Departamento de Física Teórica

LHC Phenomenology and Neutrino Physics in GUT inspired SUSY models

TESIS DOCTORAL PRESENTADA POR

Laslo Alexander Reichert

Directores de tesis: Dr. Martin Hirsch y Dr. José Wagner Furtado Valle

Paterna (Valencia), 30 de junio de 2014

Certificado

Dr. José Wagner Furtado Valle, Profesor de Investigación del CSIC,

Dr. Martin Hirsch, Investigador científico del CSIC,

CERTIFICAN:

Que la presente memoria , "LHC Phenomenology and Neutrino Physics in GUT inspired SUSY models", ha sido realizado bajo su dirección en el Departamento de Física Teórica de la Universidad de Valencia por Laslo Alexander Reichert, y que constituye su tesis doctoral para optar al grado de Doctor de Física.

Y para que así conste, en cumplimiento de la legislación vigente, presentan en el Departamento de Física Teórica de la Universidad de Valencia la referida Tesis Doctoral, y firman el presente certificado.

Firmado: Dr. José Wagner Furtado Valle

Firmado: Dr. Martin Hirsch

Acknowledgments

First of all I want to thank Jose Valle, Sergio Pastor and Martin Hirsch for providing excellent conditions in their research group for young scientists to develop and prepare a career as physicists. Particulary I want to thank Martin for his commitment and enthusiasm to work with young students on research projects in particle physics. Special thanks also to my parents for supporting and encouraging me during the whole time of my phd thesis.

Resumen

En la primera parte de la tesis investigamos un modelo supersimetrico con un mecanismo seesaw para explicar las masas de los neutrinos. El trabajo realizado resultó en dos publicaciones [1] and [2]. Implementamos el modelo en SPheno que nos permitió calcular observables de LHC (Large Hardron Collider) como por ejemplo los "Edge observables". Con la ayuda de estos observables pudimos reconstruir el espectro de masa de una teoría como SUSY y compararlo con los resultados de los experimentos. Como no hemos observado SUSY en ningún experimento calculamos para diferentes parámetros de SUSY el espectro usando errores esperados para nuestra análisis. Para poder decidir si un modelo resulta verdadero necesitamos un valor independiente que nos permita cuantificar la desviación de los resultados teóricos de los del experimento. El mismo valor nos da entonces la posibilidad de decir si dos modelos son iguales a nivel de los observables disponibles o se distinguen de manera suficiente. Nosotros usamos la prueba de χ^2 que según el nivel de confianza da lugar a verificar o discriminar modelos. El modelo depende de cinco parámetros sin tener en cuenta los acoplamientos de yukawa del sector de neutrino y un signo que aparece en el potencial de Higgs. Los cinco parámetros en cuestión son términos que rompen supersimetría de forma soft, los valores esperados del vacío de los dos campos de Higgs y la escala de seesaw. Variando estos parámetros el espectro de masa cambia lo que por lo tanto produce valores modificados en los observables. Las masas de los neutrinos son producidas por el mecanismo de seesaw. Para aplicar este mecanismo hay que introducir partículas adicionales pesadas que se transforman o bien como singletes o como tripletes bajo el grupo de simetría del modelo estándar. Hay tres mecanismos de seesaw los llamados seesaw I, II y III. Con excepción de la escala de seesaw todos los parámetros existen también en un modelo ordinario de $SU(5)$ con SUSY. Así que lo que hace el modelo distinguible de un modelo con sólo $SU(5)$ y SUSY es la escala de seesaw. Si la escala de seesaw es igual a la escala de la gran unificación no se puede distinguir el modelo conteniendo el mecanismo de seesaw del modelo sin seesaw. Esto puede entenderse a partir de las RGEs, a las cuales no contribuyen las partículas nuevas que sólo existen a escalas más allá de la escala de gran unificación. Por supuesto esto sólo es

cierto si se pueden despreciar los acoplamientos de yukawa del sector de neutrino. Como el valor de la escala de seesaw es tan importante para observar modificaciones significativas en los observables es muy importante conocer también el error de este parámetro. Descubrimos que los parámetros están muy correlacionados, por lo cual tuvimos que ajustar todos los parámetros simultáneamente. Una vez implementado el código hicimos análisis de seesaw I, II y III usando varias combinaciones de observables para ver cuáles son más y cuáles son menos importantes. Además investigamos el impacto de experimentos todavía más avanzados que el LHC como por ejemplo el ILC (International Linear Collider). Con un acelerador como el ILC los errores de los parámetros disminuyen significativamente por lo cual se puede distinguir entre un modelo de $SU(5)$ con SUSY y seesaw del que no contiene seesaw en casi todo el espacio de parámetros. A pesar de una exactitud mucho más alta del ILC respecto de la del LHC, descubrimos que únicamente con los observables del LHC ya es posible encontrar indicios de que un modelo de $SU(5)$ con SUSY y seesaw II o III explique los experimentos mejor que el que carece de seesaw.

En la segunda parte de la tesis estudiamos un modelo SUSY inspirado por la gran unificación de $SO(10)$ en el que se rompe $SO(10)$ a la escala de gran unificación a $SU(2)_L \times U(1)_B - L \times U(1)_R$. Las masas y mezclas de neutrinos se pueden explicar en este modelo con el mecanismo de seesaw. En el modelo que hemos construido usamos el mecanismo de inverse seesaw lo que nos permite romper las simetrías de gran unificación a una escala muy baja. El trabajo realizado resultó en dos publicaciones [3] and [4]. Motivado por el descubrimiento del bosón Higgs en el LHC construimos un modelo de $SU(2)_L \times U(1)_{B-L} \times U(1)_R$. Como el modelo es una extensión de las simetrías del modelo estandar hay que extender el sector de higgs. Rompiendo las simetrías adicionales a una escala muy baja además nos obliga a introducir nuevos campos. Las partículas nuevas implican una extensión de las matrices de masa lo que resulta en una modificación de la fisíca electro-débil. A diferencia con el modelo supersimetrico minimo (MSSM) en este modelo la masa del Higgs puede estar por encima de la masa del bosón Z a nivel arbol y se puede explicar la masa medida experimentalmente del order 126 GeV sin ningúna restricción sobre las masas supersimetricas. Calculamos las matrices de masa e implementamos el modelo en los programas `SPheno` y `SARAH`. Comparamos los resultados con los datos experimentales. Resulta que podemos romper las simetrías a una escala muy baja sin entrar en contradicción con los datos experimentales. Además descubrimos que en este modelo tenemos fisíca nueva que se puede comprobar en el LHC como cascadas de decaimiento de SUSY adicionales o decaimientos no-estándar del higgs.

Abstract

Motivated by current neutrino data we calculate in the first part of this thesis supersymmetric mass spectra within three variants of the seesaw mechanism, commonly known as type-I, type-II and type-III seesaw, using full 2-loop RGEs and minimal Supergravity boundary conditions. The type-II seesaw is realized using one pair of 15 and $\bar{15}$ superfields, while the type-III is realized using three copies of 24_M superfields. The 15, $\bar{15}$ and 24_M multipet are representations of a $SU(5)$ gauge group. Using published, estimated errors on SUSY mass observables attainable at the LHC and in a combined LHC+ILC analysis, we calculate expected errors for the parameters of the models, most notably the seesaw scale. Since our conclusions crucially depend on the reliability of the theoretically forecasted error bars, we discuss in some detail the accuracies which need to be achieved for the most important LHC and ILC observables before an analysis, such as the one presented here, can find any hints for seesaw mechanism in SUSY spectra. The second part of this thesis is motivated by the discovery of the new boson at around 125 GeV at the LHC. To circumvent the upper limit on the Higgs mass in the MSSM the minimal supersymmetric $U(1)_{B-L} \times U(1)_R$ extension of the standard model is discussed. Gauge couplings unify as in the MSSM, even if the scale of $U(1)_{B-L} \times U(1)_R$ breaking is as low as order TeV and the model can be embedded into an $SO(10)$ grand unified theory. The phenomenology of the model differs in some important aspects from the MSSM, leading potentially to rich phenomenology at the LHC. It predicts more light Higgs states and the mostly left CP-even Higgs has a mass reaching easily 125 GeV, with no constraints on the SUSY spectrum. Right sneutrinos can be the lightest supersymmetric particle, changing all dark matter constraints on SUSY parameter space. The model has seven neutralinos and squark/gluino decay chains involve more complicated cascades than in the MSSM. We also discuss briefly low-energy and accelerator constraints on the model, where the most important limits come from recent Z' searches at the LHC and upper limits on lepton flavour violation.

Publications

This thesis is based on the following publications:

1. M. Hirsch, L. Reichert, W. Porod, "Supersymmetric mass spectra and the seesaw scale", JHEP **1105**, 086 (2011) [arXiv:hep-ph/1101.2140]

2. C. Arbelaez, M. Hirsch, L. Reichert, "Supersymmetric mass spectra and the seesaw type-I scale", JHEP **1202**, 112 (2012) [arXiv:hep-ph/1112.4771]

3. M. Hirsch, M. Malinsky, W. Porod, L. Reichert, F. Staub, "Hefty MSSM-like light Higgs in extended gauge models", JHEP **1202**, 084 (2012) [arXiv:hep-ph/1110.3037]

4. M. Hirsch, W. Porod, L. Reichert, F. Staub, "Phenomenology of the minimal supersymmetric $U(1)_{B-L} \times U(1)_R$ extension of the standard", Phys. Rev. D **86**, 093018 (2012) [arXiv:hep-ph/1206.3516]

Contents

1 Introduction

In 2012 ATLAS and CMS announced the discovery of a new boson with a mass around 126 GeV [5; 6]. If the new particle is confirmed to be the SM Higgs boson, the SM is not only in remarkable good agreement with all precision data [7] but it also gives an answer to the last missing piece to construct a theoretically consistent model, the origin of mass. Of course, even if the new boson turns out to be the SM Higgs there remain some unanswered questions such as neutrino masses and dark matter. Also on the theoretical side the SM may not be complete. An explanation of the huge mass gaps in the spectrum of the SM particles and the so called hierarchy problem are still unsolved theoretical issues, to just name the ones most discussed in literature.

All these open questions point toward physics that can not be explained by the SM and beyond standard model (BSM) physics has to be considered to complete our understanding of what happens on microscopic scales. Unfortunately, there is still no hint for any new particles at the LHC that may shed some light on those unsolved issues. After the first CMS and ATLAS announcements [5; 6] of the discovery of a new boson with $m = 126$ GeV the decay rate into photons appeared to be too high to fit well the SM Higgs. This raised the hope that a hint for new physics beyond the standard model may have been found and therefore caused plenty of excitation [8; 9; 10; 11; 12]. However, in the latest results published by CMS this signal went down drastically [13]. It is now even below the expected value for the SM Higgs. Thus, the enhancement in the first data was perhaps just a statistical fluctuation. ATLAS still gives a value larger than the SM prediction [14], so only future data will show if the deviation is physical.

Even though the results of LHC seem to be quite sobering for the prospects of detecting physics beyond the standard model we already know from neutrino oscillations that neutrinos are massive particles. This is in contradiction with the SM prediction for massless neutrinos. The most common way to explain the smallness of neutrino masses is the so called seesaw mechanism [15; 16; 17; 18; 19; 20]. In the most minimal realization [1] a new scale M_R, the Majorana mass of the right-handed

[1] This realization is also called seesaw type I. All possible seesaw models can be classified into seesaw type I, II and

neutrinos, is introduced at high energies. Since the neutrino masses are inverse proportional to M_R, neutrinos are naturally light when M_R is large. To explain neutrino data M_R is required to be close to the scale where gauge couplings may unify [2]. Thus, neutrinos can be understood as an indirect hint for much higher scales than the scale of electroweak symmetry breaking. However, assuming the existence of high scales brings up questions such as gauge coupling unification and large "fine-tuning".

The fine-tuning in the SM comes from the quadratically divergent Higgs potential at one loop. One loop corrections to the Higgs mass scale quadratically with the mass scale of new physics. To match the Higgs mass at the electroweak scale to the Higgs mass defined at a high scale like the grand unification scale, a tremendous fine-tuning of order $\sim 10^{32}$ is required. This is also known as the hierarchy problem. In the context of grand unified theories (GUTs) we want the three gauge couplings to unify, which does not happen in the SM. For gauge coupling unification additional particles must be introduced, to change the running of the couplings in a proper way. To embed those new particles in multiplets of an enlarged symmetry group we have two well known possibilities. First, the SM gauge group is extended to a larger gauge group like $SO(10)$ and second, the Lorentz group is upgraded to supersymmetry (SUSY) [3].

We know that the SM is not valid up to all energies since gravity can not be treated classically anymore at the Planck scale (m_{Planck}) [4]. In a theory which combines at high scales gravity and SM physics at the quantum level, the SM can be understood as an effective theory. However, we currently don't have a quantum theory incorporating gravity and SM physics. Therefore, it is worth to keep in mind that challenging issues like the hierarchy problem only emerge if we introduce high scales, motivated by the smallness of neutrino masses and the idea of gauge coupling unification. There are of course different approaches to explain, e.g. the observed neutrino data like inverse seesaw [21], linear seesaw [22; 23] and radiative models [24; 25] which do not necessarily need high scales.

From astrophysical observations like clusters of galaxies, gravitational lensing and the cosmic microwave background (CMB) we know that roughly 20% of the total energy density Ω of the universe consists of dark matter (DM) [26], which only feebly interacts with the SM particles. The most popular way to add DM to the SM is to introduce weakly interacting massive particles (WIMPs) [27] but there are of course other possibilities like Axions, WIMPzillas, Q-Balls or gravitinos [27; 28; 29].

III. An introduction to seesaw type I, II and III is given in chapter 2.

[2] To get a seesaw scale close to the grand unification scale yukawa couplings of order $\mathcal{O}(10^{-1})$ are assumed. Allowing the yukawa couplings to be of order $\mathcal{O}(10^{-7})$ lowers the masses of the right-handed neutrinos down to the TeV scale.

[3] Note, that introducing a SUSY algebra or enlarging the gauge group do not automatically lead to gauge coupling unification. The running of the gauge couplings depend crucially on the chosen particle content and the scales at which new heavy particles can be produced on-shell.

[4] $m_{\text{Planck}} \cong 10^{19}$ GeV.

The minimal supersymmetric standard model (MSSM) may give an answer to many of those unsolved issues discussed before. The MSSM provides candidates for WIMP dark matter since the lightest supersymmetric particle (LSP) is stable if the MSSM lagrangian is invariant under R-Parity. A promising candidate for DM in the MSSM is the neutralino, which is a mixture of the neutral components of the Higgs and gauge boson superpartners. In the MSSM we obtain gauge coupling unification if the MSSM spectrum is not too heavy [5]. Considering all sparticle masses to be around 1 TeV SUSY terms cancel the quadratic divergences in the Higgs potential and fine-tuning is minimal.

In the SM we can distinguish between two different classes of symmetries, the Lorentz symmetry and the gauge symmetry. Therefore, to think about extensions of the SM leads naturally to think about extensions of these symmetries. The SUSY algebra is the only graded Lie algebra of symmetries of the S-matrix consistent with relativistic quantum field theory [30; 31; 32]. SUSY generalizes the notion of a Lie algebra such that the Lie algebra now includes elements whose defining relations involve anticommutators as well as commutators, which, as a consequence, connects bosonic and fermionic degrees of freedom. SUSY does not only assign a superpartner to every SM particle it also restricts the parameter space of the SM. The quartic coupling of the Higgs potential is not a free parameter anymore but a combination of the gauge couplings. This constrains the mass of the Higgs at tree level to be below the Z mass. The most challenging part of SUSY is that we don't have a dynamical well understood mechanism to break it. Since we know that the sparticle spectrum must be heavy, explicit SUSY breaking terms are introduced which split the masses of the SM particles and their superpartners. This requires the introduction of plenty new parameters since the breaking terms are not constrained by any additional symmetry. In the MSSM gauge couplings unify so it is obvious to think of GUTs in the context of SUSY. In models incorporating new physics at high scales the soft breaking terms can be motivated e.g. by supergravity or gauge mediation. This reduces the number of parameters drastically. We can understand this as a prediction from theory or just as a convenient parametrization of a parameter space, that without any simplifications is difficult to handle and looses almost any kind of predictivity.

In this work we are interested in LHC phenomenology of constrained SUSY models with extended gauge groups, which incorporate a mechanism to explain neutrino data. In chapter 3 we assume a SUSY model with CMSSM boundary conditions and a $SU(5)$ GUT group with a seesaw I, II or III mechanism. Due to additional degrees of freedom, which come from the seesaw sector, the running of the gauge couplings changes. This leads to deformations of the SUSY spectrum, what may give indirect information about the high scale parameters like the seesaw scale. To identify correlations among the high scale parameters and calculate uncertainties Monte Carlo parameter scans are used. The numerics are based on a χ-squared analysis. We show that the accuracy of such an analysis depends crucially on the assumed experimental observables and errors. Chapter 3 is based on [1] and

[5] For gauge coupling unification all supersymmetric particles should have masses below 100 TeV. In the rest of this work we consider the MSSM spectrum to be below 100 TeV.

[2]. In the first results of CMS and ATLAS a small excess at 140 GeV for a new boson was recorded [13; 14]. A Higgs with a mass of 140 GeV implies that the MSSM is in real trouble since the upper limit of the Higgs mass in the MSSM is around 130 GeV [33; 34]. Extending the gauge group can alleviate this constraint due to additional D-terms. We discuss the impact of an additional $U(1)_R$ symmetry on the Higgs mass and LHC phenomenology. To estimate the new limit for the Higgs mass in such models a detailed analysis of the parameter space is presented. To discuss sensitivities of LHC observables to new physics like additional gauge bosons, a set of benchmark points is introduced. Mass spectra and decay rates have been calculated with the programme packages Sarah [35] and SPheno [36]. All results presented in chapter 4 are based on [3] and [4].

2

Basics to get started

In this chapter an introduction to the basics of the physics discussed in chapter 3 and 4 is given. I will focus less on all technical details and instead try to review the status of the SM, Higgs physics, neutrinos and SUSY before LHC and today. In the rest of the work the SM is referred to be the SM with one Higgs doublet responsible for the spontaneous breaking of the electroweak symmetry, which is sometimes also called the minimal standard model (MSM).

The LHC was running for 2 years and ATLAS and CMS collected each more than 20fb^{-1} of data. ATLAS and CMS are the two largest experiments but there are also a couple of smaller ones like LHCb and ALICE [1]. While ATLAS and CMS were designed mainly to search for new massive particles taking advantage of the unprecedented energy available at the LHC, LHCb and ALICE have more specific roles such as measuring B-hadron physics to probe asymmetries, CP violation and heavy ions.

On March 30th 2010 the first proton-proton collision at an energy of 3.5 TeV was recorded. This defined the first time such high energies were reached in a particle accelerator [38]. In 2010 and 2011 the LHC was running at an beam energy of 7 TeV. This was increased to 8 TeV in 2012. In early 2013 the LHC was shut down for upgrades and repairs and will go into operation again in 2015 with a planned beam energy of 13 TeV.

The analysis of the LHC data taken until end of 2012 is still ongoing but it is very unlikely to find hints for new particles we have not seen until now. Therefore, a brief review of what we can already learn from LHC is given in this chapter and constraints on the parameter space of models we are interested in are presented. The first part addresses SM physics with respect to previous experiments like LEP and recent LHC data. In the second part basics of neutrino physics and GUTs are discussed and the last part gives an introduction to SUSY and current experimental limits.

[1] In [37] a complete list of all experiments at the LHC is given

2.1. Standard Model and the Higgs

The SM unifies the electromagnetic and weak force to an electroweak theory. The gauge structure is complemented by the strong interaction. Therefore the SM is based on a $SU(3)_c \times SU(2)_L \times U(1)_Y$ gauge group. After electroweak symmetry breaking (EWSB) the electromagnetic charge $Q = T_3 + Y/2$ is a linear combination of $SU(2)_L$ and $U(1)_Y$ quantum numbers. The fermionic matter fields consist of quarks which are color triplets and have electric charge $+2/3$ for up-type quarks and $-1/3$ for down-type quarks and -1 for leptons. Leptons are singlets under the $SU(3)_c$. Charged leptons (e, μ and τ) have electric charge -1 and neutrinos zero charge. In the SM neutrinos are treated as massless particles and quarks and leptons are grouped into three generations.

In 1970 the first evidence for quarks was found and the SM was established over the following years. The SM was confirmed by many experiments, starting with the detection of the charm quark in 1974 at SLAC (Stanford Linear Accelerator Center) [39; 40]. With the observation of the tau lepton in 1976 [41; 42] and the bottom quark in 1977 [43] the first third generation particles were discovered and confirmed that quarks and leptons are arranged in three families. The detection of the Z and W Boson at CERN [44; 45] was the next big step towards a complete understanding of the electroweak theory. Experiments at SLAC and CERN strengthened the assumption of three generations of fermions, affirmed by the Z Boson lifetime strongly favoring three families in the quark and lepton sector [46]. After searching at many experiments, CDF and D0 at Tevatron [2] announced in 1995 the discovery of the top quark, the last fundamental quark predicted by the SM [47; 48]. This was completed in 2000 by the detection of the tau neutrino at the DONUT (Direct Observation of the NU Tau) experiment in Fermilab [49].

In the SM, including explicit Dirac mass terms break the gauge invariance and lead to a non renormalizable theory. To give mass to fermions and the heavy gauge bosons the mechanism of spontaneous symmetry breaking is used [50; 51]. This requires a new boson charged under $SU(2)_L \times U(1)_Y$ with a potential that at low energies develops a minimum different from zero. We separate the SM lagrangian into the gauge part, which is manifestly gauge invariant, and the part including the new boson, the Higgs, that gets a vacuum expectation value (vev) at low energies breaking spontaneously the gauge symmetry:

$$\mathcal{L} = \mathcal{L}_{\text{gauge}} + \mathcal{L}_{\text{Higgs}}. \tag{2.1}$$

The gauge part reads

[2] proton antiproton accelerator at Fermilab

$$\mathcal{L}_{\text{gauge}} = -\frac{1}{4}\sum_{a=1}^{8} F^a_{\mu\nu}F^{a,\mu\nu} - \frac{1}{4}\sum_{A=1}^{3} W^A_{\mu\nu}W^{A,\mu\nu} - \frac{1}{4}B_{\mu\nu}B^{\mu\nu} + i\bar{\Psi}_L\gamma^\mu D_\mu\Psi_L + i\bar{\Psi}_R\gamma^\mu D_\mu\Psi_R \tag{2.2}$$

with

$$\begin{aligned} B_{\mu\nu} &= \partial_\mu B_\nu - \partial_\nu B_\mu \\ W^A_{\mu\nu} &= \partial_\mu W^A_\nu - \partial^A_\nu W_\mu - g\epsilon^{ABC}W_{B,\mu}W_{C,\nu} \\ F^a_{\mu\nu} &= \partial_\mu G^a_\nu - \partial^a_\nu G_\mu - g_s\epsilon^{abc}G_{b,\mu}G_{c,\nu}. \end{aligned} \tag{2.3}$$

and $a, b, c = 1, ..., 8$ the index of the adjoint representation of $SU(3)_c$ and $A, B, C = 1, ..., 3$ the index of the adjoint representation of $SU(2)_L$, respectively. The covariant derivatives are defined as

$$D_\mu\Psi_{L,R} = \left(\partial_\mu + ig_s\sum_{a=1}^{8} T^a G^a_\mu + ig\sum_{A=1}^{3} T^A_L W^A_\mu + ig'\frac{Y}{2}B_\mu\right)\Psi_{L,R}. \tag{2.4}$$

Ψ_L is the left-handed and Ψ_R the right-handed Weyl fermion transforming under $SU(2)_L$ and $SU(3)_c$ by the generators T^A and T^a, respectively.

Rearranging the electroweak terms in neutral and charged currents, one sees directly [52], that flavour changing sources can only come from charged weak interactions at tree level. Flavour changing neutral currents (FCNCs) are not present at tree level and loop contributions are highly suppressed by the GIM (Glashow, Iliopoulos and Maiani) mechanism [53]. The experimental limits on FCNCs also led to the prediction of the charm quark mass and may play an important role to test physics beyond the SM since FCNCs can be present, e.g. in models with more than one Higgs, already at tree level.

2.1.1. Spontaneous symmetry breaking

To give masses to the SM particles the Higgs must couple to fermions. Defining a gauge invariant interaction term, that turns into a mass term for right and left handed fermions after electroweak symmetry breaking, requires a SM Higgs that transforms non trivially under $SU(2)_L$ and carries hypercharge. To be in agreement with experiment the Higgs must be a $SU(2)_L$ doublet [54] and therefore the Higgs lagrangian can be written as

$$\mathcal{L}_{\text{Higgs}} = (D_\mu \Phi)^\dagger (D^\mu \Phi) - V(\Phi^\dagger \Phi) - (Y_d \bar{\Psi}_L^d \cdot \Phi \Psi_R^d + Y_u \bar{\Psi}_L^u \cdot \tilde{\Phi} \Psi_R^u + Y_e \bar{\Psi}_L^e \cdot \Phi \Psi_R^e + \text{h.c.}) \quad (2.5)$$

with

$$D_\mu \Phi = \left(\partial_\mu + ig \sum_{A=1}^{3} T^A W_\mu^A + ig' \frac{Y}{2} B_\mu \right) \Phi \quad (2.6)$$

and $\tilde{\Phi} = i\sigma^2 \Phi^*$. The Higgs potential

$$V(\Phi^\dagger \Phi) = -\mu^2 \Phi^\dagger \Phi + \frac{1}{2} \lambda \left(\Phi^\dagger \Phi \right)^2 \quad (2.7)$$

consists of a quadratic and quartic coupling with the coupling constants μ and λ. The minus sign in front of the quadratic term is essential for spontaneous symmetry breaking since it accounts for the mexican hat shape of the Higgs potential [3].

The Higgs doublet is a complex doublet, which after EWSB gets a VEV v and reads in the unitarity gauge

$$\begin{pmatrix} \Phi^+ \\ \Phi^0 \end{pmatrix} \rightarrow \begin{pmatrix} 0 \\ v + H/\sqrt{2} \end{pmatrix}. \quad (2.8)$$

Only one physical degree of freedom remains and forms the SM Higgs H. The other three constituents of the doublet are the so called would-be Goldstone bosons which become the longitudinal components of the heavy gauge bosons. Minimizing the potential defines

$$v = \sqrt{\frac{\mu^2}{\lambda}}. \quad (2.9)$$

This fixes λ, once the mass of the Higgs is known. After EWSB only one combination of gauge fields remains massless [4]. The photon stays massless whereas the tree level masses of the W and Z Boson can be defined as

[3] In the literature the minus sign in front of the quadratic coupling is usually absorbed in μ^2 and $\mu^2 < 0$.

[4] In the mass eigenbasis we get for the photon A_μ and Z boson Z_μ

$$A_\mu = \cos\theta_W B_\mu + \sin\theta_W W_\mu^3 \qquad Z_\mu = -\sin\theta_W B_\mu + \cos\theta_W W_\mu^3$$

and for the charged W boson

$$m_W^2 = \frac{1}{2}g^2v^2 \quad , \qquad m_Z^2 = \frac{g^2v^2}{2\cos^2\theta_W}. \tag{2.10}$$

An important aspect of Higgs physics are the couplings of the Higgs to the SM particles. As a consequence of spontaneous symmetry breaking the trilinear couplings to the heavy gauge bosons and fermions are proportional to their masses. The interactions for the Z and W can be written as [52]

$$\begin{aligned}\mathcal{L}[H,W,Z] = gm_W W_\mu^+ W^{-,\mu} H + \frac{g^2}{4} W_\mu^+ W^{-,\mu} H^2 \\ + \frac{gm_Z}{2\cos^2\theta_W} Z_\mu Z^\mu H + \frac{g^2}{8\cos^2\theta_W} Z_\mu Z^\mu H^2\end{aligned} \tag{2.11}$$

and for the fermions we get after EWSB masses proportional to the Yukawa couplings and the vev

$$m_{ij}^{d,u,e} = Y_{ij}^{d,u,e} v. \tag{2.12}$$

The quartic couplings in eq. 2.11 only depend on the parameter g, g' and θ_W and the couplings to fermions are proportional to their masses. Therefore all interaction terms are very well predicted by the SM and the measurement of the couplings provides a powerful tool to verify if the new boson detected at LHC is indeed the SM Higgs. The predicted Higgs decay channels into SM particles as a function of the Higgs mass are shown in fig. 2.1. The larger the fermion mass the larger the coupling and therefore the larger the branching ratio. For Higgs masses below ~ 160 GeV heavy gauge bosons can not be produced on shell and the branching ratios are suppressed. However, already for Higgs masses around 150 GeV the branching ratios into two W or Z bosons become dominant. Since photons do not couple at tree level to the Higgs, branching ratios into photons are loop suppressed.

The Higgs mass reads at tree level

$$m_H^2 = 2\mu^2 = 2\lambda v^2 \tag{2.13}$$

and is the only parameter missing in the SM to be fixed by experiment.

$$W_\mu^\pm = \frac{1}{\sqrt{2}}\left(W_\mu^1 \pm W_\mu^2\right).$$

The electromagnetic charge $e = g\sin\theta_W = g'cos\theta_W$ is proportional to the coupling constants g and g' and the rotation angle θ_W.

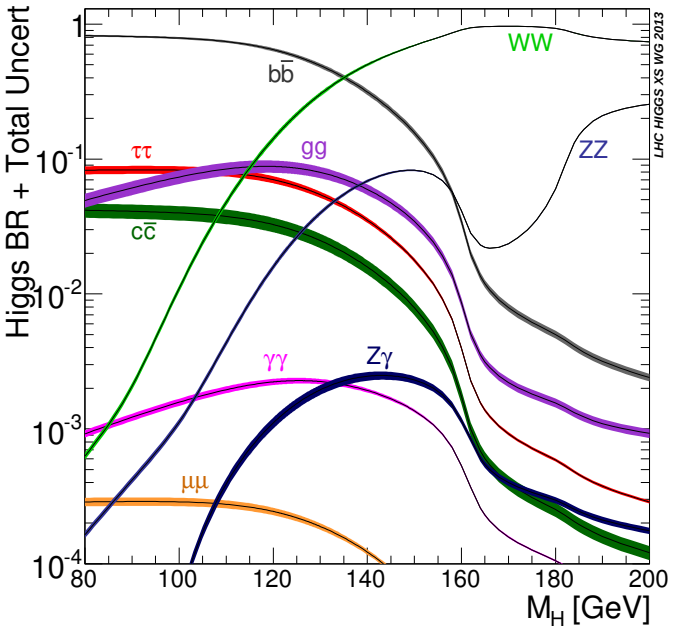

Figure 2.1: Higgs decay channels with total uncertainties as a function of the Higgs mass [55].

2.1.2. Predictions for the Higgs before LHC

Even before the Higgs was directly detected at the LHC, experimental data from previous experiments and theory lead to predictions for the SM Higgs properties. The limits discussed below are all derived for the SM with one electroweak Higgs doublet. Variations of this setup lead to different physics and usually to much less stringent bounds, unless the extension is constrained by an additional symmetry.

The most important experimental bound is the lower limit on the Higgs mass

$$m_H \gtrsim 114 \text{ GeV (at 95 \% confidence level)} \tag{2.14}$$

from LEP since no Higgs like particle was observed [7]. Also electroweak precision tests at LEP can give strong constraints on the mass range allowed for m_H once the top mass is well own. Vacuum polarization corrections of the gauge boson propagators are very precisely measured. The fit of these observables to theoretical predictions coming from loop corrections prefers a light Higgs. The experimental limits lead to an upper limit on the Higgs mass [56]

$$m_H \lesssim 185 \text{ GeV} \tag{2.15}$$

up to which the SM is still in agreement with experiment at 95 % confidence level [5].

The ρ_0 parameter

$$\rho_0 = \frac{m_W^2}{m_Z^2 \cos^2 \theta_W} \tag{2.16}$$

is exactly one at tree level considering only SM model physics. This relation can be spoiled by new physics, in particular when a non SM model Higgs acquires a vev at the electroweak scale. Including quantum corrections it has been proven that the effective Higgs must be a weak isospin doublet [46].

Also from theory side the mass of the Higgs can be constrained. In the absence of the Higgs scattering, amplitudes involving longitudinal gauge bosons lead to violations of unitarity at a few TeV. In the limit $s \gg m_Z^2$ one obtains for the WW scattering amplitude with two Z bosons in the final state [52]

$$A(W^+W^- \to ZZ) \sim i\frac{s}{v^2} \tag{2.17}$$

which has an unacceptable large energy behaviour. This can be cured by the Higgs contribution to the scattering amplitude

$$A(W^+W^- \to ZZ) \sim -i\frac{s^2}{v^2(s - m_H^2)}. \tag{2.18}$$

Combining eq. 2.17 and 2.18 leads to

$$A(W^+W^- \to ZZ) \sim -i\frac{sm_H^2}{v^2(s - m_H^2)} \tag{2.19}$$

which in the limit $m_H \ll s$ saturates at a constant value [6]. Therefore, to be consistent with unitarity bounds the Higgs mass should be $m_H^2 < 4\pi\sqrt{2}/G_F$ or $m_H < 1.5$ TeV [52]. This can also be interpreted as an upper limit for new physics that has to appear if no Higgs is found.

The non asymptotically free behaviour of the quartic coupling λ leads to a Landau pole. Requiring the Landau pole not to appear below an energy scale Λ gives upper limits on the Higgs mass [58]

[5] For the limit a top mass of $m_t = 173.3 \pm 1.1$ GeV was used [56].

[6] Note, that only the scattering amplitude saturates at a constant value. In the limit $s \gg m_W$ the cross section for $WW \to ZZ$ drops with $1/s^2$ [57].

$$\begin{aligned} m_H &\lesssim 180 \text{ GeV} && \text{for } \Lambda \sim M_{\mathsf{GUT}} - M_{\mathsf{Pl}} \\ m_H &\lesssim 500 - 800 \text{ GeV} && \text{for } \Lambda \sim 1\text{TeV} \end{aligned} \tag{2.20}$$

Last but not least also lower limits on the Higgs mass can be derived [59; 60]. For small m_H the quartic coupling λ can become negative which means that the derivative of the Higgs potential $V'[\Phi]$ is not positive anymore and therefore unbounded from below. Thus, vacuum stability requires λ to remain positive up to high scales like M_{GUT} or M_{Pl}. With a top mass of $m_t \sim 173$ GeV the lower limit is [61]

$$m_H \gtrsim (130 \pm 0.3) \text{ GeV}. \tag{2.21}$$

For Higgs masses slightly below this value the SM could still be viable up to high scales since the vacuum might be unstable but with a lifetime longer than the age of the universe [62]. Also in the case of more Higgses this constraint is softened since the bound applies only to an effective mass of all Higgses. Therefore, the lightest Higgs can be below this limit as it is the case in the MSSM. In conclusion we can constrain the Higgs mass to

$$130 \text{ GeV} \lesssim m_H \lesssim 171 \text{ GeV}. \tag{2.22}$$

Note, however, that the strong limits coming from the Landau pole and vacuum stability require the SM to be valid up to M_{GUT} and M_{Pl}, respectively, and no new physics to show up at some intermediate scale.

2.1.3. SM and the LHC

The plots in tab. 2.1 and 2.2 show the 95 $\%$ exclusion limit on the production rate ($\sigma \times L$, i.e. production cross section times luminosity) of the Higgs boson as a function of its mass [7]. This is normalized to the production rate $\sigma_{\mathsf{SM}} \times L$ of the standard model Higgs. In tab. 2.1 Higgs masses from 100 GeV to 600 GeV are plotted. This is the current mass range in which the SM Higgs can be tested at LHC. To discuss details in the energy region, where the new boson with mass around ~ 125 GeV is observed, only Higgs masses up to 200 GeV are shown in tab. 2.2.

The dashed line is the theoretical prediction for the SM background with the one and two sigma uncertainties indicated by the green and yellow error bands, respectively. The black line shows the

[7] All plots discussed in this subsection are taken from [14] and [13].

	CMS+ATLAS	
2011 Data ($L \leq 2fb^{-1}$)	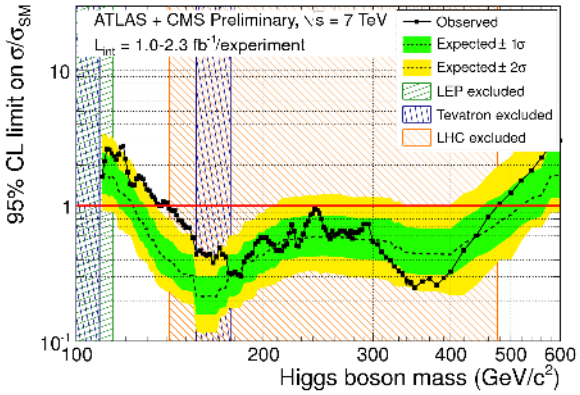	
	CMS	**ATLAS**
2011 Data ($L \leq 5fb^{-1}$)	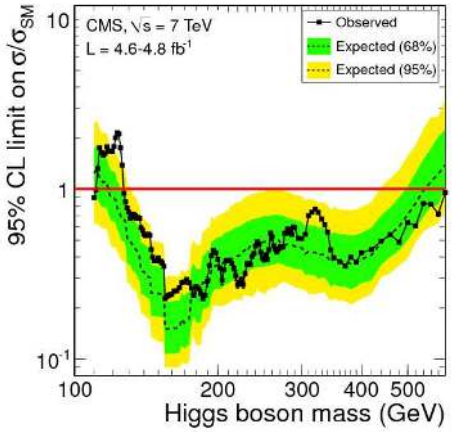	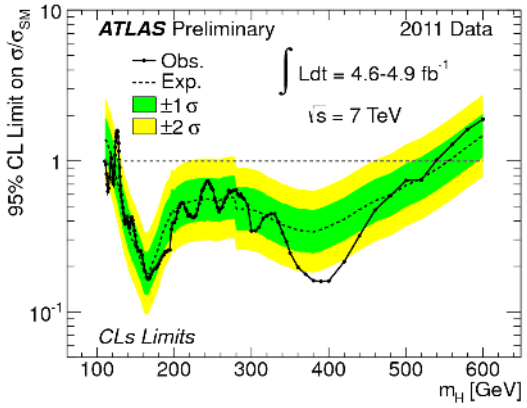
2011 + 2012 Data ($L \leq 6fb^{-1}$)		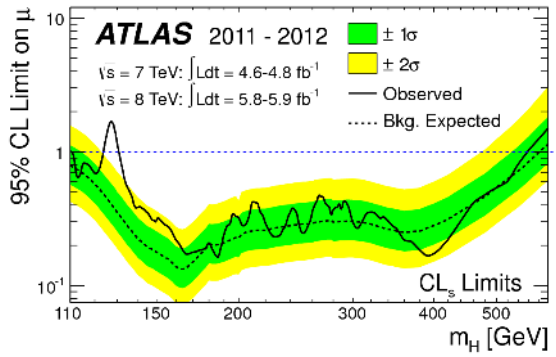

Table 2.1: The 95 % exclusion limit on the production rate of the Higgs boson as a function of its mass is shown. This is normalized to the production rate of the standard model Higgs. All plots are taken form [13] and [14].

	CMS+ATLAS	
2011 Data ($L \leq 2fb^{-1}$)	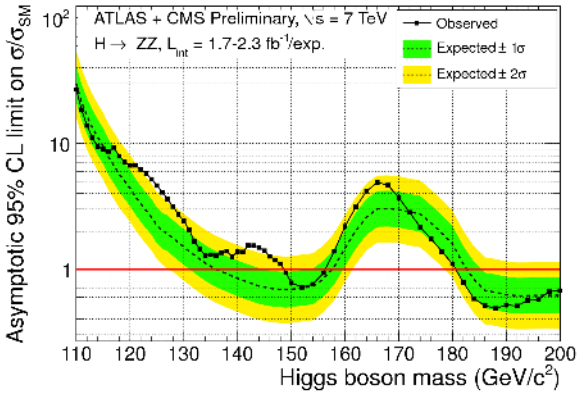	
	CMS	**ATLAS**
2011 Data ($L \leq 5fb^{-1}$)	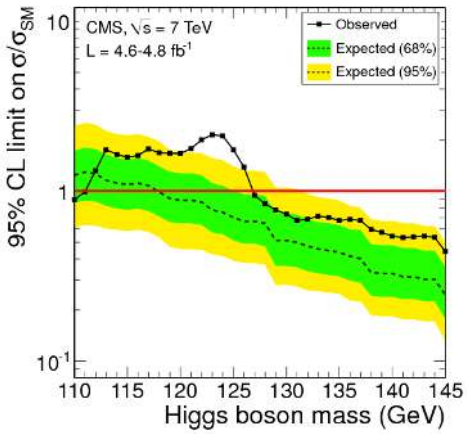	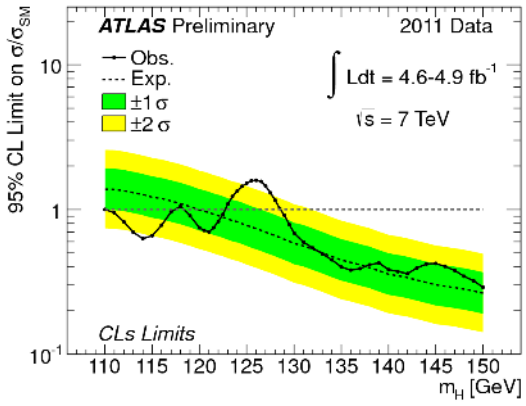
2011 + 2012 Data ($L \leq 20fb^{-1}$)		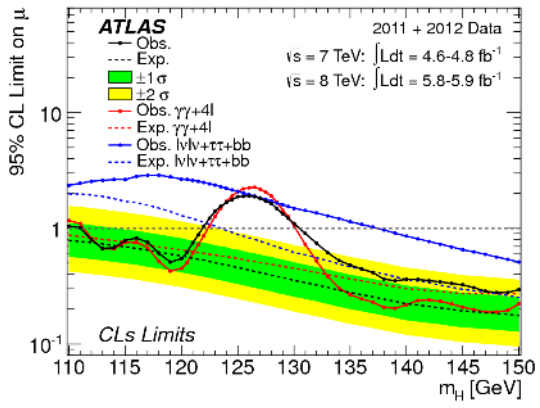

Table 2.2: The 95 % exclusion limit on the production rate of the Higgs boson as a function of its mass is shown. This is normalized to the production rate of the standard model Higgs. All plots are taken form [13] and [14].

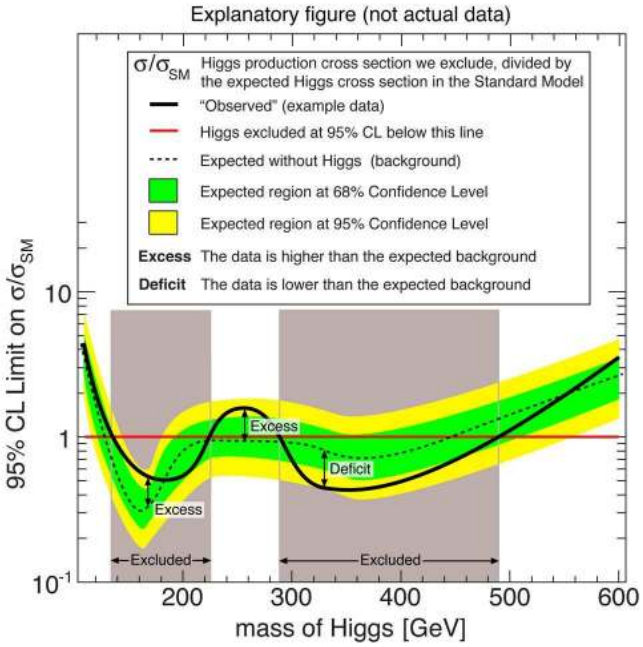

Figure 2.2: Example data set for a Higgs decay channel as a function of the Higgs mass [63].

experimental data. In the regions where the black line drops below the horizontal line at 1 the SM Higgs is excluded at 95 $\%$ confidence level. If the black curve is above one and no significant discrepancy from the SM background is observed the SM Higgs can be neither excluded nor confirmed, since the experimental error is still too large to probe this region.

To explain the standard plots used by CMS and ATLAS lets assume a simplified picture with an example data set, as shown in fig. 2.2, and only one decay channel with final state f. We denote the number of measured events as $n_{f,\text{exp}}$. For simplicity, neglect for the moment systematical errors and consider only the statistical error $\Delta n_{f,\text{exp}}$. For a given luminosity we can calculate the number of events $n_{\text{f,Higgs}}$ for the Higgs decaying to f, assuming the Higgs mass m_h to be the invariant mass of the measured final state m_f. $\sigma/\sigma_{\text{SM}}$ can be understood as the ratio of $\Delta n_{f,\text{exp}}$ and $n_{\text{f,Higgs}}$

$$\sigma/\sigma_{\text{SM}} = r = \frac{\Delta n_{f,\text{exp}}}{n_{\text{f,Higgs}}} \tag{2.23}$$

and therefore, we can distinguish between two cases. Taking into account the experimental error, events that might come from a Higgs decay are not significant, if $n_{\text{f,Higgs}} < \Delta n_{f,\text{exp}}$ and $r > 1$, respectively. The SM Higgs can not be exluded, but we can exclude Higgses with larger cross sections compared to the SM Higgs. Lets assume, e. g. $r = 2$. This implies that Higgses, which have two times the SM cross section into the final state f, can be excluded. If $n_{\text{f,Higgs}} > \Delta n_{f,\text{exp}}$

the sensitivity of the measurement [8] is sufficient to test the SM Higgs. Neglecting the theoretical error and considering $\Delta n_{f,\text{exp}}$ to be the two sigma experimental uncertainty we can exclude the SM Higgs at 95 $\%$ confidence level, if $r \leq 1$.

In the case that for a given final state more events are detected than expected from calculations of the SM background the black line is above the dotted line. In case less events are observed, the experimental curve drops below the dotted one. If such an excess or deficit, respectively, crosses the yellow error band experimental data is not in agreement with the SM background at two sigma confidence level. An excess which exactly hits the horizontal line at 1 can only be the SM Higgs or a particle which has the same production rate in this channel. If the excess is below or above 1 it may still be a Higgs but with smaller and larger cross section, respectively, compared to the SM one. However a Higgs analysis with real data is more complicated. Uncertainties coming from background events and mixing between different channels have to be included. Also the assumption, that the Higgs is produced on-shell in a s-channel and all decay final states can be measured, is a strong simplification. In case of missing energy, e.g., we do not get a peak in the invariant mass spectrum at the energy the Higgs is produced on-shell. The structure of the final state spectrum becomes more complicated and a simple reconstruction of the Higgs mass, as discussed above, is not possible anymore.

In 2011 ATLAS and CMS presented the first combined analysis for $h \to \gamma\gamma$ and $h \to ZZ$ channels (see first row in 2.1 and 2.2). Even though statistics were still too low to probe Higgs masses down to the LEP limit already a wide range of parameter space was constrained. The new limits exluded Higgs masses between 150 and 500 GeV. At around 140 GeV a small excess in the experimental data can be seen. Nevertheless more statistics were required to draw any conclusion. At the end of 2011 CMS and ATLAS presented an update of the Higgs search, including the complete 2011 data in the analysis (see second row in 2.1 and 2.2). The excess at 140 GeV went away in both experiments but a new one at around 125 GeV was observed. This was the first evidence for the existence of a spin 0 or spin 2 boson at the electroweak scale. In summer 2012 the first results, including 2012 data, were published (see third row in tab. 2.1 and 2.2). [9] Both experiments confirmed the excess at $\sim$125 GeV and presented a combined analysis of all observed decay channels (see first row in tab. 2.3). The plots show the best fit values for the coupling strength of the SM Higgs to $\tau\tau$, bb, WW, ZZ and $\gamma\gamma$ final states. ATLAS and CMS observed an enhanced decay rate into photons two sigma off the SM prediction. Therefore, the black line in the last plot in 2.1 and 2.2 crosses 1 at 125 GeV, representing the decay rate into photons. The peak is almost twice as high than the predicted one for the SM Higgs. Taken the height of the excess seriously this could be interpreted as a hint for

[8] since in this simplified case we neglect systematical errors, the experimental uncertainty depends only on the statistical error $\sqrt{n}$. Therefore, the better the statistics the better the sensitivity which means that measuring long enough, the black line goes to zero if no Higgs is found.

[9] CMS did not present their results plotting $\sigma/\sigma_{\text{SM}}$ against the Higgs mass. Therefore, on the CMS side one plot is missing in tab. 2.1 and 2.2.

physics beyond the SM. The decay rates into $\tau\tau$, bb, WW and ZZ were in good agreement with SM predictions.

In march 2013 Higgs studies using up to 25 fb^{-1} were published. In the last row in tab. 2.3 we can see that the measured decay into photons at CMS went down and is now even below the SM prediction. ATLAS still detects a larger value but since both experiments show contrary results it might be rather a statistical fluctuation than new physics. In CMS the decay into WW is slightly to small and ATLAS lacks events in the bb channel compared to the SM expectation. Also the best fit values for ZZ and $\gamma\gamma$ final states point to two slightly different Higgs masses (see tab. 2.4). CMS gets a smaller mass for $\gamma\gamma$ than for ZZ but ATLAS measurements claim the opposite. The analysis is done for only one Higgs combining both channels to get the best fit value for the mass.

As we can see in tab. 2.1 and 2.2 the lower limit on the Higgs mass becomes significantly stronger with more statistics, but the upper limit almost remains constant. This stems from the fact, that the production rate of the Higgs drops exponentially with larger m_H and therefore much more statistics is needed to push the upper bound to significantly higher values.

Also first results for the spin properties of the Higgs-like boson were published [14; 13]. Experimental data favors a spin 0 boson but more data must be taken to be conclusive. Assuming the new particle to be the SM Higgs a heavy fourth generation of fermions, which still had a small allowed window for masses slightly above m_t, are now strongly disfavored by the measured decay rates [64; 65].

If the Higgs-like boson turns out to be the SM Higgs the mass of 126 GeV fixes the quartic coupling λ to $\lambda = 0.26$. With this value we are still in the pertubative domain but vacuum stability might not be guaranteed up to M_{GUT} and M_{Pl}, respectively [61; 66].

In conclusion we can say that all measurements point towards the discovery of the SM Higgs, with small mass as preferred by the LEP electroweak precision fits [67]. Statistics must be improved to get a more detailed analysis of the couplings of the SM particles to this new boson. Thus future data must show if we really found the SM Higgs.

2.2. Neutrino physics and GUTs

2.2.1. Neutrinos and experiment

In the SM neutrinos are massless since (a) no right handed neutrinos are present, which are needed to write down a renormalizable Dirac mass term and (b) there is no Higgs triplet. From oscillation experiments we know that at least two neutrino states have non-zero mass. The measured solar (Δm^2_{12}) and atmospheric (Δm^2_{13}) mass differences [68]

	CMS	ATLAS
2011 + 2012 Data ($L \leq 6fb^{-1}$)	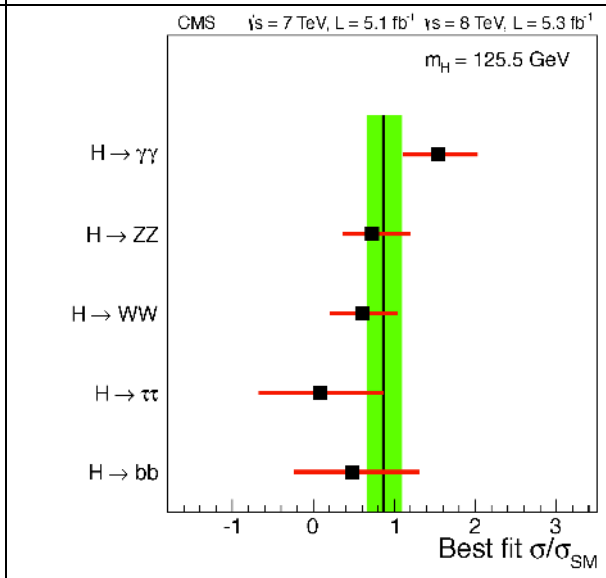	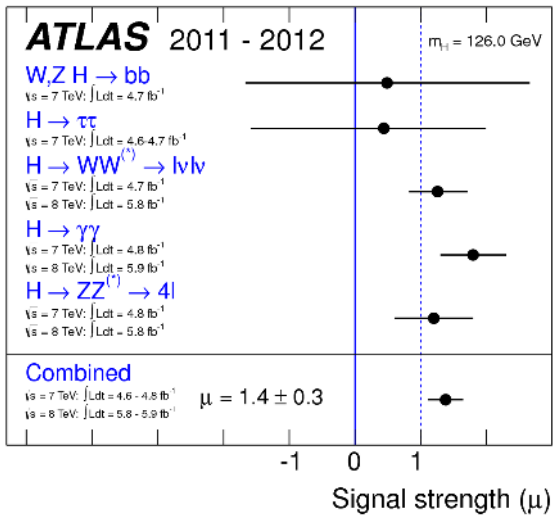
2011 + 2012 Data ($L \leq 20fb^{-1}$)	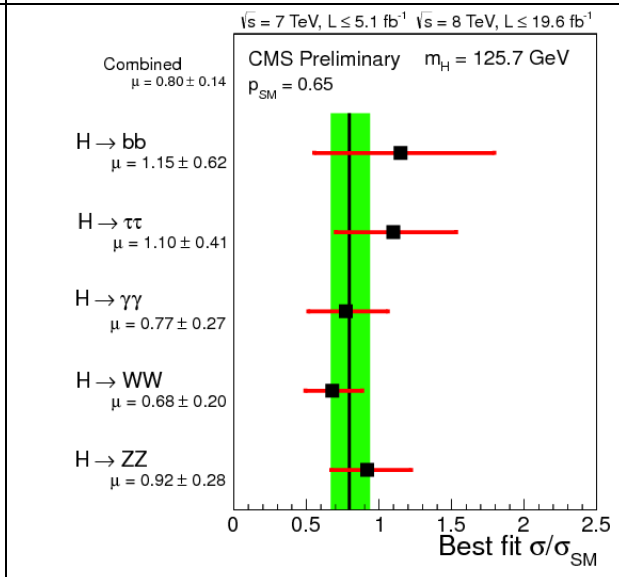	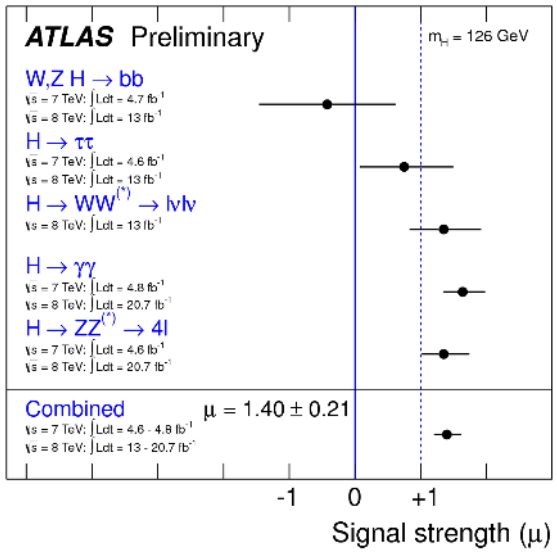

Table 2.3: The coupling strengths of the Higgs to $\gamma\gamma$, ZZ, WW, $\tau\tau$ and bb are shown as a function of $\sigma/\sigma_{\text{SM}}$. The value for μ is the best fit value for σ/σ_{SM} combining all decay channels. All plots are taken form [13] and [14].

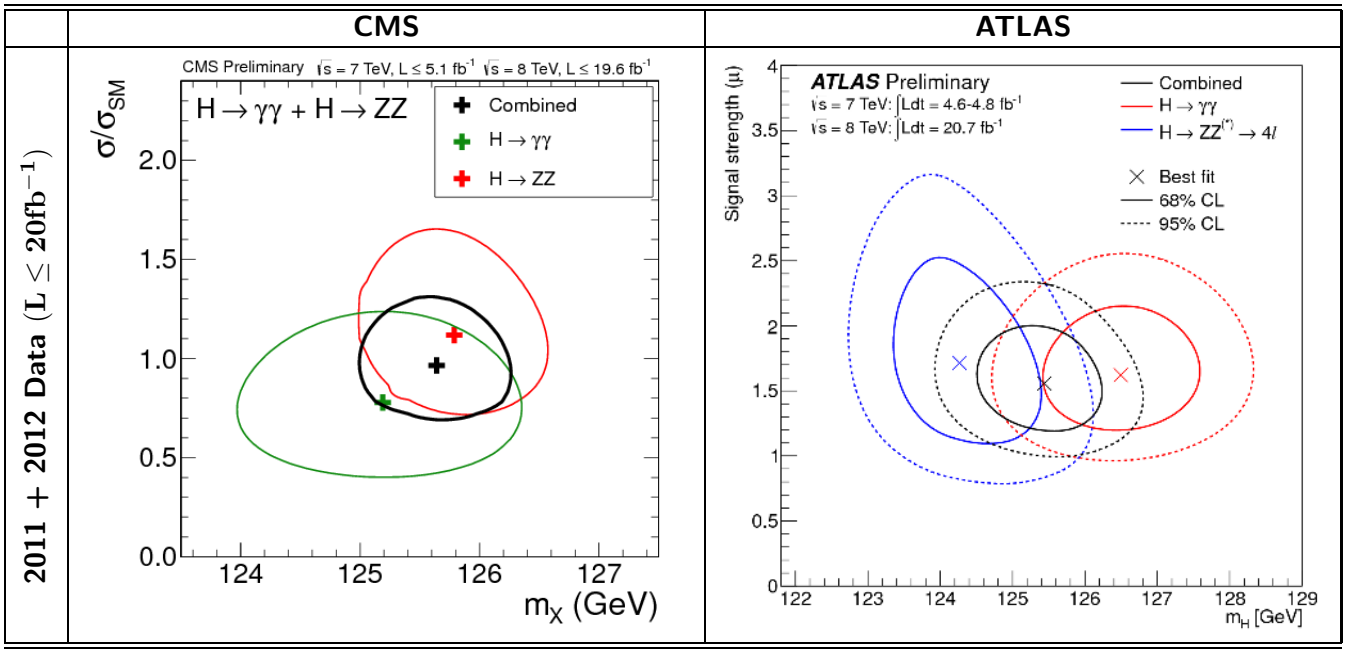

Table 2.4: The best fit values for $\gamma\gamma$ and ZZ final states are shown. σ/σ_{SM} is plotted as a function of the invariant mass m_X. The black line is the combined fit for both channels. All plots are taken form [13] and [14].

$$\Delta m^2_{12} = \Delta m^2_{\text{sol}} \sim (7.5 \pm 0.3) \times 10^{-5}\ \text{eV}^2$$
$$\Delta m^2_{13} = \Delta m^2_{\text{atm}} \sim (2.5 \pm 0.1) \times 10^{-3}\ \text{eV}^2 \tag{2.24}$$

are small but do not fix the absolute values of neutrino masses. Also the mass ordering among the three neutrino states is still an open question. In normal hierarchy the first mass state, which is dominated by the electron neutrino, is the lightest. In the inverted hierarchy the mass ordering is flipped and mass state 3 is the lightest neutrino mass eigenstate. Both are still valid solutions and more experimental data is needed to confirm or exclude one of them. Even though in oscillations only mass differences can be measured we can put an upper limit on neutrino masses. The absolute mass scale is very small and constrained by

- single beta decay $(n \to p + \bar{\nu}_e + e)$
- neutrinoless double beta decay $(2n \to 2p + 2e^-)$ in nuclei
- cosmology

Observables	most optimistic	conservative	Ref.
m_{e}	< 2.1 eV	< 2.3 eV	[70]
m_{ee}	< 0.14 eV	< 0.4 eV	[71; 72]
M_ν	< 0.32 eV	< 0.98 eV	[26]

Table 2.5: Upper limits for neutrino masses from single beta decay, neutrinoless double beta decay and cosmology.

with n and p the neutron and proton, respectively. With current accuracies we can only put limits on combinations of neutrino masses [10]. The observable in single beta decay is defined as

$$m_{\mathsf{e}}^2 = \sum_i |U_{ei}^2| m_{\nu_i}^2 \tag{2.25}$$

whereas the mass parameter derived from neutrinoless double beta decay is

$$m_{\mathsf{ee}}^2 = |\sum_i U_{ei}^2 m_{\nu_i}|^2. \tag{2.26}$$

Note, that contributions to neutrinoless double beta decay can only come from Majorana neutrinos and the measured mass parameter m_{ee}^2 depends on the Majorana phases. [11]. From cosmology we can derive limits on the sum over all neutrino mass eigenstates

$$M_\nu = \sum_i m_{\nu_i}, \tag{2.27}$$

which is independent of the mixing matrix U. Since experiments give different values for the upper limits on the observables and M_ν depends crucially on the chosen cosmological model and analysis, only the most conservative and most optimistic upper limits are presented. The values are summarized in tab. 2.5.

Neutrino oscillations are due to a mismatch of the flavour eigenstates and the mass eigenstates of neutrinos. If neutrinos are Majorana particles the mass matrix m_ν is symmetric and can be

[10] In single beta decay experiments it is in principal possible to measure masses of single neutrino mass eigenstates [69].

[11] The neutrino mixing matrix U and the Majorana phases are defined in eq. 2.28 and 2.29.

diagonalized by

$$\hat{m}_\nu = U m_\nu U^T. \tag{2.28}$$

The rotation matrix U is parametrized as

$$U = \begin{pmatrix} c_{12}c_{13} & s_{12}c_{13} & s_{13}e^{-i\delta} \\ -s_{12}c_{23} - c_{12}s_{23}s_{13}e^{i\delta} & c_{12}c_{23} - s_{12}s_{23}s_{13}e^{i\delta} & s_{23}c_{13} \\ s_{12}s_{23} - c_{12}c_{23}s_{13}e^{i\delta} & -c_{12}s_{23} - s_{12}c_{23}s_{13}e^{i\delta} & c_{23}c_{13} \end{pmatrix} \times \begin{pmatrix} e^{i\alpha_1/2} & 0 & 0 \\ 0 & e^{i\alpha_2/2} & 0 \\ 0 & 0 & 1 \end{pmatrix} \tag{2.29}$$

with $c_{ij} = \cos\theta_{ij}$ and $s_{ij} = \sin\theta_{ij}$. The angles θ_{12}, θ_{13} and θ_{23} are the solar neutrino angle, the reactor angle and the atmospheric neutrino mixing angle, respectively. δ is the Dirac phase and α_i are Majorana phases. Since U can be determined experimentally only up to an irrelevant overall phase, one can find different parameterizations of the Majorana phases in the literature.

In contrast to quarks in the neutrino sector two mixing angles are large. For a long time neutrino mixing angles were in good agreement with tribimaximal mixing [12], but recent experiments confirm a small but significant deviation from zero for θ_{13} (see tab. 2.6). Thus a lot of neutrino mass models predicting $\theta_{13} = 0$ require modifications. θ_{12} and θ_{23} are very well measured and the current experimental values are still in agreement with tribimaximal mixing expectations [73]. The recent values for mass squareds and angles of U are summarized in tab. 2.7.

2.2.2. Seesaw

To give masses to neutrinos the SM has to be extended. The simplest way is to add at least two right-handed neutrinos and write down a Yukawa term that couples the left and right handed neutrinos to the SM Higgs

$$\mathcal{L}_{Y,\text{neutrinos}} = Y_\nu \bar{\nu}_L H \nu_R \tag{2.30}$$

Thus, assuming only mass terms coming from Higgs yukawa interactions after EWSB, the same mechanism that gives masses to the SM fermions is applied in the neutrino sector. Since neutrinos are much lighter than the rest of the SM particles, very small yukawa couplings are required. However,

[12] $\theta_{12} = \sin^{-1}(1/\sqrt{3}) \simeq 35.3°$, $\theta_{23} = 45°$, $\theta_{13} = 0$ and δ is undetermined

Experiment	$\sin^2\theta_{13}$	Ref.
T2K	$0.028^{+0.019}_{-0.024}$	[74]
MINOS	$0.010^{+0.012}_{-0.008}$	[75]
DC	$0.022^{+0.019}_{-0.018}$	[76]
DYB	0.024 ± 0.005	[77]
RENO	0.029 ± 0.006	[78]

Table 2.6: Best fit values and experimental uncertainties for θ_{13} at T2K, MINOS, DC, DYB and RENO

parameter	best fit value	2σ range
$\Delta m^2_{\text{sol}}(10^{-5}\ \text{eV}^2)$	7.62	7.27-8.01
$\Delta m^2_{\text{atm}}(10^{-3}\ \text{eV}^2)$	2.55	2.38-2.68
$\sin^2\theta_{12}$	0.320	0.29-0.35
$\sin^2\theta_{23}$	0.613	0.38-0.66
$\sin^2\theta_{13}$	0.0246	0.019-0.030

Table 2.7: Best fit values and experimental uncertainties for θ_{12}, θ_{23}, θ_{13}, Δm^2_{sol} and Δm^2_{atm} for normal neutrino mass hierarchy [73].

a possible explanation for the smallness of neutrino masses can be given in terms of a Majorana term introduced for the right handed neutrinos.

In the SM the lepton and baryon number (L and B, respectively) are conserved at all orders in perturbation theory [13]. Introducing a Majorana mass for right-handed neutrinos breaks lepton number. The Majorana mass term reads

$$M_R \bar{\nu}_R^c \nu_R = \bar{\nu}_{R,i}^c M_{R,ij} \nu_{R,j}. \tag{2.31}$$

Thus the neutrino mass matrix contains after EWSB a Dirac term $m_D = Y_\nu v$ from the yukawa coupling of eq. 2.30 and the Majorana mass M_R

$$m_\nu = \begin{pmatrix} 0 & m_D \\ m_D^T & M_R \end{pmatrix}. \tag{2.32}$$

For the light neutrino mass eigenstates we get

$$\hat{m}_\nu \cong -m_D^T M_R^{-1} m_D. \tag{2.33}$$

Light neutrino masses are therefore inversely proportional to the Majorana mass. Assuming the Majorana mass to be large, neutrino masses are naturally small. This is the so called seesaw mechanism [15; 16; 17; 18; 19; 20].

Note, that without right-handed neutrinos we can still write down a Majorana mass term for ν_L. Since ν_L forms part of a $SU(2)_L$ doublet and has isospin $1/2$ we need a term with two Higgses to obtain a gauge invariant interaction. Encoding all high scale physics in one parameter M_5 the resulting effective mass term for neutrinos can be written as

$$O_5 = \frac{\lambda_{ij}}{M_5} l_i^T l_j H H. \tag{2.34}$$

O_5 is a non renormalizable five dimensional operator and was first introduced by Weinberg [82] [14].

[13] Chiral anomaly and the vacuum topology in non-abelian gauge theories leads to non-conservation of baryon and lepton number at the non-pertubative level. However, the $B-L$ symmetry is left invariant, which can be understood as a hint for grand unification. In larger symmetry groups $B-L$ invariance can be predicted by the gauge structure of the theory. From experiments we know that additional gauge symmetries like $B-L$ must be broken at some higher scale. Recent lower limits on the mass of new gauge bosons are of order a few TeV [79; 79; 80; 81].

[14] Here we can see that models incorporating the Weinberg operator do not conserve lepton number. The Weinberg operator defined in eq. 2.34 breaks lepton number by 2 ($\Delta L = 2$). In models, incorporating only Dirac neutrinos, lepton number remains unbroken. No high scale is introduced and a Yukawa coupling Y_ν of order 10^{-12} accounts for

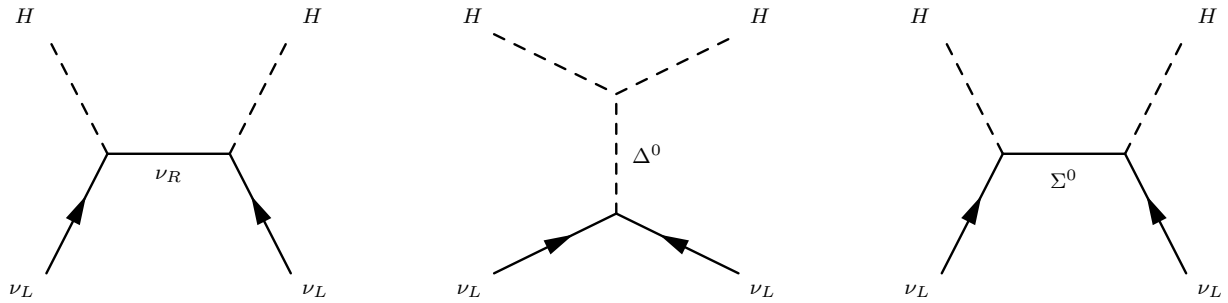

Figure 2.3: Feynman diagrams for seesaw type I, II and III.

The corresponding mass term is $m_\nu \sim \lambda v^2/M_5$ with λ a dimensionless coupling usually taken $\mathcal{O}(1)$. As in eq. (2.33) neutrino masses are inverse proportional to a new parameter with dimension mass (M_R and M_5, respectively). Therefore assuming neutrinos to be Majorana particles introduces a new scale that can explain the smallness of neutrino masses in terms of new physics present at a high scale.

At the tree level [15] we can classify the possible ultra-violet (UV) completions that lead to the effective operator defined in eq. 2.34. There are only three possibilities, including the exchange of a singlet fermion (seesaw I), a triplet scalar (seesaw II) and a triplet fermion [16].

$$\begin{aligned}
\mathcal{L}_{\text{I}} &= Y_\nu H \nu_L \nu_R + M_R \bar{\nu}_R^c \nu_R \\
\mathcal{L}_{\text{II}} &= Y_\Delta \bar{l}^c \Delta l + \lambda H \Delta H + M_\Delta \Delta\Delta \\
\mathcal{L}_{\text{III}} &= Y_\Sigma H^\dagger \bar{\Sigma} l + \frac{1}{2}\text{tr}[\bar{\Sigma} M_\Sigma \Sigma^c + \text{h.c.}].
\end{aligned} \tag{2.35}$$

with

$$\Delta = \begin{pmatrix} \Delta^+/\sqrt{2} & \Delta^{++} \\ \Delta^0 & \Delta^+/\sqrt{2} \end{pmatrix} \quad \text{and} \quad \Sigma = \begin{pmatrix} \Sigma^- & \Sigma^0/\sqrt{2} \\ \Sigma^0/\sqrt{2} & -\Sigma^+ \end{pmatrix}. \tag{2.36}$$

The Feynman diagrams for the different seesaws are shown in fig. 2.3. Note, that in the case of the seesaw II and III only the neutral component of the triplet (Δ^0 and Σ^0, respectively) contributes to m_ν. After integrating out the heavy particles ν_R, Δ^0 and Σ^0 the neutrino mass matrices read

the smallness of neutrino masses.

[15] In a recent work also all 1-loop contributions for the Weinberg operator were classified [83].

[16] Note, that in this notation seesaw models like the inverse or linear seesaw discussed in chapter 4 belong to the class of seesaw I.

$$m_\nu = -\frac{v^2}{2} Y_\nu^T M_R^{-1} Y_\nu \tag{2.37}$$

$$m_\nu = \frac{v^2}{2} \frac{\lambda}{M_\Delta} Y_\Delta \tag{2.38}$$

$$m_\nu = -\frac{v^2}{2} Y_\Sigma^T M_\Sigma^{-1} Y_\Sigma. \tag{2.39}$$

In case of seesaw I and III 21 degrees of freedom fix the neutrino sector coming from the yukawa coupling, three Majorana and three charged lepton masses [84]. For the seesaw II the parameter space is more constrained since the yukawa coupling Y_Δ is symmetric, which leads to 15 free parameters. For yukawas of $\mathcal{O}(1)$ and $m_\nu \sim \sqrt{\Delta m^2_{\text{atm}}} \sim 0.05$ eV one gets

$$\begin{aligned} M_R &\simeq 10^{15} \text{ GeV} \\ \frac{M_\Delta}{\lambda} &\simeq 10^{15} \text{ GeV} \\ M_\Sigma &\simeq 10^{15} \text{ GeV} \end{aligned} \tag{2.40}$$

In all seesaw types the seesaw scale is close to the GUT scale of order $m_{\text{GUT}} \sim 10^{16}$ GeV. Therefore Majorana neutrinos can be understood as a hint for high scales where gauge couplings may unify and all SM gauge multiplets are arranged in multiplets of a single gauge group.

2.2.3. Grand Unified Theories

Apart from being motivated by new high scales such as a seesaw scale GUTs are conceptionally appealing since they drastically simplify the gauge structure at high energies and relate Yukawa couplings of the quark and lepton sector [85]. This provides high predictivity for SM masses and couplings at the electroweak scale since the number of free parameters is drastically reduced. This also leads to strong constraints on GUT models as we will discuss in the next part.

The idea of GUTs is to extend the gauge symmetry such that the SM gauge group is a subgroup of this larger symmetry. It is clear that this larger symmetry has to be broken at some scale since we already know that SM particles do not all have the same interactions.

In all GUTs leptons and quarks couple at tree level through the additional gauge bosons which carry both electroweak charge and color. This triggers proton decay and puts strong limits on the masses of these new gauge bosons [86]. Since no proton decay has been observed [17] the GUT scale has to be at least of order a few $\sim 10^{15}$ GeV.

The breaking of GUTs down to the SM group is a challenging issue and gets the more complex the larger the GUT group. There are plenty of different GUT models in the literature due the large number of different breaking scenarios and GUT groups. In this section only the basic principles by

[17] The lower limit on the proton life time is 1×10^{34} years [87].

means of the simplest realization of unification in $SU(5)$ and $SO(10)$ GUTs are presented.

We will first discuss $SU(5)$, the smallest possible GUT group, which contains the SM as a subgroup. The fundamental representation of $SU(5)$ is a 5-plet $(\mathbf{5})$ and the adjoint representation is a 24-plet $(\mathbf{24})$. Quarks and leptons are arranged in a 5 and 10 plet $(\mathbf{10})$ [18]. In $SU(5)$ all SM particles fit exactly into a $\mathbf{5}$ and $\mathbf{10}$. Since leptons and quarks are grouped together in $SU(5)$ multiplets chiral anomaly cancellation [19], that seems to happen accidentally in the SM, is now predicted by symmetry.

$SU(5)$ is directly broken down to the SM group which in the minimal version is done with a 24-plet $(\mathbf{24_H})$. Breaking $SU(5)$ with a 24-plet leads to wrong predictions for the mass ratios of the SM particles ($m_s/m_d = m_\mu/m_e$) and is therefore already exluded by experiment. This can be cured by adding a 45 plet $\mathbf{45_H}$ to break $SU(5)$ [89].

The Higgs doublet is extended to a 5 plet $(\mathbf{5_H})$, where the first three entries are a scalar color triplet and the last two the SM Higgs. Since the additional triplet Higgs triggers proton decay it must be heavy with a lower limit on the mass around $\sim 10^{11}$ GeV [85]. The SM Higgs has mass of order the electroweak scale. To separate the scales of the doublet and the triplet a fine tuning of more than 10 orders of magnitude is required. This is called the doublet-triplet splitting problem in $SU(5)$ [90; 91]. The problem of separating scales is present in all GUTs since we need a light Higgs for EWSB, but the additional degrees of freedom, coming from the larger Higgs representations, can lead to dangerous operators for proton decay and therefore must have masses much larger than the electroweak scale.

In the minimal model with only one $\mathbf{5_H}$ for EWSB no unification is possible, since the additional color triplet only change the running of the strong coupling [20]. In the SM the running of the weak and hypercharge coupling is such that the two couplings unify at around 10^{14} GeV. Thus with only additional colored degrees of freedom, gauge coupling unification could happen only at this low scale, already exluded by experiment. It was shown in [92] that both unification and a long enough proton lifetime can be obtained in $SU(5)$ by introducing a Higgs 15-plet $(\mathbf{15_H})$ [21].

With only one $\mathbf{5}$ and $\mathbf{10}$ matter representation in $SU(5)$ neutrinos are massless since no right-handed neutrinos are present. By adding a singlet the small neutrino masses can be explained in terms of the seesaw mechanism. We will come back to neutrino GUT models in $SU(5)$ in chapter 3.

In bigger GUT groups extra matter is predicted. The extra matter can be heavy due to a breaking of the GUT group down to the SM group at a high scale, not reachable for current experiments. In

[18] All higher representations like $\mathbf{10}$ and $\mathbf{24}$, respectively can be obtained by group multiplications of the fundamental representation (e.g. $\mathbf{5} \otimes \mathbf{5} = \mathbf{10} + \mathbf{15}$ and $\mathbf{5} \otimes \bar{\mathbf{5}} = \mathbf{24} + \mathbf{1}$) [88].

[19] In any quantum field theory loop corrections to cubic gauge boson interactions can lead to non-renormalizable operators, if not all loop contributions cancel against each other.

[20] Note, that all additional degrees of freedom for the breaking of the GUT group and the new bosons from the extended gauge sector are integrated out at the GUT scale and therefore do not contribute to the running of the gauge couplings.

[21] After breaking $SU(5)$ down to the SM group the 15-plet decomposes into a color sextet, triplet and singlet, respectively. Gauge coupling unification depends crucially on the chosen masses of those multiplets [92]. In particular, with a degenerate spectrum no gauge coupling unification is possible.

$SO(10)$ one additional particle is predicted, the right handed neutrino.

The fundamental representation of $SO(10)$ is a 16 plet $(\mathbf{16})$ and the adjoint representation a 45-plet $(\mathbf{45})$ [22]. Under $SU(5)$ the $\mathbf{16}$ is decomposed as $\mathbf{16} = \mathbf{10} + \bar{\mathbf{5}} + \mathbf{1}$. Therefore all SM matter fields fit into one 16 plus a singlet, which is the right-handed neutrino.

In fig. 2.4 all possible breaking chains for Higgs representations up to $\mathbf{210}$ are shown [93]. We can divide the breaking of $SO(10)$ down to the SM group into two sectors, where we distinguish between breaking scenarios including either $SU(5)$ or the left right symmetric group in one of the intermediate breaking steps [23]. If $SO(10)$ is broken to the left right symmetric group $B + L$ is violated but $B - L$ is conserved which is now a gauge symmetry in the theory. The breaking of $SO(10)$ in several steps leads to many possibilities of breaking patterns and physics like the proton life time depends crucially on which breaking is realized.

The most economical version to break $SO(10)$ to the SM group includes a $\mathbf{45_H}$ Higgs to break the GUT symmetry and either a $\mathbf{16_H}$ or $\mathbf{126_H}$ for the subsequent breaking of $U(1)_{B-L} \times U(1)_R$ down to $U(1)_Y$. An additional $\mathbf{10_H}$ including the SM Higgs is responsible for EWSB, which is needed together with $\mathbf{16_H}$ or $\mathbf{126_H}$ to obtain realistic patterns for the fermionic masses and mixing [93].

In the case $SO(10)$ is broken first to the left right symmetric group, intermediate scales can be of order TeV predicting new physics at low scales in principle accessible for experiments [96; 97; 98; 4; 99]. In chapter 4 we concentrate on breaking patterns with $SU(2)_L \times U(1)_R \times U(1)_{B-L}$ in the intermediate scale which allows us to lower the $B - L$ breaking to around 1 TeV.

2.3. Supersymmetry

In this section a short introduction to supersymmetric theories is given. The basic principles of SUSY algebra and supersymmetric representations are discussed [32] to understand the consequences for phenomenology for SUSY models [100]. The minimal supersymmetric version of the SM, the MSSM, is introduced and a brief review of the parameter space and mass spectra of the constrained MSSM (CMSSM) is given. At the end the of this section recent limits from LHC for the CMSSM are presented.

2.3.1. Superfield formalism

The SUSY algebra is an extension of the Lorentz algebra including both commutator and anti-commutator relations. SUSY transformations map tensor (spinor) fields into spinor (tensor) fields. Since bosonic and fermionic degrees of freedom are now connected via space time transformations

[22] As in $SU(5)$ we get all higher representations by group multiplications of the fundamental representation [88].

[23] Note, that this classification does not consider the possibility to break $SO(10)$ directly to the SM group via a $\mathbf{144}$ irreducible Higgs representation [94]. This case is neglected here since an extended matter sector is required to get realistic fermion masses [95].

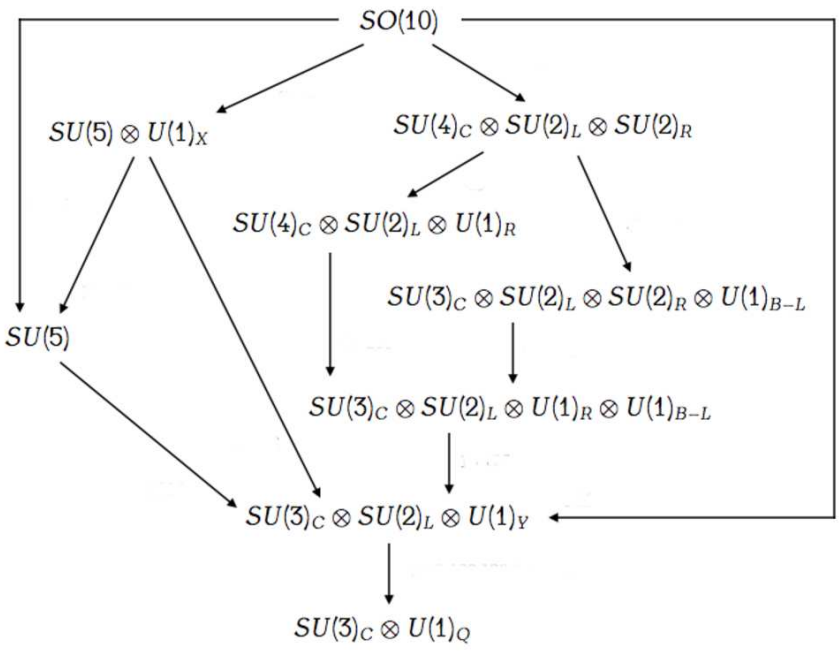

Figure 2.4: All possible breaking chains for $SO(10)$ down to the SM group 2.4.

the spin is no longer an invariant in the theory. From this it is clear that SUSY multiplets contain both bosonic and fermionic spinor representations.

An elegant method to find SUSY representations is the superfield formalism [32]. In this formalism a superspace is introduced which differs crucially from euclidean space since coordinates do not commutate anymore [24]. Superfields are analytic functions of the superspace variables θ and $\bar{\theta}$. Every superfield can be expanded in terms of θ and $\bar{\theta}$ whereas the coefficients are the so called component fields, defining the bosonic and fermionic degrees of freedom present in every multiplet. A chiral superfield Φ contains two scalar fields ϕ and F with spin 0 and a spin 1/2 field ψ

$$\Phi = \phi + i\theta\sigma^{\mu}\bar{\theta}\partial_{\mu}\phi + \frac{1}{4}\theta\theta\bar{\theta}\bar{\theta} + \sqrt{2}\theta\psi - \frac{i}{\sqrt{2}}\theta\theta\partial_{\mu}\psi\sigma^{\mu}\bar{\theta} + \theta\theta F. \tag{2.41}$$

The vector superfield is composed of a vector field A^a_{μ} and the corresponding fermionic field λ^a with spin 1/2 and the spin 0 field D^a

[24] The superspace can be defined by the anticommutating Grassman variables θ_{α} and $\bar{\theta}_{\dot{\alpha}}$ with $\{\theta_{\alpha}, \theta_{\beta}\} = 0\,, \quad \{\bar{\theta}_{\dot{\alpha}}, \bar{\theta}_{\dot{\beta}}\} = 0\,, \quad \theta^2_{\alpha} = 0\,, \qquad \bar{\theta}^2_{\dot{\alpha}} = 0.$ α and $\dot{\alpha}$ are the indices for the Weyl spinors θ and $\bar{\theta}$.

$$V^a = -\theta\sigma^\mu\bar{\theta}A^a_\mu + i\theta\theta\bar{\theta}\bar{\lambda}^a - i\bar{\theta}\bar{\theta}\theta\lambda^a + \frac{1}{2}\theta\theta\bar{\theta}\bar{\theta}D^a, \tag{2.42}$$

with a the index for the adjoint representation of the gauge group [25]. The gauge invariant superpotential of non-singlet fields is defined as

$$W(\Phi_k) = \int d\theta^2 \left(\frac{1}{2}\mu_{ij}\Phi_i\Phi_j + \frac{1}{3}y_{ijk}\Phi_i\Phi_j\Phi_k\,.\right) \tag{2.43}$$

whereas the gauge invariant kinetic term for the chiral superfields is

$$\mathcal{L}_{\text{kin,gauge}} = \int d\theta^2 d\bar{\theta}^2 \Phi^\dagger e^{2gT^aV^a}\Phi. \tag{2.44}$$

Assuming Wess-Zumino gauge we get for the exponential [26]

$$e^{2gT^aV^a} = 1 + 2V + 2g^2(T^aV^a)^2. \tag{2.45}$$

For vector fields the kinetic terms reads

$$\mathcal{L}_{\text{kin,gauge}} = \int d\theta^2 \left(\text{Tr}[W_\alpha W^\alpha] + \text{h.c.}\right) = \int d\theta^2 \left(\frac{1}{2}W^a_\alpha W^{\alpha a} + \text{h.c.}\right) \tag{2.46}$$

with $W_\alpha = \bar{D}^2 e^{-V} D_\alpha e^V$ and $\bar{D}^2 = \bar{D}_{\dot{\alpha}}\bar{D}^{\dot{\alpha}}$ [27]. To get the SUSY lagrangian for the component fields we have to integrate over the superspace. After the integration we get for the chiral part

$$\mathcal{L}_{\text{kin,chiral}} = (D_\mu\phi_i)^\dagger(D^\mu\phi_i) + i\bar{\psi}_i\bar{\sigma}^\mu D_\mu\psi_i + i\sqrt{2}g\left(\phi_i^\dagger T^a\lambda^a\psi_i - \phi_i\bar{\psi}_i T^a\bar{\lambda}^a\right) \tag{2.48}$$

with kinetic terms for the scalars ϕ_i and the fermions ψ_i but not for F_i. Since the fields F_i have no dynamics the equations of motion for F_i are only algebraic equations and defined as

[25] Note, that in general more terms in the expansion of the vector superfield are present. Since not all degrees of freedom are physical we can simplify the expression using a convenient gauge fixing. In 2.42 Wess-Zumino gauge is assumed [32].

[26] Note, that the expansion stops at second order due to the properties of the Grassman variables θ and $\bar{\theta}$.

[27] D_α and $D_{\dot{\alpha}}$ are the covariant derivatives in the superspace and defined as

$$D_\alpha = \frac{\partial}{\partial\theta^\alpha} + i\sigma^\mu_{\alpha\dot{\alpha}}\bar{\theta}^{\dot{\alpha}}\partial_\mu\,, \qquad \bar{D}_{\dot{\alpha}} = -\frac{\partial}{\partial\bar{\theta}^{\dot{\alpha}}} - i\theta^\alpha\sigma^\mu_{\alpha\dot{\alpha}}\partial_\mu \tag{2.47}$$

.

$$F_i^\dagger = -\left.\frac{\partial W(\Phi_k)}{\partial \Phi_i}\right|_{\Phi_i=\phi_i} \tag{2.49}$$

Therefore the fields F_i are only auxiliary fields and not physical degrees of freedom and can be substituted in the lagrangian by eq. 2.49. The gauge kinetic part reads after the integration over the superspace as

$$\mathcal{L}_{\text{kin,gauge}} = -\frac{1}{4}F_{\mu\nu}F^{\mu\nu} - i\lambda^a \not{D}\bar{\lambda}^a + \frac{1}{2}D^a D^a. \tag{2.50}$$

where the fields D^a, as in the case of the fields F_i, do not have dynamics and can be substituted by

$$D^a = -\sum_i g\, \phi_i^\dagger T^a \phi_i. \tag{2.51}$$

Now we can write down the complete SUSY lagrangian

$$\begin{aligned}\mathcal{L}_{\text{SUSY}} = \; & -\frac{1}{4}V^a_{\mu\nu}V^{a\mu\nu} - i\lambda^a\sigma^\mu D_\mu\bar{\lambda}^a + (D_\mu\phi_i)^\dagger(D^\mu\phi_i) \\ & + i\bar{\psi}_i\bar{\sigma}^\mu D_\mu\psi_i + i\sqrt{2}g\,(\phi_i^\dagger T^a\lambda^a\psi_i - \phi_i\bar{\psi}_i T^a\bar{\lambda}^a) \\ & - \left(\frac{1}{2}\left.\frac{\partial^2 W(\Phi_k)}{\partial\Phi_i\partial\Phi_j}\right|_{\Phi_i=\phi_i}\psi_i\psi_j + \text{h.c.}\right) - V(\phi_k)\end{aligned} \tag{2.52}$$

where the last two terms come from the superpotential defined in eq. 2.43 after the integration over the superspace. The first two terms in the 3rd line are yukawa couplings of fermionic and bosonic, respectively, component fields which come from the chiral superfields defined in the theory. $V(\phi_k)$ is the full scalar potential containing the F and D terms defined in eq. 2.49 and 2.51 and can be be written as

$$V(\phi_k) = \sum_i F_i^\dagger F_i + \sum_a \frac{1}{2}(D^a)^2 = \sum_i \left|\frac{\partial W(\phi_k)}{\partial\phi_i}\right|^2 + \frac{g^2}{2}\sum_a\left(\sum_i \phi_i^\dagger T^a\phi_i\right)^2 \tag{2.53}$$

Since $V(\phi_k)$ is completely defined by the superpotential and gauge interactions the scalar potential in supersymmetric theories is always positive definite.

We know that SUSY can not be exact since we have not observed any supersymmetric particles. SUSY can be broken spontaneously via F terms but this leads to phenomenologically unacceptable

predictions if the SM particles couple at tree level to the Higgs sector breaking SUSY. A way out is to assume another sector with superfields, that are not charged under the SM group. In this hidden sector SUSY is broken spontaneously and the breaking is communicated by so called messenger fields to the visible sector with the SM particle content. The messenger sector can be built up by gravitational or gauge interactions. The operators which come from the spontaneous SUSY breaking then appear as explicit SUSY breaking terms in the lagrangian of the visible sector. If SUSY is exact, quantum corrections of scalars do not have quadratic divergences. Operators that break SUSY explicitly and do not reintroduce quadratic divergences in the theory are called soft SUSY breaking terms and can be classified as follows [28]

1. Mass terms for the gauginos which are the fermionic part of the vector superfields
2. Mass terms for the scalar particles, $m^2_{\phi_{ij}}\ \phi^\star_i\phi_j$ with $\phi_{i,j}$ the scalar component of the chiral superfield
3. Trilinear scalar interactions, $A_{ijk}\phi_i\phi_j\phi_k$ which correspond to cubic terms in the superpotential.
4. Bilinear scalar interactions, $B_{ij}\phi_i\phi_j$ which correspond to bilinear terms in the superpotential.

Note, that in general all soft breaking parameters are free parameters in the theory.

2.3.2. MSSM

In the minimal supersymmetric version of the SM leptons and quarks are promoted to chiral superfields and therefore get a bosonic superpartner, the so called sfermions. The gauge bosons of the SM group are extended to vector superfields and acquire a fermionic superpartner, the gauginos. Since in supersymmetric theories $\Phi^\dagger\Phi$ do not give contributions to the scalar potential but $\Phi_i\Phi_j$ more than one Higgs is needed to write down a gauge invariant quadratic term required for EWSB [32]. Note, that also for the Yukawa couplings in the up and down quark sector two Higgs superfields must be defined since $\Phi\Phi'\Phi''$ and $\Phi^\dagger\Phi'\Phi'''$ can not be both supersymmetric for only one chiral superfield Φ [32]. In the MSSM two Higgs are introduced, $\hat{H}_u$ and $\hat{H}_d$ which decompose under $SU(2)_L$ as

$$\hat{H}_u = \begin{pmatrix} \hat{H}^+_u \\ \\ \hat{H}^0_u \end{pmatrix}, \qquad H_d = \begin{pmatrix} \hat{H}^0_d \\ \\ \hat{H}^-_d \end{pmatrix}, \tag{2.54}$$

The complete set of superfields of the MSSM is summarized in tab. 2.8.

[28] Breaking terms coming from a gravitational or gauge messenger sector fulfill this condition and break SUSY "softly" in the visible sector. Realizations of these breaking scenarios are "minimal supergravity" (mSUGRA) [101; 102] and gauge mediated SUSY breaking (GMSB) [103].

	Superfield	$SU(3)_c \times SU(2)_L \times U(1)_Y$	Generations
Matter	$\hat{Q}$	$(\mathbf{3}, \mathbf{2}, +\frac{1}{6})$	3
	$\hat{d}^c$	$(\overline{\mathbf{3}}, \mathbf{1}, +\frac{1}{3})$	3
	$\hat{u}^c$	$(\overline{\mathbf{3}}, \mathbf{1}, -\frac{2}{3})$	3
	$\hat{L}$	$(\mathbf{1}, \mathbf{2}, -\frac{1}{2})$	3
	$\hat{e}^c$	$(\mathbf{1}, \mathbf{1}, +1)$	3
Higgs	$\hat{H}_u$	$(\mathbf{1}, \mathbf{2}, +\frac{1}{2})$	1
	$\hat{H}_d$	$(\mathbf{1}, \mathbf{2}, -\frac{1}{2})$	1

Table 2.8: The Matter and Higgs sector field content of the MSSM.

Considering only gauge invariant terms and the superfields defined in tab. 2.8 the general Superpotential reads

$$\begin{aligned} W =& \lambda_u^{ij} \hat{Q}_i \hat{u}_j^c H_u + \lambda_d^{ij} \hat{Q}_i \hat{d}_j^c H_d + \lambda_e^{ij} \hat{L}_i \hat{e}_j^c H_d + \mu H_u H_d \\ &+ \lambda''_{ijk} \hat{u}_i^c \hat{d}_j^c \hat{d}_k^c + \lambda'_{ijk} \hat{Q}_i \hat{d}_j^c \hat{L}_k + \lambda_{ijk} \hat{L}_i \hat{e}_j^c \hat{L}_k + \mu'_i \hat{L}_i H_u. \end{aligned} \tag{2.55}$$

The terms in the second line of eq. 2.55 trigger proton decay if the B-violating coupling λ'' and one of the L-violating couplings λ', λ and μ' are non-zero. [104]. Thus, products of the couplings λ and λ' with λ'' must be either very small or λ'' equal to zero. From neutrino physics and lepton flavour violating processes also limits on λ, λ' and μ' can be derived. The couplings are usually constrained to be of order $10^{-1} - 10^{-4}$ [105; 106; 107; 108; 109] or forbidden by some additional symmetry. A symmetry which precludes dangerous operators for proton decay but still allow the yukawa couplings between the Higgs and matter sector as well as the μ term for the two Higgs is R-Parity (R_p). R-Parity is a discrete symmetry and defined as

$$R_p = (-1)^{2s+3B+L} \tag{2.56}$$

with s, the spin of the particle. R-Parity does not only protect the theory from proton decay but has also important consequences for phenomenology. First, the lightest supersymmetric particle (LSP)

is stable and might be a candidate for cold dark matter and second, super particles can be only produced (annihilated) pairwise.

As discussed in the last subsection, SUSY has to be broken softly in the visible (MSSM) sector. The soft breaking terms of the MSSM $\mathcal{L}_{\text{MSSM,soft}}$ read

$$\begin{aligned}\mathcal{L}_{\text{MSSM,soft}} = &(m_Q^2)^{ij}\tilde{Q}_i^*\tilde{Q}_j + (m_U^2)^{ij}\tilde{u^c}_i^*\tilde{u^c}_j + (m_D^2)^{ij}\tilde{d^c}_i^*\tilde{d^c}_j \\ &(m_L^2)^{ij}\tilde{L}_i^*\tilde{L}_j + (m_E^2)^{ij}\tilde{e^c}_i^*\tilde{e^c}_j + m_{H_u}^2|H_u|^2 + m_{H_d}^2|H_d|^2, \\ &A_u^{ij}\tilde{Q}_i\tilde{u^c}_j H_u + A_d^{ij}\tilde{Q}_i\tilde{d^c}_j H_d + A_l^{ij}\tilde{L}_i\tilde{e^c}_j H_d + B_\mu H_u H_d + \text{h.c.}\end{aligned} \tag{2.57}$$

where all soft masses and couplings are free parameters in the theory. Therefore the explicit breaking of SUSY introduces plenty of new parameters [29] which are neither fixed by theory nor by experiment [30]. The only sector that is more constrained than in the SM is the Higgs sector. To understand where these constraints come from we will focus in the last part of this subsection on the discussion of the Higgs potential. After integrating over the superspace and taking into account the soft terms m_{H_u}, m_{H_d} and B_μ the neutral component of the Higgses have the following potential

$$\begin{aligned}V_{\text{MSSM,Higgs}} = &\frac{g'^2}{8}\left(H_u^0 H_u^0 + H_d^0 H_d^0\right)^2 + \frac{g^2}{8}\left(H_u^0 H_u^0 + H_d^0 H_d^0\right)^2 \\ &+ \mu^2(H_u^0 H_u^0 + H_d^0 H_d^0) + m_{H_u}^2 H_u^0 H_u^0 + m_{H_d}^2 H_d^0 H_d^0 - (B_\mu H_u H_d + \text{h.c.})\end{aligned} \tag{2.58}$$

Note, that the quartic couplings are no longer free parameters but the gauge couplings g and g'. In supersymmetric theories quartic couplings, also called D-terms, are predicted by the gauge interactions [32]. After EWSB the neutral components of the Higgs doublets H_u and H_d acquire a vev

$$\langle H_u\rangle = \begin{pmatrix} 0 \\ \\ v_u \end{pmatrix}, \qquad \langle H_d\rangle = \begin{pmatrix} v_d \\ \\ 0 \end{pmatrix}. \tag{2.59}$$

Minimizing the potential leads to constraints on the parameter space. For EWSB we need

[29] After counting the physical degrees of freedom one gets more than 100 free parameters in the MSSM [110].

[30] Since no supersymmetric particles have been observed in experiment only lower limits on the soft parameters can be given.

$$\det \begin{pmatrix} \mu^2 + m_{H_u}^2 & -B\mu \\ -B\mu & \mu^2 + m_{H_d}^2 \end{pmatrix} < 0. \tag{2.60}$$

In addition

$$\mu^2 + m_{H_u}^2 + \mu^2 + m_{H_d}^2 > 2B_\mu. \tag{2.61}$$

must be satisfied to discard solutions with $v_u = v_d$. If $v_u = v_d$ the quartic term in the potential vanishes, in which case the potential may be unbounded from below. For the correct Z mass v_u and v_d are defined as

$$v_u = \frac{v}{\sqrt{2}} \sin\beta, \qquad v_d = \frac{v}{\sqrt{2}} \cos\beta, \tag{2.62}$$

with $v = \sqrt{v_u^2 + v_d^2} \sim 250\ \mathrm{GeV}$ the SM vev. Therefore we introduce $\tan\beta = v_u/v_d$ and use from now on v and $\tan\beta$ to parametrize the MSSM Higgs vevs.

Since in the MSSM we have two Higgs doublets, each containing four real scalar fields, the number of degrees of freedom is eight before the symmetry breaking. Three of them are "eaten" by the heavy gauge bosons Z, W^+ and W^- and we are left with five physical scalars. There are two CP-even scalars h^0, H^0, one CP-odd scalar A^0, and two charged scalars H^+ and H^-. The tree level masses of the CP-odd and charged scalars can be written as

$$m_A^2 = 2\mu^2 + m_{H_u}^2 + m_{H_d}^2, \qquad m_{H^\pm}^2 = m_W^2 + m_A^2 \tag{2.63}$$

and for the CP-even scalars one gets

$$m_{h^0}^2, m_{H^0}^2 = \frac{1}{2}\left(m_A^2 + m_Z^2 \mp \sqrt{(m_A^2 + m_Z^2)^2 - 4 m_Z^2 m_A^2 \cos^2 2\beta} \right). \tag{2.64}$$

The most important consequence of eq. (2.64) is that the lighter CP-even Higgs mass $m_{h^0}^2$ gets its maximal value for $\cos^2 2\beta = 1$. In this limit $m_{h^0}^2 = (m_A^2 + m_Z^2 - |m_A^2 - m_Z^2|)/2$ and therefore we obtain for $m_A < m_Z$, $m_{h^0}^2 = m_A^2 < m_Z^2$, whereas for $m_A > m_Z$, $m_{h^0}^2 = m_Z^2$ leading to an important prediction in the MSSM

$$m_{h^0} \leq m_Z. \tag{2.65}$$

That the mass of the Higgs boson mass depends on the gauge boson masses is a consequence of the quartic couplings in eq. (2.55), which are all fixed by the gauge couplings since they stem from D-terms of the scalar potential. However, this strong constraint on m_{h^0} only holds at tree level. Eq. 2.65 is modified at the one loop level [111]:

$$\Delta(m_{h^0}^2) \cong \frac{N_c}{4\pi^2} Y_t^4 v^2 \sin^4\beta \log\left(\frac{m_{\tilde{t}_1} m_{\tilde{t}_2}}{m_t^2}\right). \tag{2.66}$$

where $m_{\tilde{t}_1}$ and $m_{\tilde{t}_2}$ are the two stop masses and N_c a color factor. With a scalar top mass around $\sim$3 TeV, the lightest Higgs mass can be pushed up to about $\sim$130 GeV if 2-loop effects are included [112; 113].

Before discussing the constrained version of the MSSM let us consider the running of the gauge couplings. Additional degrees of freedom change the running in the region where the new particles can be produced on shell in the loop [31]. For simplification we assume all sparticles at a SUSY scale m_{SUSY}. At energies below this scale only SM particles contribute to the running whereas above this scale the full MSSM spectrum is considered in the loop calculation. The running of the gauge couplings at one loop can be written as

$$\begin{aligned}
\alpha_1(m_Z) =& \frac{5\alpha_{em}(m_Z)}{3\cos^2\theta_W}, \qquad \alpha_2(m_Z) = \frac{\alpha_{em}(m_Z)}{\sin^2\theta_W}, \\
\alpha_i(m_{SUSY}) =& \frac{\alpha_i(m_Z)}{1 - \frac{\alpha_i(m_Z)}{4\pi} b_i^{SM} \log\frac{m_{\text{SUSY}}^2}{m_Z^2}}, \\
\alpha_i(m_{GUT}) =& \frac{\alpha_i(m_{SUSY})}{1 - \frac{\alpha_i(m_{SUSY})}{4\pi} b_i^{MSSM} \log\frac{m_{GUT}^2}{m_{SUSY}^2}}.
\end{aligned} \tag{2.67}$$

Here, $b_i^{SM} = (b_1, b_2, b_3)^{SM} = (\frac{41}{10}, -\frac{19}{6}, -7)$ for the SM and $b_i^{MSSM} = (b_1, b_2, b_3)^{MSSM} = (\frac{33}{5}, 1, -3)$ for the MSSM. b^{SM} and b^{MSSM} account for the degrees of freedom contributing to the loop. It turns out that in the MSSM superpartners change the running between the SUSY scale and the GUT scale in such a way that gauge couplings unify at $\sim 10^{16}$ GeV if $m_{SUSY} \lesssim 100$ TeV [114].

[31] For energies, at which new heavy particles can not be produced on shell, we can integrate out these heavy degrees of freedom and are left with an effective operator suppressed by the mass of the new particle. The new dimension 5 operator does not contribute to the running of the couplings and can be neglected.

2.3.3. The constrained MSSM

In the MSSM the lightest Higgs mass is predicted to be below ~ 130 GeV and gauge couplings unify. Nevertheless, plenty of new parameters are introduced in the explicit soft SUSY breaking terms. As already mentioned soft breaking terms can be motivated by a hidden sector where SUSY is broken spontaneously and the breaking is communicated to the visible sector by messenger fields. One of the possible scenarios is Supergravity where gravitational interactions build up the messenger sector. In such models the soft breaking sector of the MSSM (eq. 2.57) simplifies at m_{GUT} as follows:

- all scalar masses are equal to a common scalar mass m_0
- all gaugino masses are equal to a common gaugino mass $M_{1/2}$
- all trilinear couplings are equal to a common trilinear coupling A_0.

The CMSSM [115] simplifies the parameter space drastically. We are left with four free SUSY parameters m_0, $M_{1/2}$, A_0 and $\tan\beta$ [32]. In the rest of this subsection some generic aspects of CMSSM phenomenology and particle spectrum are discussed.

At the GUT scale all gaugino masses are equal to $M_{1/2}$ but have different masses at the SUSY scale. Gaugino masses evolve like gauge couplings

$$M_i(m_{\mathsf{SUSY}}) = \frac{\alpha_i(m_{\mathsf{SUSY}})}{\alpha(M_{\mathsf{GUT}})} M_{1/2}. \tag{2.68}$$

Thus in the CMSSM the gauginos from $SU(3)_c$ (Gluinos) are heavier than the Winos, the gauginos of $SU(2)_L$, and the bino, the gaugino of $U(1)_Y$, is the lightest gaugino. The soft mass parameter of the first two generations can be parametrized at the SUSY scale as [116] [33]

$$m_{\tilde{f}}^2 = m_0^2 + A_{\tilde{f}} M_{1/2}^2 \tag{2.69}$$

with

[32] Note, that solving the tadpole equations fixes μ only up to a sign. Therefore the sign of μ has also to be defined since it is neither predicted by theory nor experiment.

[33] In eq. 2.69 no yukawa terms are considered since for the first two generations contributions from yukawa interactions are negligible.

$$A_{\tilde{f}} = \sum_{i=1}^{3} c_i^{\tilde{f}} f_i, \tag{2.70}$$
$$f_i = \frac{1}{b_i^{\mathsf{MSSM}}} \left(1 - \left[1 + \frac{\alpha(M_{\mathsf{GUT}})}{4\pi} b_i \log \frac{M_{\mathsf{GUT}}^2}{m_Z^2} \right]^{-2} \right).$$

$\tilde{f}$	$\tilde{E}$	$\tilde{L}$	$\tilde{D}$	$\tilde{U}$	$\tilde{Q}$
$c_1^{\tilde{f}}$	$\frac{6}{5}$	$\frac{3}{10}$	$\frac{2}{15}$	$\frac{8}{15}$	$\frac{1}{30}$
$c_2^{\tilde{f}}$	0	$\frac{3}{2}$	0	0	$\frac{3}{2}$
$c_3^{\tilde{f}}$	0	0	$\frac{8}{3}$	$\frac{8}{3}$	$\frac{8}{3}$

Table 2.9: Coefficients $c_i^{\tilde{f}}$ for eq. (2.71) [116].

With the coefficients $c_i^{\tilde{f}}$ given in table 2.9 we get for $A_{\tilde{f}}$

$$A_{\tilde{E}} \cong 0.14\ , \quad A_{\tilde{L}} \cong 0.46\ , \quad A_{\tilde{U}} \cong 3.83\ , \quad A_{\tilde{D}} \cong 3.78 \ \text{ and } \ A_{\tilde{Q}} \cong 4.19 \tag{2.71}$$

For the calculation the GUT scale has to be fixed. This can be done by using the condition $\alpha_1(M_{\mathsf{GUT}}) = \alpha_2(M_{\mathsf{GUT}})$, which gives for $\alpha_{\mathsf{em}} = 1/127.9$, $\sin^2\theta_W = 0.2312$ and $M_Z = 91.2$ GeV [117] $M_{\mathsf{GUT}} \simeq 10^{16}$ GeV. The right handed soft sfermion masses are smaller than the left handed ones. The difference of the right and left handed soft masses is much larger in the lepton sector than in the quark sector, where we have an almost degenerate spectrum. In the limit of large m_0 and small $M_{1/2}$ we get for all soft masses $m_{\tilde{f}} \sim m_0$. [34] For small m_0 and large $M_{1/2}$ we have to check that at least one gaugino is lighter than the lightest sfermion. If this condition is not fulfilled the LSP, which is stable under the assumption of R-Parity, carries electromagnetic charge [35]. Dark matter candidates charged under $U(1)_{\mathsf{em}}$ are already excluded by experiment.

For third generation soft masses yukawa interaction can not be neglected and therefore a simple parametrization as in eq. 2.69 is not possible. The contributions of the yukawa term push one of the two third generations soft masses down to smaller values. Therefore a third generation sfermion is usually the lightest sfermion in the spectrum.

[34] Note, that in this limit no EWSB is possible [118].

[35] If the left Sneutrino is assumed to be the lightest supersymmetric particle the LSP does not carry electromagnetic charge. Left Sneutrinos as dark matter candidates are already excluded by experiment [119].

2.3.4. Supersymmetry and the LHC

At the LHC we haven't seen any signal for SUSY particles. With the data taken we can only update exclusion limits on SUSY parameter space. Recent data already constrains SUSY masses to be larger than ~ 1 TeV but exact numbers depend crucially on the considered SUSY model. The present limits on the CMSSM parameter space at 95% confidence level are shown in tab. 2.10 and 2.11 [36]. In the analysis a simplified model is used that contains only a gluino octet and a neutralino within the kinematical reach. Furthermore the gluino is assumed to decay with unit probability as

$$\tilde{g} \to q + \bar{q} + \chi_1^0. \tag{2.72}$$

A more detailed discussion can be found in [122]. In tab. 2.10 the ATLAS limits on $M_{1/2}$ as a function of m_0 are presented. Already with the first analysis using 35 pb^{-1} of data limits from LEP could be significantly improved (see first row in tab. 2.10). For $M_{1/2} \lesssim 250$ GeV $m_0 \gtrsim 600$ GeV were already exluded at 95% confidence level, which corresponds to a squark mass of around 800 GeV if all squarks are assumed to be degenerate [37]. At the end of 2012 ATLAS published an update of the 2011 analysis for an integrated luminosity of $\mathcal{L} \lesssim 4.7$ fb^{-1} (see second row in tab. 2.10). $M_{1/2} < 300$ GeV were excluded for all m_0 and for $M_{1/2} > 500$ the lower limit on the squark mass was pushed to 1.4 TeV. In the last published ATLAS combined analysis for $\mathcal{L} \lesssim 20$ fb^{-1} lower limits on the CMSSM parameter space were slightly improved. Squark masses below 1.6 TeV were now excluded at 95% confidence level (see third row in tab. 2.10).

In tab. 2.11 CMS and ATLAS, respectively, exclusion limits for the lightest neutralino mass as a function of the gluino mass are shown. In both plots the regions above the grey dashed lines are kinematically forbidden. Both experiments show similar results and gluino masses of roughly 1.3 TeV are excluded for neutralino masses less than 500 GeV.

[36] All plots are taken from ref. [120] and [121].

[37] In the rest of this subsection limits on squark masses are referred to a degenerate squark spectrum. Deviations of this assumption can weaken the lower limit on squark masses significantly.

	ATLAS
2011 Data ($L \leq 35 pb^{-1}$)	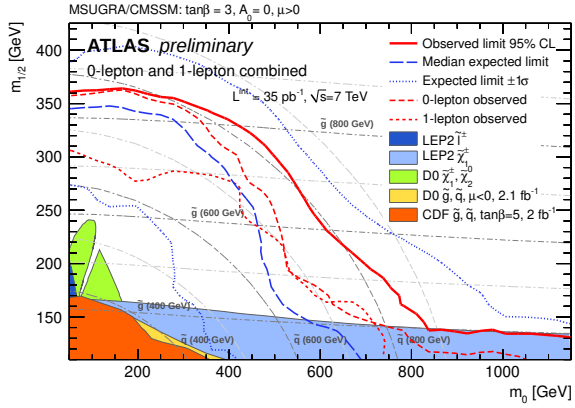
2011 + 2012 Data ($L \leq 4.7 fb^{-1}$)	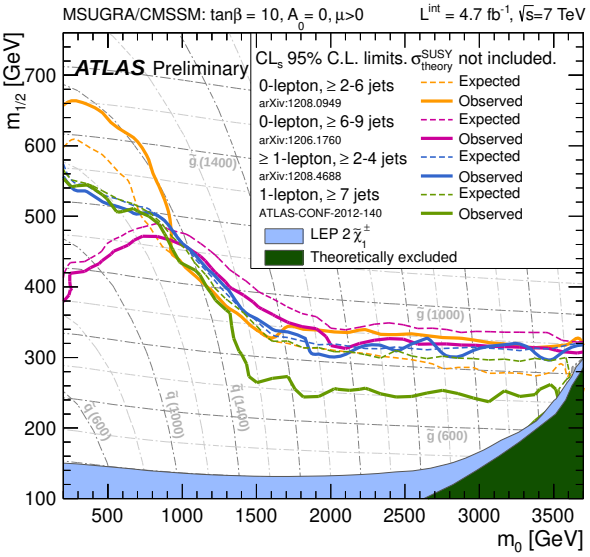
2011 + 2012 Data ($L \leq 20 fb^{-1}$)	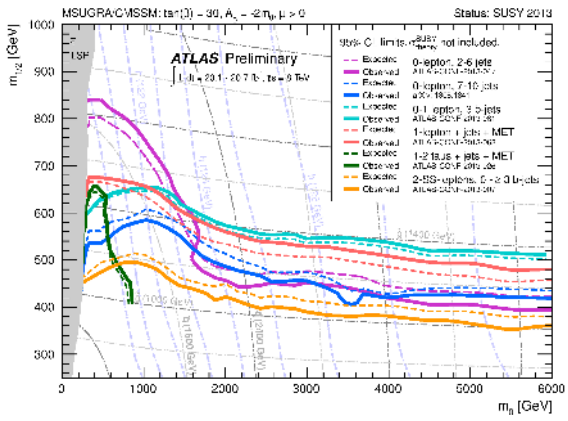

Table 2.10: Present SUSY limits on the CMSSM parameter space from ATLAS working group. All plots are taken from [120] and [121].

	CMS	ATLAS
2011 + 2012 Data ($L \leq 20 fb^{-1}$)	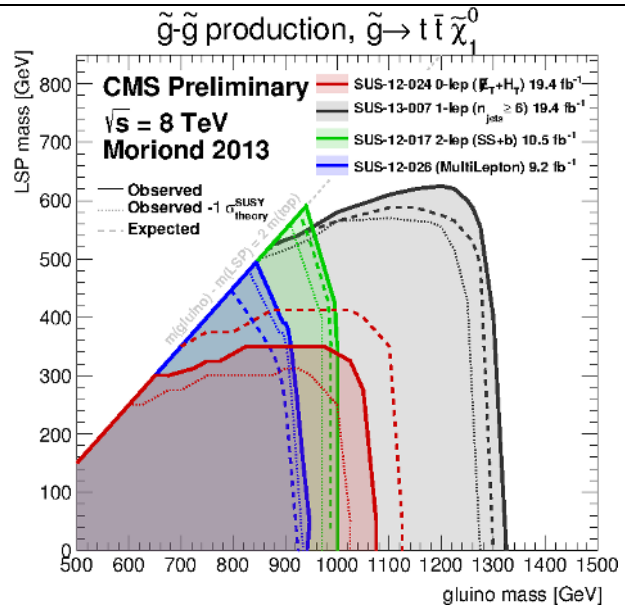	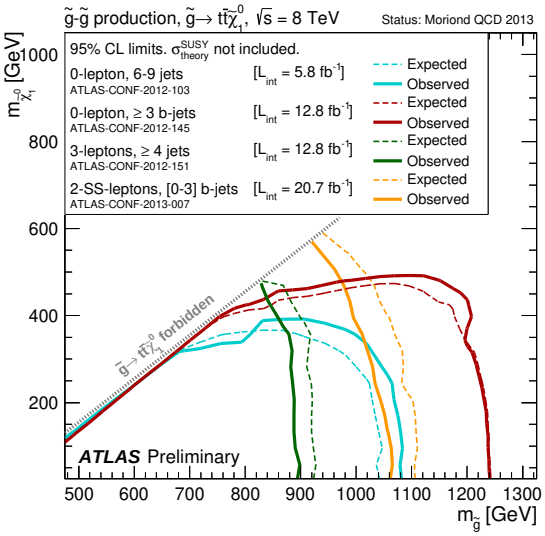

Table 2.11: Present SUSY limits on the CMSSM parameter space from CMS and ATLAS working group. All plots are taken from [120] and [121].

3

Supersymmetric seesaws

Due to the large mass scales involved in the seesaw mechanism, no direct experimental test of "the seesaw" will ever be possible. Extending the standard model (SM) only by a seesaw mechanism does not even allow for indirect tests, since all possible new observables are suppressed by (some power of) the small neutrino masses. [1]

The situation looks less bleak in the supersymmetric version of the seesaw. This is essentially so, because soft SUSY breaking parameters are susceptible to all particles and couplings which appear in the renormalization group equation (RGE) running.

In the MSSM all soft SUSY breaking mass terms are treated as free parameters, to be fixed at the electro-weak scale. However, these soft parameters potentially contain a wealth of information about physics at the high scale and understanding the nature of SUSY breaking will become the main challenge, if signals of SUSY are found at the LHC. Highly precise mass measurements will be needed to distinguish between different SUSY breaking schemes such as CMSSM, anomaly mediated SUSY breaking (AMSB) [23; 124] or GMSB, to name just the most familiar ones.

Assuming some simplified boundary conditions at an high energy scale, the SUSY softs at the electro-weak scale contain indirect information about all particles and intermediate scales. Perhaps the best known application of this idea is the example of lepton flavour violation (LFV) in seesaw type-I with CMSSM boundary conditions. A plethora of papers on LFV, both for low-energy and for accelerator experiments, have been published (for a partial list see, for example, [125; 126; 127; 128; 129; 130; 131; 132; 133; 134; 135; 136; 137; 138; 139; 140]), most of them concentrating on seesaw type-I. Much less work on SUSY seesaw type-II and type-III has been done than for type-I. For studies of LFV in SUSY seesaw type-II, see for example [141; 116], for type-III [142; 143].

Apart from the appearance of LFV, adding a seesaw to the SM particle content also leads to changes in the absolute values of SUSY masses with respect to CMSSM expectations, at least in

[1] "Low-energy" versions of the seesaw, such as inverse seesaw [123] or linear seesaw [21; 22], might allow for larger indirect effects. In this chapter we will focus exclusively on the "classical" seesaw with a high (B-L) breaking scale.

principle.

There are only very few papers, which have studied the impact of the seesaw on SUSY particle masses. Some aspects of type-I seesaw have been studied focusing on what can be learned from precision measurements in the slepton sector [133; 134; 144; 145]. Moreover, in such a scenario a splitting between the masses of the selectrons and smuons can occur which might be measurable at the LHC [146; 147; 148]. Changes in SUSY spectra can lead to changes in the expected relic density for the cold dark matter. The impact of large values of soft terms in the sneutrino sector [149] and of large values for the trilinear A_0 parameter [150; 151] have been studied in this context.

The relative scarcity of publications on SUSY spectra and the seesaw is probably explained by the fact that type-I seesaw, the undoubtedly most popular variant, adds only singlets to the MSSM particle content. If the Yukawa couplings of these singlets are smaller than, say, the gauge couplings any effects of the right-handed neutrinos on the SUSY mass eigenvalues become negligibly small. This leaves only a rather small window for the seesaw scale, m_{SS}, say, roughly $[4 \times 10^{14}, 1.2 \times 10^{15}]$ GeV where any measurable shifts in SUSY masses can be expected at all. And it is, of course, exactly this range for m_{SS} where the largest values for LFV decays are expected. Exceptions from this general rule can be found in models where one departs from the universality assumption of the CMSSM parameters. With huge soft SUSY breaking parameters in the seesaw sector one gets larger effects [152], in particular in the Higgs sector [153].

Type-II and type-III seesaw add superfields, which are charged under the SM group. Thus, the running of the gauge couplings is affected, leading to potentially large changes in SUSY spectra at the EW scale. In [154] it was pointed out, that for type-II and type-III seesaw certain combinations of soft SUSY breaking parameters are at 1-loop order nearly constant over large parts of CMSSM parameters space, but show a logarithmic dependence on m_{SS}. [2] This was studied in more detail, including 2-loop effects in the RGEs, for type-II in [116] and for type-III in [142].

However, all of the models mentioned above break SUSY at energies inaccessible for collider experiments. Thus, theoretical extrapolations from the TeV scale to the high energy scale will be needed and any "test" of SUSY breaking schemes can at best take the form of a consistency check. Based on the results of [155; 156; 157] detailed calculations have been done, quantifying the accuracy with which such tests can be done using data from LHC and a possible ILC [158; 133; 159; 160; 161]. However, these works concentrated on models with MSSM particle content and thus did not attempt to take into account the observed non-zero neutrino masses. In this chapter we study the prospects for the LHC and for a combined LHC+ILC analysis for finding indirect hints for the presence of a high-scale seesaw mechanism in SUSY spectra. Therefore we calculate the low-energy SUSY spectra for type-I, type-II and type-III seesaw in the CMSSM and confront our theoretical results with expectations for the accuracy of SUSY mass measurements at the LHC and at a possible

[2] These so-called invariants can be useful also in more complicated models in which an inverse seesaw is embedded into an extended gauge group [98].

combined LHC+ILC analysis [156; 157]. Given the estimated errors on SUSY masses obtained in detailed simulations [156; 157] we calculate expected χ^2-distributions for the two different seesaw models, in order to give a theoretical forecast on the expected errors on the model parameters, most notably the error on the "determination" of the seesaw scale m_{SS}.

3.1. Seesaw type I

Running slepton masses with a type-I seesaw have been discussed qualitatively in [133; 134; 144; 145]. In [148] it was discussed that in CMSSM extended by a type-I seesaw, splitting in the slepton sector can be considerably larger than in the pure CMSSM. This is interesting, since very small mass splittings in the smuon/selectron sector might be measurable at the LHC, if sleptons are on-shell in the decay chain $\chi_2^0 \to l^{\pm}\tilde{l}^{\mp} \to l^{\pm}l^{\mp}\chi_1^0$ [146].

In this section, we calculate SUSY spectra with CMSSM boundary conditions and a seesaw type-I. We add three generations of right-handed neutrinos and take special care that observed neutrino masses and mixing angles are always correctly fitted [3]. We then follow the procedure of [2]. Using predicted error bars on SUSY mass measurements for a combined LHC+ILC analysis, we construct fake "experimental" observables and use a χ^2-analysis to estimate errors on the parameters of our model, most notably the seesaw scale. We identify regions in parameter space, where hints for a type-I seesaw might show up at the ILC/LHC and discuss quantitatively the accuracy which need to be achieved, before a realistic analysis searching for signs of type-I seesaw in SUSY spectra can be carried out.

The rest of this section is organized as follows. In the next subsection we define the supersymmetric seesaw type-I model, fix the notation and define the CMSSM. In subsection 3.1.2 we present our results. After a short discussion of the procedures and observables in subsection 3.1.2.1, we show a simplified analysis, which allows to identify the most important observables and discuss their relevant errors in subsection 3.1.2.2. Subsection 3.1.3 then shows our full numerical results. We then close with a short summary and discussion in subsection 3.1.4.

3.1.1. Setup

3.1.1.1. Supersymmetric seesaw type-I

In the case of seesaw type-I one postulates very heavy right-handed neutrinos with the following superpotential below the GUT scale, M_G:

$$W_I \;=\; W_{MSSM} + W_{\nu}. \tag{3.1}$$

[3] Note, that in principle the input parameters of the seesaw mecanism can be reconstructed from the neutrino and sneutrino mass matrices [162].

Here W_{MSSM} is the usual MSSM part and

$$W_\nu \;=\; \widehat{N}_i^c Y_{ij}^\nu \widehat{L}_j \cdot \widehat{H}_u + \frac{1}{2}\widehat{N}_i^c M_{R,ii} \widehat{N}_i^c \,. \tag{3.2}$$

We have written eq. (3.1) in the basis where M_R and the charged lepton Yukawas are diagonal. In the seesaw one can always choose this basis without loss of generality. For the neutrino mass matrix, upon integrating out the heavy Majorana fields, one obtains the well-known seesaw formula

$$m_\nu = -\frac{v_u^2}{2} Y^{\nu,T} M_R^{-1} Y^\nu, \tag{3.3}$$

where, compared to the non-supersymmetric version of the seesaw type-I defined in eq. 2.37, the SM Higgs vev v is replaced by v_u.

Inverting the seesaw equation, eq. (3.3), allows to express Y^ν as [163]

$$Y^\nu = \sqrt{2}\frac{i}{v_u}\sqrt{\hat{M}_R}\cdot R \cdot \sqrt{\hat{m}_\nu}\cdot U^\dagger, \tag{3.4}$$

where the $\hat{m}_\nu$ and $\hat{M}_R$ are diagonal matrices containing the corresponding eigenvalues. R is in general a complex orthogonal matrix. Note that, in the special case $R = \mathbf{1}$, Y^ν contains only "diagonal" products $\sqrt{M_i m_i}$. For U we will use the standard form defined in eq. 2.29.

Eq. (2.37) contains 9 a priori unknown parameters, eq. (3.4) contains 18. The additional 9 unknowns encode the information about the high scale parameters, the three eigenvalues of M_R and the 3 moduli and 3 phases of R.

3.1.1.2. CMSSM, type-I seesaw and RGEs

The CMSSM is defined at the GUT-scale by: a common gaugino mass $M_{1/2}$, a common scalar mass m_0 and the trilinear coupling A_0, which gets multiplied by the corresponding Yukawa couplings to obtain the trilinear couplings in the soft SUSY breaking Lagrangian. In addition, at the electroweak scale, $\tan\beta = v_u/v_d$ is fixed. Here, as usual, v_d and v_u are the vacuum expectation values (vevs) of the neutral component of H_d and H_u, respectively. Finally, the sign of the μ parameter has to be chosen.

Two-loop RGEs for general supersymmetric models have been given in [164]. [4] In our numerical calculations we use `SPheno3.1.5` [36; 166], which solves the RGEs at 2-loop, including right-handed neutrinos. It is, however, useful for a qualitative understanding, to consider first the simple solutions to the RGE for the slepton mass parameters found in the leading log approximation [126; 132], given

[4] The only case not covered in [164] is models with more than one $U(1)$ gauge group. This case has been discussed recently in [165].

by

$$\begin{aligned}(\Delta M^2_{\tilde{L}})_{ij} &= -\frac{1}{8\pi^2}(3m_0^2 + A_0^2)(Y^{\nu,\dagger}LY^{\nu})_{ij} \\ (\Delta A_l)_{ij} &= -\frac{3}{8\pi^2}A_0 Y_{l_i}(Y^{\nu,\dagger}LY^{\nu})_{ij} \\ (\Delta M^2_{\tilde{E}})_{ij} &= 0,\end{aligned} \tag{3.5}$$

where only the parts proportional to the neutrino Yukawa couplings have been written. The factor L is defined as

$$L_{kl} = \log\left(\frac{M_G}{M_k}\right)\delta_{kl}. \tag{3.6}$$

Eq. (3.5) shows that, within the type-I seesaw mechanism, the right slepton parameters do not run in the leading-log approximation. Thus, LFV is restricted to the sector of left-sleptons in practice, apart from left-right mixing effects which could show up in the scalar tau sector. Also note that for the trilinear parameters running is suppressed by charged lepton masses.

It is important that the slepton mass-squareds involve a different combination of neutrino Yukawas and right-handed neutrino masses than the left-handed neutrino masses of eq. (3.3). In fact, since $(Y^{\nu,\dagger}LY^{\nu})$ is a hermitian matrix, it obviously contains only nine free parameters [127], the same number of unknowns as on the right-hand side of eq. (3.4), given that in principle all 3 light neutrino masses, 3 mixing angles and 3 CP phases are potentially measurable.

Apart from the slepton mass matrices, Y^{ν} also enters the RGEs for $m^2_{H_u}$ at 1-loop level. However, we have found that the masses of the Higgs bosons are not very sensitive to the values of Y^{ν}, see also next subsection. We thus do not give approximate expressions for $m^2_{H_u}$. For all other soft SUSY parameters, Y^{ν} enters only at the 2-loop level. Thus, the largest effects of the SUSY type-I seesaw are expected to be found in the left slepton sector.

3.1.2. Numerical results

3.1.2.1. Preliminaries

We use `SPheno3.1.5` [36; 166] to calculate all SUSY spectra and fit the neutrino data. Unless noted otherwise the fit to neutrino data is done for strict normal hierarchy (i.e. $m_{\nu_1} = 0$), best-fit values for the atmospheric and solar mass squared splitting [68] and tri-bimaximal mixing angles [167]. To reduce the number of free parameters in our fits, we assume right-handed neutrinos to be degenerate and R to be the identity. The seesaw scale, called m_{SS} below, is equal to the degenerate right-handed neutrino masses. If any of these assumptions is dropped in the next subsections, we will comment on expected changes of our results. Especially, recently there have been some indications for a non-zero reactor angle, both from the long-baseline experiment T2K [168] as well as from the first data in Double CHOOZ [169]. We will therefore comment also on non-zero values of $\theta_{13} = \theta_R$.

SPheno solves the RGEs at 2-loop level and calculates the SUSY masses at 1-loop order, except for the Higgs mass, where the most important 2-loop corrections have been implemented too. Theoretical errors in the calculation of the SUSY spectrum are thus expected to be much smaller than experimental errors at the LHC. However, since for the ILC one expects much smaller error bars, theory errors will become important at some point. We comment on theory errors in the discussion section.

Observables and their theoretically forecasted errors are taken from the tables (5.13) and (5.14) of [156] and from [157]. For the LHC we take into account the "edge variables": $(m_{ll})^{edge}$, $(m_{lq})^{\text{edge}}_{\text{low}}$, $(m_{lq})^{\text{edge}}_{\text{high}}$, $(m_{llq})_{\text{edge}}$ and $(m_{llq})_{\text{thresh}}$ from the decay chain $\tilde{q}_L \to \chi_2^0 q$ and $\chi_2^0 \to l\tilde{l} \to ll\chi_1^0$ [170; 171; 172]. In addition, we consider $(m_{llb})_{thresh}$, $(m_{\tau^+\tau^-})$ (from decays involving the lighter stau) and the mass differences $\Delta_{\tilde{g}\tilde{b}_i} = m_{\tilde{g}} - m_{\tilde{b}_i}$, with $i = 1, 2$, $\Delta_{\tilde{q}_R\chi_1^0} = m_{\tilde{q}_R} - m_{\chi_1^0}$ and $\Delta_{\tilde{l}_L\chi_1^0} = m_{\tilde{l}_L} - m_{\chi_1^0}$. Since $m_{\tilde{u}_R} \simeq m_{\tilde{d}_R} \simeq m_{\tilde{c}_R} \simeq m_{\tilde{s}_R}$ applies for a large range of the parameter space LHC measurements will not be able to distinguish between the first two generation squarks. The combined errors for an LHC+ILC analysis, tables (5.14) of [156], are dominated by the ILC for all non-coloured sparticles, except the stau. For us it is essential that both, left and right sleptons are within reach of the ILC. Also the two lightest neutralinos and the lighter chargino measured at ILC are important. The errors in [156] were calculated for relatively light SUSY spectra, thus we extrapolate them to our study points, see below, assuming constant relative errors on mass measurements. We will comment in some detail on the importance of this assumption below. Finally, we use the splitting in the selectron/smuon sector [146] as an observable:

$$\Delta(m_{\tilde{e}\tilde{\mu}}) = \frac{m_{\tilde{e}} - m_{\tilde{\mu}}}{m_{\tilde{l}}^{mean}}. \tag{3.7}$$

Here, $m_{\tilde{l}}^{mean} = \frac{1}{2}(m_{\tilde{e}} + m_{\tilde{\mu}})$. The LHC can, in principle, measure this splitting from the edge variables for both, left and right sleptons, if the corresponding scalars are on-shell. In CMSSM type-I seesaw only the left sector has a significant splitting, we therefore suppress the index "L" for brevity. For this splitting [146] quote a "one sigma observability" of $\Delta(m_{\tilde{e}\tilde{\mu}}) \sim 2.8$ ‰ for SPS1a. [5] For comparison, the errors on the left selectron and smuon mass at the ILC for this point are quoted as $\Delta(m_{\tilde{e}}) \simeq 1$ ‰ and $\Delta(m_{\tilde{\mu}}) \simeq 2.5$ ‰, respectively [156].

The negative searches for SUSY by CMS [173] and ATLAS [174] define an excluded range in CMSSM parameter space, ruling out the lightest SPS study points, such as SPS1a' [157] or SPS3 [175]. For our numerical study we define a set of five points, all of which are chosen to lie outside the LHC excluded region, but have the lightest non-coloured SUSY particles within reach of a 1 TeV linear collider. The points are defined as follows [6]:

[5] SPS1a has only the edge in the right-slepton sector on-shell, see discussion fig. (3.3).

[6] These points are ruled out now by recent LHC data (see subsection 2.3.4, but were allowed when the paper was published.

$$\begin{aligned}
\mathrm{P}_1 &\rightarrow (m_0 = 120, M_{1/2} = 600, A_0 = 0, \tan\beta = 10) \\
\mathrm{P}_2 &\rightarrow (m_0 = 120, M_{1/2} = 600, A_0 = 300, \tan\beta = 10) \\
\mathrm{P}_3 &\rightarrow (m_0 = 120, M_{1/2} = 600, A_0 = -300, \tan\beta = 10) \\
\mathrm{P}_4 &\rightarrow (m_0 = 180, M_{1/2} = 550, A_0 = 0, \tan\beta = 10) \\
\mathrm{P}_5 &\rightarrow (m_0 = 180, M_{1/2} = 550, A_0 = 300, \tan\beta = 10)
\end{aligned} \tag{3.8}$$

All points have $sgn(\mu) > 0$, masses are in units of GeV. Points P_1-P_3 lie very close to the stau-coannihilation line. We have checked by an explicit calculation with MicrOmegas [176; 177; 178; 179] that the relic density of the neutralino agrees with the current best fit value of $\Omega_{CDM}h^2$ within the quoted error bars [180] for P_1. P_4 and P_5 have been chosen such that deviations from the pure CMSSM case are larger than in P_1-P_3, see eq.(3.5), i.e. to maximize the impact of the seesaw type-I on the spectra, see below.

3.1.2.2. Observables and seesaw scale

In this subsection we will first keep all parameters at some fixed values, varying only the seesaw scale. These calculations are certainly simple-minded, but also very fast compared to the full Monte Carlo parameter scans, discussed later. However, as will be shown in the in the next subsection, there is nearly no correlation between different input parameters. Thus, the simple calculation discussed here already gives a quite accurate description of the results of the more complicated minimization procedures of the "full" calculation. Especially, this calculation allows us to identify the most important observables and discuss their maximally acceptable errors for our analysis.

In fig. (3.1) we show

$$\sigma_i = \frac{m_i^{m_{SS}} - m_i^{CMSSM}}{m_i^{CMSSM}} \Big/ \Delta(m_i), \tag{3.9}$$

where $\Delta(m_i)$ is the expected relative experimental error for the mass of sparticle i at the ILC, as a function of m_{SS}. We remind the reader that we assume that $\Delta(m_i)$ can be extrapolated to our study points. To the left results for P_1 and to the right for P_5. m_i^{CMSSM} is the value of the mass calculated in the CMSSM limit and $m_i^{m_{SS}}$ the corresponding mass for a seesaw scale of m_{SS}. These latter values have always been calculated fitting the Yukawa matrix of the neutrinos at m_{SS}, such that the best fit values of solar and atmospheric neutrino mass differences are obtained and $m_{\nu_1} \equiv 0$ is maintained. As expected the departures from the CMSSM values then increase with increasing seesaw scale. Note that the lines stop at values of $m_{SS} \sim (2-3) \times 10^{15}$ GeV, since for larger values neutrino Yukawas, which are required to fit the neutrino data, are non-perturbative.

Significant departures with respect to the CMSSM values are found (with decreasing importance)

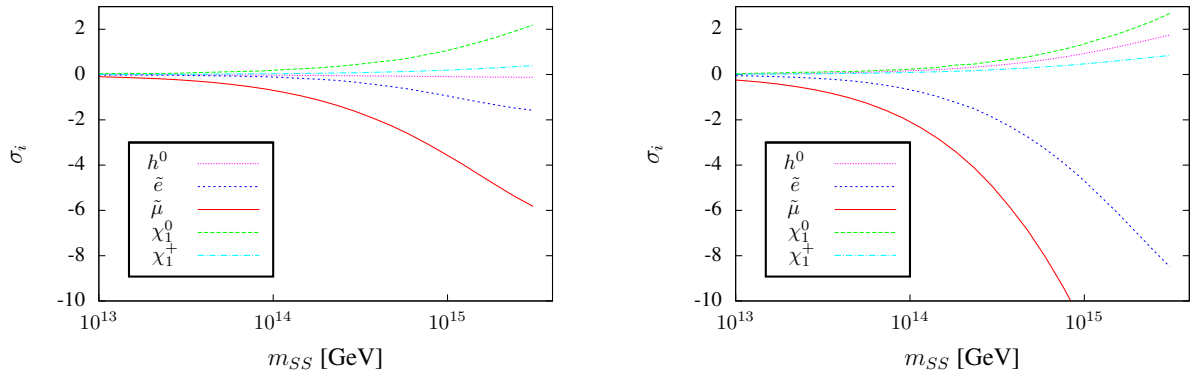

Figure 3.1: Calculated deviations of masses from their nominal CMSSM values as function of m_{SS} for the most important masses. To the left P_1, to the right P_5.

for the following observables: left smuon mass, left selectron mass, mass of χ_1^0, m_{h^0} and χ_1^+. We have checked that all other observables have much milder dependences on m_{SS}, as expected. The smuon mass is more important than the selectron mass, despite the latter having a smaller predicted error, due to our choice of degenerate right-handed neutrinos in the fits. With this assumption the running of the smuon mass has contributions from Yukawas responsible for both, atmospheric and solar scale, while the selectron has contributions from the Yukawas of the solar scale only. The change in χ_1^0 and χ_1^+ masses are small in absolute scale, but it is expected that ILC will measure these masses with very high accuracy. Also m_{h^0} shows some mild dependence on m_{SS}, but on a scale of an expected experimental error of 50 MeV [157], i.e. much smaller than our current theoretical error, see below.

As the figure shows deviations from CMSSM expectations of the order of several standard deviations are reached for left smuon and selectron for values of m_{SS} above 10^{14} GeV. Comparing the results for P_1 (left) with those for P_5 (right) it is confirmed that P_5 shows much larger deviations from CMSSM. We have checked that results for the other points P_2-P_4 fall in between the extremes of P_1 and P_5. Lines for P_2 and P_3 are nearly indistinguishable in such a plot, apart from some minor difference in the Higgs mass.

In fig. (3.2) we show the calculated χ^2 as a function of m_{SS} for 4 different CMSSM points. Here, χ^2 is calculated with respect to CMSSM expectations. To the left we show χ^2_T including all observables, to the right χ^2_T without the mass splitting in the (left) smuon-selectron sector. The figure demonstrates again that P_1 (P_5) has the smallest (largest) departures from CMSSM expectations. A non-zero value of A_0 can lead to significant departures from CMSSM expectations. Determination of A_0 from measurements involving 3rd generation sfermions and the lightest Higgs mass will therefore be important in fixing m_{SS}.

Fig. (3.2) also demonstrates that $\Delta(m_{\tilde{e}\tilde{\mu}})$ at its nominal error gives a significant contribution to the total χ^2. Thus, LHC measurements only might already give some hints for a type-I seesaw

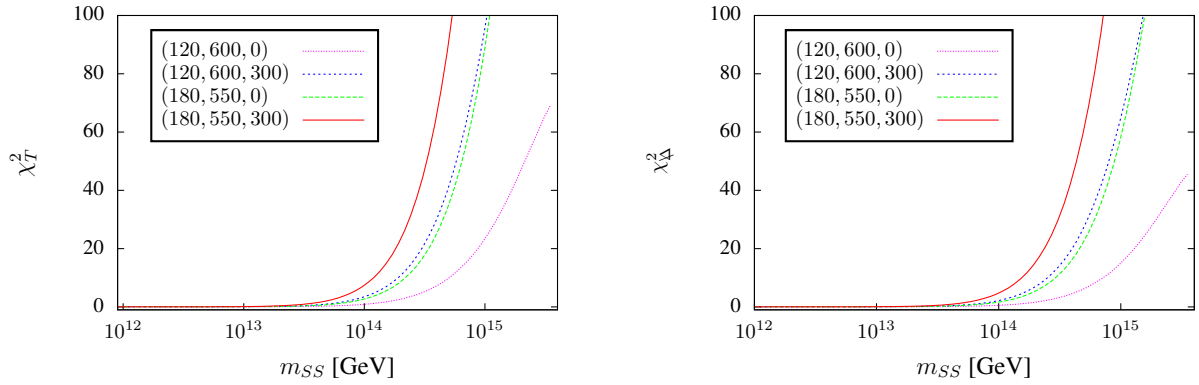

Figure 3.2: Calculated χ^2 as function of m_{SS} for 4 different CMSSM points. To the left: Total χ^2 including all observables, to the right total χ^2_Δ, i.e. χ_T without the mass splitting in the (left) smuon-selectron sector. Values quoted in the plots correspond to $(m_0, M_{1/2}, A_0)$. In all points shown we choose $\tan\beta = 10$ and $\mu > 0$.

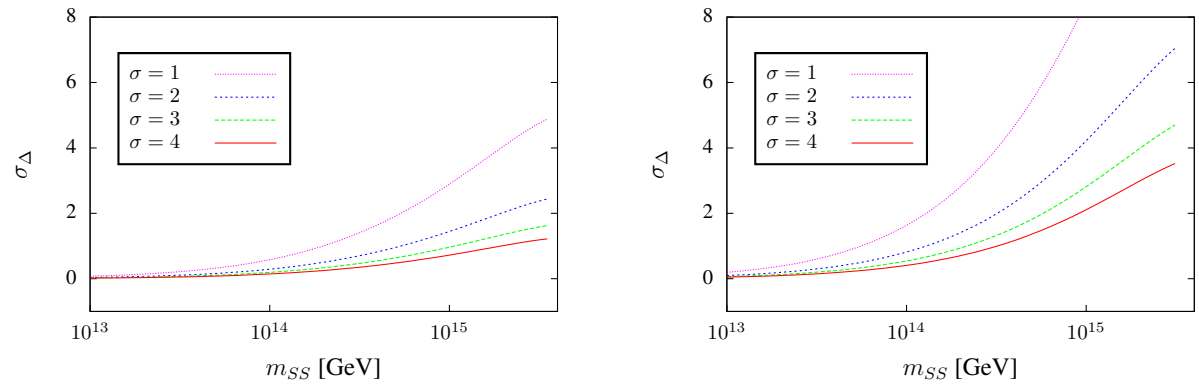

Figure 3.3: Calculated χ^2 for the observable $\Delta(m_{\tilde{e}\tilde{\mu}})$ as function of m_{SS} for different values of its error. To the left: P_1; to the right P_5.

[148]. However, with the rather large error bars of mass measurements at the LHC it will not be possible to fix the CMSSM parameters with sufficient accuracy to get a reliable error on the value of m_{SS}. Unfortunately, also the accuracy with which $\Delta(m_{\tilde{e}\tilde{\mu}})$ can be measured at the LHC is quite uncertain. According to [146] such a splitting could be found for values as low as (few) 10^{-4} or as large as (several) percent, depending on the kinematical configuration realized in nature. Moreover, our points P_1-P_5 have heavier spectra than the ones studied in [146], so larger statistical errors are to be expected.

Fig. (3.3) shows the relative deviation of $\Delta(m_{\tilde{e}\tilde{\mu}})$ for P_1 (left) and P_5 (right) for different assumed values of the error in this observable, relative to CMSSM. Here, $\sigma = 1, 2, 3, 4$ means that we have multiplied the "error" quoted in [146] by factors $1, 2, 3, 4$. The deviation drops below one sigma for any value of m_{SS} shown for P_1 (P_5) when this error is larger than twice (six times) the nominal error. This implies that no hints for seesaw type-I can be found in LHC data if the error on $\Delta(m_{\tilde{e}\tilde{\mu}})$ is larger than 5 ‰ (1.6 %) in case of P_1 (P_5).

We should also mention that the actual value of $\Delta(m_{\tilde{e}\tilde{\mu}})$ is not only a function of m_{SS} and the CMSSM parameters, but also depends on the type of fit used to explain neutrino data. We have used degenerate right-handed neutrinos and $m_{\nu_1} \equiv 0$ in the plots shown above. Much smaller splittings are found for (a) nearly-degenerate light neutrinos, i.e. $m_{\nu_1} \geq 0.05$ eV; or (b) very hierarchical right-handed neutrinos. We have checked by an explicit calculation that, for example, for P_5 and $m_{\nu_1} \equiv 0$, $\Delta\chi^2 \geq 5.89$ [7] for values of m_{SS} larger than $m_{SS} \simeq 1.6 \times 10^{14}$ GeV from $\Delta(m_{\tilde{e}\tilde{\mu}})$ alone, whereas the same $\Delta\chi^2$ is reached for $m_{\nu_1} = 0.05$ eV only for $m_{SS} \gtrsim 7 \times 10^{14}$ GeV. Consequently, even though one expects that a finite mass difference between left smuon and selectron is found in CMSSM type-I seesaw, this is by no means guaranteed.

Similar comments apply to the errors for the selectron and smuon mass at the ILC. For P_1 (P_5) the departure of the left selectron mass from the CMSSM expectations is smaller than 1 σ even for $m_{SS} \sim 3 \times 10^{15}$ if the error on this mass is larger than $1.5‰$ (1%). For the left smuon the corresponding numbers are for P_1 and P_5 approximately 1.5% and 5%, respectively.

Naively one expects LFV violation to be large, whenever the neutrino Yukawa couplings are large, i.e. for large values of m_{SS}. That is, the regions testable by SUSY mass measurements could already be excluded by upper bounds on LFV, especially the recent upper bound on $\mu \to e\gamma$ by MEG [181]. That this conjecture is incorrect is demonstrated by the example shown in fig. (3.4). In this figure we show the calculated Br($\mu \to e\gamma$) to the left and the calculated χ^2 (total and only $\Delta(m_{\tilde{e}\tilde{\mu}})$) to the right for $\delta = \pi$ and two different values of the reactor angle, θ_{13} for the point P_1. For $\theta_{13} = 0$ all values of m_{SS} above approximately $m_{SS} \sim 10^{14}$ GeV are excluded by the upper bound Br($\mu \to e\gamma$) $\leq 2.4 \times 10^{-12}$ [181]. For $\theta_{13} = 6^\circ$ nearly all values of m_{SS} become allowed. At the same time, this "small" change in the Yukawas has practically no visible effect on the calculated χ^2 from mass measurements as the plot on the right shows. This demonstrates that SUSY mass measurements

[7] $\Delta\chi^2 \geq 5.89$ corresponds to 1 σ c.l. for 5 free parameters.

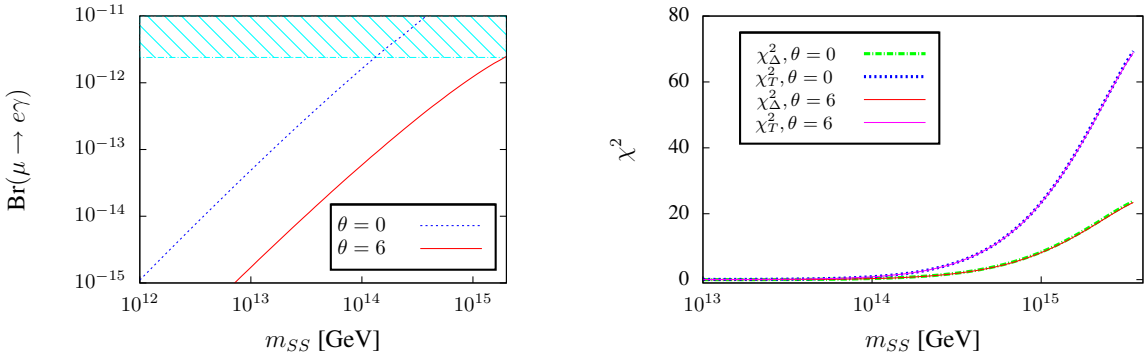

Figure 3.4: To the left $\mathrm{Br}(\mu \to e\gamma)$ and to right calculated χ^2 as function of m_{SS} for two different values of the reactor angle θ_R.

and LFV probe different portions of seesaw type-I parameter space, contrary to what is sometimes claimed in the literature. That one can fit LFV and SUSY masses independently even for such a simple model as type-I seesaw is already obvious from eq. (3.5): Even after fixing all low energy neutrino observables we still have nine unknown parameters to choose from to fit any entry of the left slepton masses independently.

Fig. (3.4) also shows that non-zero values of θ_{13}, as preferred by the most recent experimental data [168; 169], should have very little effect on our parameter scans. In our numerical scans, discussed next, we therefore keep $\theta_{13} = 0$ unless mentioned otherwise. We will, however, also briefly comment on changes of our results, when θ_{13} is allowed to float within its current error.

3.1.3. Numerical scans

For the determination of errors on the CMSSM parameters and m_{SS} we have used two independent programmes, one based on MINUIT while the other uses a simple MonteCarlo procedure to scan over the free parameters. For a more detailed discussion see [2]. Plots shown below are obtained by the MonteCarlo procedure, but we have checked that results from MINUIT and our simplistic approach described above give very similar estimates for the χ^2, with MINUIT only slightly improving the quality of the fit. In this subsection we always use all observables in the fits and quote all errors at 1 σ c.l., unless noted otherwise. Since our "fake" experimental data sets are perfect sets, the minimum of χ^2 calculated equals zero and is thus not meaningful; only $\Delta\chi^2$ calculated with respect to the best fit points has any physical meaning in the plots shown below.

Fig. (3.5) shows the allowed parameter space obtained in a MonteCarlo run for m_0, $M_{1/2}$, $\tan\beta$, A_0 and m_{SS} for 7 free parameters, P_5 and $m_{SS} = 5 \times 10^{14}$ GeV. Shown are the allowed ranges of m_0 and $M_{1/2}$ versus m_{SS}, as well as m_0 versus $M_{1/2}$ and $\tan\beta$ versus A_0. On top of the 4 CMSSM parameters and m_{SS} in this calculation we allow the solar angle (θ_{12}) and the atmospheric angle (θ_{23})

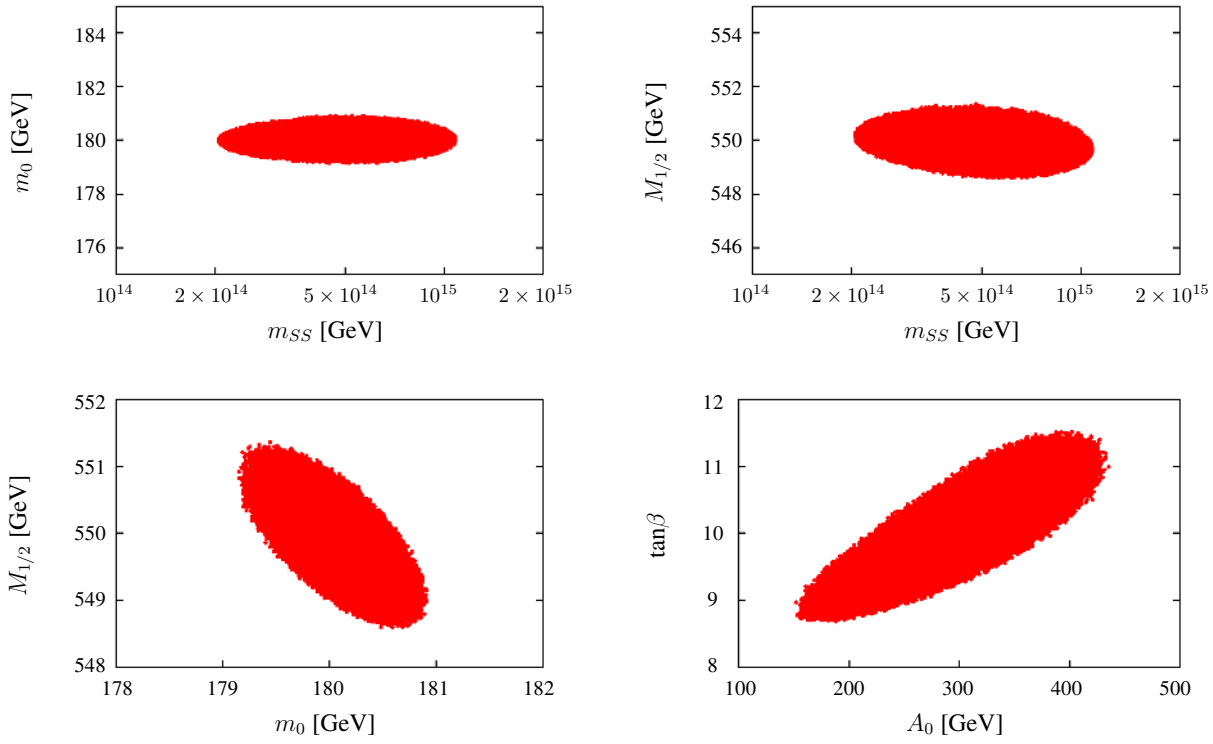

Figure 3.5: Calculated allowed parameter space for m_0, $M_{1/2}$, $\tan\beta$, A_0 and m_{SS} for 7 free parameters, P_5 and $m_{SS} = 5 \times 10^{14}$ GeV. For discussion see text.

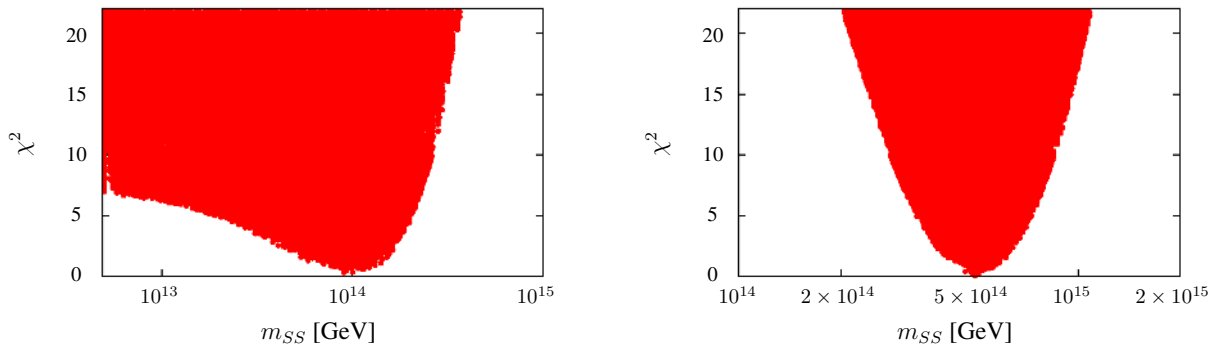

Figure 3.6: Calculated χ^2 distribution versus m_{SS} for 7 free parameters, P_5 and $m_{SS} = 10^{14}$ GeV (to the left) and $m_{SS} = 5 \times 10^{14}$ GeV (to the right).

to float freely within their allowed range. Errors on neutrino angles for this plot are taken from [182]. Plots for other points and/or different sets of free parameters look qualitatively very similar to the example shown in the figure. There is very little correlation among different parameters, contrary to the situation found in case of seesaw type-II and type-III [2]. Especially no correlations between m_0, $M_{1/2}$ and m_{SS} are found. However, there is some correlation between $\tan\beta$ and A_0, driven by the fact that $m_{h_1^0}$ alone can only fix a certain combination of these two parameters well. The correlation between $\tan\beta$ and A_0 is slightly stronger than in the CMSSM case, due to the contribution of A_0 in the running of slepton masses, see eq. (3.5).

For our assumed set of measurements, m_0 and $M_{1/2}$ are mainly determined by the highly accurate measurements of right slepton and gaugino masses of the ILC. A_0 and $\tan\beta$ are fixed by a combination of the lightest Higgs mass and the lighter stau mass. LHC measurements help to break degeneracies in parameter space, but are much less important. We stress that the highly accurate determination of CMSSM parameters shown in fig. (3.5) is a prerequisite for determining reliable errors on m_{SS}. [8]

Fig. (3.6) shows calculated χ^2 distributions versus m_{SS} for the same 7 free parameters as in fig. (3.5), P_5 and $m_{SS} = 10^{14}$ GeV (to the left) and $m_{SS} = 5 \times 10^{14}$ GeV (to the right). For the latter an upper (lower) limit of $m_{SS} \simeq 8 \times 10^{14}$ GeV ($m_{SS} \simeq 3 \times 10^{14}$ GeV) is found. For $m_{SS} = 10^{14}$ GeV a clear upper limit is found, but for low values of m_{SS} the χ^2 distribution flattens out at $\Delta\chi^2 \sim 6.5$. This different behaviour can be understood with the help of the results of the previous subsection, see fig. (3.2). For $m_{SS} = 5 \times 10^{14}$ GeV, there exists a notable difference in some observables with respect to the CMSSM expectation, especially left smuon and selectron mass can no longer be adequately fitted by varying m_0 and $M_{1/2}$ alone, without destroying the agreement with "data" for right sleptons and gauginos. Therefore both, a lower and an upper limit on m_{SS} exist for this point. The situation is different for $m_{SS} = 10^{14}$ GeV, for which the spectrum is much

[8] We have checked this explicitly in a calculation using only LHC observables.

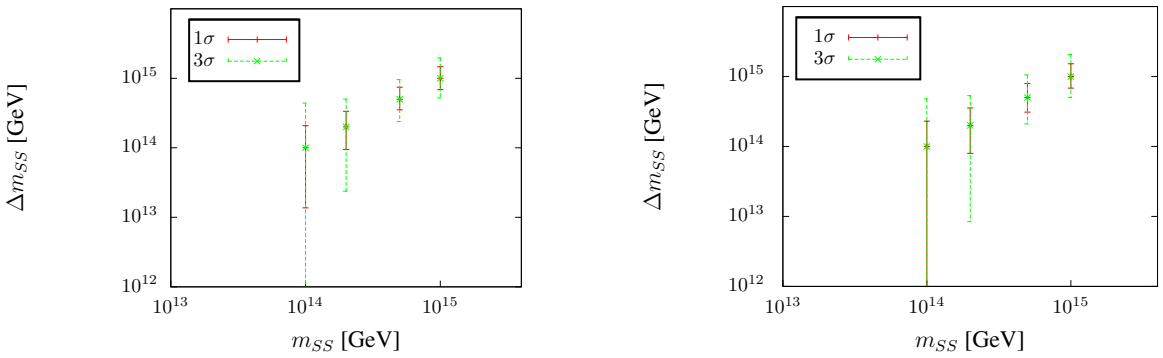

Figure 3.7: Calculated allowed range of m_{SS} versus m_{SS} for 5 (left) and 7 (right) free parameters and P_5. The two different error bars correspond to 1 and 3 σ c.l.

closer to CMSSM expectations. Larger values of m_{SS} are excluded, since they would require larger Yukawas, i.e. larger deviation from CMSSM than observed. Smaller values of m_{SS}, on the other hand, have ever smaller values of Y^ν, i.e. come closer and closer to CMSSM expectations. For an input value of m_{SS} just below $m_{SS} = 10^{14}$ GeV there is then no longer any lower limit on m_{SS}, i.e. the data becomes perfectly consistent with a pure CMSSM calculation. In this case one can only "exclude" a certain range of the seesaw, say values of m_{SS} above a few 10^{14} GeV.

One standard deviation is, of course, too little to claim an observation. We therefore show in fig. (3.7) $\Delta(m_{SS})$ versus m_{SS} for 5 (left) and 7 (right) free parameters and P_5 at 1 and 3 σ c.l. At $m_{SS} = 10^{14}$ formally a 1 sigma "evidence" could be reached, but at 3 σ c.l. the spectrum is perfectly consistent with a pure CMSSM. For larger values of m_{SS}, however, several standard deviations can be reached. For the two largest values of m_{SS} calculated in this figure, a 5 σ "discovery" is possible.

Fig. (3.7) shows $\Delta(m_{SS})$ for 5 and 7 free parameters. We have repeated this exercise for different sets of free parameters and $m_{SS} = 5 \times 10^{14}$. Here, 5 free parameters correspond to the 4 CMSSM parameters plus m_{SS}, 7 free parameters are the original 5 plus θ_{12} and θ_{23}. We have also tried other combinations such as 6 parameters: original 5 plus θ_R and 8 parameters, where we let all 3 neutrino angles float freely. Sets with larger numbers of free parameters are no longer sufficiently sampled in our MonteCarlo runs, so we do not give numbers for these, although in principle the calculation could allow also to let the neutrinos mass squared differences to float freely. Error bars are slightly larger for larger number of free parameters, as expected. However, since there is little or no correlation among the parameters, the differences are so small as to be completely irrelevant.

3.1.4. Summary and discussion

In this section we have discussed the prospects for finding indirect hints for type-I seesaw in SUSY mass measurements. Since type-I seesaw adds only singlets to the SM particle content, only very few observables are affected and all changes in masses are small, even in the most favourable

circumstances. Per-mille level accuracies will be needed, i.e. measurements at an ILC, before any quantitative attempt searching for type-I seesaw can hope for success, even assuming admittedly simplistic CMSSM boundary conditions. The SUSY parameter space used in this chapter is already excluded by recent LHC data (see subsection 2.3.4). At the time of the publication [1] the points were still allowed. Therefore, accuracies needed to find any indirect hint from seesaw type-I at LHC can not be reached anymore. Taking into account recent exclusion limits on SUSY masses from CMS and ATLAS analysis also prospects for possible mass measurements of SUSY particles at linear colliders like the ILC has to be reconsidered, since we need at least part of the SUSY spectrum within the kinematical reach of those future experiments.

Our calculation confirms quantitatively that slepton mass measurements can contain information about the type-I seesaw. Right sleptons are expected to be degenerate, while the left smuon and selectron show a potentially measurable splitting between their masses. If such a situation is indeed found, an estimate of m_{SS} might be derivable from ILC SUSY mass measurements.

Above we have commented only on experimental errors. However, given the per-mille requirements on accuracy, stressed several times, also theoretical errors in the calculation of SUSY spectra are important. Various potential sources of errors come to mind. First of all, a 1-loop calculation of SUSY masses is almost certainly not accurate enough for our purposes. We have tried to estimate the importance of higher loop orders, varying the renormalization scale in the numerical calculation. Changes of smuon and selectron mass found are of the order of the ILC error or even larger, depending on SUSY point and variation of scale. For the mass of the lightest Higgs boson it has been shown that even different calculations at 2-loop still disagree at a level of few GeV [34]. Second, our calculation assumes a perfect knowledge of the GUT scale. Changes in the GUT scale do lead to sizeable changes in the calculated spectra for the same CMSSM parameters, which can be easily of the order of the required precision of the calculation and larger. In this sense, $\Delta(m_{\tilde{e}\tilde{\mu}})$ is an especially nice observable, since here the GUT scale uncertainty nearly cancels out in the calculation. In summary, if ILC accuracies on SUSY masses can indeed be reached experimentally, progress on the theoretical side will become necessary too.

In our calculations, we have considered only SUSY masses. We have not taken into account data from lepton flavour violation, mainly because currently only upper limits are available. If in the future finite values for $l_i \to l_j + \gamma$ become available, it would be very interesting to see, how much could be learned about the type-I seesaw parameters in a combined fit. Including LFV one could maybe also allow for non-degenerate right-handed neutrinos in the fits. However, we stress again, that LFV and SUSY mass measurements test different portions of seesaw parameter space. For a more complete "reconstruction" of seesaw parameters, than what we have attempted here, both kinds of measurements would be needed.

3.2. Seesaw type II and III

In this section we calculate the low-energy SUSY spectra for type-II and type-III seesaw in CMSSM and confront our theoretical results with expectations for the accuracy of SUSY mass measurements at the LHC and at a possible combined LHC+ILC analysis [156; 157]. Given the estimated errors on SUSY masses obtained in detailed simulations [156; 157] we calculate expected χ^2-distributions for the two different seesaw models, in order to give a theoretical forecast on the expected errors on the model parameters, most notably the error on the "determination" of the seesaw scale m_{SS}.

The rest of this section is organized as follows. In the next subsection we summarize the supersymmetric variants of the seesaw type II and III, to set up the notation. We embed the new particles required by the different seesaw mechanisms in complete $SU(5)$ multiplets in order to maintain the successful unification of gauge couplings observed in the MSSM. Subsection 3.2.2 contains the bulk of this section. It first defines our setup, lists the observables we use and then discusses SUSY spectra in the different models. With these results we then proceed to calculate theoretical χ^2 distributions. We first discuss a combined LHC+ILC analysis and then go to the case of using only the less accurate LHC data. Our results, of course, depend crucially on the accuracy with which the SUSY masses can be measured in future accelerator experiments. We therefore dedicate a subsection to discuss in detail the requirements for the accuracies on the most important observables needed for our analysis. We then close with a short discussion and outlook.

3.2.1. Supersymmetric seesaw type II and III

In this subsection we define the supersymmetric versions of the tree-level variants of the seesaw type II and III. A more detailed discussion including the embedding in $SU(5)$ can be found in [183]. For brevity, we will discuss only the superpotential terms.

In supersymmetric models the simplest way to generate a type-II, while maintaining gauge coupling unification, is to add a pair of 15-plets of $SU(5)$ to eq. (2.55). The $SU(5)$ invariant superpotential than reads

$$\begin{aligned} W &= \frac{1}{\sqrt{2}}\mathbf{Y}_{15}\bar{5}_M \cdot 15 \cdot \bar{5}_M + \frac{1}{\sqrt{2}}\lambda_1 \bar{5}_H \cdot 15 \cdot \bar{5}_H + \frac{1}{\sqrt{2}}\lambda_2 5_H \cdot \overline{15} \cdot 5_H + \mathbf{Y}_5 10 \cdot \bar{5} \cdot \bar{5}_H \\ &+ \mathbf{Y}_{10} 10_M \cdot 10_M \cdot 5_H + M_{15} 15 \cdot \overline{15} + M_5 \bar{5}_H \cdot 5_H . \end{aligned} \tag{3.10}$$

Here, $\bar{5}_M$ and 10_M are the usual $SU(5)$ matter multiplets and $5_H = (H^c, H_u)$ and $\bar{5}_H = (\bar{H}^c, H_d)$. Under $SU(3) \times SU(2) \times U(1)$ the 15-plet decomposes as [141]

$$\begin{aligned} 15 &= S + T + Z \,, \\ S &\sim (6, 1, -\frac{2}{3}), \qquad T \sim (1, 3, 1), \qquad Z \sim (3, 2, \frac{1}{6}). \end{aligned} \tag{3.11}$$

Below the GUT scale, M_G, in the $SU(5)$-broken phase the superpotential reads

$$\begin{aligned} W_{II} &= \frac{1}{\sqrt{2}}(Y_T\widehat{L}\widehat{T}_1\widehat{L} + Y_S\widehat{D}^c\widehat{S}_1\widehat{D}^c) + Y_Z\widehat{D}^c\widehat{Z}_1\widehat{L} \\ &+ \frac{1}{\sqrt{2}}(\lambda_1\widehat{H}_d\widehat{T}_1\widehat{H}_d + \lambda_2\widehat{H}_u\widehat{T}_2\widehat{H}_u) + M_T\widehat{T}_1\widehat{T}_2 + M_Z\widehat{Z}_1\widehat{Z}_2 + M_S\widehat{S}_1\widehat{S}_2, \end{aligned} \tag{3.12}$$

where fields with index 1 (2) originate from the 15-plet ($\overline{15}$-plet). The first term in eq. (3.12) is responsible for the generation of neutrino masses, which at low energies are given by

$$m_\nu = \frac{v_u^2}{2}\frac{\lambda_2}{M_T}Y_T \tag{3.13}$$

As in the non-supersymmetric case defined in eq. (2.38), the seesaw scale is estimated to be $\frac{M_T}{\lambda_2} \simeq 10^{15}$ GeV.

In the case of a seesaw model type-III one needs new fermions Σ at the high scale belonging to the adjoint representation of $SU(2)$. The simplest complete $SU(5)$ embedding possible is the 24-plet [184]. The superpotential of the unbroken $SU(5)$ is then

$$W = \sqrt{2}\,\bar{5}_M\mathbf{Y_5}10_M\bar{5}_H - \frac{1}{4}10_M\mathbf{Y_{10}}10_M5_H + 5_H24_MY_N^{III}\bar{5}_M + \frac{1}{2}24_MM_{24}24_M\ . \tag{3.14}$$

The 24_M decomposes under $SU(3)\times SU(2)\times U(1)$ as

$$\begin{aligned} 24_M &= (1,1,0) + (8,1,0) + (1,3,0) + (3,2,-5/6) + (3^*,2,5/6)\ , \\ &= \widehat{B}_M + \widehat{G}_M + \widehat{W}_M + \widehat{X}_M + \widehat{\bar{X}}_M\ . \end{aligned} \tag{3.15}$$

The $\widehat{B}_M$ has the same quantum numbers as the $\widehat{N}^c$, while the fermionic component of the $\widehat{W}_M$ corresponds to the Σ. Thus, the 24_M always produces a combination of the type-I and type-III seesaw.

In the $SU(5)$ broken phase the superpotential contains

$$\begin{aligned} W_{III} &= \widehat{H}_u(\widehat{W}_MY_W - \sqrt{\frac{3}{10}}\widehat{B}_MY_B)\widehat{L} + \widehat{H}_u\widehat{\bar{X}}_MY_X\widehat{D}^c \\ &+\frac{1}{2}\widehat{B}_MM_B\widehat{B}_M + \frac{1}{2}\widehat{G}_MM_G\widehat{G}_M + \frac{1}{2}\widehat{W}_MM_W\widehat{W}_M + \widehat{X}_MM_X\widehat{\bar{X}}_M. \end{aligned} \tag{3.16}$$

Integrating out the heavy fields, as before, leads to

$$m_\nu = -\frac{v_u^2}{2}\left(\frac{3}{10}Y_B^TM_B^{-1}Y_B + \frac{1}{2}Y_W^TM_W^{-1}Y_W\right). \tag{3.17}$$

There are two contributions: (i) from the gauge singlet and (ii) from the $SU(2)$ triplet. Starting

with a common Y_N^{III}, Y_B^T evolves slightly differently from Y_W^T under the RGEs. Thus, in principle two non-zero neutrino masses are generated from one 24_M only. However, the ratio of the two non-zero neutrino masses generated in the RGE running is much too tiny to explain the observed neutrino data and thus at least 2 copies of 24_M are needed for a realistic neutrino mass spectrum. In our numerical calculations we use 3 copies of 24_M, motivated by the observed 3 generations.With $\forall Y_B^{ij}/Y_W^{ij} \simeq 1$, one can simplify eq. (3.17) to

$$m_\nu = -v_u^2 \frac{4}{10} Y_W^T M_W^{-1} Y_W \tag{3.18}$$

which is the supersymmetric version of eq. 2.39. The scale of M_W is then estimated to be $m_{SS} \sim 8 \times 10^{14}$ GeV for $Y_W^{ij} = O(1)$.

3.2.2. Results and discussion

In subsection 3.2.2.1 we will define our setup and discuss the input observables. In 3.2.2.2 we discuss the SUSY spectra in the different models and how the observables change under changes of the seesaw scale. In subsection 3.2.2.3 we present our results for a combined LHC+ILC analysis, while 3.2.2.4 shows the results for an analysis using only LHC data. Subsection 3.2.2.5 discusses the accuracies on the different observables, which need to be achieved experimentally, before any conclusions on the presence (or absence) of a seesaw mechanism can be drawn. Given the inherent unreliability of theoretical error forecasts in general, subsection 3.2.2.5 can be considered to contain the central parts of this section.

3.2.2.1. Setup, observables and data input

All the numerical results shown in the following have been obtained with the programme package SPheno [36; 185]. The RGE equations, complete at the 2-loop order, have been calculated and incorporated into SPheno with the help of SARAH [35; 186; 187]. Details and discussion of the implementation can be found in [142].

To completely specify the low-energy SUSY spectra, we have to assume a specific SUSY breaking scenario. In this subsection we use CMSSM. In the following we will call "pure CMSSM", pCMSSM for short, the version of the model with no seesaw mechanism at all. Note that this is equivalent to putting the seesaw scale m_{SS} equal to the GUT scale M_G. For brevity, we will call "type-II" and "type-III" models with CMSSM boundary conditions, to which on top of the MSSM particle content the corresponding "seesaw particles", as specified in the previous subsection, are added at scale m_{SS}.

In our numerical calculations we concentrate on some selected sets of CMSSM parameters. This is mainly motivated by the exorbitant amount of CPU time a full scan over the CMSSM space would require, see also the discussion below. The points we have studied are SPS1a' [157] and

the points SPS1b and SPS3 [175]. In addition, for reasons explained in subsection 3.2.2.2, we consider a few more points with modified CMSSM parameters. We will call these points MSP-1 $(m_0, M_{1/2}, \tan\beta, A_0) = (70, 400, 10, -300)$, MSP-2 $(220, 700, 30, 0)$ and MSP-3 $(120, 720, 10, 0)$. MSP-1 is similar to SPS1a' but with a larger value of $M_{1/2}$, MSP-2 is a point with larger $\tan\beta$ and MSP-3 is similar to SPS3, but again with a larger value of $M_{1/2}$. All these points choose $\mu > 0$. We have not found any qualitatively new features in points with negative μ, as far as the determination of m_{SS} is concerned.

Observables and their theoretically forecasted errors are taken from the tables (5.13) and (5.14) of [156] and from [157]. For the LHC we take into account the "edge variables": $(m_{ll})^{edge}$, $(m_{lq})^{\text{edge}}_{\text{low}}$, $(m_{lq})^{\text{edge}}_{\text{high}}$, $(m_{llq})_{\text{edge}}$ and $(m_{llq})_{\text{thresh}}$ from the decay chain $\tilde{q}_L \to \chi_2^0 q$ and $\chi_2^0 \to l\tilde{l} \to ll\chi_1^0$ [170; 171; 172]. In addition, we consider $(m_{llb})_{thresh}$, $(m_{\tau^+\tau^-})$ (from decays involving the lighter stau) and the mass differences $\Delta_{\tilde{g}\tilde{b}_i} = m_{\tilde{g}} - m_{\tilde{b}_i}$, with $i = 1, 2$, $\Delta_{\tilde{q}_R\chi_1^0} = m_{\tilde{q}_R} - m_{\chi_1^0}$ and $\Delta_{\tilde{l}_L\chi_1^0} = m_{\tilde{l}_L} - m_{\chi_1^0}$. Since $m_{\tilde{e}_R} \simeq m_{\tilde{\mu}_R}$ and $m_{\tilde{u}_R} \simeq m_{\tilde{d}_R} \simeq m_{\tilde{c}_R} \simeq m_{\tilde{s}_R}$ applies for a large range of the parameter space LHC measurements will not be able to distinguish between the first two generation sfermions. [9] This allows us to define the masses $m_{\tilde{l}_L} = (m_{\tilde{e}_L} + m_{\tilde{\mu}_L})/2$ and $m_{\tilde{q}_R} = (m_{\tilde{u}_R} + m_{\tilde{d}_R} + m_{\tilde{c}_R} + m_{\tilde{s}_R})/4$ which will be used from now on for the mass differences $\Delta_{\tilde{q}_R\chi_1^0}$ and $\Delta_{\tilde{l}_L\chi_1^0}$. As discussed below in subsection 3.2.2.5, especially $\Delta_{\tilde{g}\tilde{b}_i}$ and the edge variables are important for the LHC analysis. For the ILC we assume that at least $m_{\chi_1^0}$, $m_{\tilde{e}_R} \simeq m_{\tilde{\mu}_R}$ and $m_{\tilde{e}_L} \simeq m_{\tilde{\mu}_L}$ are kinematically accessible. In addition, whenever within the reach of the ILC, we also take into account $\tilde{\tau}_1$, χ_2^0, χ_1^+ and $\tilde{t}_1$, which are, however, less important. We also assume that the lighter Higgs, h^0, has been found and its mass measured with an accuracy which depends on whether the analysis is for LHC only or for LHC+ILC, see the corresponding error estimates in [157]. Errors for the ILC are taken directly from the tables of the above papers. For the error bars for the LHC, however, we have rescaled all statistical errors from the values for $300\ fb^{-1}$ to a luminosity of (only) $100\ fb^{-1}$. To be conservative the total error is obtained summing statistic and systematic error linearly. Note that we did not make use of the combined LHC and ILC errors calculated in the papers mentioned above. When we discuss the calculations for LHC and ILC observables in 3.2.2.3 we refer to an analysis in which the LHC and ILC observables are all enabled but the errors are the errors for the LHC or ILC only. Nevertheless, we have checked that using the combined errors changes the results only by an irrelevant amount. We will call this analysis therefore "ILC+LHC combined".

In [156] and [157], only standard SPS points have been studied in detail. In the calculation of the χ^2-distributions we assume that relative errors for different CMSSM points and/or seesaw points are constant. The assumption to use constant relative errors in all of our calculations is, of course, a crucial simplification which has to be checked very carefully. However, we have chosen to do so for the following two reasons: (a) It allows us to perform a χ^2 analysis for all different spectra within reasonable CPU time. And (b) uncertainties of the theoretically forecasted error bars

[9] See however [146; 147; 148].

are nearly impossible to estimate. Only experiments can finally determine total errors on observables. We thus use errors-as-predicted and discuss in subsection 3.2.2.5, how our conclusions will change as a function of these unknown errors.

To numerically estimate the allowed ranges for the model parameters we use a simple χ^2 procedure. We have found that, see below, errors on m_0, $M_{1/2}$ and m_{SS} are very strongly correlated. To assure that our estimates are reliable in all cases we have written two completely independent numerical codes. The first of these is based on MINUIT, [10]. enforcing the m_{SS} scan while MINUIT is fitting the parameters m_0, $M_{1/2}$, tanβ and A_0 for fixed m_{SS}. The second code uses a straight-forward but slow Monte Carlo random walk procedure, which can be "heated" to find separated minima. In the MC calculations we use usually a (few) 10^6 points to assure convergence. This makes the MC code slow, but reliable. We have done calculations using both codes in all cases necessary, to ensure that convergence has been reached.

Finally we need to mention that in all calculations shown below we put neutrino Yukawa couplings to negligibly small values, unless noted otherwise. Again the reason for this choice is simply to limit the amount of CPU time necessary for our fits. [11] We will comment, however, in subsection (3.2.2.5) on the differences expected with fits, where the Yukawas are chosen to fit neutrino data correctly. In general, if m_{SS} is below, say, 10^{14} GeV the differences of the full fit to our calculation with negligible Yukawas is found to be completely irrelevant. If any hints of seesaw with m_{SS} in the range $[10^{14}, 10^{15}]$ were indeed found in SUSY spectra, however, we expect that a full analysis would find results which differ by some $(10-30)$ % (depending on the exact value of m_{SS}) from our preliminary numbers.

3.2.2.2. Mass spectra and LHC and ILC observables

In this subsection we briefly summarize the differences in the calculated mass spectra of the different models and how this affects the LHC and ILC observables, which we use in our fits. In the following all numerical results shown in the figures have been calculated solving the full 2-loop RGEs numerically. Moreover, we have taken into account the 1-loop thresholds of the seesaw particles at the seesaw scale as described in [142] and include the one-loop contributions to the SUSY masses [188]. We have also included the shifts of the gauge couplings to the $\overline{DR}$-scheme. It is instructive to discuss some (semi-) analytical approximations at 1-loop order, which will allow to understand qualitatively the numerical results. We stress that none of the following approximations is used in any way in the numerical calculations.

The introduction of complete $SU(5)$ multiplets at a scale below the GUT scale changes the

[10] Minimization package from the CERN Programme Library. Documentation can be found at `http://cernlib.web.cern.ch/cernlib/`

[11] We let 5 parameters flow freely. For a type-II, for example, we have in Y_T six more complex parameters. A full fit would require minimizing χ^2 for 5+12-3=14 parameters, which can not done for all spectra we need to consider within realistic amounts of CPU time.

running of the gauge couplings. Incorporating a seesaw mechanism with full $SU(5)$ multiplets at 1-loop order in eq. 2.67 the gauge couplings at the different scales are given as [116]

$$\begin{aligned}
\alpha_1(m_Z) &= \frac{5\alpha_{em}(m_Z)}{3\cos^2\theta_W}, \qquad \alpha_2(m_Z) = \frac{\alpha_{em}(m_Z)}{\sin^2\theta_W}, \\
\alpha_i(m_{SUSY}) &= \frac{\alpha_i(m_Z)}{1-\frac{\alpha_i(m_Z)}{4\pi}b_i^{SM}\log\frac{m^2_{SUSY}}{m_Z^2}}, \\
\alpha_i(m_{SS}) &= \frac{\alpha_i(m_{SUSY})}{1-\frac{\alpha_i(m_{SUSY})}{4\pi}b_i\log\frac{m^2_{SS}}{m^2_{SUSY}}}, \\
\alpha_i(M_G) &= \frac{\alpha_i(m_{SS})}{1-\frac{\alpha_i(m_{SS})}{4\pi}(b_i+\Delta b_i)\log\frac{M_G^2}{m^2_{SS}}}.
\end{aligned} \tag{3.19}$$

m_{SS} denotes the seesaw scale, i.e. the mass of the 15-plet or the mass(es)[12] of the 24-plets. For the case of the 15-plet one finds $\Delta b_i = 7$ whereas for the case with three 24-plets one finds $\Delta b_i = 15$, since each 24_M gives a $\Delta b_i = 5$. It is easy to show that at the 1-loop level the GUT scale is not changed by the introduction of the complete $SU(5)$ multiplets. However, the $\Delta b_i \neq 0$ lead to a faster "running" of the gauge couplings and thus to a larger value of $\alpha(M_G)$ compared to the CMSSM case. For seesaw scales smaller than roughly $m_{SS} \sim 10^9$ GeV (10^{13} GeV) one then encounters a Landau pol in $\alpha(M_G)$ for seesaw type-II (type-III) [142]. This defines in each case a lower limit on the seesaw scale, if we insist on perturbativity.[13]

Gaugino masses evolve like gauge couplings:

$$M_i(m_{SUSY}) = \frac{\alpha_i(m_{SUSY})}{\alpha(M_G)} M_{1/2}. \tag{3.20}$$

Eq. (3.20) implies that the ratio M_2/M_1, which is measured at low-energies, has the usual CMSSM value, but the relationship to $M_{1/2}$ is changed. I.e. since $\alpha(M_G)$ is larger in the seesaw case than in the standard pCMSSM, M_i are smaller in seesaw than in pCMSSM.

[12] We assume that the 3 copies of 24-plets are degenerate. In principle, given enough accurately measured observables, it might be possible to drop this assumption.

[13] Note, however, the SPheno never allows us to push the seesaw scales down to these limits. Convergence problems are usually encountered already for $\alpha(M_G) \gtrsim 0.25$ depending on the CMSSM parameters.

For the soft mass parameters of the first two generations one obtains [116]

$$m_{\tilde{f}}^2 = m_0^2 + \sum_{i=1}^{3} c_i^{\tilde{f}} \left(\left(\frac{\alpha_i(m_{SS})}{\alpha(M_G)} \right)^2 f_i + f_i' \right) M_{1/2}^2, \tag{3.21}$$

$$f_i = \frac{1}{b_i} \left(1 - \left[1 + \frac{\alpha_i(m_{SS})}{4\pi} b_i \log \frac{m_{SS}^2}{m_Z^2} \right]^{-2} \right),$$

$$f_i' = \frac{1}{b_i + \Delta b_i} \left(1 - \left[1 + \frac{\alpha(M_G)}{4\pi} (b_i + \Delta b_i) \log \frac{M_G^2}{m_{SS}^2} \right]^{-2} \right). \tag{3.22}$$

The various coefficients $c_i^{\tilde{f}}$ are given in table 2.9. In the limit $m_{SS} \to M_G$ the functions f_i' go to zero and one recovers the standard CMSSM estimations for the sfermion masses. For any m_{SS} below M_G, the contribution from f_i are smaller than in the CMSSM case, due to the prefactor which is always smaller than one. The contribution from the f_i' can only partially compensate for this and thus, at low energies for a given pair of m_0 and $M_{1/2}$ one expects the sfermion masses to be smaller in seesaw than in pCMSSM. It is important, however, to note that the different coefficients c_i differ not only from sparticle to sparticle, but also are different for the same particle but different gauge groups. This observation is fundamentally the reason explaining the statement that accurate sfermion mass measurements will allow to distinguish pure CMSSM from CMSSM plus seesaw.[14] As in the case of pCMSSM, coloured particles are expected to be heavier than non-coloured ones in seesaw.

Before discussing the numerical results, we briefly comment on seesaw type-I. In type-I one only adds singlets to the MSSM particle content. Thus, $\Delta b_i = 0 \ \forall i$ and there is no deformation of the spectrum with respect to CMSSM due to the gauge part. The only change one expects for type-I is due to a different running of m_L^2, when Yukawas are taken into account. Since only m_L^2 is affected, most of the observables we have discussed above are not sensitive to the seesaw scale in type-I and our current analysis can not directly be applied to type-I seesaw.

Fig. (3.8) shows some examples of SUSY masses for two specific choices of CMSSM parameters. The top panel shows CMSSM parameters chosen as in the standard point SPS1a' [157], while the bottom panel shows MSP-1 for comparison. All plots show masses as function of m_{SS}, to the left for seesaw type-II and to the right for type-III. Shown are masses of the lighter two neutralinos, χ_1^0 and χ_2^0, and masses of charged sleptons. As is also typical in CMSSM, the mass of the lighter chargino $m_{\chi_1^+}$ is very similar to $m_{\chi_2^0}$ and smuons and selectrons are nearly degenerate. We note in passing, that the mass of the lightest Higgs, h^0, shows little or no sensitivity at all on m_{SS} but is important in the fits.

As discussed above, all masses get smaller for smaller values of m_{SS} and are always smaller than in the pCMSSM limit. Note the wide range for type-II shown and the much smaller range of m_{SS}

[14] If all c_i where the same, one could always fit the data by a simple rescaling of m_0 and $M_{1/2}$.

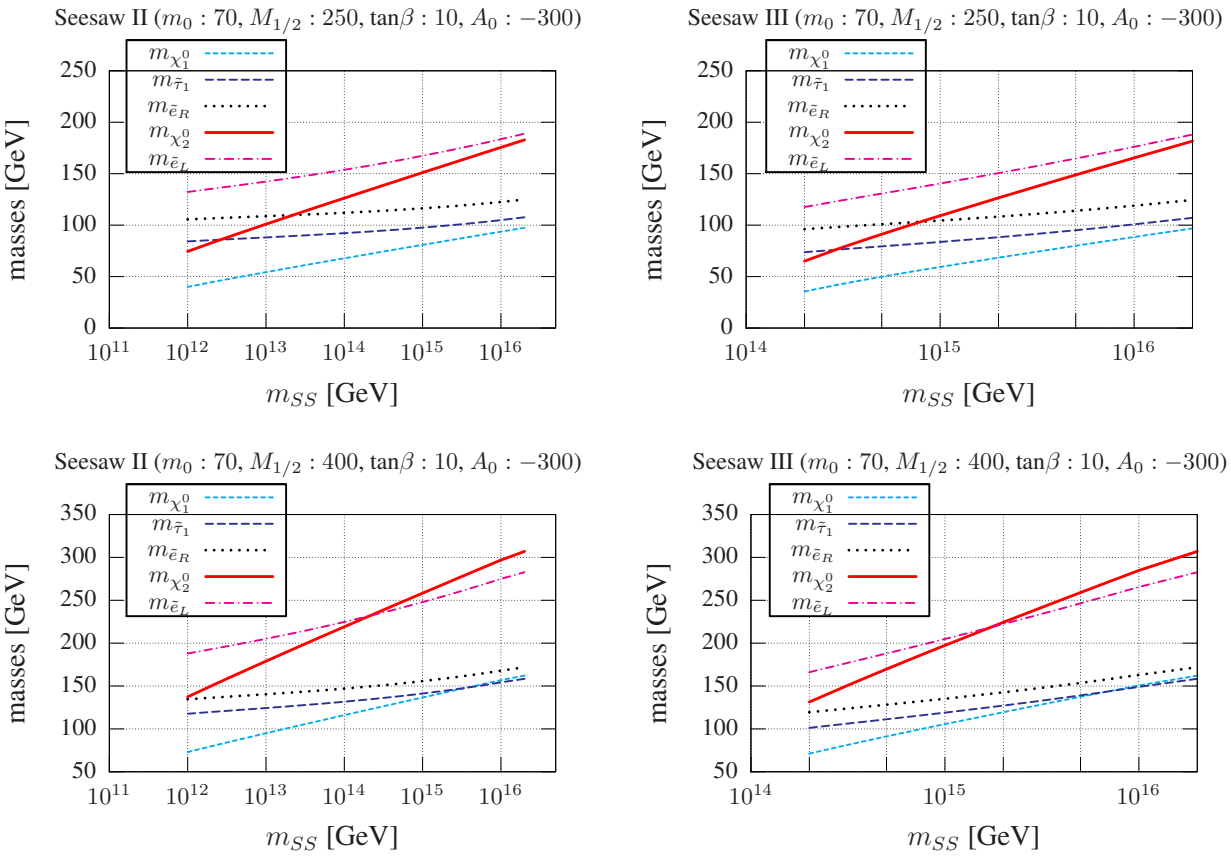

Figure 3.8: Supersymmetric masses for two specific choices of CMSSM parameters as a function of the seesaw scale. To the left: type-II. To the right: type-III. The CMSSM parameters are fixed at the values of SPS1a' (top) and to MSP-1 (bottom). Note the different scales for type-II and type-III.

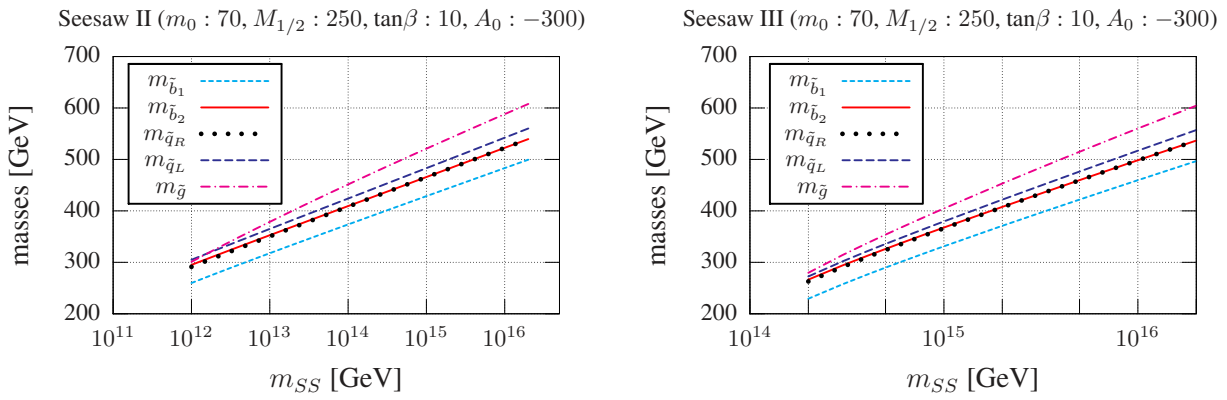

Figure 3.9: Running masses as a function of the seesaw scale, left: type-II; right: type-III. As fig. (3.8), but showing only the point SPS1a'. The masses shown in this figure are the most important coloured particles for our analysis.

plotted for type-III. Ratios of gaugino masses follow standard expectations for all values of m_{SS} and both types of seesaw. The slopes of the curves are different for different sparticles and the relative changes are larger in type-III than in type-II. This simply reflects the fact that type-III causes a larger change in the beta coefficients ($\Delta b_i = 15$) than type-II ($\Delta b_i = 7$).

For the point SPS1a' the lighter chargino becomes lighter than 105 GeV for type-II (type-III) seesaw scales below roughly $m_{SS} \sim 2\times10^{13}$ GeV ($m_{SS} \sim 10^{15}$ GeV). Thus, m_{SS} below these values are ruled out by the LEP bounds [180; 189]. Note that this implies that type-III can not explain neutrino data for CMSSM parameters as in SPS1a' with Yukawas smaller than $Y_W^{ij} \leq 1$.

Changing the seesaw scale can lead to a different mass ordering for different sparticles. For example, for SPS1a' the χ_2^0 is heavier than $\tilde{e}_R$ and $\tilde{\tau}_1$ in the CMSSM limit (seesaw scale equal to M_G), but lighter than $\tilde{e}_R$ for type-II (type-III) seesaw scales below $m_{SS} \sim 3\times10^{13}$ ($m_{SS} \sim 8\times10^{14}$). This is important for our study, since as a function of m_{SS} it can happen that some observables are kinematically open for some values of m_{SS} but not for others, see also the discussion in subsection 3.2.2.4.

The modified value of $M_{1/2} = 400$ GeV in MSP-1 with respect to SPS1a' is motivated by the fact that for this choice of parameters the edge variables from the chain $\chi_2^0 \to \tilde{l}_R l \to ll\chi_1^0$ are kinematically possible for all relevant values of m_{SS}. The larger value of $M_{1/2}$ implies heavier neutralinos and also that the LEP bounds on sparticle masses are fulfilled for all values of m_{SS} shown. Note, that all sparticles shown in the plot are kinematically accessible at an ILC with $\sqrt{s} = 1$ TeV. For MSP-1 the lighter stau is the LSP for m_{SS} larger than roughly $m_{SS} = 10^{16}$ GeV. Thus, this point formally has no cosmologically acceptable pCMSSM limit.

Fig. (3.9) shows the dependence of several coloured sparticle masses on m_{SS}. Again to the left (right) we show seesaw type-II (type-III). Note the different scales for type-II and type-III. We show

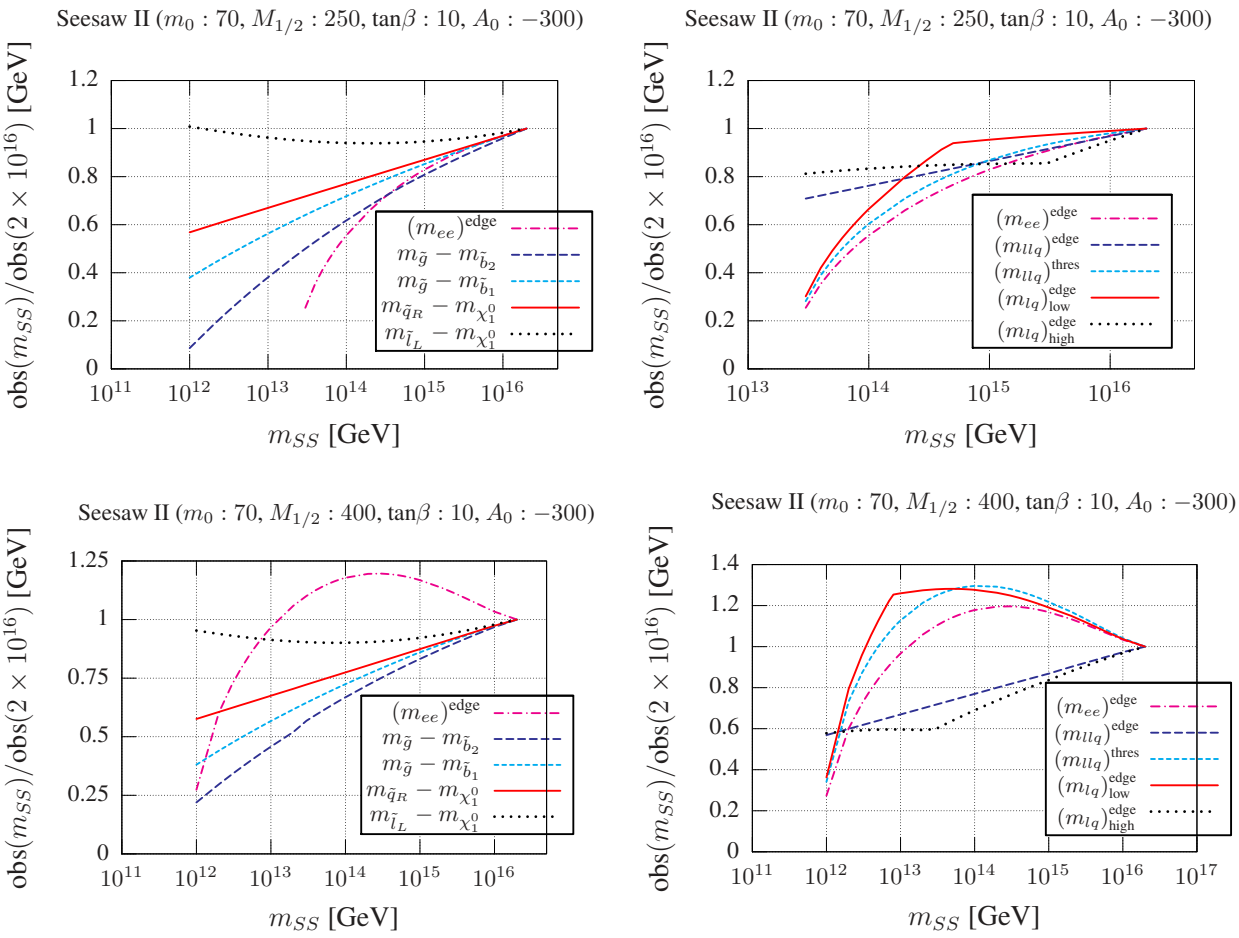

Figure 3.10: Relative change of different LHC observables as a function of the seesaw scale for type-II seesaw. Top CMSSM parameters as in SPS1a', bottom MSP-1. For an explanation see text. $(m_{ee})^{\rm edge}$ is repeated in the left plot for comparison.

only the values for SPS1a' in this figure, masses for MSP-1 are larger but behave qualitatively very similar. The relative change of masses as a function of m_{SS} is much larger than for the non-coloured sparticle masses shown in fig. (3.8). Here the range where $m_{\tilde g} \simeq m_{\tilde q_{L,R}} \lesssim 300$ GeV is excluded by Tevatron data [180; 190]. However, this region is already excluded by LEP data. Note, that $m_{\tilde g} > m_{\tilde b_1}$ for all values of m_{SS} in this point. Coloured sparticle production gives the bulk of the SUSY cross section at the LHC as usual. In these points most of the coloured sparticles are not kinematically accessible at the ILC, except for low values of m_{SS}. Except $\tilde t_1$ we therefore do not take into account measurements of coloured sparticles at the ILC in our analysis, even though they could be potentially much more accurate than the corresponding measurements at the LHC.

With the masses shown in fig. (3.8) and fig. (3.9) one obtains the LHC observables shown in

fig. (3.10) for type-II. Again in the top panel we show SPS1a' and in the bottom panel MSP-1. The figure shows several mass differences (left) and the edge variables (right) stemming from the decay chain $\tilde{q} \to q\chi_2^0$ with the subsequent decay $\chi_2^0 \to l^{\pm}\tilde{l}^{\mp} \to l^{\pm}l^{\mp}\chi_1^0$ [170; 171; 172]. We have normalized all observables to their expected values for $m_{SS} = M_G$. Thus relative changes in the different observables with respect to pCMSSM are plotted.

The two kinks in the running of $(m_{lq})^{\text{edge}}_{\text{low}}$ and $(m_{lq})^{\text{edge}}_{\text{high}}$ stem from the fact that one has to consider different cases in these observables. They can be written as [171]

$$\begin{aligned} (m_{lq})^{\text{edge}}_{\text{high}} &= \text{max}[(m^{\text{max}}_{l_{\text{near}}q})^2, (m^{\text{max}}_{l_{\text{far}}q})^2] \\ (m_{lq})^{\text{edge}}_{\text{low}} &= \text{min}[(m^{\text{max}}_{l_{\text{near}}q})^2, (m^2_{\tilde{q}} - m^2_{\chi_2^0})(m^2_{\tilde{l}_R} - m^2_{\chi_1^0})/(2m^2_{\tilde{l}_R} - m^2_{\chi_1^0})] \end{aligned} \tag{3.23}$$

where

$$\begin{aligned} (m^{\text{max}}_{l_{\text{near}}q})^2 &= (m^2_{\tilde{q}} - m^2_{\chi_2^0})(m^2_{\chi_2^0} - m^2_{\tilde{l}_R})/m^2_{\chi_2^0} \\ (m^{\text{max}}_{l_{\text{far}}q})^2 &= (m^2_{\tilde{q}} - m^2_{\chi_2^0})(m^2_{\tilde{l}_R} - m^2_{\chi_1^0})/(m^2_{\tilde{l}_R}). \end{aligned} \tag{3.24}$$

These conditions change as a function of m_{SS} causing the kinks shown in the figure. Except for the $(m_{ll})^{\text{edge}}$ different cases appear in the expressions for all edges, but only for the variables $(m_{lq})^{\text{edge}}_{\text{low}}$ and $(m_{lq})^{\text{edge}}_{\text{high}}$ do the kinematical conditions change as function of m_{SS} normally.

The plot in fig. (3.10) demonstrates the strong dependence of the LHC observables on m_{SS}. Increasing and decreasing values of the edges are possible, while mass differences usually decrease for lower values of m_{SS}. Note that in the χ^2 fits, discussed in the next subsections, observables which show (a) the largest relative change with respect to m_{SS} and (b) have the smallest expected errors will give the most important contributions. Finally we mention that fig. (3.10) shows only type-II, since results for type-III are qualitatively similar but with larger relative changes.

3.2.2.3. χ^2 analysis for combined LHC and ILC data

In this subsection we take into account all possible LHC and ILC observables. We discuss this more futuristic (but simpler) case first. Results for an analysis taking only LHC observables are discussed in the next subsection. We note in passing that we have checked that we can roughly reproduce the error on parameters for the pure CMSSM results for the point SPS1a' discussed in detail in [157].

Fig. (3.11) shows the allowed ranges of the parameters for the point MSP-1 and one specific choice of $m_{SS} = 5 \times 10^{13}$ GeV for type-II seesaw. The allowed regions have been found in a MC random walk procedure letting 5 parameters, $m_0, M_{1/2}, A_0, \tan\beta$ and m_{SS}, float freely. The ranges shown correspond to a $\Delta\chi^2 \simeq 5.89$, i.e. 1 σ c.l. for 5 free parameters, where we have taken into account the correlations between the various parameters. Plotted are different 2-dimensional

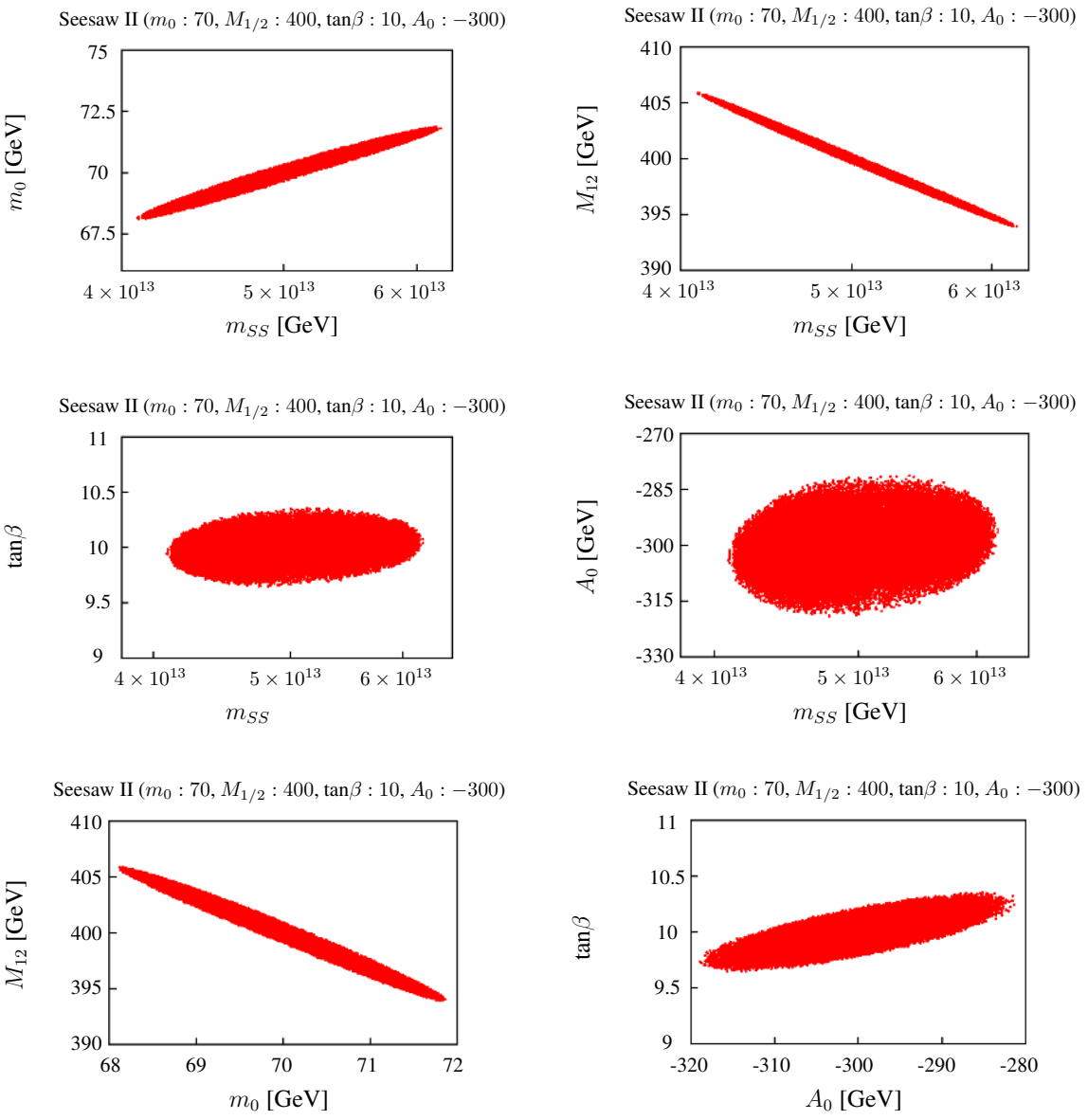

Figure 3.11: Allowed parameter space for m_0, $M_{1/2}$, $\tan\beta$, A_0 and m_{SS} for all 5 parameters varied freely. The input value for the seesaw scale is $m_{SS} = 5 \times 10^{13}$ GeV and seesaw type-II has been used.

projections of parameters.

As mentioned already above, the three parameters m_0, $M_{1/2}$ and m_{SS} are highly correlated among each other. Lower values of m_{SS} can be compensated by increasing $M_{1/2}$ and decreasing m_0 at the same time. This feature is present in all parameter space for both types of seesaw. This correlation results in errors on m_0 and $M_{1/2}$ which are larger (some times much larger, see below) than in pCMSSM for the same input errors on observables. We note that the χ^2 in this calculation is dominated by the much more accurate ILC data, see also the discussion in subsection 3.2.2.5 below.

In contrast, $\tan\beta$ and A_0 show very little correlation with m_{SS} (and m_0 and $M_{1/2}$) and only a rather moderate correlation among themselves. $\tan\beta$ and A_0 are mostly determined by the Higgs mass measurement, and to some extend by 3rd generation sfermions. Note that A_0 and $\tan\beta$ do not have much influence on the determination of m_0, $M_{1/2}$ and m_{SS}, apart from a slight increase in the errors of the latter. However if m_0 cannot be fixed a determination of A_0 and also $\tan\beta$ becomes practically impossible, because almost any shift of $\tan\beta$ and A_0 can then be compensated by changing m_0 and/or $M_{1/2}$. This will be important when we discuss the calculations using LHC observables only in subsection 3.2.2.4.

For this choice of parameters, the error on m_{SS} itself is found to be around $\Delta m_{SS} \sim 1.2 \times 10^{13}$, i.e. values of $m_{SS} = M_G$ are formally excluded by many standard deviations. However, Δm_{SS} is a very strong function of m_{SS} itself, as we will discuss below.

Fig. (3.11) shows results for a comparatively low value of m_{SS}. Fig. (3.12) shows χ^2 distributions for MSP-1 obtained by a random walk for seesaw type II and two slightly different but much higher values of m_{SS}: To the left: $m_{SS} = 10^{15}$ GeV and to the right: $m_{SS} = 1.3 \times 10^{15}$. The plots show the true χ^2-minimum and a second (fake) minimum at $m_{SS} = M_G$. For the lower value of m_{SS} this fake minimum is just excluded at 1 σ c.l., while for the slightly higher value of m_{SS} it is accepted at 1 σ c.l. These kind of false minima appear in all our calculations when m_{SS} approaches M_G. This is to be expected, since the models approach pCMSSM in this limit.

Fig. (3.13) shows the allowed range of parameters m_{SS}, m_0 and $M_{1/2}$ for $m_{SS} = 1.3 \times 10^{15}$ GeV. Two separate minima show up. For slightly larger values of m_{SS} the two solutions overlap completely. Note that this also increases the errors on m_0 and $M_{1/2}$. For slightly smaller values of m_{SS} this fake solution disappears resulting in a drastic decrease in the error bars of these three parameters. In case of type-III this fake minima does not show up separately, but indirectly by deforming the χ^2 distributions. Thus for type-III the error bars go up to M_G until it gets compatible with pCMSSM. This will be important when we discuss CMSSM plus type-III later on.

In case of the ILC+LHC analysis this kind of "false" minima are usually the only class of fake minima that appear. Using only LHC data, the χ^2 distributions are not that well behaved and false minima can also appear considerably below M_G, this will be shown in the next subsection.

Fig. (3.14) shows 1 σ, 3 σ and 5 σ c.l. error bars on the different parameters of the model as a function of the seesaw scale for one specific CMSSM set, MSP-1, for the case of type-II. The plots

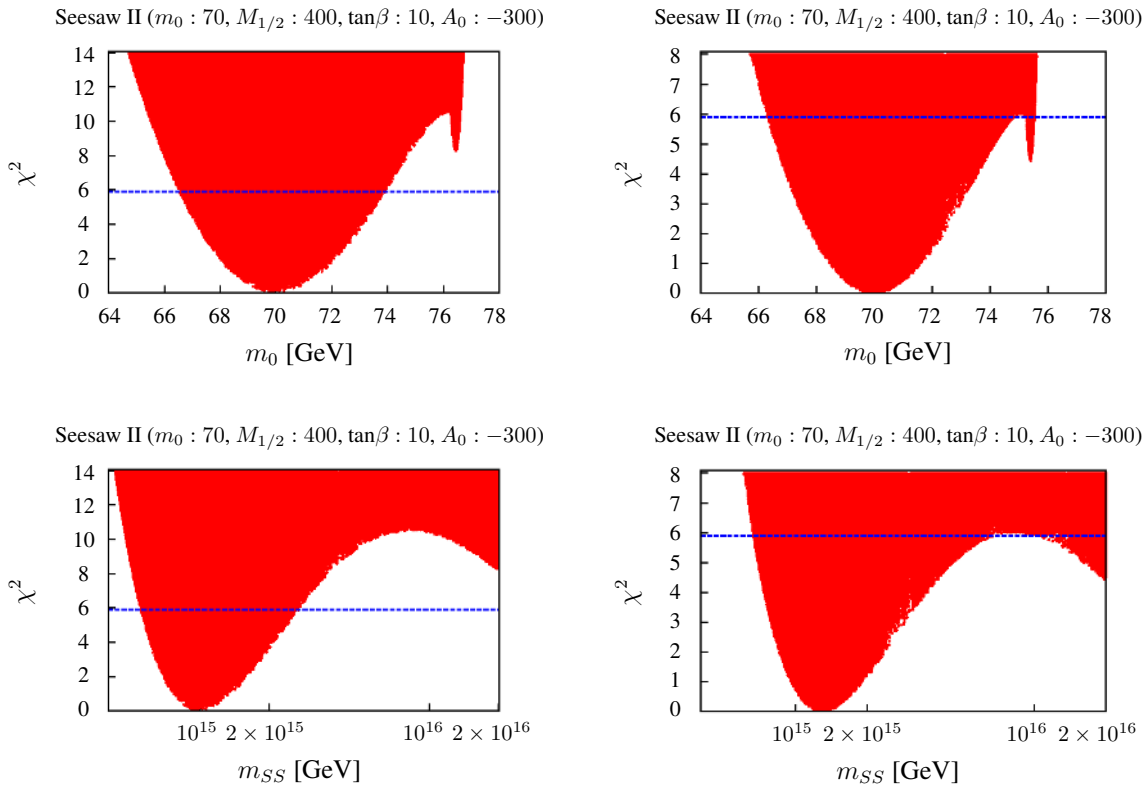

Figure 3.12: χ^2 distributions of the random walk for MSP-1 and Seesaw type II. The dashed line indicates a χ^2 of 5.89. Recall that 5.89 corresponds to a 1σ confidence level for five free parameters. The plots show the χ^2 distributions for $m_{SS} = 1 \times 10^{15}$ GeV (left) and $m_{SS} = 1.3 \times 10^{15}$ GeV (right).

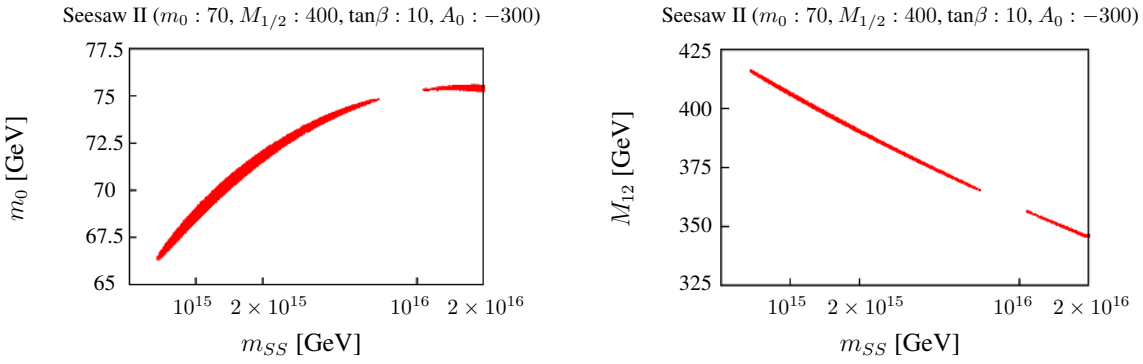

Figure 3.13: Allowed ranges of parameters m_{SS}, m_0 and $M_{1/2}$ for MSP-1 and type-II seesaw with input $m_{SS} = 1.3 \times 10^{15}$ GeV. Two separate solutions appear, one fake but acceptable minimum is at $m_{SS} = M_G$.

show a large range of m_{SS} between $[10^{12}, 10^{15}]$ GeV. Lower values of m_{SS} are in principle possible, but show no new features. Larger values of m_{SS} can not fit current neutrino data. Error bars on all parameters increase with increasing values of m_{SS}, and for values of m_{SS} larger than (roughly) $(1-2)\times10^{15}$ GeV the error $\Delta(m_{SS})$ is so large that the type-II can no longer be distinguished from pCMSSM at the 1-σ level, given the ILC+LHC observables with our "standard" errors. $\Delta(m_{SS})$ decreases very rapidly as a function of m_{SS} and for values of $m_{SS} = 6.5\times10^{14}$ (4.5×10^{14}) pCMSSM and type-II can be formally distinguished by more than 3 (5) standard deviations.

Also the errors $\Delta(m_0)$ and $\Delta(M_{1/2})$ do show dependence on m_{SS}, especially at larger values of m_{SS}. Again, the reason for this dependence is found in the strong correlation among those three parameters, as discussed above. The error $\Delta(\tan\beta)$ (and to some extend $\Delta(A_0)$), on the other hand, shows less dependence on m_{SS}. This is explained by the fact that the lightest Higgs mass, m_{h^0}, shows very little dependence on the seesaw scale. The slight dependence of $\Delta(A_0)$ on m_{SS} is due to the lightest stop mass. For simplicity in all following plots we show only the 1 σ allowed regions.

Fig. (3.15) shows two more examples of $\Delta(m_{SS})$ as a function of m_{SS}. Here results for the points MSP-2 and MSP-3 are shown for type-II seesaw. Only $\Delta(m_{SS})$ as a function of m_{SS} is shown. We do not repeat the plots for the other parameters because they are qualitatively very similar to the case shown in fig. (3.14). As the plots show results for MSP-2 and MSP-3 are similar to MSP-1. Values of m_{SS} below roughly $m_{SS} \sim 10^{15}$ GeV are inconsistent with pCMSSM. This implies that for the ILC errors as estimated in [156] and [157] a combined ILC+LHC analysis should be able to distinguish pCMSSM from type-II seesaw for nearly all values of m_{SS} relevant for neutrino data. We stress that this conclusion is correct only for those CMSSM parameters for which (both left- and right-) sleptons and the lightest neutralino are kinematically accessible at the ILC.

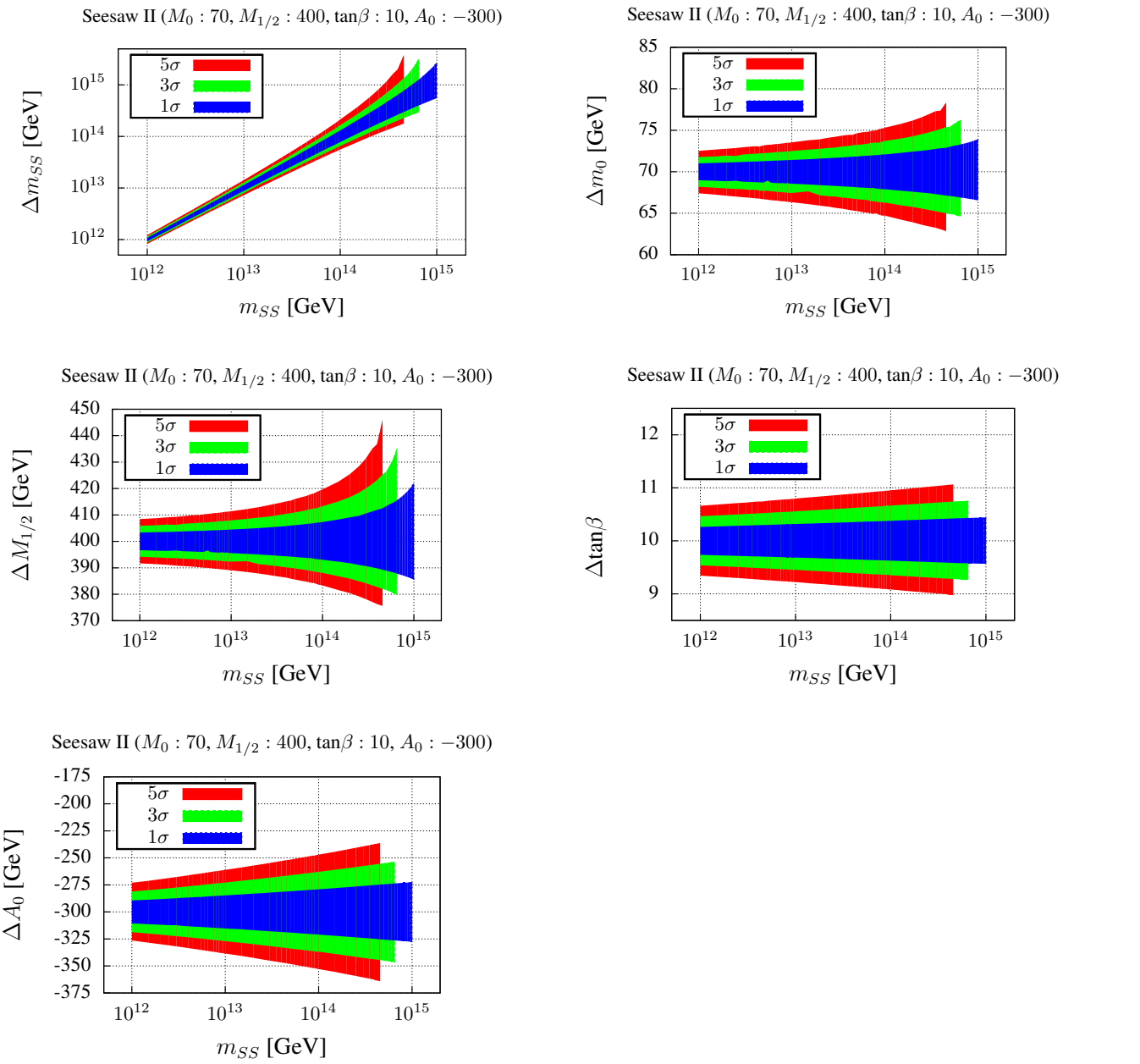

Figure 3.14: Error of m_{SS}, m_0, $M_{1/2}$, $tan\beta$ and A_0 against m_{SS} for all 5 parameters freely varied. For these plots we used the LHC and ILC observables. The chosen values for m_{SS}, m_0, $M_{1/2}$, $tan\beta$ and A_0 are the values for MSP-1. The plots show the results for seesaw type II where we used a 1σ, 3σ and 5σ c.l..

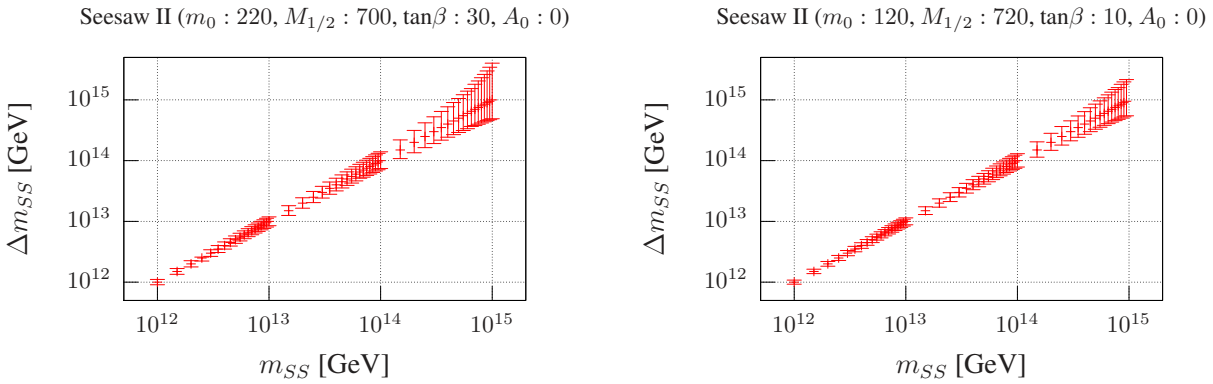

Figure 3.15: Error of m_{SS}, against m_{SS} for 5 free parameters. For these plots we used the LHC and ILC observables. The chosen values of parameters correspond to MSP-2 (left) and MSP-3 (right). The plots show the results for Seesaw type-II.

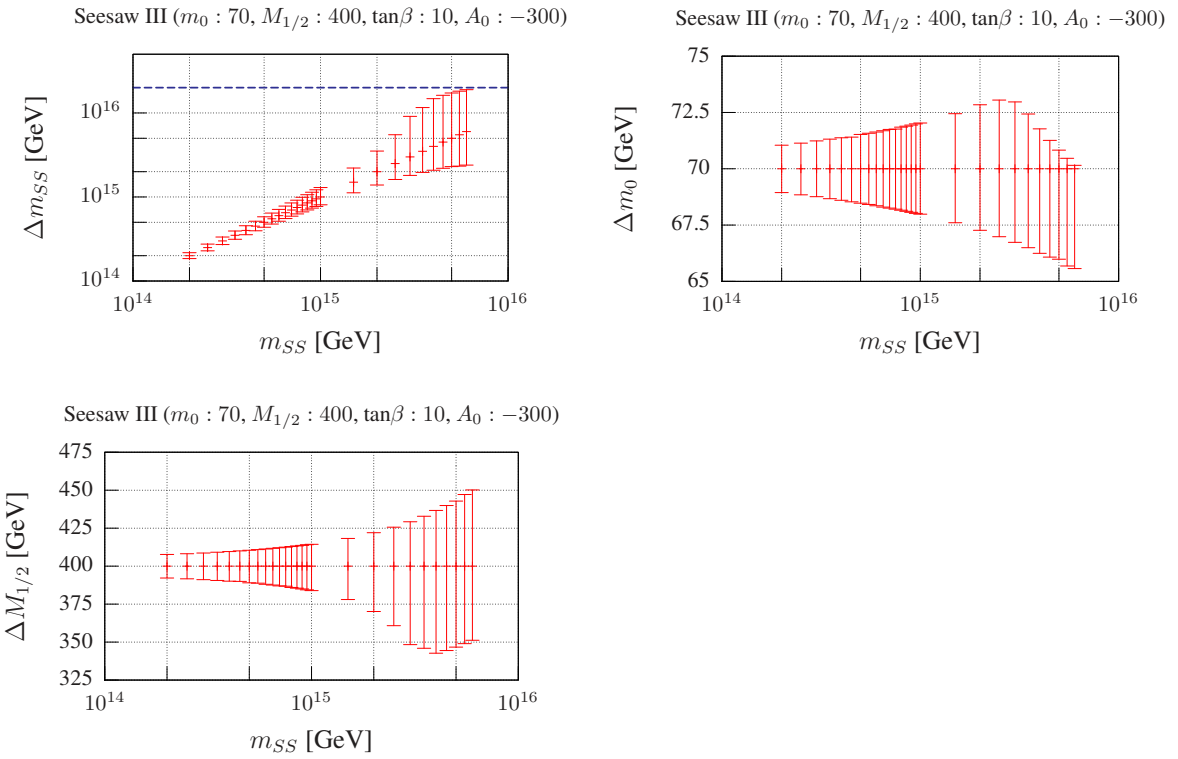

Figure 3.16: Error of m_{SS}, m_0 and $M_{1/2}$ against m_{SS} for 5 parameters varied freely. For these plots we used the LHC and ILC observables. The chosen values for m_{SS}, m_0, $M_{1/2}$, $tan\beta$ and A_0 are the values according to MSP-1. The plots show the results for seesaw type III.

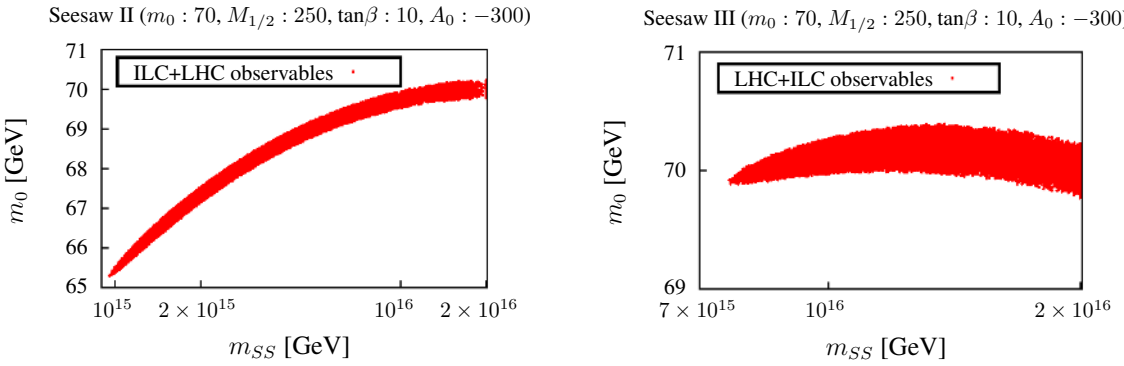

Figure 3.17: The plots show random walks in which as starting point SPS1a' was chosen. For the parameter fit we used CMSSM plus seesaw type-II and III, respectively. The runs take into account LHC and ILC observables.

Up to now we have shown only results for seesaw type-II. Fig. (3.16) shows a corresponding calculation for type-III and CMSSM parameters as in MSP-1. Again, MSP-2 and MSP-3 show similar behaviour and we do not repeat the plots for these points. Again, the scale of m_{SS} is different from the case of type-II. Since SUSY masses show a stronger dependence on m_{SS} in type-III than in type-II, larger values of m_{SS} can be distinguished from pCMSSM in this case. In the examples shown in the figure all values of m_{SS} below roughly $m_{SS} \sim 5 - 6 \times 10^{15}$ GeV can be distinguished from pCMSSM with more than 1 σ c.l. Recall that in type-III one expects $m_{SS} \lesssim 8 \times 10^{14}$ in order to explain neutrino data. Such "low" values of m_{SS} differ from pCMSSM in the fits by many standard deviations.

Errors on m_0 are similar to the values observed for type-II, while $\Delta(M_{1/2})$ is larger in type-III. The correlation between m_0, $M_{1/2}$ and m_{SS}, discussed above for type-II, is also present in type-III and with an even larger correlation between $M_{1/2}$ and m_{SS} in this case. The CMSSM solution does not show up explicitly as a second separate minimum, but deforms the χ^2 distributions, thus cutting the allowed ranges of m_0 and $M_{1/2}$.

Up to now we have always used a seesaw spectrum as input. One can also ask the opposite question: Can a pCMSSM point mimic a seesaw spectrum? An example of such a calculation is shown in fig. (3.17). In this figure we show the allowed ranges for m_{SS} and m_0 for CMSSM parameters as in SPS1a' for type-II (left) and type-III (right). As one can see m_{SS} as low as $m_{SS} \sim 10^{15}$ GeV ($m_{SS} \sim 7 \times 10^{15}$ GeV) are allowed at 1 σ c.l. for type-II (type-III) fits. Also note that $\Delta(m_0)$ is much larger than in a pCMSSM fit, due again to the observed correlation among parameters. The results shown in fig. (3.17) are consistent with the results discussed above, when a seesaw spectrum is used as input: m_{SS} compatible with M_G is reached at a very similar value of m_{SS}.

Finally we note, that distinguishing type-II from type-III requires extremely high precision, since they differ only at 2-loop order. The reason is that for 1-loop RGEs one can always cancel the shifts in the coefficient of the beta-functions by a rescaling of m_{SS}. We have checked this numerically.

Closing this subsection we note that all results shown above have been obtained for the full 2-loop calculation. We have repeated the exercise in several cases using 1-loop RGEs only. As a general result, due to the weaker running of 1-loop RGEs, differences between pCMSSM and seesaw are slightly smaller, leading to slightly larger errors on the parameters. For the case of the ILC+LHC analysis, however, differences between both calculations are rather small, with errors in parameters typically increasing in the order of (10-30) % when going from a 2-loop to a 1-loop calculation.

3.2.2.4. LHC only

In this subsection we discuss the results for an analysis using only LHC measurements. At the LHC observables do not measure SUSY masses directly. Instead, observables measure either mass differences or, in case of the edge variables, combinations of mass squared differences. Also one expects that LHC measurements will be much less precise than what can be done in case of the ILC. As a result the χ^2 distributions for an LHC-only analysis show more complicated features than for the case of LHC+ILC. Especially it should be noted that in some cases we do not have a sufficiently large number of well determined observables and fake minima can appear, which will lead to sometimes rather large error bars on parameters, as discussed below.

Fig. (3.18) shows error bars on m_{SS}, m_0, $M_{1/2}$ against m_{SS} for the point MSP-3 and seesaw type-II, again for all 5 parameters varied freely. Note the change in the scale for m_{SS}, the largest value shown is $m_{SS} = 10^{14}$ GeV. For larger values of m_{SS} type-II seesaw can no longer be distinguished in this fit from pCMSSM with at least 1 σ c.l. Note, however, that $\Delta(m_{SS})$ decreases very rapidly for decreasing values of m_{SS} and for values of m_{SS} below $m_{SS} \sim$ (few) 10^{13} GeV pCMSSM and type-II are formally different by several standard deviations.

The figure shows also that $\Delta(m_0)$ and $\Delta(M_{1/2})$ are much larger for the case of using only LHC observables than in the combined ILC+LHC analysis, as expected. Errors on m_0 and $M_{1/2}$ decrease in general with decreasing m_{SS}. The increase in $\Delta(m_0)$ and $\Delta(M_{1/2})$ around $m_{SS} \sim 7 \times 10^{12}$ GeV is due to the appearance of a fake side-minimum. Such fake minima appear only for certain ranges of m_{SS}. Depending on which side of the real minimum they appear they can lead to an asymmetric increase of the errors as observed in this figure.

Fig. (3.19) shows an example of a corresponding fit for type-III. Again, $\Delta(m_0)$ and $\Delta(M_{1/2})$ and $\Delta(m_{SS})$ are shown as a function of m_{SS} for MSP-3. Note that other points show qualitatively similar behaviour and that the range shown for m_{SS} is comparatively small. Values of m_{SS} larger than $m_{SS} \sim 5 \times 10^{14}$ are 1 σ c.l. consistent with pCMSSM. Since $m_{SS} \lesssim 8 \times 10^{14}$ to explain neutrino data, LHC-only can probe interesting parts of the parameter space, but certainly will not be able to cover all possible values of m_{SS} - unless LHC errors on mass measurements can be improved

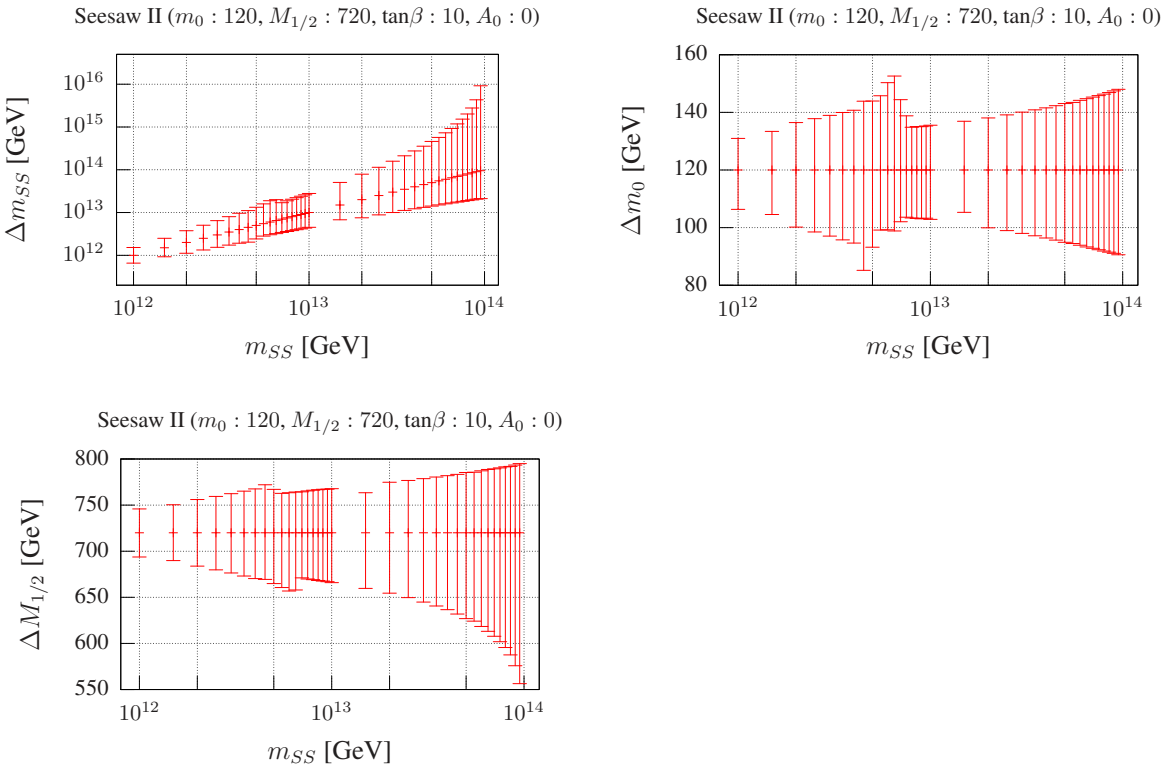

Figure 3.18: Error of m_{SS}, m_0, $M_{1/2}$, $tan\beta$ and A_0 against m_{SS} for m_{SS}, m_0, $M_{1/2}$, $tan\beta$ and A_0 varied. For these plots we used only the LHC observables. The chosen values for m_{SS}, m_0, $M_{1/2}$, $tan\beta$ and A_0 are the values according to MSP-3. The plots show the results for seesaw type II.

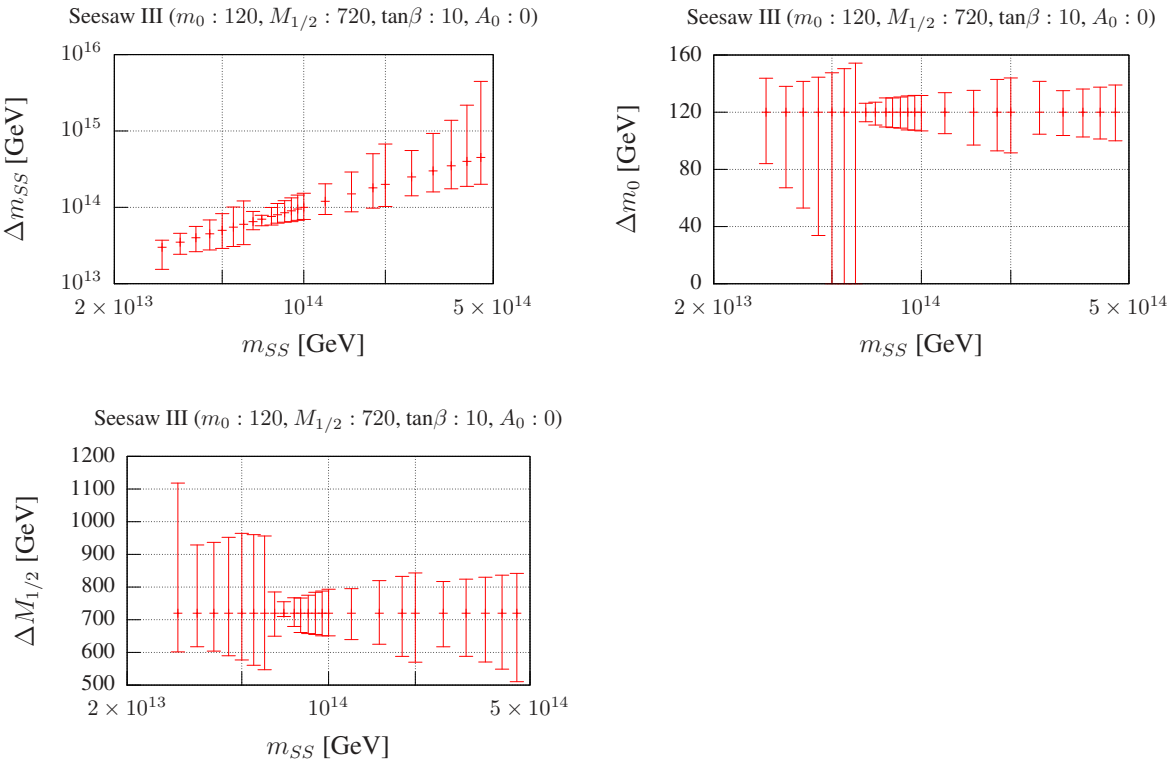

Figure 3.19: Error of m_{SS}, m_0, $M_{1/2}$ against m_{SS} for 5 parameters varied freely. For these plots we used only the LHC observables. The chosen values for m_{SS}, m_0, $M_{1/2}$, $tan\beta$ and A_0 are the values according to MSP-3. The plots show the results for seesaw type III.

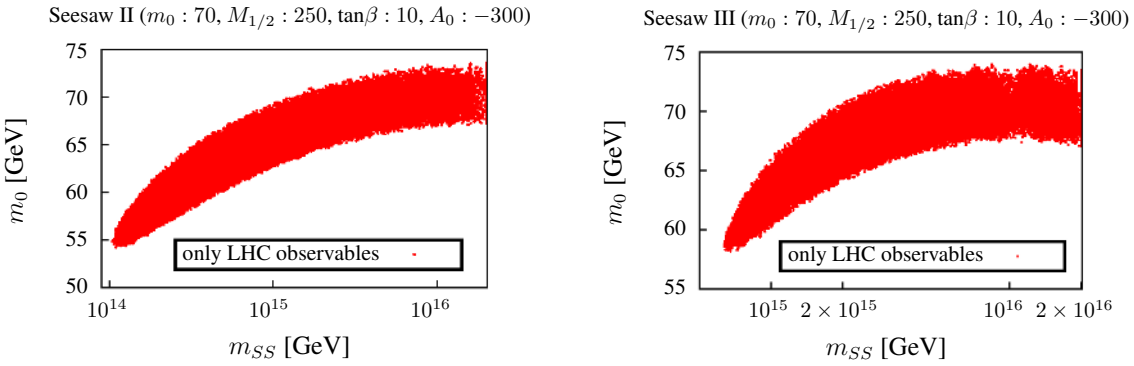

Figure 3.20: The plots show the result of a random walk in which as a starting point SPS1a' was chosen. For the parameter fit we used CMSSM plus seesaw type II and III, respectively. The runs were made for LHC observables enabled only.

compared to expectations by considerable factors.

For decreasing m_{SS} errors again decrease in general. There are two exceptions from this general rule in this plot. First, errors increase around $m_{SS} \sim 2{\times}10^{14}$ GeV. This is again due to the appearance of a fake side minimum, which slowly disappears again when going towards smaller values of m_{SS}. The large increase in the error bars around $m_{SS} \sim 6 \times 10^{13}$ GeV is due to the fact that for smaller values of m_{SS} in this calculation χ_2^0 is lighter than $\tilde{e}_R$, i.e. the edges variables are lost completely. With only a few observables in the fit, all based on mass differences, m_0 and $M_{1/2}$ can hardly be fixed at all. The dramatic increase of the error bars of m_0 can be understood easily from Eq. (3.21). As this equation shows the sfermion masses behave approximately like $m_{\tilde{f}}^2 = m_0^2 + aM_{1/2}^2$. When all edges are lost the remaining LHC observables can be fitted by varying m_{SS} and $M_{1/2}$ only.

Finally we have calculated the allowed parameter space in a seesaw fit when the true input point is pCMSSM. Two examples are shown in Fig. (3.20). The CMSSM parameters are for SPS1a' and type-II (type-III) seesaw is shown to the left (right). The allowed regions are much larger than in the combined ILC+LHC analysis, compared to the discussion in the last subsections. For type-II (type-III) values of m_{SS} as low as $m_{SS} \lesssim 10^{14}$ GeV ($m_{SS} \lesssim 6 \times 10^{14}$ GeV) are allowed at the 1 σ level. This is similar - and consistent - with the results discussed above for the opposite fit.

In summary mass measurements from the LHC only should be able to distinguish between pCMSSM and type-II (type-III) seesaw for seesaw scales below roughly $m_{SS} \lesssim 10^{14}$ GeV ($m_{SS} \lesssim 6 \times 10^{14}$ GeV). This conclusion depends critically on the possibility to measure accurately several observables, as we are going to discuss next.

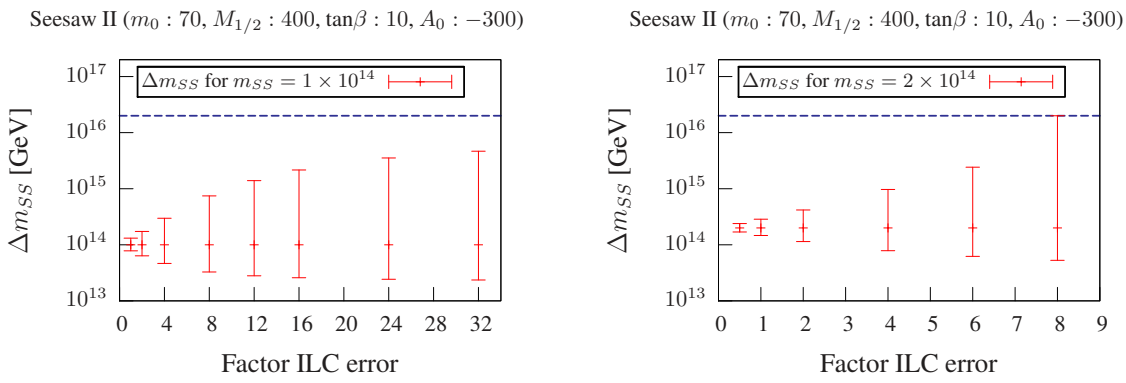

Figure 3.21: Error of m_{SS} with respect to the error of the ILC observables, f_{ILC}.

3.2.2.5. Required accuracies on mass measurements and $\Delta(m_{SS})$

All our results shown above crucially depend on the size of the expected error bars for the different observables. In this subsection we therefore discuss in some detail: (a) Which are the most important observables in our fits? And, (b) How accurately do we need to measure them to distinguish pCMSSM from seesaw for a given, fixed value of m_{SS}. Again we will discuss the ILC+LHC case first.

Fig. (3.21) shows $\Delta(m_{SS})$ for the points MSP-1 for two choices of m_{SS}. $\Delta(m_{SS})$ is shown as a function of the error of the ILC mass measurements. According to [157] it is expected that the ILC can measure SUSY masses of χ_i^0 and $\tilde{l}$ states kinematically accessible with errors of the order (0.5-2) per-mille. We define a common factor f_{ILC} and multiply all relative errors given in table 6 of [157] with this common factor. $\Delta(m_{SS})$ is then shown as a function of this factor in fig. (3.21). Note that in this calculation we keep all LHC errors unchanged at their "standard values".

As fig. (3.21) to the left shows, $\Delta(m_{SS})$ increases with the assumed errors of the ILC measurements. However, for MSP-1 and $m_{SS} = 10^{14}$ GeV, LHC measurements alone are sufficient to distinguish type-II from pCMSSM. Thus, error bars on m_{SS} hardly increase going from $f_{ILC} = 24$ to $f_{ILC} = 32$. This means that ILC data dominate the fit until errors are about one order of magnitude larger than estimated in [157], for larger ILC errors LHC measurements become more important for this choice of m_{SS}.

The situation is quite different for $m_{SS} = 2 \times 10^{14}$ GeV, see fig. (3.21) right. While $f_{ILC} = 6$ still allows to distinguish between pCMSSM and type-II, for $f_{ILC} = 8$, $\Delta(m_{SS})$ becomes to large to differentiate between type-II and pCMSSM. The required accuracy of measurements of SUSY masses at the ILC is therefore a strong function of m_{SS} itself. Errors of the order (1-2) percent are in general tolerable for seesaw scales below $m_{SS} = 10^{14}$ GeV, while per-mille level measurements are required in the interval $[10^{14}, 10^{15}]$ GeV. We note that other SUSY points behave very similar and that for type-III correspondingly larger errors are tolerable.

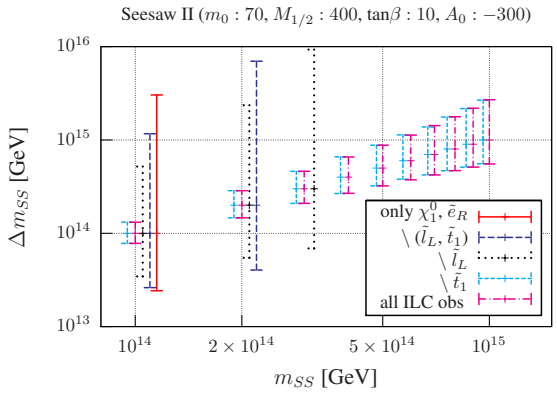

Figure 3.22: In this plot the errors of m_{SS} with respect to m_{SS} are shown. The different lines belong to different runs where different combinations of ILC observables were switched off. The different lines belong in each case to the same m_{SS} values but were a bit to be able to distinguish them. The real m_{SS} value is the value of the pink error bars which correspond to the run for all ILC observables enabled.

Fig. (3.21) treats all ILC observables equally. An interesting question to ask is, of course, which ILC observables are the most important ones for our analysis. Fig. (3.22) provides the answer. Again for the point MSP-1 and for seesaw type-II we show $\Delta(m_{SS})$ as a function of m_{SS} for different calculations taking into account different observables. We have kept all LHC observables "on" at their standard errors. "All ILC obs" is the standard fit, taking into account all kinematically accessible mass measurements with their original errors from [157]. We then switched off by hand completely the contributions from different observables. Switching off the measurement of the mass of $\tilde{t}_1$ hardly changes the result. On the other hand, it can be seen that measuring left-slepton masses is highly important. Error bars increase sizeably if this observable is not taken into account and while a set of measurements with all observables can distinguish pCMSSM from type-II all the way up to $m_{SS} = 10^{15}$ GeV, without the accurate measurement of $m_{\tilde{l}_L}$ all values of $m_{SS} \gtrsim 4 \times 10^{14}$ GeV are compatible with pCMSSM at the 1 σ level. The relative importance of $\tilde{l}_L$ despite its larger error stems from the fact that $m_{\tilde{l}_R}$ has very little sensitivity to m_{SS}, see fig. (3.8).

We now turn to the discussion of LHC errors. In this case we do not use any input from the ILC. Fig. (3.23) shows $\Delta(m_{SS})$ as a function of the assumed error. Two observables are shown: to the left as a function of $\Delta_{\tilde{g}\tilde{b}_i}$ and to the right as a function of the edge variables. Note that for SPS1a the LHC error for $\Delta_{\tilde{g}\tilde{b}_1}$ is estimated to be ~ 3.5 %, while $\Delta(m_{ll}^{\text{edge}})$ should be measured to an accuracy of 0.17 %. Note that, while $\Delta(m_{ll}^{\text{edge}})$ can possibly be accurately measured in wide ranges of CMSSM parameter space, the accuracy with which $\Delta_{\tilde{g}\tilde{b}_i}$ can be measured is far less certain. Both smaller and much larger errors on this quantity have been found in different study points, see [156].

The figure shows that for $m_{SS} = 2 \times 10^{13}$ a 7 % error on $\Delta_{\tilde{g}\tilde{b}_1}$ (which corresponds to a factor of

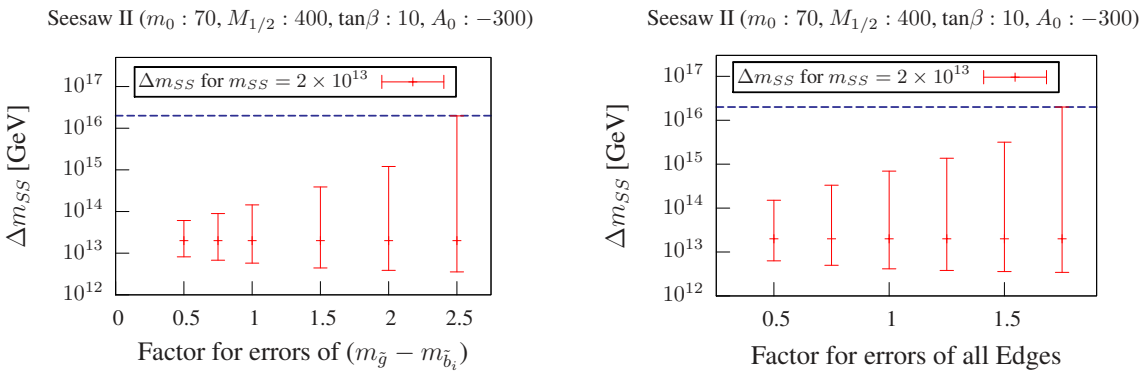

Figure 3.23: Error of m_{SS} with respect to the error of $(m_{\tilde{g}} - m_{\tilde{b}_1})$ and $(m_{ll})^{\text{edge}}$. According to [156] the error on $(m_{\tilde{g}} - m_{\tilde{b}_1})$ is expected to be $\sim 3.5\%$ and the error of $(m_{ll})^{\text{edge}}$ is estimated as $\sim 0.17\%$. Note that we also changed the error of $(m_{\tilde{g}} - m_{\tilde{b}_2})$, accordingly.

2 in the plot) is sufficient to distinguish between pCMSSM and type-II, while an error of 9 % on this quantity is not sufficient. Again, the maximum value of this error which still allows to distinguish between type-II and pCMSSM is a strong function of the (unknown) m_{SS} itself. However, we have found that always $\Delta_{\tilde{g}\tilde{b}_1}$ is a critical input observable for our analysis. [15] The importance of $\Delta_{\tilde{g}\tilde{b}_1}$ can be understood from Fig. (3.9) and (3.10): coloured sparticle masses depend much more strongly on m_{SS} than masses of, for example, sleptons. Thus, despite the larger relative error on $\Delta_{\tilde{g}\tilde{b}_1}$ compared to the edge variables,it is nearly as important as demonstrated in fig. (3.23) to the right.

Fig. (3.24) shows the results of different runs, where we have switched off artificially different combinations of observables. As noted above, $\Delta_{\tilde{g}\tilde{b}_1}$ and the edges are the most important observables for fixing $\Delta(m_{SS})$. However, the Higgs mass measurement is not negligible, despite the fact that $\Delta(m_{SS})$ does not increase much in the figure, when m_{h^0} is switched off. This importance lies in the fact that without m_{h^0} the largest value of m_{SS} not compatible with M_G is 2×10^{13} GeV, compared to $m_{SS} = 10^{14}$ GeV for m_{h^0} switched on.

We do not repeat the discussion for type-III seesaw. Results are very similar qualitatively, but again larger values of m_{SS} can be tested for the same errors on the observables.

Finally, we turn to the question of Yukawa couplings. Fig. (3.25) shows again $\Delta(m_{SS})$ as a function of m_{SS} for two different calculations: (i) a calculation with triplet Yukawa couplings negligibly small (all $(Y_T)_{ij} \sim \mathcal{O}(10^{-4})$) and (ii) a calculation in which Y_T has been fitted to give the atmospheric and solar neutrino mass squareds at their best fit values with neutrino angles taking tri-bimaximal values. As can be seen, differences between both calculations become negligible below roughly $m_{SS} = 10^{14}$ GeV, as expected. For larger values of m_{SS} correctly fitting the Yukawas leads to slightly smaller errors on m_{SS}. This can be understood, since for finite Yukawas SUSY masses

[15] We also consider $\Delta_{\tilde{g}\tilde{b}_2}$, which, however, is less important due to its larger error.

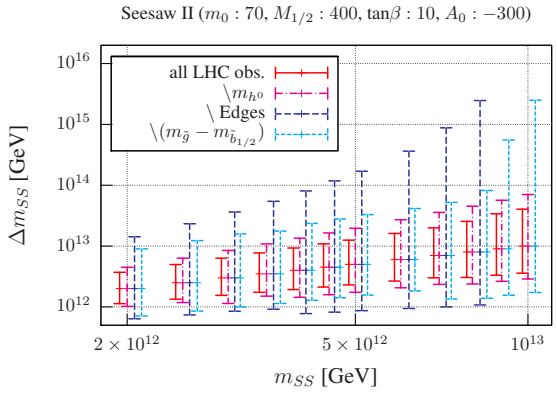

Figure 3.24: In this plot the errors of m_{SS} with respect to m_{SS} are shown. The different lines belong to different runs at which we switched off different combinations of LHC observables. The different lines belong in each case to the same m_{SS} values but we separated them in the plot a bit to be able to distinguish them. The real m_{SS} value is the value of the pink error bars that correspond to the run in which the Higgs mass measurement is disabled.

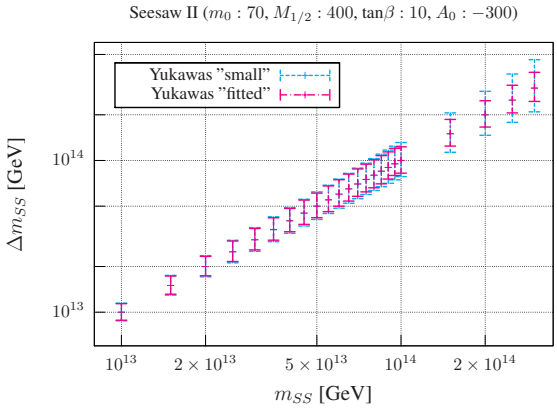

Figure 3.25: In this plot the errors of m_{SS} with respect to m_{SS} are shown. The different lines belong to two different runs at which we set the Yukawa couplings to very small values ($\sim 10^{-4}$) in the first run and in the second one we fitted the Yukawa couplings to neutrino data and calculated the error with the fitted values.

change slightly stronger than for infinitesimal values of Y_T, making the fit easier. Note, however, that we have not scanned over all allowed range of Y_T in this calculation. In a complete 14 parameter χ^2 fit errors might be larger. Note also, we can not find any good neutrino solution for m_{SS} larger than $m_{SS} = 6 \times 10^{14}$, since in this calculation we have chosen for the coupling $\lambda_2 = 0.5$. In conclusion, a full fit including Yukawa couplings will be necessary only if signs of $m_{SS} \gtrsim 10^{14}$ GeV have been found in SUSY mass data.

3.2.3. Conclusions and discussion

In this section we have studied the possibility to obtain indirect information on the seesaw scale from SUSY mass measurements at future colliders in case of seesaw type II and III. Assuming CMSSM boundary conditions and taking error estimates as forecasted by study groups we find that a combination of LHC and ILC measurements should be able to distinguish pure CMSSM from CMSSM plus either type-II or type-III seesaw for nearly any relevant values of the seesaw scale, if (a) at least χ_1^0, $\tilde{e}_R/\ \tilde{\mu}_R$ and $\tilde{e}_L/\ \tilde{\mu}_L$ are kinemetically accessible at the ILC and (b) the LHC can measure $m_{\tilde{g}} - m_{\tilde{b}_1}$ and the edge observables accurately. We always assume that the lightest Higgs has been found. The degree of confidence with which pCMSSM can be distinguished from CMSSM plus seesaw depends sensitively on the actual value of the seesaw scale. At the "critical" value of $m_{SS} \sim 10^{15}$, beyond which neutrino data can no longer be explained with Yukawas smaller than 1, the difference between type-II + CMSSM and pCMSSM could be as low as only 1 σ c.l. However, the difference between pCMSSM and CMSSM + seesaw rises very sharply with decreasing m_{SS} and formally more than 5 σ c.l. could be reached already at $(5-6) \times 10^{14}$ for type-II. Differences between pCMSSM and CMSSM plus type-III are always found to be larger than for CMSSM plus type-II for the same value of m_{SS}.

As expected, the future is not as bright, if we take into account only LHC data. We found that one can distinguish pure CMSSM and CMSSM plus seesaw in some favourable parts of parameter space. However, recent LHC data was not included in our analysis. Already with the first published results from CMS and ATLAS the SUSY parameter space used for this work was excluded (see subsection 2.3.4). With recent LHC data it has become unlikely that one can distinguish pure CMSSM and CMSSM plus seesaw. Nevertheless, it is important to keep in mind that the lower the real value of the seesaw scale m_{SS} is, the easier it becomes to distinguish pure CMSSM from CMSSM plus seesaw. Therefore, at the lower limit of m_{SS} may remain the possibility to see deviations from a seesaw mechanism in the SUSY spectrum but with much less accuracy than presented in this work. To evaluate in which regions of the parameter space our analysis is possible we have discussed the most important measurements for the LHC and the ILC and the relative errors with which these observables need to be measured. In our analysis we used exclusively CMSSM SUSY breaking boundary conditions, but other, more involved SUSY breaking schemes with more free parameters could, in principle, be "tested" in a similar way.

Of course, the analysis presented in this paper is far from being complete. If SUSY is found at the LHC, one would need to redo our calculations with real data. However, the experimentalist would not, as we have always assumed in our fits, know the real values of the parameters. We have tried for a few points, whether the correct input parameters can be retrieved for arbitrary starting points in our MC random walk procedure and - given enough CPU-time - are able to find the correct minimum. However, our "observables" are theoretically calculated observables and thus perfect in contrast to real data which are expected to scatter around the true values and might show tension between different observables. Thus, finding the correct minimum in real data might be more difficult. Moreover, the underlying model will not be known a priori and, thus, χ^2_{Min} for different models need to be calculated and compared.

4

Higgs, LHC and extended gauge groups

Within the MSSM the gauge couplings unify nearly perfectly around an energy scale of approximately $m_G \simeq 2 \times 10^{16}$ GeV, if SUSY particles exist with masses of the order of $\mathcal{O}(1)$ TeV. Extending the MSSM with non-singlet superfields tends to destroy this attractive feature, unless (a) the additional fields come in complete $SU(5)$ multiplets or (b) the standard model gauge group is extended too. Here we study a model in which the SM group is enlarged to $SU(3)_c \times SU(2)_L \times U(1)_{B-L} \times U(1)_R$. It is a variant of the models first proposed in [97] and later discussed in more detail in [98].

Our main motivation for studying this model can be summarized as: (i) It unifies, in the same way the MSSM does, even if the scale of $U(1)_{B-L} \times U(1)_R$ breaking is as low as the electro-weak scale; (ii) it can be easily embedded into an $SO(10)$ grand unified theory; (iii) it has the right ingredients to explain neutrino masses (and angles) by either an inverse [123] or a linear [21; 22] seesaw; (iv) it allows for Higgs masses significantly larger than the MSSM without the need for a very heavy SUSY spectrum [3] and (v) it potentially leads to rich phenomenology at the LHC.

As already discussed in chapter 2 both ATLAS [191] and CMS [192] announced the discovery of a new boson which might be the SM Higgs boson with a mass of roughly $m_h \sim 125$ GeV. This result, perhaps unsurprisingly, has triggered an avalanche of papers studying the impact of such a relatively hefty Higgs on the supersymmetric parameter space [193; 194; 195; 196; 197; 198; 199; 200; 201; 8; 202; 203; 204; 205; 206; 207; 208; 209; 210; 211; 212; 213; 214; 215; 216; 217; 218; 219; 220; 221; 222; 223; 224; 225; 226]. The general consensus seems to be, that the MSSM can generate $m_h \sim 125$ GeV only if squarks and gluinos have masses in the multi-TeV range. While this is, of course, perfectly consistent with the lower bounds on SUSY masses obtained from $E_T \!\!\!/$ searches at the LHC [227; 228], such a heavy spectrum could make it quite difficult indeed for the LHC to find direct signals for SUSY.

There are, of course, several possibilities to circumvent this conclusion. First of all, it is well-known that the loop corrections to h^0 are dominated by the top quark-squark loops. Thus, little or no constraints on sleptons and on squarks of the first two generations can in fact be derived

from Higgs mass measurements, once the assumption of universal boundary conditions for the soft SUSY parameters is abandoned. Second, in the next-to-minimal SSM (NMSSM) the h^0 can be heavier than in the MSSM due to the presence of new F-terms from the additional singlet Higgs [8; 226], especially in models with non-universal boundary conditions for the (soft) Higgs mass terms [208] or in the generalized NMSSM [209; 210]. And, third, in models with an extended gauge group additional D-terms contribute to the Higgs mass matrices, relaxing the MSSM upper limit considerably [229; 230; 231; 232; 233]. This latter possibility is the case we have studied in a previous paper [3] using the minimal $U(1)_{B-L} \times U(1)_R$ models of [97]. In this chapter we extend the analysis of [3], including both Higgs and SUSY phenomenology.

Due to the extended gauge structure the model necessarily has more Higgses than the MSSM. Near D-flatness of the $U(1)_{B-L} \times U(1)_R$ breaking then results in one additional light Higgs, h^0_{BLR} [3]. Mixing between the MSSM $h^0 \equiv h^0_L$ and h^0_{BLR} enhances the mass of the mostly MSSM Higgs and, potentially, affects its decays. This is reminiscent to the situation in the NMSSM, where an additional light and mostly singlet Higgs state seems to be preferred [8; 226] if the signals found by ATLAS [191] and CMS [192] are indeed due to a 125 GeV Higgs.

The MSSM-like h^0_L in our model can have some exotic decays. For example, the h^0_L will decay to two lighter Higgses, if kinematically possible, although this decay can never be dominant due to constraints coming from LEP. The model also includes right-handed neutrinos with electro-weak scale masses and there is a small but interesting part in parameter space where $m_{Z^0} \leq m_{\nu_R} \leq m_{h^0_L}$, where the Higgs decays to two neutrinos. These decays always lead to one light and one heavy neutrino, with the latter decaying promptly to either $W^{\pm} l^{\mp}$ or $Z^0 \nu$. (Mostly right) sneutrinos can be lighter than the h^0_L, in which case the Higgs can have invisible decays.

The SUSY spectrum of the model is also richer than the MSSM: It has seven neutralinos and nine sneutrino states. These additional sneutrinos can easily be the lightest supersymmetric particle (LSP) and thus change all the constraints on SUSY parameter space, usually derived from the requirement that the neutralino be a good dark matter candidate with the correct relic density [180][1]. Even though the lightest sneutrino can also be the LSP in the MSSM, direct detection experiments have ruled out this possibility a long time ago [119]. In SUSY decays, within the MSSM right squarks decay directly to the bino-like neutralino, leading to the standard missing momentum signature of supersymmetry. Due to the extended gauge group, right squarks can decay also to heavier neutralinos, leading to longer decay chains and potentially to multiple lepton edges[2]. Decays of the heavier neutralinos also produce Higgses, both the h^0_L and the h^0_{BLR} appear, with ratios depending on the right higgsino content of the neutralinos in the decay chains.

The rest of this chapter is organized as follows. In the next section we discuss the setup of

[1] Also for the case of a neutralino LSP, constraints on the SUSY parameter space from dark matter can change in case the right Higgsino is light.

[2] Longer SUSY cascades from larger number of neutralino states have also been discussed in [234; 235].

the model, its particle content, superpotential and soft terms and the symmetry breaking. The phenomenologically most interesting mass matrices of the spectrum are given in section 4.2 where we also discuss numerical results on the SUSY and Higgs mass eigenstates. Here, we focus on Higgs and slepton/sneutrino masses, which are the phenomenologically most interesting. We will discuss in detail how far the lightest Higgs mass can be pushed to larger values compared to MSSM expectations. In section 4.3 we define some benchmark points for the model and discuss their phenomenologically most interesting decay chains. We then close with a short summary. In the appendix we give mass matrices not presented in the text, formulas for the 1-loop corrections in the Higgs sector and more information about the calculation of the RGEs, including anomalous dimensions as well as the 1-loop β functions for gauge couplings and gauginos.

4.1. The model: $SU(3)_c \times SU(2)_L \times U(1)_{B-L} \times U(1)_R$

In this section we present the particle content of the model, its superpotential and discuss the symmetry breaking. We consider the simplest model based on the gauge group $SU(3)_c \times SU(2)_L \times U(1)_R \times U(1)_{B-L}$. We will call this the mBLR model below. As has been shown in [97] it can emerge as the low-energy limit of a certain class of $SO(10)$ GUTs broken along the "minimal" left-right symmetric chain [236; 237]

$$\begin{aligned} SO(10) &\rightarrow SU(3)_c \times SU(2)_L \times SU(2)_R \times U(1)_{B-L} \\ &\rightarrow SU(3)_c \times SU(2)_L \times U(1)_R \times U(1)_{B-L}. \end{aligned} \tag{4.1}$$

The main virtue of this setting is that an MSSM-like gauge coupling unification is achieved with a sliding $U(1)_R \times U(1)_{B-L}$ breaking scale, i.e. this last stage can stretch down even to the electroweak scale. Different from the previous works [97; 98], we assume that the first two breaking steps down to $U(1)_R \times U(1)_{B-L}$ happen both at (or sufficiently close to) the GUT scale. This assumption is used only for simplifying our setup, it does not lead to any interesting changes in phenomenology.

4.1.1. Particle content, superpotential and soft terms

The transformation properties of all matter and Higgs superfields of the model are summarized in table 4.1. Apart from the MSSM fields, in the matter sector we have $\hat{\nu^c}$ and $\hat{S}$. The former are necessary in the extended gauge group for anomaly cancellation,[3] while the fields $\hat{S}$ are included to explain neutrino masses by either an inverse [123] or a linear [21; 22] seesaw mechanism. Our Higgs sector, including the new fields $\hat{\chi}_R$ and $\hat{\bar{\chi}}_R$, is the minimal one for the breaking of $U(1)_{B-L} \times U(1)_R$ to $U(1)_{EM}$.

[3] $\hat{\nu^c}$ is automatically part of the theory due to its $SO(10)$ origin.

	Superfield	$SU(3)_c \times SU(2)_L \times U(1)_R \times U(1)_{B-L}$	Generations
	$\hat{Q}$	$(\mathbf{3}, \mathbf{2}, 0, +\frac{1}{6})$	3
	$\hat{d^c}$	$(\overline{\mathbf{3}}, \mathbf{1}, +\frac{1}{2}, -\frac{1}{6})$	3
	$\hat{u^c}$	$(\overline{\mathbf{3}}, \mathbf{1}, -\frac{1}{2}, -\frac{1}{6})$	3
	$\hat{L}$	$(\mathbf{1}, \mathbf{2}, 0, -\frac{1}{2})$	3
	$\hat{e^c}$	$(\mathbf{1}, \mathbf{1}, +\frac{1}{2}, +\frac{1}{2})$	3
	$\hat{\nu^c}$	$(\mathbf{1}, \mathbf{1}, -\frac{1}{2}, +\frac{1}{2})$	3
	$\hat{S}$	$(\mathbf{1}, \mathbf{1}, 0, 0)$	3
	$\hat{H}_u$	$(\mathbf{1}, \mathbf{2}, +\frac{1}{2}, 0)$	1
	$\hat{H}_d$	$(\mathbf{1}, \mathbf{2}, -\frac{1}{2}, 0)$	1
	$\hat{\chi}_R$	$(\mathbf{1}, \mathbf{1}, +\frac{1}{2}, -\frac{1}{2})$	1
	$\hat{\bar{\chi}}_R$	$(\mathbf{1}, \mathbf{1}, -\frac{1}{2}, +\frac{1}{2})$	1

Table 4.1: The Matter and Higgs sector field content of the $U(1)_R \times U(1)_{B-L}$ model. Generation indices have been suppressed. The $\hat{S}$ superfields are included to generate neutrino masses via the inverse seesaw mechanism. Under matter parity, the matter fields are odd while the Higgses are even.

The fields χ_R and $\bar{\chi}_R$ can be viewed as the (electric charge neutral) remnants of $SU(2)_R$ doublets, which remain light in the spectrum when the $SU(2)_R$ gauge factor is broken by the vev of a $B-L$ neutral triplet down to the $U(1)_R$ [97]. The presence of $\hat{\chi}_R$ and $\hat{\bar{\chi}}_R$ makes it necessary to introduce an extra Z_2^M matter parity, since otherwise R-parity is broken in a potentially disastrous way, once these scalars acquire vacuum expectation values. This Z_2^M is not a particular feature of our setup; it is always needed in models where $U(1)_{B-L}$ is broken with doublets [238]. [4]

Models with a sliding $U(1)_R \times U(1)_{B-L}$ scale and $(B-L)$-even Higgses can be constructed as well. These would simply require that the fields $\hat{\chi}_R$ (and its partner) are replaced by fields which transform as $(1,1,1/2,\pm 1)$. These can be understood as the neutral components of $SU(2)_R$ triplets, remaining light in the spectrum when $SU(2)_R$ is broken to $U(1)_R$. Such a construction has the advantage that R-parity is automatically conserved, different from the model we study here, which needs the introduction of matter parity to guarantee the stability of the LSP. However, the disadvantage of these models is that they necessarily lead to a type-I seesaw instead of an inverse seesaw. Note that such a low-scale type-I seesaw would overshoot experimental bounds on neutrino masses, unless the neutrino Yukawa couplings are assumed to be tiny, $\mathcal{O}(10^{-6})$ or smaller. [5]

For the particle content of table 4.1 the relevant R-parity and Z_2^M conserving superpotential is given by

$$W = W_{\rm MSSM} + W_S. \tag{4.2}$$

Here,

$$\begin{aligned} W_{\rm MSSM} &= Y_u \hat{u^c} \hat{Q} \hat{H}_u - Y_d \hat{d^c} \hat{Q} \hat{H}_d - Y_e \hat{e^c} \hat{L} \hat{H}_d + \mu \hat{H}_u \hat{H}_d \\ W_S &= Y_\nu \hat{\nu^c} \hat{L} \hat{H}_u + Y_s \hat{\nu^c} \hat{\chi}_R \hat{S} - \mu_R \hat{\bar{\chi}}_R \hat{\chi}_R + \mu_S \hat{S} \hat{S}. \end{aligned} \tag{4.3}$$

where Y_e, Y_d and Y_u are the usual MSSM Yukawa couplings for the charged leptons and the quarks. In addition there are the neutrino Yukawa couplings Y_ν and Y_s; the latter mixes the ν^c fields with the S fields giving rise to heavy SM-singlet pseudo-Dirac mass eigenstates. The term μ_R is completely analogous to the MSSM μ term. Note that the term μ_S is included to generate non-zero neutrino mass with an inverse seesaw mechanism. However, as always is done in inverse seesaw, we assume that μ_S is much smaller than all other dimensionful parameters of the model. Apart from neutrino masses themselves it will therefore not affect any of the mass matrices (or decays) of our interest.

Note that, besides the role it plays in neutrino physics, the Y_s coupling is relevant also for the Higgs phenomenology at the loop level as it enters the mixing of χ_R and $\bar{\chi}_R$ Higgs fields with the $SU(2)_L$ Higgs doublets as well as the RGEs for χ_R, see below.

[4] In the normalization of [238] doublets have $U(1)_{B-L} = 1$, i.e are "odd" under B-L.
[5] For discussion of R-parity in LR-models see [239; 240; 241].

Following the notation and conventions of [242] the soft SUSY breaking Lagrangian reads

$$\begin{aligned} V_{soft} &= \sum_{ij} m_{ij}^2 \phi_i^* \phi_j + \Big(\sum_a M_a \lambda_a \lambda_a + T_u \tilde{u}_R^* \tilde{Q} H_u - T_d \tilde{d}_R^* \tilde{Q} H_d + T_\nu \tilde{\nu}_R^* \tilde{L} H_u \\ &\quad - T_e \tilde{e}_R^* \tilde{L} H_d + B_\mu H_u H_d - B_{\mu_R} \bar{\chi}_R \chi_R + T_s \tilde{\nu}_R^* \chi_R \tilde{S} + B_{\mu_S} \tilde{S} \tilde{S} + h.c. \Big) . \end{aligned} \tag{4.4}$$

The first sum contains the scalar masses squared and the second sum runs over all gauginos for the different gauge groups (called λ_{BL}, λ_R, λ_L^i and λ_G^α in the following) and the second one contains the scalar masses squared. While B_{μ_S} is in principle a free parameter, a naive order of magnitude expectation for it is $B_{\mu_S} \sim \mu_S m_{SUSY}$. Thus, one expects that B_{μ_S} is much smaller than all other soft terms and can be safely neglected, see discussion of sneutrinos below.

To reduce the number of free parameters, in our numerical studies we will consider a scenario motivated by minimal supergravity. This means that we assume a GUT unification of all soft-breaking sfermion masses as well as a unification of all gaugino mass parameters

$$\begin{aligned} m_0^2 \delta_{ij} = m_D^2 \delta_{ij} = m_U^2 \delta_{ij} = m_Q^2 \delta_{ij} = m_E^2 \delta_{ij} = m_L^2 \delta_{ij} = m_{\nu^c}^2 \delta_{ij} \\ M_{1/2} = M_{BL} = M_R = M_2 = M_3 \end{aligned} \tag{4.5}$$

Also, for the trilinear soft-breaking coupling, the ordinary CMSSM conditions are assumed

$$T_i = A_0 Y_i, \qquad i = e, d, u, \nu, s \; . \tag{4.6}$$

The GUT scale is chosen as the unification scale of g_{BL}, g_R and g_L, while we allow g_3 to be slightly different, exactly as in the MSSM. A complete unification is assumed to happen due to GUT threshold corrections. For the remaining soft parameters in the Higgs sector, $m_{H_d}^2$, $m_{H_u}^2$, $m_{\chi_R}^2$, $m_{\bar{\chi}_R}^2$ and μ, B_μ, μ_R and B_{μ_R}, we have implemented two different options. These are discussed in subsection 4.1.2.

The presence of two Abelian groups gives rise to gauge kinetic mixing

$$-\chi_{ab} \hat{F}^{B-L,\mu\nu} \hat{F}^R_{\mu\nu} \, . \tag{4.7}$$

This is allowed by gauge and Lorentz invariance [243], as $\hat{F}^{B-L,\mu\nu}$ and $\hat{F}^{R,\mu\nu}$ are gauge invariant, see e.g. [244]. Even if $U(1)_R$ and $U(1)_{B-L}$ are orthogonal in $SO(10)$ the kinetic mixing term will be induced during the RGE running below the $SU(2)_R$ breaking scale because the light fields remaining below the GUT scale can't be arranged in complete $SO(10)$ multiplets: while all matter fields form three generations of 16-plets, $\hat{\chi}_R$ and $\hat{\bar{\chi}}_R$ induce off-diagonal elements already in the 1-loop matrix

of the anomalous dimensions defined by $\gamma_{RBL} = \frac{1}{16\pi^2}\text{Tr}Q_R Q_{B-L}$. The matrix reads

$$\gamma = \frac{1}{16\pi^2} N \begin{pmatrix} \frac{15}{2} & -\frac{1}{2} \\ -\frac{1}{2} & \frac{9}{2} \end{pmatrix} N. \tag{4.8}$$

$N = \text{diag}(1, \sqrt{\frac{3}{2}})$ contains the GUT normalization of the two Abelian gauge groups. Our implementation follows the description of [165], where it is shown that terms of the form as in eq. (4.7) can be absorbed in the covariant derivative by a re-definition of the gauge fields. Therefore, we are going to work in the following with covariant derivatives of the form

$$D_\mu = \partial_\mu - i Q_\Phi^T G A_\mu \,, \tag{4.9}$$

where Q_Φ^T is a vector containing the charges of the field Φ with respect to the two Abelian gauge groups and G is the gauge coupling matrix

$$G = \begin{pmatrix} g_R & g_{RBL} \\ g_{BLR} & g_{BL} \end{pmatrix}. \tag{4.10}$$

A_μ contains the gauge bosons $A_\mu = (A_\mu^R, A_\mu^{BL})^T$. Since the off-diagonal elements in eq. (4.8) are negative and roughly one order smaller than the diagonal ones, it can be expected that the off-diagonal gauge couplings at the SUSY scale are positive but also much smaller than the diagonal ones. This is in some contrast to models in which kinetic mixing arises due to the presence of $U(1)_Y \times U(1)_{B-L}$ [245]. In addition, a mixing term of the form

$$M_{BLR} \lambda_{BL} \lambda_R \tag{4.11}$$

between the two gaugino λ_{BL} and λ_R will be present [246]. Since we have chosen the $SU(2)_R$ breaking scale to be very close to the GUT scale we demand as additional boundary conditions that the new parameters arising from kinetic mixing vanish at the GUT scale, *i.e.*

$$g_{RBL} = g_{BLR} = 0 \,, \qquad M_{BLR} = 0 \,. \tag{4.12}$$

For more details on $U(1)$ mixing and its physical impact we refer the interested reader also to recent papers [247; 248; 245; 249]. Our focus will be on the additional terms in the scalar mass matrices due to the presence of non-diagonal couplings.

4.1.2. Tadpole equations and boundary conditions

The $U(1)_R \times U(1)_{B-L}$ gauge symmetry is spontaneously broken to the hypercharge $U(1)_Y$ by the vevs v_{χ_R} and $v_{\bar{\chi}_R}$ of the scalar components of the $\hat{\chi}_R$ and $\hat{\bar{\chi}}_R$ superfields while the $SU(2)_L \otimes U(1)_Y \to U(1)_Q$ is governed by the vevs v_d and v_u of the neutral scalar components of the $SU(2)_L$ Higgs doublets H_d and H_u up to gauge kinetic mixing effects. One can write

$$\chi_R = \frac{1}{\sqrt{2}}(\sigma_R + i\varphi_R + v_{\chi_R}) \ , \ \bar{\chi}_R = \frac{1}{\sqrt{2}}(\bar{\sigma}_R + i\bar{\varphi}_R + v_{\bar{\chi}_R}) \ , \tag{4.13}$$

$$H_d^0 = \frac{1}{\sqrt{2}}(\sigma_d + i\varphi_d + v_d) \ , \quad H_u^0 = \frac{1}{\sqrt{2}}(\sigma_u + i\varphi_u + v_u) \ , \tag{4.14}$$

where the generic symbols σ and φ denote the CP-even and CP-odd components of the relevant fields, respectively.

The minimum conditions for the four different vevs can be written at tree-level as

$$t_d = -B_\mu v_u + v_d \left(m_{H_d}^2 + |\mu|^2 + \frac{1}{8}A_{LR,3}(v_d^2 - v_u^2) + \frac{1}{8}A_{LR,2}(v_{\bar{\chi}_R}^2 - v_{\chi_R}^2) \right) \tag{4.15}$$

$$t_u = -B_\mu v_d + v_u \left(m_{H_u}^2 + |\mu|^2 - \frac{1}{8}A_{LR,3}(v_d^2 - v_u^2) - \frac{1}{8}A_{LR,2}(v_{\bar{\chi}_R}^2 - v_{\chi_R}^2) \right) \tag{4.16}$$

$$t_{\bar{\chi}_R} = -B_{\mu_R} v_{\chi_R} + v_{\bar{\chi}_R} \left(m_{\bar{\chi}_R}^2 + |\mu_R|^2 + \frac{1}{8}A_{LR,1}(v_{\bar{\chi}_R}^2 - v_{\chi_R}^2) + \frac{1}{8}A_{LR,2}(v_d^2 - v_u^2) \right) \tag{4.17}$$

$$t_{\chi_R} = -B_{\mu_R} v_{\bar{\chi}_R} + v_{\chi_R} \left(m_{\chi_R}^2 + |\mu_R|^2 - \frac{1}{8}A_{LR,1}(v_{\bar{\chi}_R}^2 - v_{\chi_R}^2) - \frac{1}{8}A_{LR,2}(v_d^2 - v_u^2) \right) \tag{4.18}$$

where we defined

$$\begin{aligned} A_{LR,1} &= g_{BL}^2 + g_R^2 + g_{BLR}^2 + g_{RBL}^2 - 2g_R g_{BLR} - 2g_{BL} g_{RBL} \\ A_{LR,2} &= g_R^2 + g_{RBL}^2 - g_R g_{BLR} - g_{BL} g_{RBL} \\ A_{LR,3} &= g_L^2 + g_R^2 + g_{RBL}^2 \, . \end{aligned} \tag{4.19}$$

For the vacuum expectation values we use the following parameterization:

$$\begin{aligned} v_R^2 = v_{\chi_R}^2 + v_{\bar{\chi}_R}^2 \ , \quad v^2 = v_d^2 + v_u^2 \\ \tan\beta_R = \frac{v_{\chi_R}}{v_{\bar{\chi}_R}} \ , \quad \tan\beta = \frac{v_u}{v_d} . \end{aligned} \tag{4.20}$$

The tadpole equations can analytically be solved for either (i) $(\mu, B_\mu, \mu_R, B_{\mu_R})$ or (ii) $(\mu, B_\mu, m_{\chi_R}^2, m_{\bar{\chi}_R}^2)$ or (iii) $(m_{H_d}^2, m_{H_u}^2, m_{\chi_R}^2, m_{\bar{\chi}_R}^2)$. Option (i) can be considered the minimal version. We call this option CmBLR (constrained mBLR), since it allows to define boundary conditions for all scalar soft masses, $m_{H_d}^2 = m_{H_u}^2 = m_0^2$ and $m_{\chi_R}^2 = m_{\bar{\chi}_R}^2 = m_0$ at m_{GUT}, reducing the number of free parameters by four. This assumption, however, leads to some important constraints on the

parameter space, as we will discuss next. Options (ii) and (iii) are more flexible. Option (ii) is similar to the CMSSM with non-universal soft masses (NUHM) [250; 251; 252], albeit the non-universality is only in the $B-L$ sector. We will call this the χ_RmBLR (non-universal χ_R masses mBLR), and most of our numerical results are based on this option. We mention option (iii) for completeness, but we have not used it in our numerical studies.

As will be shown in subsection 4.2.1, the mass of the Z'-boson in the mBLR model is approximately given by

$$m_{Z'}^2 \simeq \frac{1}{4} A_{LR,1} v_R^2 \tag{4.21}$$

We can use this expression and eqs (4.15)-(4.18) to obtain an approximate relation between $m_{Z'}$ and μ_R, $m_{\chi_R}^2$, $m_{\tilde{\chi}_R}^2$ and $\tan\beta_R$. This leads to

$$m_{Z'}^2 \simeq -2(|\mu_R|^2 + m_{\tilde{\chi}_R}^2) + \frac{g_R^2}{4} v^2 \cos(2\beta) \frac{\tan\beta_R^2 + 1}{\tan\beta_R^2 - 1} + \Delta m_{\chi_R}^2 \frac{2\tan\beta_R^2}{\tan\beta_R^2 - 1} \tag{4.22}$$

where $\Delta m_{\chi_R}^2 = m_{\tilde{\chi}_R}^2 - m_{\chi_R}^2$. We can roughly estimate $\Delta m_{\chi_R}^2$, if we make a CMSSM-like assumption for the boundary conditions, $m_{\tilde{\chi}_R}^2 = m_{\chi_R}^2 = m_0^2$ at the GUT scale. The running value of $\Delta m_{\chi_R}^2$ can then be found by a one-step integration of the RGEs at 1-loop level as:

$$\Delta m_{\chi_R}^2 \simeq \frac{1}{4\pi^2} \mathrm{Tr}(Y_s Y_s^\dagger)(3m_0^2 + A_0^2) \log\left(\frac{m_{GUT}}{M_{SUSY}}\right) \tag{4.23}$$

with $T_s \simeq A_0 Y_s$. As eq.(4.23) shows, with these assumptions $\Delta m_{\chi_R}^2 > 0$ and the condition that $m_{Z'}$ of eq.(4.22) has to fulfill the experimental lower bound will define an excluded area in the 3-dimensional parameter space [$\mathrm{Tr}(Y_s Y_s^\dagger)$, $\tan\beta_R, m_{RGE}^2$], where $m_{RGE}^2 = (3m_0^2 + A_0^2)$. If we assume in addition that Y_s is small enough to remain perturbative anywhere between the weak and the GUT scale, a lower bound on m_{RGE}^2 as a function of $\tan\beta_R - 1$ will result in the CmBLR.

This can be understood in more details as follows. In the CmBLR $\Delta m_{\chi_R}^2 \geq 0$, as shown by eq. (4.23) and the last term in eq. (4.22) is positive only if $\tan\beta_R > 1$. Since $\cos(2\beta) < 0$ the second term in eq. (4.22) is positive only if $\tan\beta_R < 1$. If $\Delta m_{\chi_R}^2 \gtrsim |\frac{g_R^2}{4} v^2 \cos(2\beta)|$, only solutions with $\tan\beta_R > 1$ can be found. Since finally $|\mu_R|^2$ must be $|\mu_R|^2 > 0$ and $m_{\tilde{\chi}_R}^2 > 0$ in the CmBLR we get the constraints on the parameter space shown in fig. 4.1. Here we show for two choices of v_R contour lines of μ_R in the plane $(\tan\beta_R, m_0)$. Just above the lines for $\mu_R = -200$ GeV $|\mu_R|^2 = 0$, i.e. larger values of $\tan\beta_R$ do not lead to consistent solutions of the tadpole equations (for fixed m_0 and A_0). This restricts the model to values of $\tan\beta_R$ very close to 1, as is clearly demonstrated in the figure. Note that for low values of m_0 the constraints on the viable region of $\tan\beta_R$ actually becomes stronger. [6]

[6] $\tan\beta_R \simeq 1$ is also needed for a spectrum without tachyons since the additional D-terms can give large negative

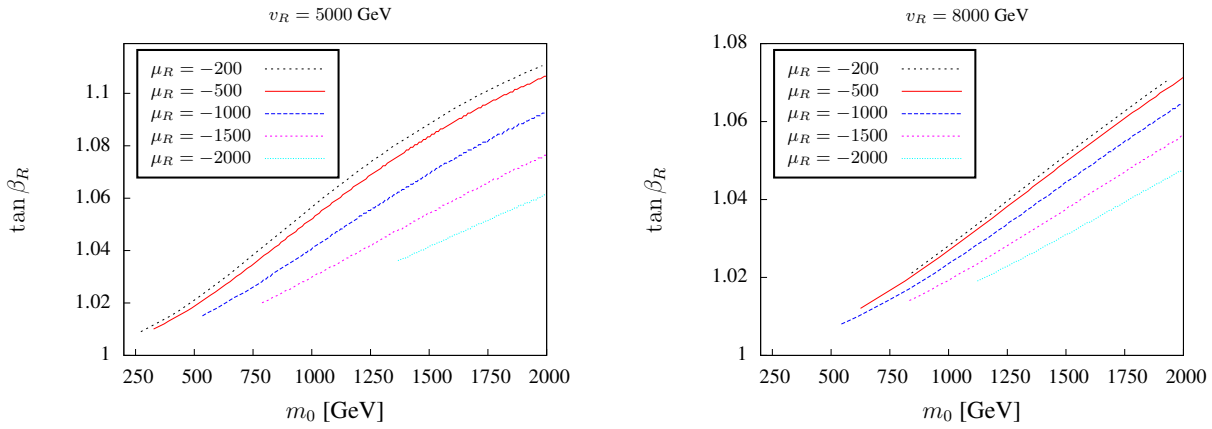

Figure 4.1: Constraints on the CmBLR parameter space from the condition of correct symmetry breaking, to the left: $v_R = 5$ TeV, to the right $v_R = 8$ TeV. In both plots $M_{1/2} = 1000$ GeV, $\tan\beta = 10$ and $A_0 = 0$. Just above the lines for $\mu_R = -200$ GeV $|\mu_R|^2 = 0$, i.e. larger values of $\tan\beta_R$ do not lead to consistent solutions of the tadpole equations (for fixed m_0 and A_0). For detailed explanation see text.

No such constraint on m_0 and A_0 exists in the χ_RmBLR, since here $\Delta m^2_{\chi_R}$ is a free parameter. However, if $(\Delta m^2_{\chi_R}/m^2_{\chi_R}) \ll 1$, values of $\tan\beta_R$ very close to 1 are preferred by eq. (4.22) in both, the CmBLR and the χ_RmBLR.

4.2. Masses

In this section we give the most important mass matrices of the model at tree-level. In the numerical calculations we take also the 1-loop corrections [188] into account, see appendix for more details. The numerical implementation of the model has been done using `SPheno` [36; 166], for which the necessary subroutines and input files were generated using the package `SARAH` [35; 186; 187]. The model files used are included in the public version 3.1.0 of `SARAH`.

contributions to the sfermion masses, see below.

4.2.1. Gauge bosons

In the basis (W^0, B_{B-L}, B_R) the mass matrix for the neutral gauge bosons reads at tree-level

$$M_{VV}^2 = \frac{1}{4}\begin{pmatrix} g_L^2 v^2 & -g_L g_{RBL} v^2 & -g_L g_R v^2 \\ -g_L g_{RBL} v^2 & g_{RBL}^2 v^2 + \tilde{g}_{BL}^2 v_R^2 & g_R g_{RBL} v^2 - \tilde{g}_R \tilde{g}_{BL} v_R^2 \\ -g_L g_R v^2 & g_R g_{RBL} v^2 - \tilde{g}_R \tilde{g}_{BL} v_R^2 & g_R^2 v^2 + \tilde{g}_R^2 v_R^2 \end{pmatrix} \tag{4.24}$$

where

$$\tilde{g}_{BL} = (g_{BL} - g_{RBL}) \ , \quad \tilde{g}_R = (g_R - g_{BLR}) \, . \tag{4.25}$$

From eq. (4.24) the masses of the photon, the Z and the Z' can be calculated analytically

$$m_\gamma = 0 \ , \quad m_{Z,Z'}^2 = \frac{1}{8}\left(A v^2 + B v_R^2 \mp v_R^2 \sqrt{-4C\left(\frac{v^2}{v_R^2}\right) + \left(A\left(\frac{v^2}{v_R^2}\right) + B\right)^2} \right) \tag{4.26}$$

with

$$\begin{aligned} A &= g_L^2 + g_R^2 + g_{RBL}^2 \\ B &= g_{BL}^2 + g_R^2 + g_{BLR}^2 + g_{RBL}^2 - 2 g_{BLR} g_R - 2 g_{RBL} g_{BL} \\ C &= g_L^2 (g_R - g_{BLR})^2 + g_{BL}^2 (g_L^2 + g_R^2) - 2 g_{BL} (g_L^2 + g_{BLR} g_R) g_{RBL} + (g_{BLR}^2 + g_L^2) g_{RBL}^2 \, . \end{aligned} \tag{4.27}$$

Expanding eq. 4.26 in powers of v^2/v_R^2, we find up to first order

$$m_Z^2 = \frac{C v^2}{4B} \ , \quad m_{Z'}^2 = \frac{(AB - C) v^2 + B^2 v_R^2}{4B} \, . \tag{4.28}$$

In the limit $g_{BLR} = 0$ and $g_{RBL} = 0$ we then get

$$m_Z^2 = \frac{(g_{BL}^2 g_L^2 + g_{BL}^2 g_R^2 + g_L^2 g_R^2) v^2}{4(g_{BL}^2 + g_R^2)} \ , \quad m_{Z'}^2 = \frac{g_R^4 v^2}{4(g_{BL}^2 + g_R^2)} + \frac{1}{4}(g_{BL}^2 + g_R^2) v_R^2 \, . \tag{4.29}$$

ATLAS has recently published updated lower limits on Z' searches [253]. Our Z' corresponds to the Z_χ in the notation of [254], i.e. [253] gives a lower limit of $Z' \gtrsim 1.8$ TeV, which corresponds to roughly $v_R \gtrsim 5$ TeV for our choice of couplings[7], see, however, the discussion in subsection 4.3.4.

[7] The condition that the gauge couplings reproduce correctly the standard model hypercharge, plus the assumption of unification lead to values of roughly $g_{BL} \sim 0.57$, $g_R \sim 0.45$, $g_{BLR} \sim 0.014$ and $g_{RBL} \sim 0.012$ at the SUSY scale.

Mixing between Z and Z' states lead to a shift in the ρ-parameter [255], measured very accurately at LEP [256]. Expanding eq. 4.26 up to second order, we estimate the shift to be of order

$$\Delta\rho = \frac{v^2/v_R^2}{v^2/v_R^2 + B^2/(C-2AB)} \ . \tag{4.30}$$

For our choice of couplings g_L, g_R and g_{B-L} (fixed by the experimental inputs and gauge coupling unification) this leads to a lower limit of roughly $v_R \gtrsim 3.3$ TeV, similar to but less stringent than the direct search bound.

4.2.2. Higgs bosons

4.2.2.1. Pseudoscalar Higgs bosons

At the tree level we find that in the $(\varphi_d, \varphi_u, \bar{\varphi}_R, \varphi_R)$ basis the pseudoscalar sector has a block-diagonal form and reads in Landau gauge

$$M_{AA}^2 = \begin{pmatrix} M_{AA,L}^2 & 0 \\ 0 & M_{AA,R}^2 \end{pmatrix} \tag{4.31}$$

with

$$M_{AA,L}^2 = B_\mu \begin{pmatrix} \tan\beta & 1 \\ 1 & \cot\beta \end{pmatrix} \ , \ M_{AA,R}^2 = B_{\mu_R} \begin{pmatrix} \tan\beta_R & 1 \\ 1 & \cot\beta_R \end{pmatrix} \ . \tag{4.32}$$

From these four states two are Goldstone bosons which become the longitudinal parts of the massive neutral vector bosons Z and a Z'. In the physical spectrum there are two pseudoscalars A^0 and A_R^0 with masses

$$m_A^2 = B_\mu(\tan\beta + 1/\tan\beta) \, , \qquad m_{A_R}^2 = B_{\mu_R}(\tan\beta_R + 1/\tan\beta_R) \, . \tag{4.33}$$

4.2.2.2. Scalar Higgs bosons

The tree-level CP-even Higgs mass matrix in the $(\sigma_d, \sigma_u, \bar{\sigma}_R, \sigma_R)$ basis reads

$$M^2_{hh} = \begin{pmatrix} m^2_{LL} & m^2_{LR} \\ m^{2,T}_{LR} & m^2_{RR} \end{pmatrix}, \tag{4.34}$$

where

$$m^2_{LL} = \begin{pmatrix} (g^2_Z + \frac{1}{4}g^2_{RBL})v^2 c^2_\beta + m^2_A s^2_\beta & -\frac{1}{2}\left(m^2_A + (g^2_Z + \frac{1}{4}g^2_{RBL})v^2\right) s_{2\beta} \\ -\frac{1}{2}\left(m^2_A + (g^2_Z + \frac{1}{4}g^2_{RBL})v^2\right) s_{2\beta} & (g^2_Z + \frac{1}{4}g^2_{RBL})v^2 s^2_\beta + m^2_A c^2_\beta \end{pmatrix}, \tag{4.35}$$

$$m^2_{LR} = \frac{1}{4}\begin{pmatrix} (\tilde{g}_R g_R - \tilde{g}_{BL} g_{RBL}) v v_R c_\beta c_{\beta_R} & -(\tilde{g}_R g_R - \tilde{g}_{BL} g_{RBL}) v v_R c_\beta s_{\beta_R} \\ -(\tilde{g}_R g_R - \tilde{g}_{BL} g_{RBL}) v v_R s_\beta c_{\beta_R} & (\tilde{g}_R g_R - \tilde{g}_{BL} g_{RBL}) v v_R s_\beta s_{\beta_R} \end{pmatrix}, \tag{4.36}$$

$$m^2_{RR} = \begin{pmatrix} \tilde{g}^2_{Z_R} v^2_R c^2_{\beta_R} + m^2_{A_R} s^2_{\beta_R} & -\frac{1}{2}\left(m^2_{A_R} + \tilde{g}^2_{Z_R} v^2_R\right) s_{2\beta_R} \\ -\frac{1}{2}\left(m^2_{A_R} + \tilde{g}^2_{Z_R} v^2_R\right) s_{2\beta_R} & \tilde{g}^2_{Z_R} v^2_R s^2_{\beta_R} + m^2_{A_R} c^2_{\beta_R} \end{pmatrix}, \tag{4.37}$$

$s_x = \sin(x)$, $c_x = \cos(x)$ $(x = \beta, \beta_R, 2\beta, 2\beta_R)$, $g^2_Z = (g^2_L + g^2_R)/4$, $\tilde{g}^2_{Z_R} = (\tilde{g}^2_{BL} + \tilde{g}^2_R)/4$. The matrix m^2_{LL} contains the standard MSSM doublet mass matrix. To see this explicitly one has to integrate out the additional Higgs fields in the $v_R \to \infty$ limit which yields a shift in the gauge couplings such that the MSSM limit is achieved. m^2_{RR} corresponds to the $U(1)_R \times U(1)_{B-L}$ Higgs bosons and m^2_{LR} provides the essential mixing between the two sectors.

Note that it is straightforward to show that the determinant of the mass matrix eq. (4.34) goes to zero, whenever one of the parameters $((\tan\beta - 1), m_A, (\tan\beta_R - 1), m_{A_R})$ goes to zero. One can also calculate analytically that in the limit of $v_R \to \infty$ the lightest eigenvalue of eq. (4.34) obeys the MSSM tree-level limit for h^0. For finite v_R corrections to m^2_{LL} appear, of the order of $g^2_R v^3/v_R$, which lead to a shift in the lightest eigenvalue. Thus the MSSM tree-level upper bound of $m^{\text{tree}}_{h^0} \leq m_{Z^0}$ for the lightest Higgs can be violated.

4.2.2.3. Numerical examples

The numerical results given below have been calculated in SPheno [36; 166] for which the necessary subroutines and input files were generated by the relevant extension of SARAH [257]. Hence, the complete one-loop corrections in the extended Higgs sector have been included [4]. We will concentrate the discussion on the lightest two mass eigenstates, since here the changes with respect to the MSSM are expected to be most important for the choice of m_A and m_{A_R} used below. We always check that we are at the minimum of the potential, by solving the (1-loop improved) tadpole equations for the soft Higgs masses.

Throughout the numerical analysis we have adopted a CMSSM-like configuration specified by $M_{1/2} = 600$ GeV, $m_0 = 120$ GeV, $A_0 = 0$ and $\tan\beta = 10$. The stop-sector soft masses in (4.4) were chosen as $m_{\tilde{Q}_3} = m_{\tilde{U}_3} = 2$ TeV, $T_{u33} = 3$ TeV and the top quark mass has been fixed to $m_t = 172.9$ GeV. In addition we have assumed $v_R = 5$ TeV, $\mu = 800$ GeV, $m_A = 800$ GeV, $\mu_\chi = -500$ GeV, $m_{A_R} = 2$ TeV and $\tan\beta_R = 1.1$ unless specified otherwise [8]. For the sake of completeness [9] we have taken $g_{BL} = 0.46$ and $g_R = 0.48$.

Some further remarks concerning the parameters of the extended Higgs sector are in order here. The experimental constraints on the Z' mass yield a lower bound on v_R of about 2.5 TeV [10] for the assumed gauge couplings. This VEV, however, also enters the sfermion mass matrices via the D-term contributions. Focusing, e.g., at the charged sleptons the relevant mass matrix reads

$$M_{\tilde{l}}^2 = \begin{pmatrix} M_{\tilde{L}}^2 + \frac{1}{8}M_{DL}^2 + m_f^2 & \frac{1}{\sqrt{2}}(v_d T_l - \mu Y_l v_u) \\ \frac{1}{\sqrt{2}}(v_d T_l - \mu Y_l v_u) & M_{\tilde{E}}^2 + \frac{1}{8}M_{DR}^2 + m_f^2 \end{pmatrix}, \tag{4.38}$$

where

$$M_{DL}^2 = g_{BL}^2(v_{\chi_R}^2 - v_{\tilde{\chi}_R}^2) + g_L^2(v_u^2 - v_d^2) \quad \text{and} \quad M_{DR}^2 = (g_R^2 - g_{BL}^2)(v_{\chi_R}^2 - v_{\tilde{\chi}_R}^2) + g_R^2(v_u^2 - v_d^2) \tag{4.39}$$

are just the D-terms, $M_{\tilde{L}}^2$ and $M_{\tilde{E}}^2$ are the soft SUSY masses for the L-type and R-type sleptons and all flavour indices have been suppressed in the above formula.

[8] At the time of the publication CMS and ATLAS data showed a small excess at 140 GeV (see subsection 2.1.3) For this choice of parameters m_{h^0} in the MSSM limit is about 125 GeV (1-loop), which is needed to explain a Higgs mass of 140 GeV. For a Higgs mass of around 125 GeV, as indicated by recent LHC data, we have less stringent constraints on the soft parameters. For $m_{\tilde{Q}_3} = 1.1$ TeV, $m_{\tilde{U}_3} = 0.96$ TeV and $T_{u33} = 1.1$ TeV corresponding to the RGE solutions for these CMSSM one finds $m_{h^0} = 111$ GeV at 1-loop.

[9] It is perhaps worth mentioning that from the effective theory point of view the specific values of g_{BL} and g_R do not matter as long as they yield the correct MSSM hypercharge coupling. Indeed, we have verified that different choices lead to results very similar to those quoted in the text.

[10] At the time of the publication the lower limit on Z' was around 1 TeV. For an update and a more detailed discussion see subsection 4.3.4.

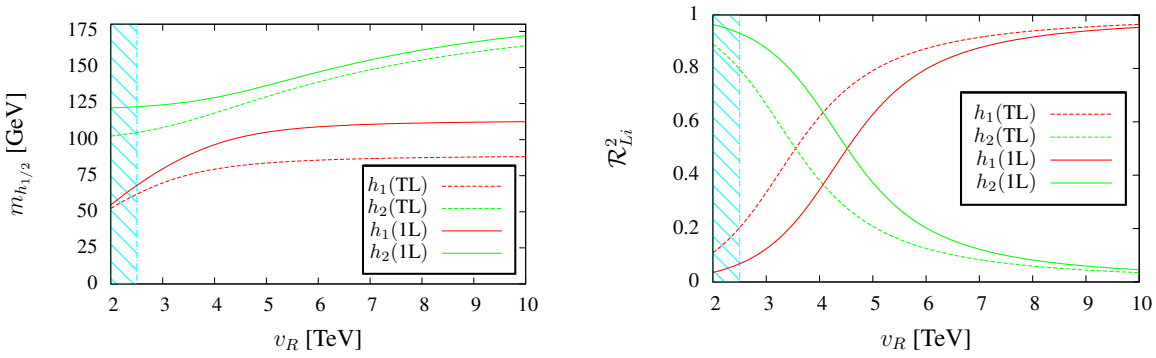

Figure 4.2: The tree level and one-loop masses of the two lightest Higgs bosons $h_{1,2}$ (left) and $\mathcal{R}^2_{Li}$ (right) as a function of v_R; at tree level (TL) in dashed and at one loop (1L) in solid lines. The values of all the other parameters are given in the text. The shaded area is excluded by the Z' searches.

Since the (dominant) v_R^2-parts of the two D-terms have opposite signs, the breaking of the extra gauge group must be nearly "D-flat", i.e., $\tan\beta_R \simeq 1$ as otherwise one of the sleptons would become tachyonic[11]. For completeness we also note that the cases of $\tan\beta = 1$ and $\tan\beta_R = 1$ lead to saddle points of the potential but not to minima which is a well known fact within the MSSM. In a complete analogy with the MSSM one can also show that for $\tan\beta_R \to 1$ one of the Higgs states gets massless at the tree level. Thus, since $\tan\beta_R$ has to be close to one, we generally expect two light Higgs bosons in the spectrum, which holds even at the one-loop level.

In Figure 4.2 we show the masses of the two lightest Higgs bosons together with

$$\mathcal{R}^2_{Li} \equiv R^2_{i1} + R^2_{i2} \tag{4.40}$$

as a function of v_R where $i = 1, 2$ labels the light Higgs scalars in the model. Note that the quantity $\mathcal{R}^2_{Li}$, which reaches one in the MSSM limit, is a rough measure of how much the corresponding Higgs with index i resembles an MSSM Higgs boson. Roughly speaking, the smaller this quantities is, the smaller is the i-th Higgs coupling to the Z- and W-bosons, implying a reduced production cross sections at LEP, Tevatron and the LHC.

As claimed above there are two light CP-even states $h_{1,2}$ which essentially correspond to an admixture of the "standard" MSSM-like doublet component h^0 and its counterpart h^0_R spanning over the $\chi_R - \bar{\chi}_R$ sector; this can also be seen by noticing that $\mathcal{R}^2_{L1} + \mathcal{R}^2_{L2} \simeq 1$ as displayed on the right hand side of Figure 4.2. We stress that the state which mainly resembles the MSSM h^0 (i.e., the one with a large $\mathcal{R}^2_{Li}$) has already a tree-level mass of around 110 GeV or larger and reaches

[11] Let us note that this is indeed the case in all supersymmetric models featuring a spontaneously broken extended gauge symmetry well above the TeV scale (like, e.g., SUSY GUTs) and as such this requirement should be viewed as a phenomenological constraint rather than a fine-tuning.

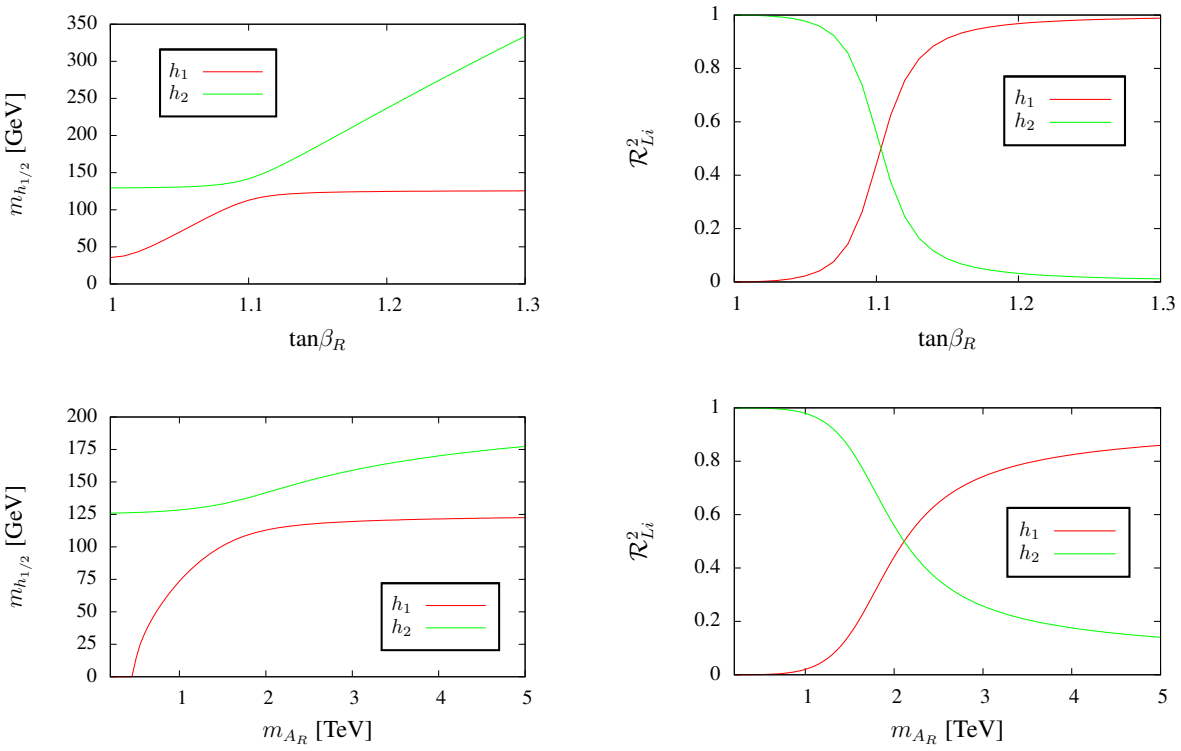

Figure 4.3: One-loop masses of the two lightest Higgs bosons (left column) and $\mathcal{R}^2_{Li}$ (right column) as a function of tanβ_R (upper row) and m_{A_R} (lower row). The values of all the other parameters are given in the text.

up to 140 GeV once loop corrections are included[12]. The lighter state with a mass below 100 GeV hardly couples to the Z-boson and, thus, the LEP constraints from the Higgs searches do not apply for it. To this end, we have used the `HiggsBounds` package [258; 259] to check explicitly that all the configurations of our concern here are experimentally allowed. Note also that the large variation in $\mathcal{R}^2_{Li}$ as seen on the right panel of the Figure 4.2 and, in particular, its high sensitivity to radiative corrections is expected because the parameters have been deliberately chosen close to a level-crossing region.

This can be also seen in Figure 4.3 where we display the $m_{h_{1,2}}$ dependence on tanβ_R and m_{A_R}. All results shown in this figure are at the one-loop level. The upper bound on tanβ_R is given by the requirement that for a given value of v_R all sfermions masses are consistent with existing data (which, however, depends also on the sfermion mass parameters). The observed dependence on tanβ_R is, indeed, rather strong. Note also that very light h_1 can be obtained for[13] tan$\beta_R \lesssim 1.05$.

[12] Actually, even larger values can be obtained when varying the parameters, e.g. m_{A_R}.
[13] The exact value as well as the others given below depend on the other parameters.

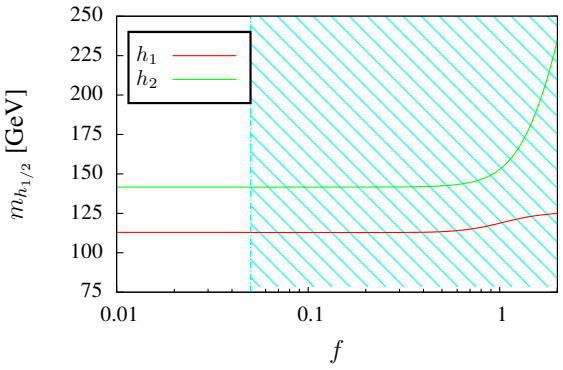

Figure 4.4: One-loop masses of the two lightest Higgs bosons as functions of f. The values of all the other parameters are given in the text. The shaded area is excluded by $\mu \to e\gamma$.

As in this regime it is mainly a combination of $\bar{\chi}_R$ and χ_R (see the right panel) the usual bounds do not apply. However, the second lightest Higgs boson (similar to the MSSM h^0) can decay into a pair of these states with sizable branching ratio which in turn can change the Higgs phenomenology drastically [4]. For $1.2 \lesssim \tan\beta_R \lesssim 1.3$ the lightest state becomes mainly the MSSM h^0 with a mass close to 130 GeV which is a consequence of the stop-sector parameter choice. In this figure one also sees that there is still quite some mixing between the two lightest states even for $m_{A_R} = 5$ TeV; this implies a change in the phenomenology with respect to that of the MSSM (for a given set of the MSSM parameters).

We checked that in this model, in general, the loops due to third generation sfermions (in particular the stops) give the largest contribution. In reference [260] it has been shown that in inverse seesaw models also the sneutrino loops can give large contributions. Indeed, we find that there can be huge contributions if the neutrino Yukawa couplings are $O(1)$ or larger as can be seen in Figure 4.4. The neutrino Yukawa couplings are parametrized as

$$Y_\nu = f \begin{pmatrix} 0 & 0 & 0 \\ a & a & -a \\ 0 & 1 & 1 \end{pmatrix} , \tag{4.41}$$

with

$$a = \left(\Delta m^2_\odot / \Delta m^2_{\rm A}\right)^{\frac{1}{4}} \sim 0.4 \, , \tag{4.42}$$

and the structure has been chosen such that one correctly accommodates the neutrino data. However,

we find that the bound BR($\mu \to e\gamma$) $\lesssim 2.4 \cdot 10^{-12}$ [181] [14] severely constrains this option as, for large f, one gets a large contribution to $\mu \to e\gamma$ due to the chargino-sneutrino and W-neutrino loops.

There are, of course, several ways to tune the parameters such that this bound is avoided. For example, one can add a non-minimal flavour structure into the slepton sector [262] or tune the structure of the neutrino Yukawa couplings so that very specific values for θ_{13}, the reactor mixing angle, are obtained [130; 142]. This implies that, in principle, larger values for the neutrino Yukawa couplings are possible, hence rendering the corresponding loops more important.

Finally we note, that in the plots in this subsection we have not shown the regions excluded by LEP or the LHC searches, since we were interested only in showing the parameter dependencies of our numerical results. In the study points of the next subsection, however, we have taken care that our points survive all known experimental constraints.

4.2.3. Neutrinos

The mBLR model contains beside the usual three left-handed neutrinos six additional states which are singlets with respect to the SM group. The corresponding mass matrix is in the basis (ν_L, ν^c, S) given by

$$m_\nu = \begin{pmatrix} 0 & \frac{1}{\sqrt{2}} v_u Y_\nu^T & 0 \\ \frac{1}{\sqrt{2}} v_u Y_\nu & 0 & \frac{1}{\sqrt{2}} v_{\chi_R} Y_s \\ 0 & \frac{1}{\sqrt{2}} v_{\chi_R} Y_s^T & \mu_S \end{pmatrix} . \tag{4.43}$$

This matrix is diagonalized by U^ν:

$$U^{\nu,*} m_\nu U^{\nu,\dagger} = m_\nu^{dia}. \tag{4.44}$$

Eigenvalues for the three light (and mostly left-handed) neutrinos can be found in the seesaw approximation as:

$$m_\nu^{\text{eff}} = -\frac{v_u^2}{v_R^2} Y_\nu^T (Y_s^T)^{-1} \mu_S Y_s^{-1} Y_\nu \, . \tag{4.45}$$

Neutrino data implies that either Y_ν and/or μ_S is small and in inverse seesaw the smallness of neutrino mass is attributed to the smallness of the latter [15].

The smallness of μ_S implies that the six heavy states form three "quasi-Dirac" pairs. For vanishing

[14] At the time the paper was published the experimental limit was BR($\mu \to e\gamma$) $\lesssim 2.4 \cdot 10^{-12}$ [181]. Note, that meanwhile the bound has been improved to BR($\mu \to e\gamma$) $\lesssim 5.7 \cdot 10^{-13}$ [261].

[15] The bounds on rare lepton decays imply that the off-diagonal terms of Y_s and Y_ν have to be small compared to their diagonal entries, unless their diagonal values are small too.

off-diagonal entries in Y_s and Y_ν a good estimate of the masses of the heavy states is:

$$m_{\nu_h,ii} \simeq \pm\sqrt{|Y_{\nu,ii}|^2 v_u^2 + |Y_{s,ii}|^2 v_{\chi_R}^2}\,. \tag{4.46}$$

4.2.4. Sparticles

4.2.4.1. Neutralinos

The mass matrix of the neutralinos reads in the basis $(\lambda_{BL}, \lambda_L^0, \tilde{h}_d^0, \tilde{h}_u^0, \lambda_R, \tilde{\bar{\chi}}_R, \tilde{\chi}_R)$:

$$M_{\tilde{\chi}^0} = \begin{pmatrix} M_{BL} & 0 & -\frac{1}{2}g_{RBL}v_d & \frac{1}{2}g_{RBL}v_u & \frac{M_{BLR}}{2} & \frac{1}{2}v_{\bar{\chi}_R}\tilde{g}_{BL} & -\frac{1}{2}v_{\chi_R}\tilde{g}_{BL} \\ 0 & M_2 & \frac{1}{2}g_L v_d & -\frac{1}{2}g_L v_u & 0 & 0 & 0 \\ -\frac{1}{2}g_{RBL}v_d & \frac{1}{2}g_L v_d & 0 & -\mu & -\frac{1}{2}g_R v_d & 0 & 0 \\ \frac{1}{2}g_{RBL}v_u & -\frac{1}{2}g_L v_u & -\mu & 0 & \frac{1}{2}g_R v_u & 0 & 0 \\ \frac{M_{BLR}}{2} & 0 & -\frac{1}{2}g_R v_d & \frac{1}{2}g_R v_u & M_R & -\frac{1}{2}v_{\bar{\chi}_R}\tilde{g}_R & \frac{1}{2}v_{\chi_R}\tilde{g}_R \\ \frac{1}{2}v_{\bar{\chi}_R}\tilde{g}_{BL} & 0 & 0 & 0 & -\frac{1}{2}v_{\bar{\chi}_R}\tilde{g}_R & 0 & -\mu_R \\ -\frac{1}{2}v_{\chi_R}\tilde{g}_{BL} & 0 & 0 & 0 & \frac{1}{2}v_{\chi_R}\tilde{g}_R & -\mu_R & 0 \end{pmatrix}. \tag{4.47}$$

The eigenvalues of this matrix are not completely arbitrary. Since $U(1)_{B-L} \times U(1)_R$ is broken in such a way as to produce correctly the SM group $U(1)_Y$ in the limit of $v << v_R$ the matrix contains one state which corresponds to the MSSM bino, $\tilde{B}$, which is a superposition of λ_{BL} and λ_R. In addition the matrix contains an orthogonal state, which we will call $\tilde{B}_\perp$ in the following.

For CMSSM like boundary conditions, $M_{BL} = M_2 = M_R = M_{1/2}$, the bino is usually the lightest of the three gaugino like states, with the $\tilde{W}$ being approximately twice as heavy. The $\tilde{B}_\perp$ is very often mixed with one of the right higgsinos, and, since M_{BL} at low energies is much smaller than v_R this mixing is often important. In addition, there is the standard quasi-Dirac pair of "left" higgsinos, plus two more states which are mostly right higgsinos. Of the latter one is usually rather heavy, while the other can be light, if μ_R is small.

In fig. 4.5 the neutralino masses and $\mathcal{R}^2_{\perp i}$ for CmBLR are plotted against v_R for some arbitrary choice of other parameters. As discussed, there are in total seven eigenstates. Of special interest is the $\tilde{B}_\perp$, so in the plot on the right we show the percentage of $\tilde{B}_\perp$ ($\mathcal{R}^2_{\perp i}$) in the corresponding

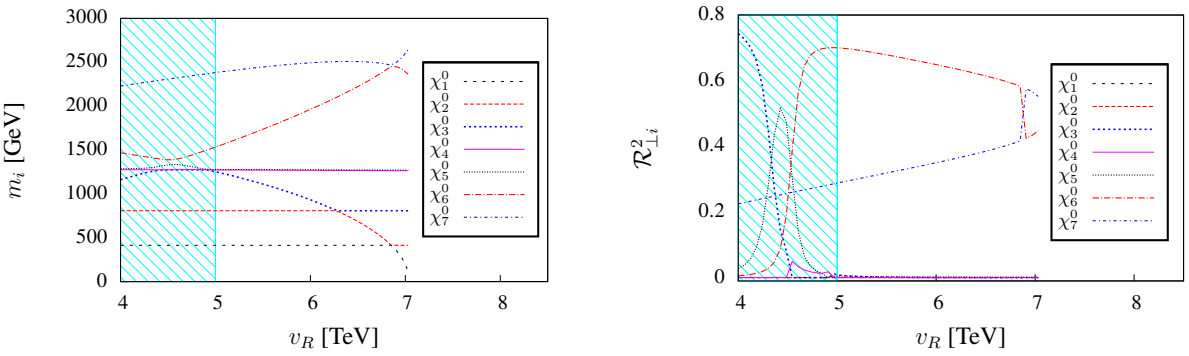

Figure 4.5: Neutralino masses (left) and $\mathcal{R}^2_{\perp i}$ (right) versus v_R for otherwise fixed choice of parameters: $m_0 = 1000$ GeV, $M_{1/2} = 1000$ GeV, $\tan\beta = 10$, $A_0 = -600$, $\tan\beta_R = 1.04$. This plot uses the CmBLR version of the model.

mass eigenstate. Here $\mathcal{R}^2_{\perp i} = 1$ means that the i-th neutralino is a pure $\tilde{B}_\perp$. As one can see in fig. 4.6 the masses and mixing of the three new states depend strongly on v_R. For small v_R all three states mix to each other. Increasing v_R leads to a decoupling of the lighter higgsino-right from the $\tilde{B}_\perp$ which decreases in mass since μ_R becomes smaller for large v_R while the masses of the two remaining states get large. Since the MSSM Neutralinos mix very little with the new states, there are four eigenvalues which show almost no dependence on the parameters v_R and μ_R.

In fig. 4.6 the neutralino masses and $\mathcal{R}^2_{\perp i}$ are plotted against v_R for the case of χ_RmBLR. In this calculation, μ_R and m_{A_R} can take fixed values while v_R is varied freely. Two of the three new Neutralino states are a mixture of the higgsino-right and $\tilde{B}_\perp$ and therefore depend on v_R. Since the lighter higgsino-right hardly mix to the $\tilde{B}_\perp$ it has a constant mass at $m_{\tilde{h}_R} \simeq |\mu_R| = 1700$ GeV in this example. The lighter of the two new states that show dependence on v_R is mostly a $\tilde{B}_\perp$, whereas the one with larger mass is mostly a higgsino-right. The smaller v_R the smaller the mixing between these two states and thus the larger the coupling of the mostly $\tilde{B}_\perp$-state to the MSSM particles. This will be important when we discuss LHC phenomenology in subsection 4.3.4.

The dependence of the neutralino masses and $\mathcal{R}^2_{\perp i}$ on μ_R is shown in fig. 4.7. Since the higgsino-right and the $\tilde{B}_\perp$ mix, all three states show a dependence on μ_R. The state which hardly mixes to the $\tilde{B}_\perp$ decreases in mass for small $|\mu_R|$. So we can easily have a higgsino-right as LSP choosing μ_R close to zero. The state which is mostly the $\tilde{B}_\perp$ gets a smaller mass for large $|\mu_R|$, while the one which is mostly a higgsino-right increases in mass.

4.2.4.2. Sleptons and sneutrinos

In models in which lepton number is broken, the scalar neutrinos split into a real and an imaginary part with slightly different masses [263]. Since we assume that the smallness of neutrino masses is

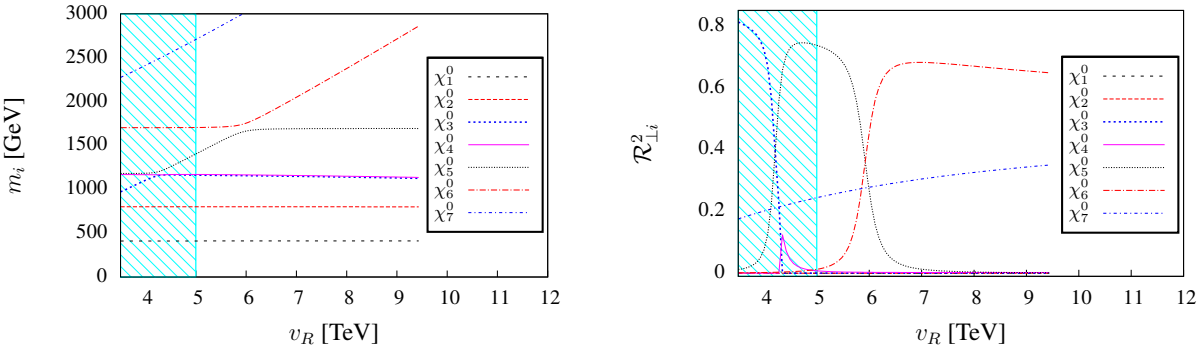

Figure 4.6: Neutralino masses (left) and $\mathcal{R}^2_{\perp i}$ (right) versus v_R for otherwise fixed choice of parameters: $m_0 = 630$ GeV, $M_{1/2} = 1000$ GeV, $\tan\beta = 10$, $A_0 = 0$, $\tan\beta_R = 1.05$, $\mu_R = -1700$ GeV, $m_{A_R} = 4800$ GeV. This plot uses the χ_RmBLR version of the model.

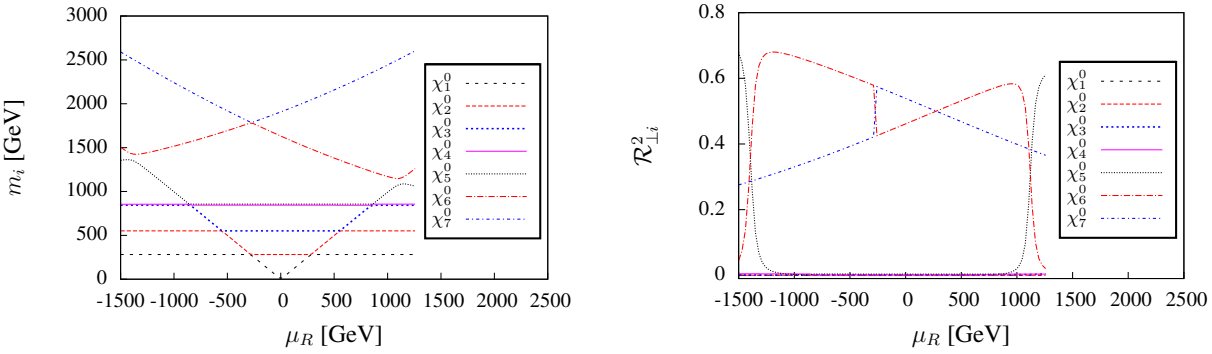

Figure 4.7: Neutralino masses (left) and $\mathcal{R}^2_{\perp i}$ (right) versus μ_R for otherwise fixed choice of parameters: $m_0 = 400$ GeV, $M_{1/2} = 700$ GeV, $\tan\beta = 10$, $A_0 = 0$, $v_R = 5000$ GeV, $\tan\beta_R = 1.05$, $m_{A_R} = 3000$ GeV.

due to the smallness of the parameter μ_S (and, therefore, B_{μ_S} is supposed to be small too), this splitting between sneutrino mass eigenstates is too small to be of any relevance, except neutrino masses themselves.

Neglecting μ_S and B_{μ_S} the sneutrino mass matrix is given by

$$M^2_{\tilde{\nu}} = \begin{pmatrix} m^2_{LL,\tilde{\nu}} & \frac{1}{\sqrt{2}} v_u (T^\dagger_\nu - Y^\dagger_\nu \cot\beta\mu) & \frac{1}{2} v_u v_{\chi_R} Y^\dagger_\nu Y_s \\ \frac{1}{\sqrt{2}} v_u (T_\nu - Y_\nu \cot\beta\mu^*) & m^2_{RR,\tilde{\nu}} & \frac{1}{\sqrt{2}} v_{\chi_R} (T_s - Y_s \cot\beta_R \mu^*_R) \\ \frac{1}{2} v_u v_{\chi_R} Y^\dagger_s Y_\nu & \frac{1}{\sqrt{2}} v_{\chi_R} (T^\dagger_s - Y^\dagger_s \cot\beta_R \mu_R) & m^2_S + \frac{v^2_{\chi_R}}{2} Y^\dagger_s Y_s \end{pmatrix} \tag{4.48}$$

where

$$\begin{aligned} m^2_{LL,\tilde{\nu}} &= m^2_L + \frac{v^2_u}{2} Y^\dagger_\nu Y_\nu - \\ &\quad \frac{1}{8}\left((g^2_{BL} + g^2_{BLR} - g_{BL} g_{RBL})(v^2_{\bar{\chi}_R} - v^2_{\chi_R}) + (g^2_L + g^2_R + g_{BL} g_{RBL})(v^2_d - v^2_u)\right) \mathbf{1} \\ m^2_{RR,\tilde{\nu}} &= m^2_\nu + \frac{v^2_u}{2} Y_\nu Y^\dagger_\nu \; + \frac{v^2_{\chi_R}}{2} Y^\dagger_s Y_s + \\ &\quad \frac{1}{8}\left((g^2_{BL} + g^2_R + g^2_{BLR} + g^2_{RBL} - 2 g_{BL} g_{RBL} - 2 g_R g_{BLR})(v^2_{\bar{\chi}_R} - v^2_{\chi_R}) + \right. \\ &\quad \left. (g^2_R + g^2_{RBL} - g_{BL} g_{RBL} - g_R g_{BLR})(v^2_d - v^2_u)\right) \mathbf{1} \end{aligned} \tag{4.49}$$

For charged sleptons one gets:

$$M^2_{\tilde{l}} = \begin{pmatrix} m^2_{LL,\tilde{l}} & \frac{1}{\sqrt{2}} v_d (T^\dagger_l - Y^\dagger_l \tan\beta\mu) \\ \frac{1}{\sqrt{2}} v_d (T_l - Y_l \tan\beta\mu^*) & m^2_{RR,\tilde{l}} \end{pmatrix} \tag{4.50}$$

where

$$\begin{aligned} m^2_{LL,\tilde{l}} &= m^2_L + \frac{v^2_d}{2} Y^\dagger_l Y_l - \frac{1}{8}\Big((g^2_{BL} + g^2_{BLR} - g_{BL} g_{RBL} - g_R g_{BLR})(v^2_{\bar{\chi}_R} - v^2_{\chi_R}) \\ &\qquad - (g^2_L - g_{BL} g_{RBL} - g_R g_{BLR})(v^2_d - v^2_u)\Big)\mathbf{1} \\ m^2_{RR,\tilde{l}} &= m^2_E + \frac{v^2_d}{2} Y_l Y^\dagger_l + \frac{1}{8}\Big((g^2_{BL} - g^2_R + g^2_{BLR} - g^2_{RBL})(v^2_{\bar{\chi}_R} - v^2_{\chi_R}) \\ &\qquad - (g^2_R + g^2_{RBL} + g_{BL} g_{RBL} + g_R g_{BLR})(v^2_d - v^2_u)\Big)\mathbf{1} \end{aligned} \tag{4.51}$$

In fig. 4.8 sneutrino and slepton masses are plotted against v_R, $\tan\beta_R$ and μ_R. The figures on the left show a zoom into the region of the lightest states, whereas the figures on the right show a larger range of masses for a better understanding of the overall behavior. To see which particle is the LSP, while varying v_R, $\tan\beta_R$ and μ_R, we included in all plots on the left the mass of the lightest neutralino state. This state is always a Bino, except for the plot against μ_R. Here the LSP becomes a higgsino-right for $|\mu_R| < 250$ GeV. The plots show that the masses depend strongly on the choice of v_R and $\tan\beta_R$. In the case of charged sleptons the dependence on v_R and $\tan\beta_R$ comes only from additional D-terms at the tree level. This is different for sneutrinos. Here we can have an interplay between new D-terms and terms coming from the coupling Y_s which both depend on v_R and $\tan\beta_R$. The additional D-terms force left sparticle to become light for $\tan\beta_R < 1$ while for $\tan\beta_R > 1$ right sparticle masses decrease. Up to $v_R = 6$ TeV $\tilde{\nu}_1$ is a right handed sneutrino and therefore the mass increases for increasing v_R. For $v_R > 6$ TeV the mass of $\tilde{\nu}_1$ drops down again since here it is mainly a left handed sneutrino. Thus, increasing v_R leads to a level-crossing in the mass spectrum of left and right handed sneutrinos. The same holds for the sleptons. In the plot against v_R the mass of the right sneutrino decreases much faster for $v_R < 6$ TeV than the mass of the right sleptons. This is due to the off-diagonal terms proportional to Y_s, which contain also μ_R in the sneutrino mass matrix. These terms mix the scalar component of $\hat{S}$ to $\tilde{\nu}_R$. Thus for low values of v_R in this example the LSP is neutral, which is allowed, whereas for larger values of v_R (with left sleptons being light) there are parts of the parameter space, where the lightest slepton is charged, which is phenomenologically forbidden. Whether in the left sector charged or neutral states are lighter, depends heavily on the choice of parameters.

Varying $\tan\beta_R$ the right slepton masses decrease faster than the right sneutrino masses for $\tan\beta_R > 0.95$ due the additional sneutrino mixing. Since the sneutrino and slepton masses depend strongly on the choice of v_R, $\tan\beta_R$ and μ_R one obtains limits on combination on these parameters. On the one hand, one has to avoid tachyonic states and on the other hand one has to take care not to get charged sleptons as LSP. The combination of both conditions forces us to choose $\tan\beta_R$ close to one and gives us an upper limit on v_R and $|\mu_R|$ as function of $|\tan\beta_R - 1|$.

4.3. Constraints, sample spectra and decays

In this section we discuss several interesting phenomenological aspects which potentially allow the BLR model to be discriminated from the MSSM at the LHC and exemplify the most important features for a few study points. We include a discussion of the direct production of new states and characteristic changes in the cascade decays of supersymmetric particles.

For brevity we will call these benchmark points BLRSP1- BLRSP5, the corresponding input parameters are listed in table 4.2. All of these points have been calculated with the χ_RmBLR version of the model. However, note that for BLRSP5 the input is chosen to be consistent with the CmBLR

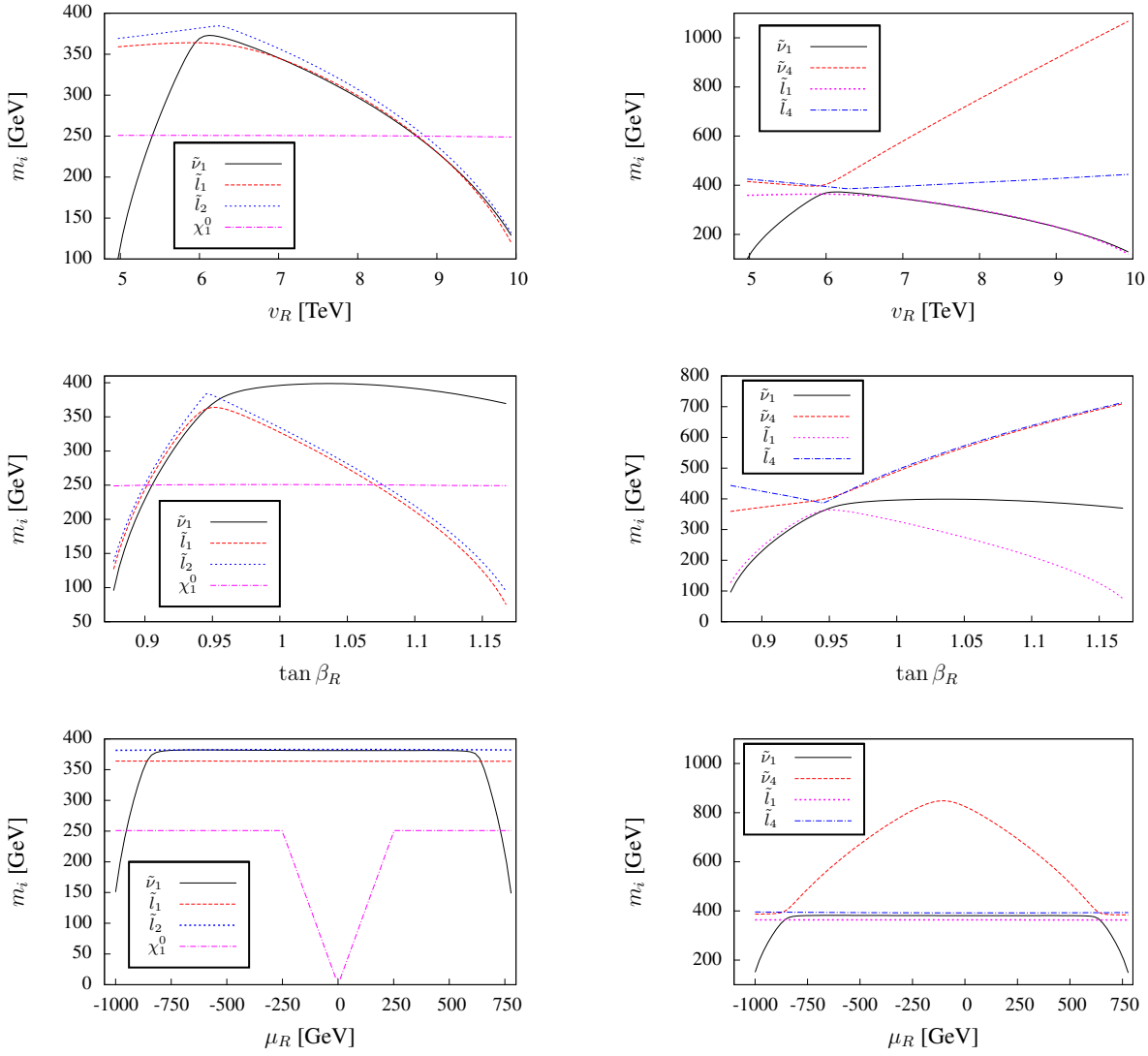

Figure 4.8: Lightest slepton (and neutralino) masses as function of v_R, $\tan\beta_R$ and μ_R for a fixed but arbitrary choice of other parameters: $m_0 = 220$ GeV, $M_{1/2} = 630$ GeV, $\tan\beta = 10$, $A_0 = 0$, $\tan\beta_R = 0.95$, $v_R = 6000$, $\mu_R = -850$ GeV, $m_{A_R} = 2200$ GeV, $Y_{s,ii} = 0.3$. Plots on the left show a zoom into the light mass region, such that mass differences between the lightest sneutrino and the lightest charged slepton are resolved, figures to the right show the overall dependence, for a discussion see text.

variant.

A few comments on the input parameters and the resulting mass spectra are in order, before we discuss the phenomenology in detail. As shown below, the bounds on rare lepton flavour violating decays require Y_ν and Y_s to be essentially flavour-diagonal, unless these couplings are very small. Therefore we have chosen Y_ν and Y_s diagonal as starting point implying that all points satisfy trivially the LFV constraints. A correct explanation for the neutrino angles then requires flavour violating entries in the parameter μ_S, which we do not give in table 4.2, since they are irrelevant for collider phenomenology.

The input values of table 4.2 lead to the mass spectrum shown in tables 4.3 and 4.4. We give the masses and in brackets the particle character. In case of mixed states the two largest components, for example $(\tilde{W}, \tilde{h}_L)$, are given where the first entry accounts for the larger contribution. If the ordering in the composition changes like in the case of $m_{\tilde{u}_{5,6}}$ we use squared brackets. Therefore we have $(\tilde{c}_L, \tilde{u}_L)$ for $m_{\tilde{u}_5}$ and $(\tilde{u}_L, \tilde{c}_L)$ for $m_{\tilde{u}_6}$. In all cases input parameters have been chosen such, that the squark and gluino masses are outside the region currently excluded by pure CMSSM searches at ATLAS [227] and CMS [228]. Since (a) we expect the missing momentum signal to be smaller in these points than in a true CMSSM spectrum and (b) our squark spectra are less degenerate than the CMSSM case, we believe this is a conservative choice. Two of the points have a sneutrino LSP (BLRSP1 and BLRSP3), while three points have a neutralino LSP (for BLRSP2 and BLRSP5 mostly a bino, for BLRSP4 a state which is mostly a $\tilde{h}_R$).

Note that the ordering of sfermion mass eigenstates does in many cases not follow the standard CMSSM patterns: $m_{\tilde{\tau}_1} \leq m_{\tilde{\mu}_R} \simeq m_{\tilde{e}_R} < m_{\tilde{\mu}_L} \simeq m_{\tilde{e}_L} \leq m_{\tilde{\tau}_2}$ and $m_{\tilde{t}_1} \leq m_{\tilde{c}_R} \simeq m_{\tilde{u}_R} < m_{\tilde{c}_L} \simeq m_{\tilde{u}_L} \leq m_{\tilde{t}_2}$ (similar for sdowns). These patterns are distorted in the study points due to the unconventional D-terms of the model and this feature gets enhanced for larger $|\tan\beta_R - 1|$ and/or larger values of v_R. We note also that for sneutrinos and charged sleptons many states are quite degenerate. For example $\tilde{\mu}_R$ and $\tilde{e}_R$ have practically the same mass in all points. While these degeneracies are always true in CMSSM spectra, in our case this is not necessarily so, but simply reflects the fact that both Y_ν and Y_s have been chosen generation independent in all points, except BLRSP1. As this point shows, even a rather moderate generation dependent value of Y_s can lead to large mass splittings in the sneutrino sector. A generation dependent value of Y_ν would not only split sneutrino masses but also charged slepton masses.

4.3.1. Higgs physics, direct production

In all study points of table 4.2 there is one Higgs boson with mass between 120 and 125 GeV. In addition, there is a second state with masses varying between 19 and 140 GeV. In BLRSP1, BLRSP3 and BLRSP5 the mass eigenstate h_2 is SM-like, with $R^2_{L2} > 0.9$. In BLRSP2 it is h_1, which has a large content of H_d and H_u and BLRSP4 is a case where h_1 and h_2 have large mixing. Since we have often a mass eigenstate below the LEP limit of 115 GeV for a standard model Higgs boson,

	BLRSP1	BLRSP2	BLRSP3	BLRSP4	BLRSP5
CMSSM					
m_0 [GeV]	470	1000	120	165	500
$M_{1/2}$ [GeV]	700	1000	780	700	850
$\tan\beta$	20	10	10	10	10
A_0	0	-3000	-300	0	-600
Extended gauge sector					
v_R [GeV]	4700	6000	6000	5400	5000
$\tan\beta_R$	1.05	1.025	0.85	1.06	1.023
μ_R [GeV]	-1650	-780	-1270	260	(-905)
m_{A_R} [GeV]	4800	7600	800	2350	(1482)
Yukawas					
$Y_{\nu,11}$	0.04	0.1	0.1	0.1	0.1
$Y_{\nu,22}$	0.04	0.1	0.1	0.1	0.1
$Y_{\nu,33}$	0.04	0.1	0.1	0.1	0.1
$Y_{s,11}$	0.04	0.042	0.3	0.3	0.3
$Y_{s,22}$	0.05	0.042	0.3	0.3	0.3
$Y_{s,33}$	0.05	0.042	0.3	0.3	0.3

Table 4.2: Parameters of the various study points. In BLRSP1-BLRSP4 μ_R and m_{A_R} are input whereas in BLRSP5 the constrained version of the model has been used and, thus, these two parameters are output. For a discussion of these points see text.

	BLRSP1	BLRSP2	BLRSP3	BLRSP4	BLRSP5
Sneutrinos and Sleptons					
$m_{\tilde{\nu}_1}$ [GeV]	102.3 $(\tilde{\nu}_R)$	797.0 $(\tilde{\nu}_R)$	91.6 $(\tilde{\nu}_R, \tilde{\nu}_L)$	542.3 $(\tilde{\nu}_R, \tilde{\nu}_L)$	753.4 $(\tilde{\nu}_R, \tilde{\nu}_L)$
$m_{\tilde{\nu}_2}$ [GeV]	102.3 $(\tilde{\nu}_R)$	797.0 $(\tilde{\nu}_R)$	92.6 $(\tilde{\nu}_R, \tilde{\nu}_L)$	542.3 $(\tilde{\nu}_R, \tilde{\nu}_L)$	753.9 $(\tilde{\nu}_R, \tilde{\nu}_L)$
$m_{\tilde{\nu}_3}$ [GeV]	203.0 $(\tilde{\nu}_R)$	797.0 $(\tilde{\nu}_R)$	92.6 $(\tilde{\nu}_R, \tilde{\nu}_L)$	542.3 $(\tilde{\nu}_R, \tilde{\nu}_L)$	753.9 $(\tilde{\nu}_R, \tilde{\nu}_L)$
$m_{\tilde{\nu}_4}$ [GeV]	573.8 $(\tilde{\nu}_R)$	1120.1 $(\tilde{\nu}_R, \tilde{\nu}_L)$	253.4 $(\tilde{\nu}_L, \tilde{\nu}_R)$	585.4 $(\tilde{\nu}_L, \tilde{\nu}_R)$	785.5 $(\tilde{\nu}_L, \tilde{\nu}_R)$
$m_{\tilde{\nu}_{5,6}}$ [GeV]	604.4 $(\tilde{\nu}_R)$	1120.3 $(\tilde{\nu}_R, \tilde{\nu}_L)$	258.2 $(\tilde{\nu}_L, \tilde{\nu}_R)$	586.7 $(\tilde{\nu}_L, \tilde{\nu}_R)$	789.0 $(\tilde{\nu}_L, \tilde{\nu}_R)$
$m_{\tilde{\nu}_7}$ [GeV]	725.2 $(\tilde{\nu}_L)$	1220.0 $(\tilde{\nu}_L, \tilde{\nu}_R)$	1374.0 $(\tilde{\nu}_L, \tilde{\nu}_R)$	953.4 $(\tilde{\nu}_R)$	950.1 $(\tilde{\nu}_R)$
$m_{\tilde{\nu}_{8,9}}$ [GeV]	734.1 $(\tilde{\nu}_L)$	1236.6 $(\tilde{\nu}_L, \tilde{\nu}_R)$	1374.0 $(\tilde{\nu}_R)$	953.4 $(\tilde{\nu}_R)$	950.1 $(\tilde{\nu}_R)$
$m_{\tilde{e}_1}$ [GeV]	484.1 $(\tilde{\tau}_R)$	1013.9 $(\tilde{\tau}_R)$	254.7 $(\tilde{\tau}_L, \tilde{\tau}_R)$	263.0 $(\tilde{\tau}_R)$	580.4 $(\tilde{\tau}_R)$
$m_{\tilde{e}_{2,3}}$ [GeV]	512.7 $(\tilde{\mu}_R)/(\tilde{e}_R)$	1055.3 $(\tilde{\mu}_R)/(\tilde{e}_R)$	265.6 $(\tilde{\mu}_L)/(\tilde{e}_L)$	270.5 $(\tilde{\mu}_R)/(\tilde{e}_R)$	592.3 $(\tilde{\mu}_R)/(\tilde{e}_R)$
$m_{\tilde{e}_4}$ [GeV]	732.1 $(\tilde{\tau}_L)$	1222.4 $(\tilde{\tau}_L)$	447.7 $(\tilde{\tau}_R, \tilde{\tau}_L)$	591.6 $(\tilde{\tau}_L)$	788.0 $(\tilde{\tau}_L)$
$m_{\tilde{e}_{5,6}}$ [GeV]	738.8 $(\tilde{\mu}_L)/(\tilde{e}_L)$	1237.9 $(\tilde{\mu}_L)/(\tilde{e}_L)$	450.6 $(\tilde{\mu}_R)/(\tilde{e}_R)$	592.2 $(\tilde{\mu}_L)/(\tilde{e}_L)$	790.9 $(\tilde{\mu}_L)/(\tilde{e}_L)$
Squarks					
$m_{\tilde{u}_1}$ [GeV]	1144.0 $(\tilde{t}_R, \tilde{t}_L)$	1185.4 $(\tilde{t}_R, \tilde{t}_L)$	1247.0 $(\tilde{t}_R, \tilde{t}_L)$	1111.3 $(\tilde{t}_R, \tilde{t}_L)$	1316.0 $(\tilde{t}_R, \tilde{t}_L)$
$m_{\tilde{u}_2}$ [GeV]	1392.1 $(\tilde{t}_L, \tilde{t}_R)$	1851.9 $(\tilde{t}_L, \tilde{t}_R)$	1526.9 $(\tilde{t}_L, \tilde{t}_R)$	1361.4 $(\tilde{t}_L, \tilde{t}_R)$	1643.2 $(\tilde{t}_L, \tilde{t}_R)$
$m_{\tilde{u}_{3,4}}$ [GeV]	1456.0 $(\tilde{c}_R)/(\tilde{u}_R)$	2154.7 $(\tilde{c}_R)/(\tilde{u}_R)$	1565.9 $(\tilde{c}_R)/(\tilde{u}_R)$	1392.4 $(\tilde{c}_R)/(\tilde{u}_R)$	1728.0 $(\tilde{c}_R)/(\tilde{u}_R)$
$m_{\tilde{u}_{5,6}}$ [GeV]	1509.0 $[\tilde{c}_L, \tilde{u}_L]$	2227.3 $[\tilde{c}_L, \tilde{u}_L]$	1634.0 $[\tilde{c}_L, \tilde{u}_L]$	1448.8 $[\tilde{c}_L, \tilde{u}_L]$	1795.8 $[\tilde{c}_L, \tilde{u}_L]$
$m_{\tilde{d}_1}$ [GeV]	1359.2 $(\tilde{b}_L, \tilde{b}_R)$	1819.2 $(\tilde{b}_L)$	1409.8 $(\tilde{b}_R, \tilde{b}_L)$	1326.3 $(\tilde{b}_L)$	1611.8 $(\tilde{b}_L)$
$m_{\tilde{d}_2}$ [GeV]	1464.0 $(\tilde{b}_R, \tilde{b}_L)$	2148.1 $(\tilde{b}_R)$	1462.3 $(\tilde{s}_R)$	1420.1 $(\tilde{b}_R)$	1724.5 $(\tilde{b}_R)$
$m_{\tilde{d}_3}$ [GeV]	1489.8 $(\tilde{s}_R)$	2175.9 $(\tilde{s}_R)$	1462.3 $(\tilde{d}_R)$	1426.2 $(\tilde{s}_R)$	1734.8 $(\tilde{s}_R)$
$m_{\tilde{d}_4}$ [GeV]	1489.8 $(\tilde{d}_R)$	2175.9 $(\tilde{d}_R)$	1496.2 $(\tilde{b}_L, \tilde{b}_R)$	1426.2 $(\tilde{d}_R)$	1734.8 $(\tilde{d}_R)$
$m_{\tilde{d}_{5,6}}$ [GeV]	1509.0 $[\tilde{s}_L, \tilde{d}_L]$	2228.9 $[\tilde{s}_L, \tilde{d}_L]$	1635.9 $[\tilde{s}_L, \tilde{d}_L]$	1450.9 $[\tilde{s}_L, \tilde{d}_L]$	1795.8 $[\tilde{s}_L, \tilde{d}_L]$
Neutralinos					
$m_{\chi_1^0}$ [GeV]	282.2 $(\tilde{B})$	416.7 $(\tilde{B})$	312.9 $(\tilde{B})$	258.5 $(\tilde{h}_R)$	346.6 $(\tilde{B})$
$m_{\chi_2^0}$ [GeV]	552.3 $(\tilde{W}, \tilde{h}_L)$	780.0 $(\tilde{h}_R)$	615.3 $(\tilde{W}, \tilde{h}_L)$	279.7 $(\tilde{B})$	679.5 $(\tilde{W}, \tilde{h}_L)$
$m_{\chi_3^0}$ [GeV]	828.9 $(\tilde{h}_L)$	817.5 $(\tilde{W})$	1086.6 $(\tilde{h}_L)$	549.0 $(\tilde{W}, \tilde{h}_L)$	902.7 $(\tilde{h}_R)$
$m_{\chi_4^0}$ [GeV]	838.9 $(\tilde{h}_L, \tilde{W})$	1865.5 $(\tilde{h}_L)$	1092.8 $(\tilde{h}_L, \tilde{W})$	844.9 $(\tilde{h}_L)$	1133.1 $(\tilde{h}_L)$
$m_{\chi_5^0}$ [GeV]	1230.4 $(\tilde{B}_\perp, \tilde{h}_R)$	1865.7 $(\tilde{h}_L)$	1232.2 $(\tilde{h}_R, \tilde{B}_\perp)$	856.8 $(\tilde{h}_L, \tilde{W})$	1139.4 $(\tilde{h}_L, \tilde{W})$
$m_{\chi_6^0}$ [GeV]	1650.9 $(\tilde{h}_R)$	2017.6 $(\tilde{B}_\perp, \tilde{h}_R)$	1811.3 $(\tilde{B}_\perp, \tilde{h}_R)$	1639.0 $(\tilde{B}_\perp, \tilde{h}_R)$	1489.8 $(\tilde{B}_\perp, \tilde{h}_R)$
$m_{\chi_7^0}$ [GeV]	2608.3 $(\tilde{h}_R, \tilde{B}_\perp)$	2392.3 $(\tilde{h}_R, \tilde{B}_\perp)$	2741.4 $(\tilde{h}_R, \tilde{B}_\perp)$	2174.6 $(\tilde{h}_R, \tilde{B}_\perp)$	2056.5 $(\tilde{h}_R, \tilde{B}_\perp)$

Table 4.3: Susy spectra of our study points, for discussion see text. $(\tilde{\nu}_R)$ is a nearly maximal mixture of the right sneutrinos and the S-fields.

	BLRSP1	BLRSP2	BLRSP3	BLRSP4	BLRSP5
Light higgses (1-loop/2-loop)					
m_{h_1} [GeV]	59.1/59.6	119.2/125.4	92.7/93.1	100.8/102.6	18.8/18.8
m_{h_2} [GeV]	119.0/124.1	139.7/140.4	114.5/120.1	121.0/124.8	115.7/121.8
$\mathcal{R}^2_{L1}$	0.05/0.04	0.90/0.83	0.07/0.04	0.33/0.22	0.001/0.001
$\mathcal{R}^2_{L2}$	0.95/0.96	0.10/0.17	0.93/0.96	0.67/0.78	0.999/0.999
Heavy scalars/pseudoscalars					
m_{h_3} [GeV]	971.5	2176.5	1268.2	948.2	1345.6
m_{h_4} [GeV]	5074.9	7883.3	2268.2	3024.7	2227.2
m_{A_1} [GeV]	972.8	2177.5	796.3	949.2	1346.8
m_{A_2} [GeV]	4789.4	7581.1	1269.3	2345.1	1477.8

Table 4.4: Higgs spectra of our study points, for discussion see text.

we have checked the consistency of these eigenstates with data using `HiggsBounds 3.4.0beta` [258; 259]. All points are allowed by accelerator constraints, but sometimes very close to existing bounds, especially BLRSP4 and also BLRSP2. As an indication for the theoretical uncertainties in the mass calculation we give the masses using the complete 1-loop formulas and the ones adding the dominant 2-loop corrections to the MSSM sector [264; 265; 266; 267; 268; 34] [16].

In BLRSP1 and BLRSP5 h_1 is so light that the decay $h_2 \to h_1 h_1$ is kinematically allowed. However, the mixing between both sectors is so small that for BLRSP1 the corresponding branching ratio is about 1 per-cent whereas for BLRSP5 it is a few per-mile. The smallness of this decay is a direct consequence of the bounds imposed by LEP and the decay $h_2 \to h_1 h_1$ can never be dominant in the BLR model. The h_2 can also decay into a combination of heavy and light neutrinos with a branching ratio of a few per-cent, as for example in case of BLRSP1 leading to the final states

$$h_2 \quad \to \quad \nu_i \nu_k \to \nu_i l^{\pm} W^{\mp} \tag{4.52}$$

$$h_2 \quad \to \quad \nu_i \nu_k \to \nu_i \nu_j Z \tag{4.53}$$

with $i, j = 1, 2, 3$ and $k = 4, \ldots, 9$. These final states can also be obtained via intermediate states containing an off-shell vector boson, e.g. WW^* and ZZ^*. However, their existence implies that ratio of quark versus lepton final states will not correspond to the branching ratios of the vector bosons. Note, however, that for hadronic W-boson decays the invariant mass of jj+lepton system would show a peak at the heavy neutrino mass, which allows to identify this signature, in principle. Apart from these decays, the h_2 can also decay to two scalar neutrinos and, if kinematically allowed, this decay can become dominant, leading to a (nearly) invisible Higgs boson.

For a 125 GeV Higgs boson the excess [191; 192], see also [269], indicates a slightly larger than expected branching ratio into the two-photon final state. In [8] it was shown that the NMSSM can, in principle, explain such an enhanced di-photon rate, due to a possible mixing of the singlet and the Higgs, which reduces the coupling of the Higgs to bottom quarks, thus reducing the total width, without affecting the production cross section. In the case of the BLR model, such a construction is not possible, since our singlets are charged under $U(1)_R$ and the mixing between SM and BLR sectors is controlled by $\tan\beta_R$. Since we have to choose $\tan\beta_R$ close to one, the singlets mix to the up and down components of the Higgs equally. Therefore a reduction of $h \to b\bar{b}$ causes a reduction of the coupling for gluon fusion as well. Thus, a sizeable enhancement of Br($h \to \gamma\gamma$) by reducing simply the total width is not possible in the BLR model. Currently the discrepancy of the data with expectations is only at the level of about 1 σ c.l. and, as already mentioned before, only ATLAS confirmed the enhanced decay rate into photons in the latest published results. However, should future data show indeed an enhanced rate for the $\gamma\gamma$ final state, this would be hard to explain in the

[16] Note, that χ_R and $\bar{\chi}_R$ do not couple at tree-level to quarks. Therefore the 2-loop contributions from the extended higgs sector to the higgs mass are expected to be small and neglected in the presented calculation.

BLR model.

In the four points (BLRSP1, BLRSP3-BLRSP5) h_1 has approximately the same branching ratios for the decays into SM-fermions as a SM Higgs boson of the same mass. However, the corresponding widths are suppressed by the mixing with the usual MSSM sector which reduces the width by a factor between 10^2 and 10^4. At the LHC the main production of this particle is via SUSY cascade decays, e.g. it appears in the decays of $\tilde{\nu}_{4,5,6}$ (BLRSP1, BLRSP3), $\tilde{\chi}_3^0$ (BLRSP4) or in the decays of the heavy neutrinos which are produced via the Z' (BLRSP1, BLRSP4) as discussed in subsection . However, in case of BLRSP5 LHC will miss h_1 as it only appears in the decays of the heavy Higgs bosons which have masses in the TeV range.

Study point BLRSP2 differs from the others as here h_1 is the MSSM-like Higgs boson and h_2 has a mass of 140 GeV which could explain the slight excess in this region observed by ATLAS and CMS in the early data [270; 271]. In this region of the parameter space the Higgs at 125 GeV is made as in the MSSM, implying a rather heavy SUSY spectrum. This is due to the fact that a 140 GeV Higgs with reduced couplings can only be the h_{BLR}, i.e. this points exist to the right of the level-crossing region shown in fig. 4.2. Due to the choice of a rather small Y_s in this point the heavy neutrinos masses are below the mass of h_2. This leads to non-standard decays into the heavy neutrinos which dominantly decay to a lepton and a W-boson.

4.3.2. Z' physics

As already mentioned in sect. 4.2.1, our Z' corresponds essentially to the Z_χ in the notation of [254]. In previous studies usually two assumptions have been made in the construction of mass bounds: (i) the Z' decays only into the known SM particles [272] and (ii) the effects of gauge kinetic mixing are neglected. Both assumptions are not truly valid in the BLR model. For a recent study of Z' bounds without these assumptions see [273]. As shown in table 4.5 we find in all our points that the heavy neutrinos appear as final states beside the SM-fermions. Moreover, in all but BLRSP5 also supersymmetric particles appear as decay products, in particular sneutrinos and sleptons. On the other hand, gauge kinetic effects are in this model less important and were only important if one could measure the branching with a precision of 1 per-cent or better.

The Z' couples to leptons and quarks as follows

$$Z'_\mu \bar{f} \gamma^\mu (c_L^f P_L + c_R^f P_R) f \tag{4.54}$$

The different coefficients are given in table 4.6.

Note, that in the couplings to the u-quarks a partial cancellation occurs in contrast to the ones to d-quarks, which get enhanced. Moreover, the same feature appears in the vertex $\tilde{q}$-q-$\tilde{B}_\perp$ which leads to some interesting consequences discussed in subsection 4.3.4.

We find that the decays into the heavy neutrino states are always possible and have a sizable

final state	BLRSP1	BLRSP2	BLRSP3	BLRSP4	BLRSP5
$BR(dd)$	0.31	0.35	0.35	0.37	0.43
$BR(uu)$	0.06	0.07	0.07	0.07	0.08
$BR(ll)$	0.12	0.14	0.14	0.14	0.16
$BR(\nu_l\nu_l)$	0.10	0.11	0.12	0.12	0.12
$BR(\nu_h\nu_h)$	0.27	0.30	0.13	0.11	0.13
$BR(\tilde{\nu}\tilde{\nu})$	0.05	—	0.05	0.03	—
$BR(\tilde{l}\tilde{l})$	—	—	0.05	0.03	—
$BR(\tilde{\chi}_2^+\tilde{\chi}_2^-)$	—	—	—	0.02	—
$BR(\tilde{\chi}_4^0\tilde{\chi}_5^0)$	—	—	—	0.02	—

Table 4.5: Branching ratios of the dominant Z' decay modes. Here we have summed over the generations in case of the charged fermions and sfermions. For the neutrinos we have splitted this sum into a sum over the light (heavy) states denoted by ν_l (ν_h).

	c_L	c_R
d	$-\frac{i}{6}\left(-3g_L Z^{13} + g_{BL} Z^{23} + g_{BLR} Z^{33}\right)$	$-\frac{i}{6}\left((g_{BL} - 3g_{RBL}) Z^{23} + (g_{BLR} - 3g_R) Z^{33}\right)$
u	$-\frac{i}{6}\left(3g_L Z^{13} + g_{BL} Z^{23} + g_{BLR} Z^{33}\right)$	$-\frac{i}{6}\left((g_{BL} + 3g_{RBL}) Z^{23} + (g_{BLR} + 3g_R) Z^{33}\right)$
l	$\frac{i}{2}\left(g_L Z^{13} + g_{BL} Z^{23} + g_{BLR} Z^{33}\right)$	$\frac{i}{2}\left((g_{BL} + g_{RBL}) Z^{23} + (g_{BLR} + g_R) Z^{33}\right)$
ν	$\frac{i}{2}\Big[\sum_{x=1}^{3} Z_\nu^{j3+x,*} Z_\nu^{i3+x}\big((-g_{BL} + g_{RBL}) Z^{23} + (g_R - g_{BLR}) Z^{33}\big) + \sum_{x=1}^{3} Z_\nu^{jx,*} Z_\nu^{ix}\left(g_{BL} Z^{23} - g_L Z^{13} + g_{BLR} Z^{33}\right)\Big]$	$-\frac{i}{2}\Big[\sum_{x=1}^{3} Z_\nu^{i3+x,*} Z_\nu^{j3+x}\big((-g_{BL} + g_{RBL}) Z^{23} + (g_R - g_{BLR}) Z^{33}\big) + \sum_{x=1}^{3} Z_\nu^{ix,*} Z_\nu^{jx}\left(g_{BL} Z^{23} - g_L Z^{13} + g_{BLR} Z^{33}\right)\Big]$

Table 4.6: Coefficients c_L^f and c_R^f for the coupling between Z_R and two leptons or quarks. Here, Z is the rotation matrix diagonalizing the neutral gauge boson mass matrix and Z_ν is the neutrino mixing matrix. For the explicit expression of Z_μ we refer to the output of `SARAH`.

branching ratio provided $\mathrm{Tr}(|Y_s|) \lesssim 1$. In table 4.5 we summarize the most important final states of the Z' for the different scenarios. As can be seen the heavy neutrino final states have always a sizable branching ratios with up to about 30 per-cent when summing over the generations. But even for rather heavy neutrinos as in BLRSP5 own finds for this channel a 15 per-cent branching ratio. In several cases also channels into SUSY particles are open, in particular in scenarios with sneutrino LSPs. In case of supersymmetric particles the final states containing sleptons or sneutrinos have the largest branching ratios. Channels into neutralinos or charginos are suppressed. They proceed either via the mixing with the Z which is rather small or via the projection of the higgsino-right onto the corresponding neutralino state.

The appearance of additional final states leads to a reduction of the event numbers in the most sensitive search channels, i.e. reducing cross section times branching ratio, and, thus, the bounds obtained by the LHC collaborations [253; 274; 275] are less constraining in the BLR model. This is depicted in fig. 4.9 where we show the production cross section $\sigma(pp \to \mu^+\mu^-)$ around the Z' resonance. [17] In case that the width of the Z' is calculated using only SM final states the cross section is increased roughly by a factor 1.6 in comparison to the case where also right handed neutrinos and SUSY particle contribute to the width of Z'. With this choice of parameters, the main effect is due to R-neutrinos. We attribute the remaining difference to the official ATLAS result to slightly different values in the couplings and slightly different branching ratios of the final states. Our results agree also with the ones of ref. [254]. We conclude that, although in our benchmark points we take always $m_{Z'} > 1.8$ TeV, a significantly lower mass is possible consistent with data.

4.3.3. Heavy neutrinos

As discussed above, the heavy neutrino states can be produced via the Z' with a considerable branching ratio of about 30 per-cent when summing over all heavy neutrinos. Moreover, see below, they can also be produced in the cascade decays of supersymmetric particles. These heavy neutrinos mix with the light neutrino states implying a reduction of the couplings of the light neutrinos to the Z-boson and, thus, also a reduction of the invisible width of the Z-boson. Taking the data from ref. [180] this can be translated into the following condition on the 3×3 sub-block U^ν_{ij}, $i, j \leq 3$, of the neutrino mixing matrix:

$$\left| 1 - \sum_{ij=1, i\leq j}^{3} \left| \sum_{k=1}^{3} U^\nu_{ik} U^{\nu,*}_{jk} \right|^2 \right| < 0.009 \tag{4.55}$$

at the 3-σ level. We have checked that all our benchmark points fulfill this condition.

[17] For the calculation of the cross section we used `WHIZARD` [276; 277] and implemented the model using the `SUSY Toolbox` [257].

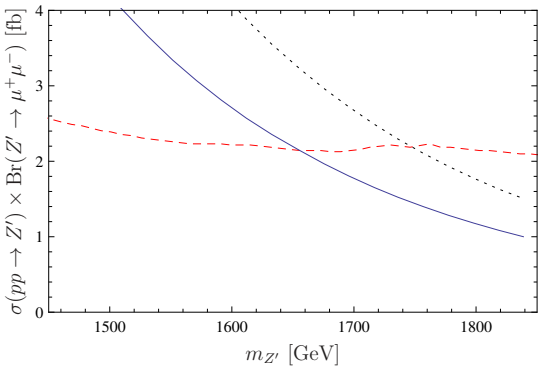

Figure 4.9: Cross section of $pp \to Z' \to \mu^+\mu^-$ near the Z' peak as function of $m_{Z'}$ taking into account a K-factor of 1.3 [278]. For the black, dotted line the Z' width has been calculated allowing only SM final states, while the blue solid includes also right-handed neutrinos and SUSY states. The red line shows the ATLAS exclusion limit [253]. We have used as input BLRSP1 and varied $v_R = [4.1, 5.1]$ TeV. Best experimental available limits are used. For details we refer to the output of SARAH.

The main decay modes of the heavy neutrinos are[18]

$$\nu_j \to W^\pm l^\mp \tag{4.56}$$
$$\nu_j \to Z\nu_i \tag{4.57}$$
$$\nu_j \to h_k\nu_i \tag{4.58}$$

where $j \geq 4$, $i \leq 3$, $k = 1, 2$ and $l = e, \mu, \tau$, provided they are kinemtically allowed. If there is no kinematical suppression we find in general the branching ratios scale like $BR(\nu_j \to W^\pm l^\mp) : BR(\nu_j \to Z\nu_i) : BR(\nu_j \to h_k\nu_i) \simeq 0.5 : 0.25 : 0.25$ where we have summed over the light Higgs bosons, the light neutrinos and leptons, respectively. We stress that these states are quasi-Dirac neutrinos and, thus, for six heavy neutrinos at LHC the existence of up to three new particles could be established. Note, that the final states containing a W-boson allow for a direct mass measurement.

Beside the above decay modes, also decays into SUSY particle are possible if kinematics allow for it. For example we find that for BLRSP4 the decay into $\tilde{\nu}_{1,2,3}\tilde{\chi}_1^0$ are possible and have branching ratios of about 3 per-cent. In scenarios like BLRSP3, BLRSP4 and BLRSP5 the main production of the heavy neutrinos is via the Z' and, thus, a high luminosity will be required to observe such final states.

[18] For related discussions see e.g. [279; 280; 281] and references therein.

4.3.4. SUSY cascade decays

In this subsection we point out several features which distinguish the BLR model from the usual MSSM. For the sake of preparing the ground, let us first summarize the main features of the MSSM relevant for the LHC, focusing for the time being on scenarios where the gluino is heavier than the squarks: (i) The gluino decays dominantly into squarks and quarks. (ii) L-squarks and L-sleptons decay dominantly into the chargino and the neutralino which are mainly $SU(2)_L$-gauginos. Apart from kinematical effects the branching ratio for decays into the charged wino divided by the branching ratio into the neutral wino is about 2:1. (iii) R-squarks and R-sleptons decay dominantly into the bino-like neutralino with a branching ratio often quite close to 100 per-cent. (iv) In case of third generation sfermions also decays into higgsinos are important.

In the BLR model one has two main new features: (i) there are additional neutralinos and (ii) the sneutrino sector is enlarged as well. The latter implies that sneutrino LSPs are possible consistent with all astrophysical constraints and direct dark matter searches [282; 283; 284; 285; 286; 287; 288]. This feature is for example realized in study points BLRSP1 and BLRSP3[19].

Let us start the discussion with BLRSP1. In this point the four lighter neutralinos are the usual MSSM neutralinos with the standard hierarchy. The fifth state corresponds to the additional $U(1)$-gaugino, which we call $\tilde{B}_\perp$, whereas the two additional states are the additional higgsinos. Note that the lightest neutralino is not stable anymore but decays into final states containing all nine neutrinos as well as the three lightest sneutrinos. Of the latter ones the second lightest is so long lived that it will lead to a displaced vertex in a typical collider detector. The third sneutrino decays dominantly via three-body decays into $l^+l^-\tilde{\nu}_i$ and $\nu_k\nu_l\tilde{\nu}_i$ with $i = 1, 2$ and $k, l = 1, 2, 3$. As discussed in subsection 4.3.3 the heavy neutrinos decay dominantly into W-bosons and charged leptons, thus the decays of the lightest neutralino are not invisible.

$\tilde{B}_\perp$ appears for example in the decays of $\tilde{d}_R$ and $\tilde{s}_R$ with branching ratios BR($q\tilde{\chi}_1^0$) $\simeq 0.8$ and BR($q\tilde{\chi}_5^0$) $\simeq 0.2$. For completeness we remark that the decays of $\tilde{u}_R$ and $\tilde{c}_R$ into $\tilde{\chi}_5^0$ is suppressed as the corresponding coupling is suppressed as are the couplings of Z' to u-type quarks in this model. $\tilde{\chi}_5^0$ decays dominantly into sleptons and sneutrinos. Combining all the above together one gets a much richer structure for the decays of the R-squarks, e.g. the following decay chains:

$$\tilde{q}_R \rightarrow q\tilde{\chi}_1^0 \rightarrow q\nu_k\tilde{\nu}_1 \rightarrow q\nu_j Z\tilde{\nu}_1 \tag{4.59}$$

$$\tilde{q}_R \rightarrow q\tilde{\chi}_1^0 \rightarrow q\nu_k\tilde{\nu}_1 \rightarrow ql^\pm W^\mp\tilde{\nu}_1 \tag{4.60}$$

$$\tilde{q}_R \rightarrow q\tilde{\chi}_1^0 \rightarrow q\nu_k\tilde{\nu}_3 \rightarrow ql^\pm W^\mp\tilde{l}'^+ l'^- \nu_1 \tag{4.61}$$

$$\tilde{q}_R \rightarrow q\tilde{\chi}_5^0 \rightarrow ql^\pm\tilde{l}_i^\mp \rightarrow ql^\pm l^\mp\tilde{\chi}_1^0 \rightarrow ql^\pm l^\mp\nu_k\tilde{\nu}_1 \rightarrow ql^\pm l^\mp l'^\pm W^\mp\tilde{\nu}_1 \tag{4.62}$$

[19] We note for completeness, that the relic abundance is actually somewhat too large in this point but can easily be adjusted by changing for example in BLRSP1 $\tan\beta_R$ from 1.05 to 1.0475 without changing the collider features of BLRSP1.

with $k \in \{4,5,6,7,8,9\}$ and $j \in \{1,2,3\}$. Of course, several other combinations are possible as well.

From equations (4.59) to (4.62) one sees immediately that the standard signature of R-squarks, namely jet and missing energy, is only realized in a few cases in this study point, e.g. if in eq. (4.59) the Z decays into neutrinos. Interestingly, the chain via $\tilde{\chi}_5^0$ into sleptons leads to a characteristic edge in the invariant mass of the lepton which can be used to determine the corresponding masses once combined with information from other decay chains. Also in the study points BLRSP2 and BLRSP5 $\tilde{d}_R$ and $\tilde{s}_R$ decay into heavy neutralinos, which contain sizable content of the extra $U(1)$ gaugino, with a sizable branching ratio. However, there the situation is somewhat less involved as in these study points the lightest bino-like neutralino is the LSP.

Another interesting feature is, that $\tilde{\chi}_5^0$ decays also into the heavier sneutrinos which themselves decay into the LSP plus h_1. Similarly h_1 can be produced in the decays of the heavy neutrinos implying that this state can be produced with sizable rate in SUSY cascade decays. However, as the corresponding final states are quite complicated a dedicated Monte Carlo study will be necessary to decide if this is indeed a discovery channel for h_1.

From the point of view of SUSY cascade decays BLRSP2 looks essentially like a standard MSSM point. Inspection of the spectrum shows that $\tilde{\chi}_2^0$ is essentially a higgsino corresponding to the extended $U(1)$ sector but it shows hardly up in the cascade decays. Its main production channel is via an s-channel Z' but even in this case the corresponding cross section is so low that it will not be detected at the LHC even with an integrated luminosity of 300 fb^{-1}. Another interesting feature shows up in the decays of $\tilde{\chi}_3^0$ which is mainly the neutral wino and gets copiously produced in the decays of the L-squarks: it decays with about 77 (15) per-cent into h_1 (h_2), implying that the cascade decays are an important source of Higgs bosons.

In case of BLRSP3 one has sneutrino LSPs like in BLRSP1 but with a different hierarchy in the spectrum, as the three lightest sleptons are lighter then the lightest neutralino. Therefore the $\tilde{\chi}_1^0$ has also sizable decay rates into charged sleptons which sum to about 30 per-cent. The sleptons decay then further into $W^-\tilde{\nu}_{1,2,3}$ and $\nu_{2,3}$ via 3-body decays into $f\bar{f}$-pairs. The latter, however, are rather soft due to the small mass difference. In addition we have the decay channel into a light neutrino and one of the heavier sneutrinos which themselves decay into a lighter sneutrino and either one of the Higgs boson or the Z-boson. Putting again all these decays together one obtains for the $\tilde{\chi}_1^0$

decays

$$\begin{aligned}
\tilde{\chi}_1^0 &\to l^\pm \tilde{l}^\mp \to l^\pm W^\mp \tilde{\nu}_1 && (4.63)\\
\tilde{\chi}_1^0 &\to l^\pm \tilde{l}^\mp \to l^\pm W^\mp \tilde{\nu}_{2,3} \to l^\pm W^\mp f \bar{f} \tilde{\nu}_1 && (4.64)\\
\tilde{\chi}_1^0 &\to \nu_j \tilde{\nu}_{2,3} \to \nu_{1,2,3} f \bar{f} \tilde{\nu}_1 && (4.65)\\
\tilde{\chi}_1^0 &\to \nu_j \tilde{\nu}_1 && (4.66)\\
\tilde{\chi}_1^0 &\to \nu_j \tilde{\nu}_k \to \nu_j h_{1,2} \tilde{\nu}_1 && (4.67)\\
\tilde{\chi}_1^0 &\to \nu_j \tilde{\nu}_k \to \nu_j h_{1,2} f \bar{f} \tilde{\nu}_1 && (4.68)
\end{aligned}$$

with $j = 1, 2, 3$ and $k = 4, 5, 6$. This implies that the decays of the R-squarks show again a more complicated structure compared to the usual CMSSM expectations. Channels (4.67) and (4.68) give h_1 in about 15 per-cent of the final states of $\tilde{\chi}_1^0$. Moreover, $\tilde{\chi}_2^0$ and $\tilde{\chi}_1^+$ decay dominantly into sleptons and sneutrinos. Here a new feature is found for $\tilde{\chi}_1^+$, as also the following chains

$$\begin{aligned}
\tilde{\chi}_1^+ &\to l^+ \tilde{\nu}_{5,6} \to l^+ Z \tilde{\nu}_1 && (4.69)\\
\tilde{\chi}_1^+ &\to l^+ \tilde{\nu}_{5,6} \to l^+ h_{1,2} \tilde{\nu}_1 && (4.70)
\end{aligned}$$

gives rise to sharp edge structures. However, as the main final states of Z and $h_{1,2}$ are two jets, the feasibility still needs to be investigated.

In BLRSP4 we have chosen $\mu_R = 260$ GeV in order to construct an LSP which is essentially a $\tilde{h}_R$. Here, the R-sleptons are lighter than $\tilde{\chi}_2^0$, which is essentially bino-like in this point, giving rise to the following decay chain of the down-type R-squarks

$$\tilde{d}_R \to d \tilde{\chi}_2^0 \to d l^\pm \tilde{l}^\mp \to d l^\pm l^\mp \tilde{\chi}_1^0 \qquad (4.71)$$

Nearly all cascade decays end in a $\tilde{\chi}_2^0$ or one of the lighter sleptons. Due to the fact, that in this particular case the additional sneutrino states are hardly produced, it might be difficult to distinguish it from the NMSSM, at least as long as the Z' is not discovered. The heavier L-sleptons do not show up in the cascade decays of squarks and gluinos but can be produced via the Z' as discussed in subsection .

BLRSP5 is similar to BLRSP1 but compatible with pure GUT conditions, e.g. μ_R and m_{A_R} are not input in this case put derived quantities. To fulfill the tadpole equations we have to choose $Y_s = 0.3$ and $\tan\beta_R = 1.03$ if we want a relatively low $m_0 = 500$ GeV while $M_{1/2} = 850$ GeV. The choice of Y_s leads automatically to large masses for the heavy neutrinos such that the lightest Higgs can not decay into those states. As in BLRSP1 the down-type R-squarks decay not only into $\tilde{\chi}_1^0$ but also into $\tilde{\chi}_6^0$ with a branching ratio of about 13 per-cent. For completeness, we note that here $\tilde{\chi}_3^0 \simeq \tilde{h}_R$. However this state gets hardly produced in any of the SUSY decays or via the Z'.

Therefore, it is likely that LHC will miss it and also at a linear collider such as ILC or CLIC it will be difficult to study, due to the small production cross section.

4.4. Conclusions

In this chapter we have studied the minimal supersymmetric $U(1)_{B-L} \times U(1)_R$ extension of the standard model. The model is minimal in the sense that the extended gauge symmetry is broken with the minimal number of Higgs fields. In the matter sector the model contains (three copies of) a superfield $\hat{\nu}^c$, to cancel anomalies. Adding three singlet superfields $\hat{S}$ allows to generate small neutrino masses with an inverse seesaw mechanism.

In particular, we have shown that, already at the tree-level, the CP-even Higgs boson resembling the lightest neutral Higgs h^0 of the MSSM, can have a mass well above m_Z. At the one loop level, masses of 140 GeV and even above can easily be reached. In addition to such an h^0-like Higgs, one can also have a second light state which, however, hardly couples to the SM vector bosons as it predominantly spans over the SM-neutral components. We have found regions where the h^0-like Higgs can decay into two such states which, however, alters the standard search techniques at the LHC. Finally, we would like to stress that the general features discussed here also apply to other extensions of the SM gauge group, e.g., to full-featured left-right symmetric models, provided the MSSM Higgs doublets are charged with respect to the extended gauge symmetry.

The phenomenology of the model differs from the MSSM in a number of interesting aspects. We have focused on the Higgs phenomenology and discussed changes in SUSY spectra and decays with respect to the MSSM. The model is less constrained then the CMSSM from the possible measurement of a Higgs with a mass of the order of 125 GeV. If the hints found in LHC data [191; 192] is indeed correct our model predicts two relatively light states should exist, with the second h^0 corresponding (mostly) to the lightest of the "right" Higgses, added to break the extended gauge group.

It is interesting, as we have discussed, that very often a right sneutrino is found to be the LSP. This will affect all constraints on CMSSM parameter space derived from constraints on the dark matter abundance. In fact, if the right sneutrino is indeed the LSP in our model, no constraint on any CMSSM parameters can be derived from DM constraints.

The model has new D-terms in all scalar mass matrices, which can lead to sizeable changes in the SUSY spectra, of potential phenomenological interest. We have discussed a few benchmark points, covering a number of features which could allow to distinguish the model from the CMSSM. Obviously this includes the discovery of a Z' at the LHC where we have shown that the current bounds from LHC data depend on the details of the particle spectrum. Also the cascade decays of supersymmetric particles can be significantly more involved than in the usual CMSSM as the additional neutralinos, neutrinos and sneutrinos lead to enhancement of the multiplicities in the final states. This implies that the existing limits on the CMSSM parameter space get modified as

standard final states have reduced branching ratios and at the same time additional final states are present. In case that the mBLR model is indeed realized these new cascade decays will offer additional kinematical information on the particle spectrum. Possible scenarios to distinguish the model presented in this section from the MSSM are a Z' within the kinematical reach of the LHC, the observation of three light non-degenerate higgs states and the right sneutrino to be the LSP.

5 Conclusions

In the first part of this thesis we calculate supersymmetric mass spectra with CMSSM boundary conditions and a type-I, type-II and type-III seesaw mechanism, respectively, added to explain current neutrino data. All results are based on [1] and [2]. Using published, estimated errors on SUSY mass observables for LHC and ILC analysis, we perform a theoretical χ^2 analysis to identify parameter regions where pure CMSSM and CMSSM plus seesaw might be distinguishable with LHC and/or ILC data. In case of seesaw type-I the most important observables are determined to be the (left) smuon and selectron masses and the splitting between them, respectively. Splitting in the (left) smuon and selectrons is tiny in most of CMSSM parameter space, but can be quite sizeable for large values of the seesaw scale, m_{SS}. Thus, for very roughly $m_{SS} \geq 10^{14}$ GeV hints for type-I seesaw might appear in SUSY mass measurements for a combined LHC and ILC analysis. Taking into account recent exclusion limits on SUSY masses from LHC accuracies, needed to distinguish a CMSSM and a CMSSM plus type-I scenario, can not be achieved anymore. If SUSY particles are within the reach of the ILC, CMSSM can be distinguished from CMSSM plus type-II or type-III seesaw for nearly all relevant values of the seesaw scale. In the case when only the much less accurate LHC measurements are used, we find that indications for the seesaw can be found in favourable parts of the parameter space. The lower the real value of the seesaw scale m_{SS} is, the easier it becomes to distinguish CMSSM from CMSSM plus seesaw. Nevertheless, with recent LHC data it is very unlikely to detect deformations in a CMSSM spectra coming from a seesaw type-II and type-II, respectively.

Motivated by the discovery of the new boson at around 125 GeV at the LHC we study in the second part of this thesis the minimal supersymmetric $U(1)_{B-L} \times U(1)_R$ extension of the standard model. All results are based on [3] and [4]. In the MSSM the lightest neutral Higgs h_0 must be, at the tree level, lighter than the Z boson and that the loop corrections shift this stringent upper bound up to about 130 GeV. Extending the MSSM gauge group in a suitable way, the new Higgs sector dynamics can push the tree-level mass of h_0 well above the tree-level MSSM limit if it couples to the new gauge sector. We found that at the loop level h_0 masses in the 140 GeV ballpark can be

reached easily. Therefore a Higgs mass at around 125 GeV could be easily explained by this model. The second light state in the Higgs sector hardly couples to the SM vector bosons but we have found regions where the h^0-like Higgs can decay into two such states. Due to the extended gauge sector $U(1)$ new D-terms in all scalar mass matrices are present. This can lead to significant changes in the the SUSY spectra, of potential phenomenological interest. The discussed benchmark points, present a number of features which could provide the possibility to distinguish the model from the CMSSM. The discovery of a Z' would give strong hints for an extra $U(1)$ present at low scales. Additional neutralinos, neutrinos and sneutrinos contribute to cascade decays of supersymmetric particles and enhance the multiplicity in the final states. Therefore limits on the CMSSM parameter space change since CMSSM final states have reduced branching ratios and new final states, coming from the extended multiplets, are present. In this work we have focused on the Higgs phenomenology and discussed changes in SUSY spectra and decays with respect to the MSSM. However, also DM phenomenology may change drastically. Due to the extended neutrino sector also sneutrinos are found to be the LSP. With such a dark matter candidate constraints on the CMSSM space coming from limits on the dark matter abundance are changed. If the right sneutrino is the LSP no constraint on any CMSSM parameters can be derived from DM constraints.

A

Appendix

A.1. Mass matrices

Here we list the tree-level mass matrices of the model not given in the main text.

- **Mass matrix for Down-Squarks**, Basis: $\left(\tilde{d}_L, \tilde{d}_R\right)$

$$m^2_{\tilde{d}} = \begin{pmatrix} m^2_{LL} & \frac{1}{\sqrt{2}}\left(v_d T_d^\dagger - v_u \mu Y_d^\dagger\right) \\ \frac{1}{\sqrt{2}}\left(v_d T_d - v_u Y_d \mu^*\right) & m^2_{RR} \end{pmatrix} \tag{A.1}$$

$$\begin{aligned} m^2_{LL} = m^2_q + \frac{v_d^2}{2} Y_d^\dagger Y_d - \frac{1}{24}\Big(\Big(g^2_{BL} + g^2_{BLR} - g_{BLR} g_R - g_{BL} g_{RBL}\Big)\Big(v^2_{\chi_R} - v^2_{\bar{\chi}_R}\Big) \\ + \Big(3 g^2_L + g_{BL} g_{RBL} + g_{BLR} g_R\Big)\Big(v_d^2 - v_u^2\Big)\Big)\mathbf{1} \end{aligned} \tag{A.2}$$

$$\begin{aligned} m^2_{RR} = m^2_d + \frac{v_d^2}{2} Y_d Y_d^\dagger \\ + \frac{1}{24}\Big(\Big(g^2_{BL} + g^2_{BLR} - 4(g_{BLR} g_R + g_{BL} g_{RBL}) + 3(g^2_R + g^2_{RBL})\Big)\Big(v^2_{\chi_R} - v^2_{\bar{\chi}_R}\Big) \\ + \Big(g_{BL} g_{RBL} + g_{BLR} g_R - 3(g^2_R + g^2_{RBL})\Big)\Big(v_d^2 - v_u^2\Big)\Big)\mathbf{1} \end{aligned} \tag{A.3}$$

- **Mass matrix for Up-Squarks**, Basis: $(\tilde{u}_L, \tilde{u}_R)$

$$m^2_{\tilde{u}} = \begin{pmatrix} m^2_{LL} & \frac{1}{\sqrt{2}}\Big(- v_d \mu Y_u^\dagger + v_u T_u^\dagger\Big) \\ \frac{1}{\sqrt{2}}\Big(- v_d Y_u \mu^* + v_u T_u\Big) & m^2_{RR} \end{pmatrix} \tag{A.4}$$

$$m_{LL}^2 = m_q^2 + \frac{v_u^2}{2} Y_u^\dagger Y_u - \frac{1}{24}\Big(\Big(g_{BL}^2 + g_{BLR}^2 - g_{BLR}g_R - g_{BL}g_{RBL}\Big)\Big(v_{\chi_R}^2 - v_{\bar{\chi}_R}^2\Big) + \Big(3g_L^2 - g_{BL}g_{RBL} - g_{BLR}g_R\Big)\Big(v_u^2 - v_d^2\Big)\Big)\mathbf{1} \tag{A.5}$$

$$m_{RR}^2 = m_u^2 + \frac{v_u^2}{2} Y_u Y_u^\dagger + \frac{1}{24}\Big(\Big(g_{BL}^2 + g_{BLR}^2 + 2(g_{BLR}g_R + g_{BL}g_{RBL}) - 3(g_R^2 + g_{RBL}^2)\Big)\Big(v_{\chi_R}^2 - v_{\bar{\chi}_R}^2\Big) + \Big(g_{BL}g_{RBL} + g_{BLR}g_R + 3(g_R^2 + g_{RBL}^2)\Big)\Big(v_d^2 - v_u^2\Big)\Big)\mathbf{1} \tag{A.6}$$

- **Mass of the Charged Higgs boson**: One obtains the same expression as in the MSSM:

$$m_{H^+}^2 = B_\mu \left(\tan\beta + \cot\beta\right) + m_W^2 \tag{A.7}$$

- **Mass matrix for Charginos**, Basis: $\left(\tilde{W}^-, \tilde{H}_d^-\right), \left(\tilde{W}^+, \tilde{H}_u^+\right)$

$$m_{\tilde{\chi}^-} = \begin{pmatrix} M_2 & \frac{1}{\sqrt{2}} g_L v_u \\ \frac{1}{\sqrt{2}} g_L v_d & \mu \end{pmatrix} \tag{A.8}$$

A.2. Calculation of the mass spectrum

We are going to present now the basic steps to calculate the mass spectrum. As starting point we use electroweak precision data to get the gauge and Yukawa couplings: the SM-like Yukawa couplings are calculated from the fermion masses and the one-loop relations of ref. [188] which have been adjusted to our model. Similarly, also the standard model gauge couplings are calculated by the same procedure presented in ref. [188], but again, including all new contributions of the mode under consideration. Since the entire RGE running is performed in the basis $SU(3)_C \times SU(2)_L \times U(1)_R \times U(1)_{B-L}$, the value of the GUT normalized g_{BL} and g_R are matched to the GUT normalized hypercharge coupling g_Y by

$$g_R = c_{RY}\, g_Y\,, \tag{A.9}$$

$$g_{BL} = \frac{5 g_{BLR} g_{RBL} g_R - \sqrt{6} g_{RBL} g_Y^2 + \sqrt{(3 g_{BLR}^2 - 2\sqrt{6} g_{BLR} g_R + 2 g_R^2)(5(g_R^2 + g_{RBL}^2 - 3 g_Y^2) g_Y^2}}{5 g_R^2 - 3 g_Y^2}\,. \tag{A.10}$$

This is nothing else then an inversion of the well known relation between the gauge couplings for $U(1)_R \times U(1)_{B-L} \to U(1)_Y$ including the off-diagonal gauge couplings given in eq. (A.11). We are

using the $SO(10)$ GUT normalization of $\sqrt{\frac{3}{5}}$ for $U(1)_Y$ and $\sqrt{\frac{3}{2}}$ for $U(1)_{B-L}$. To get the correct values of c_{RY} as well as g_{RBL} and g_{BLR} an iterative procedure is used: c_{RY} is calculated as ratio of the g_Y and g_{BL} when running down from the GUT scale and applying

$$g_Y = \sqrt{\frac{5(g_{BL}g_R - g_{BLR}g_{RBL})^2}{3(g_{BL}^2 + g_{BLR}) + 2(g_R^2 + g_{RBL}^2) - 2\sqrt{6}(g_R g_{BLR} + g_{BL}g_{RBL})}} \tag{A.11}$$

When the gauge and Yukawa couplings are derived, the RGEs are then evaluated up to the GUT scale where the corresponding boundary conditions of eqs. (4.5), (4.6) and (4.12) are applied. Afterwards a RGE running of the full set of parameters to the SUSY scale is performed. We use always 2-loop RGEs which include the full effect of kinetic mixing [164; 165].

The running parameters are then used to calculate the tree level mass spectrum. However, it is well known that the one-loop corrections can be very important for particular particles and have to be taken into account. The best known example is the light MSSM Higgs boson which get shifted by up to 50% per-cent in case of heavy stops. Similar effects can be expected in the extended Higgs sector especially since these can be very light at tree-level. Similarly, the gauginos arising in an extended gauge sector can be potentially light and receive important corrections at one-loop [245]. To take these and all other possible effects into account we use a complete one-loop correction of the entire mass spectrum. Our procedure to calculate the one-loop masses is based on the method proposed in Ref.[188]: first, all running $\overline{\text{DR}}$ parameters are calculated at the SUSY scale and the SUSY masses at tree-level are derived. The EW vevs v_d and v_u are afterwards re-calculated using the one-loop corrected Z mass and demanding

$$m_Z^2 + \delta m_Z^2 = \frac{(g_{BL}^2 g_L^2 + g_{BL}^2 g_R^2 + g_L^2 g_R^2)v^2}{4(g_{BL}^2 + g_R^2)}(v_d^2 + v_u^2) \tag{A.12}$$

in addition with the running value of $\tan\beta$. Note that δm_Z^2 as well as all other self-energies include the corrections originated by all particles present in the mBLR. These calculations are performed in $\overline{\text{DR}}$ scheme and 't Hooft gauge. Also the complete dependence on the external momenta are taken into account. The re-calculated vevs are afterwards used to solve the tree-level tadpole equations again and to re-calculate the tree-level mass spectrum as well as all vertices entering the one-loop corrections. Using these vertices and masses, the one-loop corrections δt_i to the tadpole equations are derived and we use as renormalization condition

$$t_i - \delta t_i = 0\,. \tag{A.13}$$

These one-loop corrected tadpole equations are solved with respect to the same parameter as at tree level resulting in new parameters $\mu^{(1)}, B_\mu^{(1)}, \mu_R^{(1)}$, $B_{\mu_R}^{(1)}$ respectively $\mu^{(1)}, B_\mu^{(1)}$, $m_{\chi_R}^{2,(1)}$, $m_{\bar{\chi}_R}^{2,(1)}$. The final step is to calculate all self-energies for different particles and to use those to get the one-loop

corrected mass spectrum [1].

1. **Real scalars**: for a real scalar ϕ, the one-loop corrections are included by calculating the real part of the poles of the corresponding propagator matrices [188]

$$\text{Det}\left[p_i^2\mathbf{1} - m^2_{\phi,1L}(p^2)\right] = 0, \tag{A.14}$$

where

$$m^2_{\phi,1L}(p^2) = \tilde{m}^2_{\phi,T} - \Pi_\phi(p^2). \tag{A.15}$$

Equation (A.14) has to be solved for each eigenvalue $p^2 = m_i^2$ which can be achieved in an iterative procedure. This has to be done also for charged scalars as well as the fermions. Note, $\tilde{m}^2_T$ is the tree-level mass matrix but for the parameters fixed by the tadpole equations the one-loop corrected values $X^{(1)}$ are used.

2. **Complex scalars**: for a complex scalar η field we use at one-loop level

$$m^{2,\eta}_{1L}(p_i^2) = \tilde{m}^{2,\eta}_T - \Pi_\eta(p_i^2), \tag{A.16}$$

While in case of sfermions $\tilde{m}^{2,\eta}_T$ agrees exactly with the tree-level mass matrix, for charged Higgs bosons $\mu^{(1)}$ and $B^{(1)}_\mu$ or $m^{(1)}_{H_d}$ and $m^{(1)}_{H_d}$ has to be used depending on the set of parameters the tadpole equations are solved for.

3. **Majorana fermions**: the one-loop mass matrix of a Majorana χ fermion is related to the tree-level mass matrix by

$$\begin{aligned} M^\chi_{1L}(p_i^2) \;=\; & M^\chi_T - \frac{1}{2}\Big[\Sigma^0_S(p_i^2) + \Sigma^{0,T}_S(p_i^2) + \left(\Sigma^{0,T}_L(p_i^2) + \Sigma^0_R(p_i^2)\right) M^\chi_T \\ & + M^{\tilde{\chi}^0}_T \left(\Sigma^{0,T}_R(p_i^2) + \Sigma^0_L(p_i^2)\right)\Big], \end{aligned} \tag{A.17}$$

where we have denoted the wave-function corrections by Σ^0_R, Σ^0_L and the direct one-loop contribution to the mass by Σ^0_S.

4. **Dirac fermions**: for a Dirac fermion Ψ one has to add the self-energies as

$$M^\Psi_{1L}(p_i^2) = M^\Psi_T - \Sigma^+_S(p_i^2) - \Sigma^+_R(p_i^2)M^\Psi_T - M^\Psi_T\Sigma^+_L(p_i^2). \tag{A.18}$$

Note, this procedure agrees with the method implemented in `SPheno 3.1.10` to calculate the loop masses in the MSSM as well as with the code produced by `SARAH 3.0.39` or later. However, there

[1] Note, that for all calculations simple $\overline{\text{DR}}$ scheme is used and we assume that all new divergencies coming from the extended gauge sector vanish.

are small differences to earlier versions of SPheno as well as other spectrum calculators: the MSSM equivalent of condition eq (A.12) is often solved in an iterative way using the one-loop corrected parameters from the tadpole equations to calculate δm_Z^2 until $m_Z^2 + \delta m_Z^2$ has converged. In this context also $\mu^{(1)}$ and $B_\mu^{(1)}$ are used in the vertices entering the one-loop corrections. However, these steps mix tree- and one-loop level and break therefore gauge invariance: when we tried this approach the relation between Goldstone and gauge bosons mass is violated. However, the numerical differences in case of the MSSM turned out to be rather small.

As example we give the necessary formulae to calculate the one-loop corrections to the tadpole equations and the scalar Higgs masses in appendix A.3.

A.3. 1-loop corrections of the Higgs sector

As discussed in section A.2 we have calculated the entire mass spectrum at one-loop. For that purpose it is necessary to calculate all possible 1-loop diagrams for the one- and two-point functions. As example we here give the corresponding expressions for the one-loop corrections of the tadpoles as well as the self-energy for the scalar Higgs fields. For all other self-energies we refer to the output of SARAH. The results are expressed via Passarino Veltman integrals [188]. The basic integrals are

$$A_0(m) = 16\pi^2 Q^{4-n} \int \frac{d^n q}{i\,(2\pi)^n} \frac{1}{q^2 - m^2 + i\varepsilon}\,, \tag{A.19}$$

$$B_0(p, m_1, m_2) = 16\pi^2 Q^{4-n} \int \frac{d^n q}{i\,(2\pi)^n} \frac{1}{\left[q^2 - m_1^2 + i\varepsilon\right]\left[(q-p)^2 - m_2^2 + i\varepsilon\right]}\,, \tag{A.20}$$

with the renormalization scale Q. All the other, necessary functions can be expressed by A_0 and B_0. For instance,

$$B_1(p, m_1, m_2) = \frac{1}{2p^2}\left[A_0(m_2) - A_0(m_1) + (p^2 + m_1^2 - m_2^2) B_0(p, m_1, m_2)\right]\,, \tag{A.21}$$

and

$$F_0(p, m_1, m_2) = A_0(m_1) - 2A_0(m_2) - (2p^2 + 2m_1^2 - m_2^2) B_0(p, m_1, m_2)\,, \tag{A.22}$$

$$G_0(p, m_1, m_2) = (p^2 - m_1^2 - m_2^2) B_0(p, m_1, m_2) - A_0(m_1) - A_0(m_2) \tag{A.23}$$

The numerical evalution of all loop-integrals is performed by SPheno. With this conventions we can write the one-loop tadpoles as

$$\delta t_{\sigma_i}^{(1)} = +\frac{3}{2} A_0\Big(m_Z^2\Big)\Gamma_{\sigma_i, Z, Z} + \frac{3}{2} A_0\Big(m_{Z_R}^2\Big)\Gamma_{\sigma_i, Z_R, Z_R} + 3A_0\Big(m_{W^-}^2\Big)\Gamma_{\sigma_i, W^+, W^-}$$

$$
\begin{aligned}
&+ 16A_0\Big(m^2_{\nu_1}\Big)\Gamma_{\sigma_i,\nu_1,\nu_1}m^2_{\nu_1} - \sum_{a=1}^{2} A_0\Big(m^2_{H_a^-}\Big)\Gamma_{\sigma_i,H_a^+,H_a^-} \\
&+ 4\sum_{a=1}^{2} A_0\Big(m^2_{\tilde{\chi}_a^-}\Big)\Gamma^L_{\sigma_i,\tilde{\chi}_a^+,\tilde{\chi}_a^-}m^2_{\tilde{\chi}_a^-} + 12\sum_{a=1}^{3} A_0\Big(m^2_{d_a}\Big)\Gamma^L_{\sigma_i,\bar{d}_a,d_a}m^2_{d_a} \\
&+ 4\sum_{a=1}^{3} A_0\Big(m^2_{e_a}\Big)\Gamma^L_{\sigma_i,\bar{e}_a,e_a}m^2_{e_a} + 12\sum_{a=1}^{3} A_0\Big(m^2_{u_a}\Big)\Gamma^L_{\sigma_i,\bar{u}_a,u_a}m^2_{u_a} \\
&- \frac{1}{2}\sum_{a=1}^{4} A_0\Big(m^2_{A_{0,a}}\Big)\Gamma_{\sigma_i,A_{0,a},A_{0,a}} - \frac{1}{2}\sum_{a=1}^{4} A_0\Big(m^2_{h_a}\Big)\Gamma_{\sigma_i,h_a,h_a} - 3\sum_{a=1}^{6} A_0\Big(m^2_{\tilde{d}_a}\Big)\Gamma_{\sigma_i,\tilde{d}_a^*,\tilde{d}_a} \\
&- \sum_{a=1}^{6} A_0\Big(m^2_{\tilde{e}_a}\Big)\Gamma_{\sigma_i,\tilde{e}_a^*,\tilde{e}_a} - 3\sum_{a=1}^{6} A_0\Big(m^2_{\tilde{u}_a}\Big)\Gamma_{\sigma_i,\tilde{u}_a^*,\tilde{u}_a} \\
&+ 2\sum_{a=1}^{7} A_0\Big(m^2_{\tilde{\chi}_a^0}\Big)\Gamma^L_{\sigma_i,\tilde{\chi}_a^0,\tilde{\chi}_a^0}m^2_{\tilde{\chi}_a^0} - \sum_{a=1}^{9} A_0\Big(m^2_{\tilde{\nu}_a}\Big)\Gamma_{\sigma_i,\tilde{\nu}_a^*,\tilde{\nu}_a} \\
&+ 2\sum_{a=1}^{9} A_0\Big(m^2_{\nu_a}\Big)\Gamma_{\sigma_i,\nu_a,\nu_a}m^2_{\nu_a}
\end{aligned}
\tag{A.24}
$$

with $\sigma_i = (\sigma_d, \sigma_u, \sigma_R, \bar{\sigma}_R)_i^T$. Γ_{xyz} denotes the vertex of the three particles x, y z, while Γ_{wxyz} will be used for four-point interactions. For chiral couplings we use Γ^L as coefficient of the left and Γ^R as coefficient of the right polarization operator. For instance, $\Gamma_{\sigma_d,Z,Z}$ is the coupling of a pure down-type Higgs to a Z boson while $\Gamma^L_{\sigma_R,\tilde{\chi}_2^0,\tilde{\chi}_2^0}$ corresponds to the left-chiral part of the interaction of a R-Higgs to a neutralino of the second generation. The expressions for all vertices can be obtained with `SARAH`.

Using these conventions the self-energy for the scalar Higgs fields reads

$$
\begin{aligned}
\Pi_{\sigma_i,\sigma_j}(p^2) = &\frac{7}{4}B_0\Big(p^2, m_Z^2, m_Z^2\Big)\Gamma^*_{\sigma_j,Z,Z}\Gamma_{\sigma_i,Z,Z} \\
&+ \frac{7}{2}B_0\Big(p^2, m_Z^2, m_{Z_R}^2\Big)\Gamma^*_{\sigma_j,Z_R,Z}\Gamma_{\sigma_i,Z_R,Z} + \frac{7}{4}B_0\Big(p^2, m_{Z_R}^2, m_{Z_R}^2\Big)\Gamma^*_{\sigma_j,Z_R,Z_R}\Gamma_{\sigma_i,Z_R,Z_R} \\
&+ \frac{7}{2}B_0\Big(p^2, m_{W^-}^2, m_{W^-}^2\Big)\Gamma^*_{\sigma_j,W^+,W^-}\Gamma_{\sigma_i,W^+,W^-} + 2A_0\Big(m_Z^2\Big)\Gamma_{\sigma_i,\sigma_i,Z,Z} + 2A_0\Big(m_{Z_R}^2\Big)\Gamma_{\sigma_i,\sigma_i,Z_R,Z_R} \\
&+ 4A_0\Big(m_{W^-}^2\Big)\Gamma_{\sigma_i,\sigma_i,W^+,W^-} - \sum_{a=1}^{2} A_0\Big(m^2_{H_a^-}\Big)\Gamma_{\sigma_i,\sigma_i,H_a^+,H_a^-} \\
&+ \sum_{a=1}^{2}\sum_{b=1}^{2} B_0\Big(p^2, m^2_{H_a^-}, m^2_{H_b^-}\Big)\Gamma^*_{\sigma_j,H_a^+,H_b^-}\Gamma_{\sigma_i,H_a^+,H_b^-} \\
&- 2\sum_{a=1}^{2} m_{\tilde{\chi}_a^+}\sum_{b=1}^{2} B_0\Big(p^2, m^2_{\tilde{\chi}_a^-}, m^2_{\tilde{\chi}_b^-}\Big)m_{\tilde{\chi}_b^-}\Big(\Gamma^{L*}_{\sigma_j,\tilde{\chi}_a^+,\tilde{\chi}_b^-}\Gamma^R_{\sigma_i,\tilde{\chi}_a^+,\tilde{\chi}_b^-} + \Gamma^{R*}_{\sigma_j,\tilde{\chi}_a^+,\tilde{\chi}_b^-}\Gamma^L_{\sigma_i,\tilde{\chi}_a^+,\tilde{\chi}_b^-}\Big)
\end{aligned}
$$

$$
\begin{aligned}
&+\sum_{a=1}^{2}\sum_{b=1}^{2} G_0\Big(p^2, m^2_{\tilde{\chi}^-_a}, m^2_{\tilde{\chi}^-_b}\Big)\Big(\Gamma^{L*}_{\sigma_j,\tilde{\chi}^+_a,\tilde{\chi}^-_b}\Gamma^{L}_{\sigma_i,\tilde{\chi}^+_a,\tilde{\chi}^-_b} + \Gamma^{R*}_{\sigma_j,\tilde{\chi}^+_a,\tilde{\chi}^-_b}\Gamma^{R}_{\sigma_i,\tilde{\chi}^+_a,\tilde{\chi}^-_b}\Big)\\
&-6\sum_{a=1}^{3} m_{\bar{d}_a}\sum_{b=1}^{3} B_0\Big(p^2, m^2_{d_a}, m^2_{\bar{d}_b}\Big) m_{d_b}\Big(\Gamma^{L*}_{\sigma_j,\bar{d}_a,d_b}\Gamma^{R}_{\sigma_i,\bar{d}_a,d_b} + \Gamma^{R*}_{\sigma_j,\bar{d}_a,d_b}\Gamma^{L}_{\sigma_i,\bar{d}_a,d_b}\Big)\\
&+3\sum_{a=1}^{3}\sum_{b=1}^{3} G_0\Big(p^2, m^2_{d_a}, m^2_{\bar{d}_b}\Big)\Big(\Gamma^{L*}_{\sigma_j,\bar{d}_a,d_b}\Gamma^{L}_{\sigma_i,\bar{d}_a,d_b} + \Gamma^{R*}_{\sigma_j,\bar{d}_a,d_b}\Gamma^{R}_{\sigma_i,\bar{d}_a,d_b}\Big)\\
&-2\sum_{a=1}^{3} m_{\bar{e}_a}\sum_{b=1}^{3} B_0\Big(p^2, m^2_{e_a}, m^2_{\bar{e}_b}\Big) m_{e_b}\Big(\Gamma^{L*}_{\sigma_j,\bar{e}_a,e_b}\Gamma^{R}_{\sigma_i,\bar{e}_a,e_b} + \Gamma^{R*}_{\sigma_j,\bar{e}_a,e_b}\Gamma^{L}_{\sigma_i,\bar{e}_a,e_b}\Big)\\
&+\sum_{a=1}^{3}\sum_{b=1}^{3} G_0\Big(p^2, m^2_{e_a}, m^2_{\bar{e}_b}\Big)\Big(\Gamma^{L*}_{\sigma_j,\bar{e}_a,e_b}\Gamma^{L}_{\sigma_i,\bar{e}_a,e_b} + \Gamma^{R*}_{\sigma_j,\bar{e}_a,e_b}\Gamma^{R}_{\sigma_i,\bar{e}_a,e_b}\Big)\\
&-6\sum_{a=1}^{3} m_{\bar{u}_a}\sum_{b=1}^{3} B_0\Big(p^2, m^2_{u_a}, m^2_{\bar{u}_b}\Big) m_{u_b}\Big(\Gamma^{L*}_{\sigma_j,\bar{u}_a,u_b}\Gamma^{R}_{\sigma_i,\bar{u}_a,u_b} + \Gamma^{R*}_{\sigma_j,\bar{u}_a,u_b}\Gamma^{L}_{\sigma_i,\bar{u}_a,u_b}\Big)\\
&+3\sum_{a=1}^{3}\sum_{b=1}^{3} G_0\Big(p^2, m^2_{u_a}, m^2_{\bar{u}_b}\Big)\Big(\Gamma^{L*}_{\sigma_j,\bar{u}_a,u_b}\Gamma^{L}_{\sigma_i,\bar{u}_a,u_b} + \Gamma^{R*}_{\sigma_j,\bar{u}_a,u_b}\Gamma^{R}_{\sigma_i,\bar{u}_a,u_b}\Big)\\
&-\frac{1}{2}\sum_{a=1}^{4} A_0\Big(m^2_{A_{0,a}}\Big)\Gamma_{\sigma_i,\sigma_i,A_{0,a},A_{0,a}} - \frac{1}{2}\sum_{a=1}^{4} A_0\Big(m^2_{h_a}\Big)\Gamma_{\sigma_i,\sigma_i,h_a,h_a}\\
&+\frac{1}{2}\sum_{a=1}^{4}\sum_{b=1}^{4} B_0\Big(p^2, m^2_{A_{0,a}}, m^2_{A_{0,b}}\Big)\Gamma^{*}_{\sigma_j,A_{0,a},A_{0,b}}\Gamma_{\sigma_i,A_{0,a},A_{0,b}}\\
&+\frac{1}{2}\sum_{a=1}^{4}\sum_{b=1}^{4} B_0\Big(p^2, m^2_{h_a}, m^2_{h_b}\Big)\Gamma^{*}_{\sigma_j,h_a,h_b}\Gamma_{\sigma_i,h_a,h_b} - 3\sum_{a=1}^{6} A_0\Big(m^2_{\tilde{d}_a}\Big)\Gamma_{\sigma_i,\sigma_i,\tilde{d}^*_a,\tilde{d}_a}\\
&-\sum_{a=1}^{6} A_0\Big(m^2_{\tilde{e}_a}\Big)\Gamma_{\sigma_i,\sigma_i,\tilde{e}^*_a,\tilde{e}_a} - 3\sum_{a=1}^{6} A_0\Big(m^2_{\tilde{u}_a}\Big)\Gamma_{\sigma_i,\sigma_i,\tilde{u}^*_a,\tilde{u}_a}\\
&+3\sum_{a=1}^{6}\sum_{b=1}^{6} B_0\Big(p^2, m^2_{\tilde{d}_a}, m^2_{\tilde{d}_b}\Big)\Gamma^{*}_{\sigma_j,\tilde{d}^*_a,\tilde{d}_b}\Gamma_{\sigma_i,\tilde{d}^*_a,\tilde{d}_b} + \sum_{a=1}^{6}\sum_{b=1}^{6} B_0\Big(p^2, m^2_{\tilde{e}_a}, m^2_{\tilde{e}_b}\Big)\Gamma^{*}_{\sigma_j,\tilde{e}^*_a,\tilde{e}_b}\Gamma_{\sigma_i,\tilde{e}^*_a,\tilde{e}_b}\\
&+3\sum_{a=1}^{6}\sum_{b=1}^{6} B_0\Big(p^2, m^2_{\tilde{u}_a}, m^2_{\tilde{u}_b}\Big)\Gamma^{*}_{\sigma_j,\tilde{u}^*_a,\tilde{u}_b}\Gamma_{\sigma_i,\tilde{u}^*_a,\tilde{u}_b}\\
&-\sum_{a=1}^{7} m_{\tilde{\chi}^0_a}\sum_{b=1}^{7} B_0\Big(p^2, m^2_{\tilde{\chi}^0_a}, m^2_{\tilde{\chi}^0_b}\Big) m_{\tilde{\chi}^0_b}\Big(\Gamma^{L*}_{\sigma_j,\tilde{\chi}^0_a,\tilde{\chi}^0_b}\Gamma^{R}_{\sigma_i,\tilde{\chi}^0_a,\tilde{\chi}^0_b} + \Gamma^{R*}_{\sigma_j,\tilde{\chi}^0_a,\tilde{\chi}^0_b}\Gamma^{L}_{\sigma_i,\tilde{\chi}^0_a,\tilde{\chi}^0_b}\Big)\\
&+\frac{1}{2}\sum_{a=1}^{7}\sum_{b=1}^{7} G_0\Big(p^2, m^2_{\tilde{\chi}^0_a}, m^2_{\tilde{\chi}^0_b}\Big)\Big(\Gamma^{L*}_{\sigma_j,\tilde{\chi}^0_a,\tilde{\chi}^0_b}\Gamma^{L}_{\sigma_i,\tilde{\chi}^0_a,\tilde{\chi}^0_b} + \Gamma^{R*}_{\sigma_j,\tilde{\chi}^0_a,\tilde{\chi}^0_b}\Gamma^{R}_{\sigma_i,\tilde{\chi}^0_a,\tilde{\chi}^0_b}\Big)\\
&-\sum_{a=1}^{9} A_0\Big(m^2_{\tilde{\nu}_a}\Big)\Gamma_{\sigma_i,\sigma_i,\tilde{\nu}^*_a,\tilde{\nu}_a} + \sum_{a=1}^{9}\sum_{b=1}^{9} B_0\Big(p^2, m^2_{\tilde{\nu}_a}, m^2_{\tilde{\nu}_b}\Big)\Gamma^{*}_{\sigma_j,\tilde{\nu}^*_a,\tilde{\nu}_b}\Gamma_{\sigma_i,\tilde{\nu}^*_a,\tilde{\nu}_b}
\end{aligned}
$$

$$
\begin{aligned}
&- \sum_{a=1}^{9} m_{\nu_a} \sum_{b=1}^{9} B_0\Big(p^2, m_{\nu_a}^2, m_{\nu_b}^2\Big) m_{\nu_b} \Big(\Gamma^{L*}_{\sigma_j,\nu_a,\nu_b} \Gamma^{R}_{\sigma_i,\nu_a,\nu_b} + \Gamma^{R*}_{\sigma_j,\nu_a,\nu_b} \Gamma^{L}_{\sigma_i,\nu_a,\nu_b}\Big) \\
&+ \frac{1}{2} \sum_{a=1}^{9} \sum_{b=1}^{9} G_0\Big(p^2, m_{\nu_a}^2, m_{\nu_b}^2\Big) \Big(\Gamma^{L*}_{\sigma_j,\nu_a,\nu_b} \Gamma^{L}_{\sigma_i,\nu_a,\nu_b} + \Gamma^{R*}_{\sigma_j,\nu_a,\nu_b} \Gamma^{R}_{\sigma_i,\nu_a,\nu_b}\Big) \\
&+ 2 \sum_{b=1}^{2} \Gamma^{*}_{\sigma_j,W^+,H_b^-} \Gamma_{\sigma_i,W^+,H_b^-} F_0\Big(p^2, m_{H_b^-}^2, m_{W^-}^2\Big) + \sum_{b=1}^{4} \Gamma^{*}_{\sigma_j,\gamma,A_{0,b}} \Gamma_{\sigma_i,\gamma,A_{0,b}} F_0\Big(p^2, m_{A_{0,b}}^2, 0\Big) \\
&+ \sum_{b=1}^{4} \Gamma^{*}_{\sigma_j,Z,A_{0,b}} \Gamma_{\sigma_i,Z,A_{0,b}} F_0\Big(p^2, m_{A_{0,b}}^2, m_Z^2\Big) + \sum_{b=1}^{4} \Gamma^{*}_{\sigma_j,Z_R,A_{0,b}} \Gamma_{\sigma_i,Z_R,A_{0,b}} F_0\Big(p^2, m_{A_{0,b}}^2, m_{Z_R}^2\Big)
\end{aligned}
\tag{A.25}
$$

A.4. RGEs

The calculation of the renormalization group equations performed by SARAH is based on the generic expression of [164]. In addition, the results of [165] are used to include the effect of kinetic mixing.

The β functions for the parameters of a general superpotential written as

$$W(\phi) = \frac{1}{2}\mu^{ij}\phi_i\phi_j + \frac{1}{6}Y^{ijk}\phi_i\phi_j\phi_k \tag{A.26}$$

can be easily obtained from the results shown for the anomalous dimensions by using the relations [289; 290]

$$\beta_Y^{ijk} = Y^{p(ij}\gamma_p{}^{k)} \,, \tag{A.27}$$

$$\beta_\mu^{ij} = \mu^{p(i}\gamma_p{}^{j)} \,. \tag{A.28}$$

For the results of the other parameters as well as for the two-loop results, which we skip here because of their length, one can use the function `CalcRGEs[]` of SARAH.

A.4.1. Anomalous dimensions

$$\gamma_{\hat{q}}^{(1)} = \frac{1}{12}\Big(12\Big(Y_d^\dagger Y_d + Y_u^\dagger Y_u\Big) - \Big(18g_L^2 + 32g_s^2 + g_{BL}^2 + g_{BLR}^2\Big)\mathbf{1}\Big) \tag{A.29}$$

$$\gamma_{\hat{l}}^{(1)} = -\frac{3}{4}\Big(2g_L^2 + g_{BL}^2 + g_{BLR}^2\Big)\mathbf{1} + Y_e^\dagger Y_e + Y_v^\dagger Y_v \tag{A.30}$$

$$\gamma_{\hat{H}_d}^{(1)} = \frac{1}{2}\Big(2\mathsf{Tr}\Big(Y_e Y_e^\dagger\Big) - 3g_L^2 + 6\mathsf{Tr}\Big(Y_d Y_d^\dagger\Big) - g_R^2 - g_{RBL}^2\Big) \tag{A.31}$$

$$\gamma^{(1)}_{\hat{H}_u} = \frac{1}{2}\Big(2\mathsf{Tr}\Big(Y_v Y_v^\dagger\Big) - 3g_L^2 + 6\mathsf{Tr}\Big(Y_u Y_u^\dagger\Big) - g_R^2 - g_{RBL}^2\Big) \tag{A.32}$$

$$\gamma^{(1)}_{\hat{\chi}_R} = \frac{1}{4}\Big(- 2g_R^2 - 2g_{RBL}^2 + 2\sqrt{6}g_{BL}g_{RBL} + 2\sqrt{6}g_{BLR}g_R - 3g_{BL}^2 - 3g_{BLR}^2 + 4\mathsf{Tr}\Big(Y_s Y_s^\dagger\Big)\Big) \tag{A.33}$$

$$\gamma^{(1)}_{\hat{\bar{\chi}}_R} = \frac{1}{4}\Big(- 2\Big(g_R^2 + g_{RBL}^2\Big) + 2\sqrt{6}g_{BL}g_{RBL} + 2\sqrt{6}g_{BLR}g_R - 3g_{BL}^2 - 3g_{BLR}^2\Big) \tag{A.34}$$

$$\gamma^{(1)}_{\hat{S}} = Y_s^\dagger Y_s \tag{A.35}$$

$$\gamma^{(1)}_{\hat{u}} = \frac{1}{12}\Big(24Y_u^* Y_u^T - \Big(2\sqrt{6}g_{BL}g_{RBL} + 2\sqrt{6}g_{BLR}g_R + 32g_s^2 + 6g_R^2 + 6g_{RBL}^2 + g_{BL}^2 + g_{BLR}^2\Big)\mathbf{1}\Big) \tag{A.36}$$

$$\gamma^{(1)}_{\hat{d}} = \frac{1}{12}\Big(24Y_d^* Y_d^T - \Big(- 2\sqrt{6}g_{BL}g_{RBL} - 2\sqrt{6}g_{BLR}g_R + 32g_s^2 + 6g_R^2 + 6g_{RBL}^2 + g_{BL}^2 + g_{BLR}^2\Big)\mathbf{1}\Big) \tag{A.37}$$

$$\gamma^{(1)}_{\hat{\nu}} = \frac{1}{4}\Big(- \Big(2\Big(g_R^2 + g_{RBL}^2\Big) - 2\sqrt{6}g_{BL}g_{RBL} - 2\sqrt{6}g_{BLR}g_R + 3g_{BL}^2 + 3g_{BLR}^2\Big)\mathbf{1} + 4\Big(2Y_v^* Y_v^T + Y_s^* Y_s^T\Big)\Big) \tag{A.38}$$

$$\gamma^{(1)}_{\hat{e}} = \frac{1}{4}\Big(- \Big(2\Big(g_R^2 + g_{RBL}^2\Big) + 2\sqrt{6}g_{BL}g_{RBL} + 2\sqrt{6}g_{BLR}g_R + 3g_{BL}^2 + 3g_{BLR}^2\Big)\mathbf{1} + 8Y_e^* Y_e^T\Big) \tag{A.39}$$

A.4.2. Gauge Couplings

$$\beta^{(1)}_{g_{BL}} = \frac{1}{4}\Big(27g_{BL}^3 - 2\sqrt{6}g_{BL}^2 g_{RBL} + g_{BL}\Big(27g_{BLR}^2 + 30g_{RBL}^2 - \sqrt{6}g_{BLR}g_R\Big) + g_{BLR}\Big(30g_R - \sqrt{6}g_{BLR}\Big)g_{RBL}\Big) \tag{A.40}$$

$$\beta^{(1)}_{g_R} = \frac{1}{4}\Big(27g_{BL}g_{BLR}g_{RBL} + 27g_{BLR}^2 g_R - 2\sqrt{6}g_{BLR}g_R^2 + 30g_R^3 + 30g_R g_{RBL}^2 - \sqrt{6}g_{BL}g_R g_{RBL} - \sqrt{6}g_{BLR}g_{RBL}^2\Big) \tag{A.41}$$

$$\beta^{(1)}_{g_{BLR}} = \frac{1}{4}\Big(g_{BL}^2\Big(27g_{BLR} - \sqrt{6}g_R\Big) + g_{BL}\Big(30g_R g_{RBL} - \sqrt{6}g_{BLR}g_{RBL}\Big) + g_{BLR}\Big(27g_{BLR}^2 - 2\sqrt{6}g_{BLR}g_R + 30g_R^2\Big)\Big) \tag{A.42}$$

$$\beta^{(1)}_{g_{RBL}} = \frac{1}{4}\Big(27g_{BL}^2 g_{RBL} + 30g_{RBL}\Big(g_R^2 + g_{RBL}^2\Big) + g_{BL}\Big(27g_{BLR}g_R - \sqrt{6}\Big(2g_{RBL}^2 + g_R^2\Big)\Big) - \sqrt{6}g_{BLR}g_R g_{RBL}\Big) \tag{A.43}$$

$$\beta^{(1)}_{g_L} = g_L^3 \tag{A.44}$$

$$\beta^{(1)}_{g_s} = -3g_s^3 \tag{A.45}$$

A.4.3. Gaugino Mass Parameters

$$\beta^{(1)}_{M_{BL}} = \frac{1}{2}\Big(27g^2_{BL}M_{BL} - g_{BL}\Big(- 27g_{BLR}M_{BR} + 2\sqrt{6}g_{RBL}M_{BL} + \sqrt{6}g_RM_{BR}\Big) + g_{RBL}\Big(30g_{RBL}M_{BL} + 30g_RM_{BR} - \sqrt{6}g_{BLR}M_{BR}\Big)\Big) \tag{A.46}$$

$$\beta^{(1)}_{M_R} = \frac{1}{2}\Big(27g^2_{BLR}M_R + 30g_R\Big(g_{RBL}M_{BR} + g_RM_R\Big) + g_{BL}\Big(27g_{BLR} - \sqrt{6}g_R\Big)M_{BR} - \sqrt{6}g_{BLR}\Big(2g_RM_R + g_{RBL}M_{BR}\Big)\Big) \tag{A.47}$$

$$\beta^{(1)}_{M_{BR}} = \frac{1}{4}\Big(27g^2_{BL}M_{BR} + 27g^2_{BLR}M_{BR} - \sqrt{6}g_{BLR}\Big(2g_RM_{BR} + g_{RBL}\Big(M_{BL} + M_R\Big)\Big) + 30\Big(g^2_RM_{BR} + g^2_{RBL}M_{BR} + g_Rg_{RBL}\Big(M_{BL} + M_R\Big)\Big) + g_{BL}\Big(27g_{BLR}\Big(M_{BL} + M_R\Big) - \sqrt{6}\Big(2g_{RBL}M_{BR} + g_R\Big(M_{BL} + M_R\Big)\Big)\Big)\Big) \tag{A.48}$$

$$\beta^{(1)}_{M_2} = 2g^2_LM_2 \tag{A.49}$$

$$\beta^{(1)}_{M_3} = -6g^2_sM_3 \tag{A.50}$$

Bibliography

[1] C. Arbelaez, M. Hirsch, and L. Reichert, "Supersymmetric mass spectra and the seesaw type-I scale," JHEP **1202** (2012) 112, arXiv:1112.4771 [hep-ph].

[2] M. Hirsch, L. Reichert, and W. Porod, "Supersymmetric mass spectra and the seesaw scale," JHEP **1105** (2011) 086, arXiv:1101.2140 [hep-ph].

[3] M. Hirsch, M. Malinsky, W. Porod, L. Reichert, and F. Staub, "Hefty MSSM-like light Higgs in extended gauge models," JHEP **1202** (2012) 084, arXiv:1110.3037 [hep-ph].

[4] M. Hirsch, W. Porod, L. Reichert, and F. Staub, "Phenomenology of the minimal supersymmetric $U(1)_{B-L} \times U(1)_R$ extension of the standard model," Phys.Rev. **D86** (2012) 093018, arXiv:1206.3516 [hep-ph].

[5] **ATLAS Collaboration** Collaboration, G. Aad et al., "Observation of a new particle in the search for the Standard Model Higgs boson with the ATLAS detector at the LHC," Phys.Lett. **B716** (2012) 1–29, arXiv:1207.7214 [hep-ex].

[6] **CMS Collaboration** Collaboration, S. Chatrchyan et al., "Observation of a new boson at a mass of 125 GeV with the CMS experiment at the LHC," Phys.Lett. **B716** (2012) 30–61, arXiv:1207.7235 [hep-ex].

[7] **ALEPH Collaboration, DELPHI Collaboration, L3 Collaboration, OPAL Collaboration, LEP Electroweak Working Group, SLD Heavy Flavor and Electroweak Groups** Collaboration, D. Abbaneo et al., "A Combination of preliminary electroweak measurements and constraints on the standard model," arXiv:hep-ex/0112021 [hep-ex].

[8] U. Ellwanger, "A Higgs boson near 125 GeV with enhanced di-photon signal in the NMSSM," JHEP **1203** (2012) 044, arXiv:1112.3548 [hep-ph].

[9] A. Joglekar, P. Schwaller, and C. E. Wagner, "Dark Matter and Enhanced Higgs to Di-photon Rate from Vector-like Leptons," JHEP **1212** (2012) 064, arXiv:1207.4235 [hep-ph].

[10] H. An, T. Liu, and L.-T. Wang, "125 GeV Higgs Boson, Enhanced Di-photon Rate, and Gauged $U(1)_{\rm PQ}$-Extended MSSM," Phys.Rev. **D86** (2012) 075030, arXiv:1207.2473 [hep-ph].

[11] J. Baglio, A. Djouadi, and R. Godbole, "The apparent excess in the Higgs to di-photon rate at the LHC: New Physics or QCD uncertainties?," Phys.Lett. **B716** (2012) 203–207, arXiv:1207.1451 [hep-ph].

[12] L. G. Almeida, E. Bertuzzo, P. A. Machado, and R. Z. Funchal, "Does $H \to \gamma\gamma$ Taste like vanilla New Physics?," JHEP **1211** (2012) 085, arXiv:1207.5254 [hep-ph].

[13] CMS working group, "CMS experiment - Public Higgs Results," 2014. https://twiki.cern.ch/twiki/bin/view/CMSPublic/PhysicsResultsHIG.

[14] ATLAS working group, "ATLAS experiment - Public Higgs Results," 2014. https://twiki.cern.ch/twiki/bin/view/AtlasPublic/HiggsPublicResults.

[15] P. Minkowski, "mu $\to$ e gamma at a Rate of One Out of 1-Billion Muon Decays?," Phys.Lett. **B67** (1977) 421.

[16] T. Yanagida, "KEK lectures, edited by Sawada, O. and Sugamoto, A. (Word Scientific, Tsukuba, Japan, 1979),".

[17] M. Gell-Mann, P. Ramond, R. Slansky, P. van Niewenhuizen, and D. Freedman, "Supergravity,".

[18] R. Mohapatra and G. Senjanovic, "Neutrino Mass and Spontaneous Parity Nonconservation," Phys.Rev.Lett. **44** (1980) 912.

[19] J. Schechter and J. W. F. Valle, "Neutrino Masses In SU(2) X U(1) Theories," Phys.Rev.D **22** (1980) 2227.

[20] T. Cheng and L.-F. Li, "Neutrino Masses, Mixings and Oscillations in SU(2) x U(1) Models of Electroweak Interactions," Phys.Rev. **D22** (1980) 2860.

[21] E. K. Akhmedov, M. Lindner, E. Schnapka, and J. Valle, "Dynamical left-right symmetry breaking," Phys.Rev. **D53** (1996) 2752–2780, arXiv:hep-ph/9509255 [hep-ph].

[22] E. K. Akhmedov, M. Lindner, E. Schnapka, and J. Valle, "Left-right symmetry breaking in NJL approach," Phys.Lett. **B368** (1996) 270–280, arXiv:hep-ph/9507275 [hep-ph].

[23] G. F. Giudice, M. A. Luty, H. Murayama, and R. Rattazzi, "Gaugino mass without singlets," JHEP **9812** (1998) 027, arXiv:hep-ph/9810442 [hep-ph].

[24] A. Zee, "A Theory of Lepton Number Violation, Neutrino Majorana Mass, and Oscillation," Phys.Lett. **B93** (1980) 389.

[25] K. Babu, "Model of 'Calculable' Majorana Neutrino Masses," Phys.Lett. **B203** (1988) 132.

[26] **Planck Collaboration** Collaboration, P. Ade et al., "Planck 2013 results. XVI. Cosmological parameters," arXiv:1303.5076 [astro-ph.CO].

[27] D. Hooper, "TASI 2008 Lectures on Dark Matter," arXiv:0901.4090 [hep-ph].

[28] A. Kusenko and M. E. Shaposhnikov, "Supersymmetric Q balls as dark matter," Phys.Lett. **B418** (1998) 46–54, arXiv:hep-ph/9709492 [hep-ph].

[29] F. D. Steffen, "Dark Matter Candidates - Axions, Neutralinos, Gravitinos, and Axinos," Eur.Phys.J. **C59** (2009) 557–588, arXiv:0811.3347 [hep-ph].

[30] S. R. Coleman and J. Mandula, "All Possible Symmetries of the S Matrix," Phys.Rev. **159** (1967) 1251–1256.

[31] R. Haag, J. T. Lopuszanski, and M. Sohnius, "All Possible Generators of Supersymmetries of the s Matrix," Nucl.Phys. **B88** (1975) 257.

[32] J. Bagger and J. Wess, "Supersymmetry and supergravity,".

[33] S. Heinemeyer, W. Hollik, and G. Weiglein, "The Masses of the neutral CP - even Higgs bosons in the MSSM: Accurate analysis at the two loop level," Eur.Phys.J. **C9** (1999) 343–366, arXiv:hep-ph/9812472 [hep-ph].

[34] B. Allanach, A. Djouadi, J. Kneur, W. Porod, and P. Slavich, "Precise determination of the neutral Higgs boson masses in the MSSM," JHEP **0409** (2004) 044, arXiv:hep-ph/0406166 [hep-ph].

[35] F. Staub, "SARAH," arXiv:0806.0538 [hep-ph].

[36] W. Porod, "SPheno, a program for calculating supersymmetric spectra, SUSY particle decays and SUSY particle production at e+ e- colliders," Comput.Phys.Commun. **153** (2003) 275–315, arXiv:hep-ph/0301101 [hep-ph].

[37] CERN, "Lhc experiments." http://home.web.cern.ch/about/experiments.

[38] LHCb working group, "LHCb experiment," 2012. http://lhcb-public.web.cern.ch/lhcb-public/Welcome_270811.html.

[39] **E598 Collaboration** Collaboration, J. Aubert et al., "Experimental Observation of a Heavy Particle J," Phys.Rev.Lett. **33** (1974) 1404–1406.

[40] **SLAC-SP-017 Collaboration** Collaboration, J. Augustin et al., "Discovery of a Narrow Resonance in e+ e- Annihilation," Phys.Rev.Lett. **33** (1974) 1406–1408.

[41] M. L. Perl, G. Abrams, A. Boyarski, M. Breidenbach, D. Briggs, et al., "Evidence for Anomalous Lepton Production in e+ - e- Annihilation," Phys.Rev.Lett. **35** (1975) 1489–1492.

[42] G. Goldhaber, F. Pierre, G. Abrams, M. Alam, A. Boyarski, et al., "Observation in e+ e- Annihilation of a Narrow State at 1865-MeV/c**2 Decaying to K pi and K pi pi pi," Phys.Rev.Lett. **37** (1976) 255–259.

[43] S. Herb, D. Hom, L. Lederman, J. Sens, H. Snyder, et al., "Observation of a Dimuon Resonance at 9.5-GeV in 400-GeV Proton-Nucleus Collisions," Phys.Rev.Lett. **39** (1977) 252–255.

[44] **UA1 Collaboration** Collaboration, G. Arnison et al., "Experimental Observation of Isolated Large Transverse Energy Electrons with Associated Missing Energy at s**(1/2) = 540-GeV," Phys.Lett. **B122** (1983) 103–116.

[45] **UA2 Collaboration** Collaboration, M. Banner et al., "Observation of Single Isolated Electrons of High Transverse Momentum in Events with Missing Transverse Energy at the CERN anti-p p Collider," Phys.Lett. **B122** (1983) 476–485.

[46] **ALEPH Collaboration, DELPHI Collaboration, L3 Collaboration, OPAL Collaboration, SLD Collaboration, LEP Electroweak Working Group, SLD Electroweak Group, SLD Heavy Flavour Group** Collaboration, S. Schael et al., "Precision electroweak measurements on the Z resonance," Phys.Rept. **427** (2006) 257–454, arXiv:hep-ex/0509008 [hep-ex].

[47] **D0 Collaboration** Collaboration, S. Abachi et al., "Observation of the top quark," Phys.Rev.Lett. **74** (1995) 2632–2637, arXiv:hep-ex/9503003 [hep-ex].

[48] **CDF Collaboration** Collaboration, F. Abe et al., "Observation of top quark production in $\bar{p}p$ collisions," Phys.Rev.Lett. **74** (1995) 2626–2631, arXiv:hep-ex/9503002 [hep-ex].

[49] **DONUT Collaboration** Collaboration, K. Kodama et al., "Observation of tau neutrino interactions," Phys.Lett. **B504** (2001) 218–224, arXiv:hep-ex/0012035 [hep-ex].

[50] P. W. Higgs, "Broken symmetries, massless particles and gauge fields," Phys.Lett. **12** (1964) 132–133.

[51] F. Englert and R. Brout, "Broken Symmetry and the Mass of Gauge Vector Mesons," Phys.Rev.Lett. **13** (1964) 321–323.

[52] G. Altarelli, "Collider Physics within the Standard Model: a Primer," arXiv:1303.2842 [hep-ph].

[53] S. Glashow, J. Iliopoulos, and L. Maiani, "Weak Interactions with Lepton-Hadron Symmetry," Phys.Rev. **D2** (1970) 1285–1292.

[54] G. Altarelli and M. W. Grunewald, "Precision electroweak tests of the standard model," Phys.Rept. **403-404** (2004) 189–201, arXiv:hep-ph/0404165 [hep-ph].

[55] LHC working group, "LHC experiment," 2012. https://twiki.cern.ch/twiki/bin/view/LHCPhysics.

[56] **ALEPH Collaboration, CDF Collaboration, D0 Collaboration, DELPHI Collaboration, L3 Collaboration, OPAL Collaboration, SLD Collaboration, LEP Electroweak Working Group, Tevatron Electroweak Working Group, SLD Electroweak and Heavy Flavour Groups** Collaboration, "Precision Electroweak Measurements and Constraints on the Standard Model," arXiv:1012.2367 [hep-ex].

[57] M. Maggiore, "A Modern introduction to quantum field theory,".

[58] T. Hambye and K. Riesselmann, "Matching conditions and Higgs mass upper bounds revisited," Phys.Rev. **D55** (1997) 7255–7262, arXiv:hep-ph/9610272 [hep-ph].

[59] N. Cabibbo, L. Maiani, G. Parisi, and R. Petronzio, "Bounds on the Fermions and Higgs Boson Masses in Grand Unified Theories," Nucl.Phys. **B158** (1979) 295–305.

[60] M. Sher, "Electroweak Higgs Potentials and Vacuum Stability," Phys.Rept. **179** (1989) 273–418.

[61] G. Degrassi, S. Di Vita, J. Elias-Miro, J. R. Espinosa, G. F. Giudice, et al., "Higgs mass and vacuum stability in the Standard Model at NNLO," JHEP **1208** (2012) 098, arXiv:1205.6497 [hep-ph].

[62] M. Lindner, M. Sher, and H. W. Zaglauer, "Probing Vacuum Stability Bounds at the Fermilab Collider," Phys.Lett. **B228** (1989) 139.

[63] ATLAS working group, "ATLAS experiment," 2012. http://atlas.ch/news/2011/simplified-plots.html.

[64] **ATLAS Collaboration** Collaboration, S. N. Collaboration), "Searches for Fourth Generation, Vector-like Quarks and Resonances with the ATLAS Detector," EPJ Web Conf. **60** (2013) 17009.

[65] **CMS Collaborations** Collaboration, A. Ivanov, "Limits on Fourth Generation Fermions," arXiv:1308.3084 [hep-ex].

[66] D. Buttazzo, G. Degrassi, P. P. Giardino, G. F. Giudice, F. Sala, et al., "Investigating the near-criticality of the Higgs boson," arXiv:1307.3536 [hep-ph].

[67] **LEP Working Group for Higgs boson searches, ALEPH Collaboration, DELPHI Collaboration, L3 Collaboration, OPAL Collaboration** Collaboration, R. Barate et al., "Search for the standard model Higgs boson at LEP," Phys.Lett. **B565** (2003) 61–75, arXiv:hep-ex/0306033 [hep-ex].

[68] T. Schwetz, M. Tortola, and J. W. Valle, "Three-flavour neutrino oscillation update," New J.Phys. **10** (2008) 113011, arXiv:0808.2016 [hep-ph].

[69] S. Masood, S. Nasri, J. Schechter, M. Tortola, J. Valle, et al., "Exact relativistic beta decay endpoint spectrum," Phys.Rev. **C76** (2007) 045501, arXiv:0706.0897 [hep-ph].

[70] M. Steidl, "Experiments for the absolute neutrino mass measurement," arXiv:0906.0454 [nucl-ex].

[71] **EXO Collaboration** Collaboration, M. Auger et al., "Search for Neutrinoless Double-Beta Decay in ^{136}Xe with EXO-200," Phys.Rev.Lett. **109** (2012) 032505, arXiv:1205.5608 [hep-ex].

[72] **GERDA Collaboration** Collaboration, M. Agostini et al., "Results on neutrinoless double beta decay of 76Ge from GERDA Phase I," Phys.Rev.Lett. **111** (2013) 122503, arXiv:1307.4720 [nucl-ex].

[73] D. Forero, M. Tortola, and J. Valle, "Global status of neutrino oscillation parameters after Neutrino-2012," Phys.Rev. **D86** (2012) 073012, arXiv:1205.4018 [hep-ph].

[74] **T2K Collaboration** Collaboration, K. Abe et al., "Indication of Electron Neutrino Appearance from an Accelerator-produced Off-axis Muon Neutrino Beam," Phys.Rev.Lett. **107** (2011) 041801, arXiv:1106.2822 [hep-ex].

[75] **MINOS Collaboration** Collaboration, P. Adamson et al., "Improved search for muon-neutrino to electron-neutrino oscillations in MINOS," Phys.Rev.Lett. **107** (2011) 181802, arXiv:1108.0015 [hep-ex].

[76] **DOUBLE-CHOOZ Collaboration** Collaboration, Y. Abe et al., "Indication for the disappearance of reactor electron antineutrinos in the Double Chooz experiment," Phys.Rev.Lett. **108** (2012) 131801, arXiv:1112.6353 [hep-ex].

[77] **DAYA-BAY Collaboration** Collaboration, F. An et al., "Observation of electron-antineutrino disappearance at Daya Bay," Phys.Rev.Lett. **108** (2012) 171803, arXiv:1203.1669 [hep-ex].

[78] **RENO collaboration** Collaboration, J. Ahn et al., "Observation of Reactor Electron Antineutrino Disappearance in the RENO Experiment," Phys.Rev.Lett. **108** (2012) 191802, arXiv:1204.0626 [hep-ex].

[79] **for the CMS Collaboration** Collaboration, R. Kogler, "Search for heavy resonances decaying to top quarks," arXiv:1310.8183 [hep-ex].

[80] **ATLAS Collaboration, CMS Collaboration** Collaboration, P. Van Mulders, "Searches for new fermions and new bosons," arXiv:1212.2339 [hep-ex].

[81] **ATLAS Collaboration** Collaboration, G. Aad et al., "ATLAS search for a heavy gauge boson decaying to a charged lepton and a neutrino in pp collisions at $\sqrt{s} = 7$ TeV," Eur.Phys.J. **C72** (2012) 2241, arXiv:1209.4446 [hep-ex].

[82] S. Weinberg, "Baryon and Lepton Nonconserving Processes," Phys.Rev.Lett. **43** (1979) 1566–1570.

[83] F. Bonnet, M. Hirsch, T. Ota, and W. Winter, "Systematic study of the d=5 Weinberg operator at one-loop order," JHEP **1207** (2012) 153, arXiv:1204.5862 [hep-ph].

[84] A. Santamaria, "Masses, mixings, Yukawa couplings and their symmetries," Phys.Lett. **B305** (1993) 90–97, arXiv:hep-ph/9302301 [hep-ph].

[85] P. Langacker, "Grand Unified Theories and Proton Decay," Phys.Rept. **72** (1981) 185.

[86] H. Georgi and S. Glashow, "Unity of All Elementary Particle Forces," Phys.Rev.Lett. **32** (1974) 438–441.

[87] **Super-Kamiokande Collaboration** Collaboration, K. Abe et al., "A Search for Nucleon Decay via $n \to \bar{\nu}\pi^0$ and $p \to \bar{\nu}\pi^+$ in Super-Kamiokande," arXiv:1305.4391 [hep-ex].

[88] R. Slansky, "Group Theory for Unified Model Building," Phys.Rept. **79** (1981) 1–128.

[89] H. Georgi and C. Jarlskog, "A New Lepton - Quark Mass Relation in a Unified Theory," Phys.Lett. **B86** (1979) 297–300.

[90] S. Weinberg, "Supersymmetry at Ordinary Energies. 1. Masses and Conservation Laws," Phys.Rev. **D26** (1982) 287.

[91] S. Dimopoulos, S. Raby, and F. Wilczek, "Proton Decay in Supersymmetric Models," Phys.Lett. **B112** (1982) 133.

[92] I. Dorsner, P. Fileviez Perez, and R. Gonzalez Felipe, "Phenomenological and cosmological aspects of a minimal GUT scenario," Nucl.Phys. **B747** (2006) 312–327, arXiv:hep-ph/0512068 [hep-ph].

[93] L. Di Luzio, "Aspects of symmetry breaking in Grand Unified Theories," arXiv:1110.3210 [hep-ph].

[94] K. Babu, I. Gogoladze, P. Nath, and R. M. Syed, "A Unified framework for symmetry breaking in SO(10)," Phys.Rev. **D72** (2005) 095011, arXiv:hep-ph/0506312 [hep-ph].

[95] P. Nath and R. M. Syed, "Yukawa Couplings and Quark and Lepton Masses in an SO(10) Model with a Unified Higgs Sector," Phys.Rev. **D81** (2010) 037701, arXiv:0909.2380 [hep-ph].

[96] P. B. Dev and R. Mohapatra, "TeV Scale Inverse Seesaw in SO(10) and Leptonic Non-Unitarity Effects," Phys.Rev. **D81** (2010) 013001, arXiv:0910.3924 [hep-ph].

[97] M. Malinsky, J. Romao, and J. Valle, "Novel supersymmetric SO(10) seesaw mechanism," Phys.Rev.Lett. **95** (2005) 161801, arXiv:hep-ph/0506296 [hep-ph].

[98] V. De Romeri, M. Hirsch, and M. Malinsky, "Soft masses in SUSY SO(10) GUTs with low intermediate scales," Phys.Rev. **D84** (2011) 053012, arXiv:1107.3412 [hep-ph].

[99] C. Arbelaez, R. M. Fonseca, M. Hirsch, and J. C. Romao, "Supersymmetric SO(10) GUTs with sliding scales," Phys.Rev. **D87** (2013) 075010, arXiv:1301.6085 [hep-ph].

[100] M. Drees, R. Godbole, and P. Roy, "Theory and phenomenology of sparticles: An account of four-dimensional N=1 supersymmetry in high energy physics,".

[101] A. H. Chamseddine, R. L. Arnowitt, and P. Nath, "Locally Supersymmetric Grand Unification," Phys.Rev.Lett. **49** (1982) 970.

[102] H. P. Nilles, "Supersymmetry, Supergravity and Particle Physics," Phys.Rept. **110** (1984) 1–162.

[103] G. Giudice and R. Rattazzi, "Theories with gauge mediated supersymmetry breaking," Phys.Rept. **322** (1999) 419–499, arXiv:hep-ph/9801271 [hep-ph].

[104] R. Barbier, C. Berat, M. Besancon, M. Chemtob, A. Deandrea, et al., "R-parity violating supersymmetry," Phys.Rept. **420** (2005) 1–202, arXiv:hep-ph/0406039 [hep-ph].

[105] S. Rakshit, G. Bhattacharyya, and A. Raychaudhuri, "R-parity violating trilinear couplings and recent neutrino data," Phys.Rev. **D59** (1999) 091701, arXiv:hep-ph/9811500 [hep-ph].

[106] M. Hirsch and J. Valle, "Neutrinoless double beta decay in supersymmetry with bilinear R parity breaking," Nucl.Phys. **B557** (1999) 60–78, arXiv:hep-ph/9812463 [hep-ph].

[107] M. Hirsch, M. Diaz, W. Porod, J. Romao, and J. Valle, "Neutrino masses and mixings from supersymmetry with bilinear R parity violation: A Theory for solar and atmospheric neutrino oscillations," Phys.Rev. **D62** (2000) 113008, arXiv:hep-ph/0004115 [hep-ph].

[108] M. Hirsch, J. Romao, J. Valle, and A. Villanova del Moral, "Production and decays of supersymmetric Higgs bosons in spontaneously broken R-parity," Phys.Rev. **D73** (2006) 055007, arXiv:hep-ph/0512257 [hep-ph].

[109] H. Dreiner, K. Nickel, F. Staub, and A. Vicente, "New bounds on trilinear R-parity violation from lepton flavor violating observables," Phys.Rev. **D86** (2012) 015003, arXiv:1204.5925 [hep-ph].

[110] D. Chung, L. Everett, G. Kane, S. King, J. D. Lykken, et al., "The Soft supersymmetry breaking Lagrangian: Theory and applications," Phys.Rept. **407** (2005) 1–203, arXiv:hep-ph/0312378 [hep-ph].

[111] H. Murayama, "Supersymmetry phenomenology," arXiv:hep-ph/0002232 [hep-ph].

[112] T. Hahn, S. Heinemeyer, W. Hollik, H. Rzehak, and G. Weiglein, "Two-loop corrections to the charged Higgs-boson mass in the MSSM," Nucl.Phys.Proc.Suppl. **183** (2008) 86–90.

[113] T. Hahn, S. Heinemeyer, W. Hollik, H. Rzehak, and G. Weiglein, "FeynHiggs 2.7," Nucl.Phys.Proc.Suppl. **205-206** (2010) 152–157, arXiv:1007.0956 [hep-ph].

[114] U. Amaldi, W. de Boer, and H. Furstenau, "Comparison of grand unified theories with electroweak and strong coupling constants measured at LEP," Phys.Lett. **B260** (1991) 447–455.

[115] M. Drees, "An Introduction to supersymmetry," arXiv:hep-ph/9611409 [hep-ph].

[116] M. Hirsch, S. Kaneko, and W. Porod, "Supersymmetric seesaw type. II. LHC and lepton flavour violating phenomenology," Phys.Rev. **D78** (2008) 093004, arXiv:0806.3361 [hep-ph].

[117] Particle Data Group, "Review of Particle Physics," 2012. http://pdg.lbl.gov/.

[118] G. Cho, K. Hagiwara, C. Kao, and R. Szalapski, "Constraints on the mSUGRA parameter space from electroweak precision data," arXiv:hep-ph/9901351 [hep-ph].

[119] T. Falk, K. A. Olive, and M. Srednicki, "Heavy sneutrinos as dark matter," Phys.Lett. **B339** (1994) 248–251, arXiv:hep-ph/9409270 [hep-ph].

[120] CMS working group, "CMS experiment - Public SUSY Results," 2014. https://twiki.cern.ch/twiki/bin/view/CMSPublic/PhysicsResultsSUS.

[121] ATLAS working group, "ATLAS experiment - Public SUSY Results," 2014. https://twiki.cern.ch/twiki/bin/view/AtlasPublic/SupersymmetryPublicResults.

[122] **ATLAS Collaboration** Collaboration, G. Aad et al., "Search for new phenomena in final states with large jet multiplicities and missing transverse momentum at sqrt(s)=8 TeV proton-proton collisions using the ATLAS experiment," JHEP **1310** (2013) 130, arXiv:1308.1841 [hep-ex].

[123] R. Mohapatra and J. Valle, "Neutrino Mass and Baryon Number Nonconservation in Superstring Models," Phys.Rev. **D34** (1986) 1642.

[124] Z. Chacko, M. A. Luty, I. Maksymyk, and E. Ponton, "Realistic anomaly mediated supersymmetry breaking," JHEP **0004** (2000) 001, arXiv:hep-ph/9905390 [hep-ph].

[125] J. Hisano, T. Moroi, K. Tobe, M. Yamaguchi, and T. Yanagida, "Lepton flavor violation in the supersymmetric standard model with seesaw induced neutrino masses," Phys.Lett. **B357** (1995) 579–587, arXiv:hep-ph/9501407 [hep-ph].

[126] J. Hisano, T. Moroi, K. Tobe, and M. Yamaguchi, "Lepton flavor violation via right-handed neutrino Yukawa couplings in supersymmetric standard model," Phys.Rev. **D53** (1996) 2442–2459, arXiv:hep-ph/9510309 [hep-ph].

[127] J. R. Ellis, J. Hisano, M. Raidal, and Y. Shimizu, "A New parametrization of the seesaw mechanism and applications in supersymmetric models," Phys.Rev. **D66** (2002) 115013, arXiv:hep-ph/0206110 [hep-ph].

[128] F. Deppisch, H. Pas, A. Redelbach, R. Ruckl, and Y. Shimizu, "Probing the Majorana mass scale of right-handed neutrinos in mSUGRA," Eur.Phys.J. **C28** (2003) 365–374, arXiv:hep-ph/0206122 [hep-ph].

[129] E. Arganda and M. J. Herrero, "Testing supersymmetry with lepton flavor violating tau and mu decays," Phys.Rev. **D73** (2006) 055003, arXiv:hep-ph/0510405 [hep-ph].

[130] S. Antusch, E. Arganda, M. Herrero, and A. Teixeira, "Impact of theta(13) on lepton flavour violating processes within SUSY seesaw," JHEP **0611** (2006) 090, arXiv:hep-ph/0607263 [hep-ph].

[131] E. Arganda, M. Herrero, and A. Teixeira, "mu-e conversion in nuclei within the CMSSM seesaw: Universality versus non-universality," JHEP **0710** (2007) 104, arXiv:0707.2955 [hep-ph].

[132] J. Hisano, M. M. Nojiri, Y. Shimizu, and M. Tanaka, "Lepton flavor violation in the left-handed slepton production at future lepton colliders," Phys.Rev. **D60** (1999) 055008, arXiv:hep-ph/9808410 [hep-ph].

[133] G. Blair, W. Porod, and P. Zerwas, "The Reconstruction of supersymmetric theories at high-energy scales," Eur.Phys.J. **C27** (2003) 263–281, arXiv:hep-ph/0210058 [hep-ph].

[134] A. Freitas, W. Porod, and P. Zerwas, "Determining sneutrino masses and physical implications," Phys.Rev. **D72** (2005) 115002, arXiv:hep-ph/0509056 [hep-ph].

[135] S. Petcov, S. Profumo, Y. Takanishi, and C. Yaguna, "Charged lepton flavor violating decays: Leading logarithmic approximation versus full RG results," Nucl.Phys. **B676** (2004) 453–480, arXiv:hep-ph/0306195 [hep-ph].

[136] S. Pascoli, S. Petcov, and C. Yaguna, "Quasidegenerate neutrino mass spectrum, mu $\to$ e + gamma decay and leptogenesis," Phys.Lett. **B564** (2003) 241–254, arXiv:hep-ph/0301095 [hep-ph].

[137] S. Petcov, T. Shindou, and Y. Takanishi, "Majorana CP-violating phases, RG running of neutrino mixing parameters and charged lepton flavor violating decays," Nucl.Phys. **B738** (2006) 219–242, arXiv:hep-ph/0508243 [hep-ph].

[138] S. Petcov and T. Shindou, "Charged lepton decays l(i) $\to$ l(j) + gamma, leptogenesis CP-violating parameters and Majorana phases," Phys.Rev. **D74** (2006) 073006, arXiv:hep-ph/0605151 [hep-ph].

[139] M. Hirsch, J. Valle, W. Porod, J. Romao, and A. Villanova del Moral, "Probing minimal supergravity in type I seesaw with lepton flavour violation at the LHC," Phys.Rev. **D78** (2008) 013006, arXiv:0804.4072 [hep-ph].

[140] M. Hirsch, "Charged lepton flavour violation," Nucl.Phys.Proc.Suppl. **217** (2011) 318–323.

[141] A. Rossi, "Supersymmetric seesaw without singlet neutrinos: Neutrino masses and lepton flavor violation," Phys.Rev. **D66** (2002) 075003, arXiv:hep-ph/0207006 [hep-ph].

[142] J. Esteves, J. Romao, M. Hirsch, F. Staub, and W. Porod, "Supersymmetric type-III seesaw: lepton flavour violating decays and dark matter," Phys.Rev. **D83** (2011) 013003, arXiv:1010.6000 [hep-ph].

[143] C. Biggio and L. Calibbi, "Phenomenology of SUSY SU(5) with type I+III seesaw," JHEP **1010** (2010) 037, arXiv:1007.3750 [hep-ph].

[144] F. Deppisch, A. Freitas, W. Porod, and P. Zerwas, "Determining Heavy Mass Parameters in Supersymmetric SO(10) Models," Phys.Rev. **D77** (2008) 075009, arXiv:0712.0361 [hep-ph].

[145] K. Kadota and J. Shao, "Enhanced Tau Lepton Signatures at LHC in Constrained Supersymmetric Seesaw," Phys.Rev. **D80** (2009) 115004, arXiv:0910.5517 [hep-ph].

[146] B. Allanach, J. Conlon, and C. Lester, "Measuring Smuon-Selectron Mass Splitting at the CERN LHC and Patterns of Supersymmetry Breaking," Phys.Rev. **D77** (2008) 076006, arXiv:0801.3666 [hep-ph].

[147] A. J. Buras, L. Calibbi, and P. Paradisi, "Slepton mass-splittings as a signal of LFV at the LHC," JHEP **1006** (2010) 042, arXiv:0912.1309 [hep-ph].

[148] A. Abada, A. Figueiredo, J. Romao, and A. Teixeira, "Interplay of LFV and slepton mass splittings at the LHC as a probe of the SUSY seesaw," JHEP **1010** (2010) 104, arXiv:1007.4833 [hep-ph].

[149] L. Calibbi, Y. Mambrini, and S. Vempati, "SUSY-GUTs, SUSY-seesaw and the neutralino dark matter," JHEP **0709** (2007) 081, arXiv:0704.3518 [hep-ph].

[150] K. Kadota, K. A. Olive, and L. Velasco-Sevilla, "A Sneutrino NLSP in the nu CMSSM," Phys.Rev. **D79** (2009) 055018, arXiv:0902.2510 [hep-ph].

[151] K. Kadota and K. A. Olive, "Heavy Right-Handed Neutrinos and Dark Matter in the nuCMSSM," Phys.Rev. **D80** (2009) 095015, arXiv:0909.3075 [hep-ph].

[152] S. K. Kang, T. Morozumi, and N. Yokozaki, "Effects of Large Threshold Corrections in Supersymmetric Type-I Seesaw Model," JHEP **1011** (2010) 061, arXiv:1005.1354 [hep-ph].

[153] S. Heinemeyer, M. Herrero, S. Penaranda, and A. Rodriguez-Sanchez, "Higgs Boson Masses in the MSSM with Heavy Majorana Neutrinos," JHEP **1105** (2011) 063, arXiv:1007.5512 [hep-ph].

[154] M. R. Buckley and H. Murayama, "How can we test seesaw experimentally?," Phys.Rev.Lett. **97** (2006) 231801, arXiv:hep-ph/0606088 [hep-ph].

[155] **ECFA/DESY LC Physics Working Group** Collaboration, J. Aguilar-Saavedra et al., "TESLA: The Superconducting electron positron linear collider with an integrated x-ray laser laboratory. Technical design report. Part 3. Physics at an e+ e- linear collider," arXiv:hep-ph/0106315 [hep-ph].

[156] **LHC/LC Study Group** Collaboration, G. Weiglein et al., "Physics interplay of the LHC and the ILC," Phys.Rept. **426** (2006) 47–358, arXiv:hep-ph/0410364 [hep-ph].

[157] J. A. Aguilar-Saavedra, A. Ali, B. C. Allanach, R. L. Arnowitt, H. A. Baer, et al., "Supersymmetry parameter analysis: SPA convention and project," Eur.Phys.J. **C46** (2006) 43–60, arXiv:hep-ph/0511344 [hep-ph].

[158] G. Blair, W. Porod, and P. Zerwas, "Reconstructing supersymmetric theories at high-energy scales," Phys.Rev. **D63** (2001) 017703, arXiv:hep-ph/0007107 [hep-ph].

[159] P. Bechtle, K. Desch, W. Porod, and P. Wienemann, "Determination of MSSM parameters from LHC and ILC observables in a global fit," Eur.Phys.J. **C46** (2006) 533–544, arXiv:hep-ph/0511006 [hep-ph].

[160] R. Lafaye, T. Plehn, M. Rauch, and D. Zerwas, "Measuring Supersymmetry," Eur.Phys.J. **C54** (2008) 617–644, arXiv:0709.3985 [hep-ph].

[161] C. Adam, J.-L. Kneur, R. Lafaye, T. Plehn, M. Rauch, et al., "Measuring Unification," Eur.Phys.J. **C71** (2011) 1520, arXiv:1007.2190 [hep-ph].

[162] S. Davidson and A. Ibarra, "Determining seesaw parameters from weak scale measurements?," JHEP **0109** (2001) 013, arXiv:hep-ph/0104076 [hep-ph].

[163] J. Casas and A. Ibarra, "Oscillating neutrinos and muon $\to$ e, gamma," Nucl.Phys. **B618** (2001) 171–204, arXiv:hep-ph/0103065 [hep-ph].

[164] S. P. Martin and M. T. Vaughn, "Two loop renormalization group equations for soft supersymmetry breaking couplings," Phys.Rev. **D50** (1994) 2282, arXiv:hep-ph/9311340 [hep-ph].

[165] R. M. Fonseca, M. Malinsky, W. Porod, and F. Staub, "Running soft parameters in SUSY models with multiple U(1) gauge factors," Nucl.Phys. **B854** (2012) 28–53, arXiv:1107.2670 [hep-ph].

[166] W. Porod and F. Staub, "SPheno 3.1: Extensions including flavour, CP-phases and models beyond the MSSM," Comput.Phys.Commun. **183** (2012) 2458–2469, arXiv:1104.1573 [hep-ph].

[167] P. Harrison, D. Perkins, and W. Scott, "Tri-bimaximal mixing and the neutrino oscillation data," Phys.Lett. **B530** (2002) 167, arXiv:hep-ph/0202074 [hep-ph].

[168] **T2K Collaboration** Collaboration, M. Khabibullin, "Latest oscillation results from T2K," arXiv:1111.0183 [hep-ex].

[169] H. D. Kerrect, "Double CHOOZ experiment." http://workshop.kias.re.kr/lownu11/. 6th International Workshop on low energy neutrino physics.

[170] H. Bachacou, I. Hinchliffe, and F. E. Paige, "Measurements of masses in SUGRA models at CERN LHC," Phys.Rev. **D62** (2000) 015009, arXiv:hep-ph/9907518 [hep-ph].

[171] B. Allanach, C. Lester, M. A. Parker, and B. Webber, "Measuring sparticle masses in nonuniversal string inspired models at the LHC," JHEP **0009** (2000) 004, arXiv:hep-ph/0007009 [hep-ph].

[172] C. G. Lester, "Model independent sparticle mass measurements at ATLAS,".

[173] **CMS Collaboration** Collaboration, S. Chatrchyan et al., "Search for Supersymmetry at the LHC in Events with Jets and Missing Transverse Energy," Phys.Rev.Lett. **107** (2011) 221804, arXiv:1109.2352 [hep-ex].

[174] **ATLAS Collaboration** Collaboration, G. Aad et al., "Search for squarks and gluinos using final states with jets and missing transverse momentum with the ATLAS detector in $\sqrt{s} = 7$ TeV proton-proton collisions," Phys.Lett. **B710** (2012) 67–85, arXiv:1109.6572 [hep-ex].

[175] B. Allanach, M. Battaglia, G. Blair, M. S. Carena, A. De Roeck, et al., "The Snowmass points and slopes: Benchmarks for SUSY searches," Eur.Phys.J. **C25** (2002) 113–123, arXiv:hep-ph/0202233 [hep-ph].

[176] G. Belanger, F. Boudjema, A. Pukhov, and A. Semenov, "micrOMEGAs: Version 1.3," Comput.Phys.Commun. **174** (2006) 577–604, arXiv:hep-ph/0405253 [hep-ph].

[177] G. Belanger, F. Boudjema, A. Pukhov, and A. Semenov, "MicrOMEGAs 2.0: A Program to calculate the relic density of dark matter in a generic model," Comput.Phys.Commun. **176** (2007) 367–382, arXiv:hep-ph/0607059 [hep-ph].

[178] G. Belanger, F. Boudjema, A. Pukhov, and A. Semenov, "Dark matter direct detection rate in a generic model with micrOMEGAs 2.2," Comput.Phys.Commun. **180** (2009) 747–767, arXiv:0803.2360 [hep-ph].

[179] G. Belanger, F. Boudjema, P. Brun, A. Pukhov, S. Rosier-Lees, et al., "Indirect search for dark matter with micrOMEGAs2.4," Comput.Phys.Commun. **182** (2011) 842–856, arXiv:1004.1092 [hep-ph].

[180] **Particle Data Group** Collaboration, K. Nakamura et al., "Review of particle physics," J.Phys. **G37** (2010) 075021.

[181] **MEG collaboration** Collaboration, J. Adam et al., "New limit on the lepton-flavour violating decay $\mu^+ \to e^+\gamma$," Phys.Rev.Lett. **107** (2011) 171801, arXiv:1107.5547 [hep-ex].

[182] T. Schwetz, M. Tortola, and J. Valle, "Global neutrino data and recent reactor fluxes: status of three-flavour oscillation parameters," New J.Phys. **13** (2011) 063004, arXiv:1103.0734 [hep-ph].

[183] F. Borzumati and T. Yamashita, "Minimal supersymmetric SU(5) model with nonrenormalizable operators: Seesaw mechanism and violation of flavour and CP," Prog.Theor.Phys. **124** (2010) 761–868, arXiv:0903.2793 [hep-ph].

[184] E. Ma, "Pathways to naturally small neutrino masses," Phys.Rev.Lett. **81** (1998) 1171–1174, arXiv:hep-ph/9805219 [hep-ph].

[185] W. Porod, "SPheno." For the latest version of spheno, see the web page: http://www.physik.uni-wuerzburg.de/$\sim$porod/SPheno.html.

[186] F. Staub, "From Superpotential to Model Files for FeynArts and CalcHep/CompHep," Comput.Phys.Commun. **181** (2010) 1077–1086, arXiv:0909.2863 [hep-ph].

[187] F. Staub, "Automatic Calculation of supersymmetric Renormalization Group Equations and Self Energies," Comput.Phys.Commun. **182** (2011) 808–833, arXiv:1002.0840 [hep-ph].

[188] D. M. Pierce, J. A. Bagger, K. T. Matchev, and R.-j. Zhang, "Precision corrections in the minimal supersymmetric standard model," Nucl.Phys. **B491** (1997) 3–67, arXiv:hep-ph/9606211 [hep-ph].

[189] http://lepsusy.web.cern.ch/lepsusy/.

[190] J. Yamaoka, "Tevatron Bounds," 2010. Talk given at PASCOS, Valencia (Spain).

[191] **ATLAS Collaboration** Collaboration, G. Aad et al., "Combined search for the Standard Model Higgs boson using up to 4.9 fb^{-1} of pp collision data at $\sqrt{s} = 7$ TeV with the ATLAS detector at the LHC," Phys.Lett. **B710** (2012) 49–66, arXiv:1202.1408 [hep-ex].

[192] **CMS Collaboration** Collaboration, S. Chatrchyan et al., "Combined results of searches for the standard model Higgs boson in pp collisions at $\sqrt{s} = 7$ TeV," Phys.Lett. **B710** (2012) 26–48, arXiv:1202.1488 [hep-ex].

[193] L. J. Hall, D. Pinner, and J. T. Ruderman, "A Natural SUSY Higgs Near 126 GeV," JHEP **1204** (2012) 131, arXiv:1112.2703 [hep-ph].

[194] H. Baer, V. Barger, and A. Mustafayev, "Implications of a 125 GeV Higgs scalar for LHC SUSY and neutralino dark matter searches," Phys.Rev. **D85** (2012) 075010, arXiv:1112.3017 [hep-ph].

[195] J. L. Feng, K. T. Matchev, and D. Sanford, "Focus Point Supersymmetry Redux," Phys.Rev. **D85** (2012) 075007, arXiv:1112.3021 [hep-ph].

[196] S. Heinemeyer, O. Stal, and G. Weiglein, "Interpreting the LHC Higgs Search Results in the MSSM," Phys.Lett. **B710** (2012) 201–206, arXiv:1112.3026 [hep-ph].

[197] A. Arbey, M. Battaglia, A. Djouadi, F. Mahmoudi, and J. Quevillon, "Implications of a 125 GeV Higgs for supersymmetric models," Phys.Lett. **B708** (2012) 162–169, arXiv:1112.3028 [hep-ph].

[198] A. Arbey, M. Battaglia, and F. Mahmoudi, "Constraints on the MSSM from the Higgs Sector: A pMSSM Study of Higgs Searches, $B_s^0 \to \mu^+\mu^-$ and Dark Matter Direct Detection," Eur.Phys.J. **C72** (2012) 1906, arXiv:1112.3032 [hep-ph].

[199] P. Draper, P. Meade, M. Reece, and D. Shih, "Implications of a 125 GeV Higgs for the MSSM and Low-Scale SUSY Breaking," Phys.Rev. **D85** (2012) 095007, arXiv:1112.3068 [hep-ph].

[200] T. Moroi, R. Sato, and T. T. Yanagida, "Extra Matters Decree the Relatively Heavy Higgs of Mass about 125 GeV in the Supersymmetric Model," Phys.Lett. **B709** (2012) 218–221, arXiv:1112.3142 [hep-ph].

[201] M. Carena, S. Gori, N. R. Shah, and C. E. Wagner, "A 125 GeV SM-like Higgs in the MSSM and the $\gamma\gamma$ rate," JHEP **1203** (2012) 014, arXiv:1112.3336 [hep-ph].

[202] O. Buchmueller, R. Cavanaugh, A. De Roeck, M. Dolan, J. Ellis, et al., "Higgs and Supersymmetry," Eur.Phys.J. **C72** (2012) 2020, arXiv:1112.3564 [hep-ph].

[203] S. Akula, B. Altunkaynak, D. Feldman, P. Nath, and G. Peim, "Higgs Boson Mass Predictions in SUGRA Unification, Recent LHC-7 Results, and Dark Matter," Phys.Rev. **D85** (2012) 075001, arXiv:1112.3645 [hep-ph].

[204] M. Kadastik, K. Kannike, A. Racioppi, and M. Raidal, "Implications of the 125 GeV Higgs boson for scalar dark matter and for the CMSSM phenomenology," JHEP **1205** (2012) 061, arXiv:1112.3647 [hep-ph].

[205] J. Cao, Z. Heng, D. Li, and J. M. Yang, "Current experimental constraints on the lightest Higgs boson mass in the constrained MSSM," Phys.Lett. **B710** (2012) 665–670, arXiv:1112.4391 [hep-ph].

[206] A. Arvanitaki and G. Villadoro, "A Non Standard Model Higgs at the LHC as a Sign of Naturalness," JHEP **1202** (2012) 144, arXiv:1112.4835 [hep-ph].

[207] M. Gozdz, "Lightest Higgs boson masses in the R-parity violating supersymmetry," arXiv:1201.0875 [hep-ph].

[208] J. F. Gunion, Y. Jiang, and S. Kraml, "The Constrained NMSSM and Higgs near 125 GeV," Phys.Lett. **B710** (2012) 454–459, arXiv:1201.0982 [hep-ph].

[209] G. G. Ross and K. Schmidt-Hoberg, "The Fine-Tuning of the Generalised NMSSM," Nucl.Phys. **B862** (2012) 710–719, arXiv:1108.1284 [hep-ph].

[210] G. G. Ross, K. Schmidt-Hoberg, and F. Staub, "The Generalised NMSSM at One Loop: Fine Tuning and Phenomenology," JHEP **1208** (2012) 074, arXiv:1205.1509 [hep-ph].

[211] P. Fileviez Perez, "SUSY Spectrum and the Higgs Mass in the BLMSSM," Phys.Lett. **B711** (2012) 353–359, arXiv:1201.1501 [hep-ph].

[212] N. Karagiannakis, G. Lazarides, and C. Pallis, "Dark Matter and Higgs Mass in the CMSSM with Yukawa Quasi-Unification," J.Phys.Conf.Ser. **384** (2012) 012012, arXiv:1201.2111 [hep-ph].

[213] S. King, M. Muhlleitner, and R. Nevzorov, "NMSSM Higgs Benchmarks Near 125 GeV," Nucl.Phys. **B860** (2012) 207–244, arXiv:1201.2671 [hep-ph].

[214] Z. Kang, J. Li, and T. Li, "On Naturalness of the MSSM and NMSSM," JHEP **1211** (2012) 024, arXiv:1201.5305 [hep-ph].

[215] C.-F. Chang, K. Cheung, Y.-C. Lin, and T.-C. Yuan, "Mimicking the Standard Model Higgs Boson in UMSSM," JHEP **1206** (2012) 128, arXiv:1202.0054 [hep-ph].

[216] L. Aparicio, D. Cerdeno, and L. Ibanez, "A 119-125 GeV Higgs from a string derived slice of the CMSSM," JHEP **1204** (2012) 126, arXiv:1202.0822 [hep-ph].

[217] L. Roszkowski, E. M. Sessolo, and Y.-L. S. Tsai, "Bayesian Implications of Current LHC Supersymmetry and Dark Matter Detection Searches for the Constrained MSSM," Phys.Rev. **D86** (2012) 095005, arXiv:1202.1503 [hep-ph].

[218] J. Ellis and K. A. Olive, "Revisiting the Higgs Mass and Dark Matter in the CMSSM," Eur.Phys.J. **C72** (2012) 2005, arXiv:1202.3262 [hep-ph].

[219] H. Baer, V. Barger, and A. Mustafayev, "Neutralino dark matter in mSUGRA/CMSSM with a 125 GeV light Higgs scalar," JHEP **1205** (2012) 091, arXiv:1202.4038 [hep-ph].

[220] N. Desai, B. Mukhopadhyaya, and S. Niyogi, "Constraints on Invisible Higgs Decay in MSSM in the Light of Diphoton Rates from the LHC," arXiv:1202.5190 [hep-ph].

[221] J.-J. Cao, Z.-X. Heng, J. M. Yang, Y.-M. Zhang, and J.-Y. Zhu, "A SM-like Higgs near 125 GeV in low energy SUSY: a comparative study for MSSM and NMSSM," JHEP **1203** (2012) 086, arXiv:1202.5821 [hep-ph].

[222] L. Maiani, A. Polosa, and V. Riquer, "Probing Minimal Supersymmetry at the LHC with the Higgs Boson Masses," New J.Phys. **14** (2012) 073029, arXiv:1202.5998 [hep-ph].

[223] T. Cheng, J. Li, T. Li, D. V. Nanopoulos, and C. Tong, "Electroweak Supersymmetry around the Electroweak Scale," arXiv:1202.6088 [hep-ph].

[224] N. D. Christensen, T. Han, and S. Su, "MSSM Higgs Bosons at The LHC," Phys.Rev. **D85** (2012) 115018, arXiv:1203.3207 [hep-ph].

[225] D. A. Vasquez, G. Belanger, C. Boehm, J. Da Silva, P. Richardson, et al., "The 125 GeV Higgs in the NMSSM in light of LHC results and astrophysics constraints," Phys.Rev. **D86** (2012) 035023, arXiv:1203.3446 [hep-ph].

[226] U. Ellwanger and C. Hugonie, "Higgs bosons near 125 GeV in the NMSSM with constraints at the GUT scale," Adv.High Energy Phys. **2012** (2012) 625389, arXiv:1203.5048 [hep-ph].

[227] "ATLAS results." Updated results can be found on the web-page: https://twiki.cern.ch/twiki/bin/view/AtlasPublic; especially: ATLAS-CONF-2012-033.

[228] "CMS results." Updated results can be found on the web-page: https://twiki.cern.ch/twiki/bin/view/CMSPublic/PhysicsResults.

[229] H. E. Haber and M. Sher, "Higgs mass bound in E(6) based supersymmetric theories," Phys.Rev. **D35** (1987) 2206.

[230] M. Drees, "Comment on 'Higgs boson mass bound in E(6) based supersymmetric theories.'," Phys.Rev. **D35** (1987) 2910–2913.

[231] M. Cvetic, D. A. Demir, J. Espinosa, L. Everett, and P. Langacker, "Electroweak breaking and the mu problem in supergravity models with an additional U(1)," Phys.Rev. **D56** (1997) 2861, arXiv:hep-ph/9703317 [hep-ph].

[232] Y. Zhang, H. An, X.-d. Ji, and R. N. Mohapatra, "Light Higgs Mass Bound in SUSY Left-Right Models," Phys.Rev. **D78** (2008) 011302, arXiv:0804.0268 [hep-ph].

[233] E. Ma, "Exceeding the MSSM Higgs Mass Bound in a Special Class of U(1) Gauge Models," Phys.Lett. **B705** (2011) 320–323, arXiv:1108.4029 [hep-ph].

[234] A. Ali, D. A. Demir, M. Frank, and I. Turan, "Search for Gauge Extensions of the MSSM at the LHC," Phys.Rev. **D79** (2009) 095001, arXiv:0902.3826 [hep-ph].

[235] A. Belyaev, J. P. Hall, S. F. King, and P. Svantesson, "Novel gluino cascade decays in E_6 inspired models," Phys.Rev. **D86** (2012) 031702, arXiv:1203.2495 [hep-ph].

[236] R. Mohapatra, "New Contributions to Neutrinoless Double beta Decay in Supersymmetric Theories," Phys.Rev. **D34** (1986) 3457–3461.

[237] C. S. Aulakh, K. Benakli, and G. Senjanovic, "Reconciling supersymmetry and left-right symmetry," Phys.Rev.Lett. **79** (1997) 2188–2191, arXiv:hep-ph/9703434 [hep-ph].

[238] S. P. Martin, "Some simple criteria for gauged R-parity," Phys.Rev. **D46** (1992) 2769–2772, arXiv:hep-ph/9207218 [hep-ph].

[239] C. Aulakh and R. N. Mohapatra, "Neutrino as the Supersymmetric Partner of the Majoron," Phys.Lett. **B119** (1982) 136.

[240] M. J. Hayashi and A. Murayama, "Radiative breaking of SU(2)-R x U(1)-(B-L) gauge symmetry induced by broken N=1 Supergravity in a left-right symmetric model," Phys.Lett. **B153** (1985) 251.

[241] R. Mohapatra, "Mechanism for understanding small neutrino mass in superstring theories," Phys.Rev.Lett. **56** (1986) 561–563.

[242] B. Allanach, C. Balazs, G. Belanger, M. Bernhardt, F. Boudjema, et al., "SUSY Les Houches Accord 2," Comput.Phys.Commun. **180** (2009) 8–25, arXiv:0801.0045 [hep-ph].

[243] B. Holdom, "Two U(1)'s and Epsilon Charge Shifts," Phys.Lett. **B166** (1986) 196.

[244] K. Babu, C. F. Kolda, and J. March-Russell, "Implications of generalized Z - Z-prime mixing," Phys.Rev. **D57** (1998) 6788–6792, arXiv:hep-ph/9710441 [hep-ph].

[245] B. O'Leary, W. Porod, and F. Staub, "Mass spectrum of the minimal SUSY B-L model," JHEP **1205** (2012) 042, arXiv:1112.4600 [hep-ph].

[246] F. Braam and J. Reuter, "A Simplified Scheme for GUT-inspired Theories with Multiple Abelian Factors," Eur.Phys.J. **C72** (2012) 1885, arXiv:1107.2806 [hep-ph].

[247] E. J. Chun, J.-C. Park, and S. Scopel, "Dark matter and a new gauge boson through kinetic mixing," JHEP **1102** (2011) 100, arXiv:1011.3300 [hep-ph].

[248] Y. Mambrini, "The ZZ' kinetic mixing in the light of the recent direct and indirect dark matter searches," JCAP **1107** (2011) 009, arXiv:1104.4799 [hep-ph].

[249] T. G. Rizzo, "Gauge Kinetic Mixing in the E_6SSM," Phys.Rev. **D85** (2012) 055010, arXiv:1201.2898 [hep-ph].

[250] D. Matalliotakis and H. P. Nilles, "Implications of nonuniversality of soft terms in supersymmetric grand unified theories," Nucl.Phys. **B435** (1995) 115–128, arXiv:hep-ph/9407251 [hep-ph].

[251] N. Polonsky and A. Pomarol, "Nonuniversal GUT corrections to the soft terms and their implications in supergravity models," Phys.Rev. **D51** (1995) 6532–6549, arXiv:hep-ph/9410231 [hep-ph].

[252] V. Berezinsky, A. Bottino, J. R. Ellis, N. Fornengo, G. Mignola, et al., "Neutralino dark matter in supersymmetric models with nonuniversal scalar mass terms," Astropart.Phys. **5** (1996) 1–26, arXiv:hep-ph/9508249 [hep-ph].

[253] "ATLAS conference note ATLAS-CONF-2012-007, see [227].".

[254] J. Erler, P. Langacker, S. Munir, and E. Rojas, "Z' Bosons at Colliders: a Bayesian Viewpoint," JHEP **1111** (2011) 076, arXiv:1103.2659 [hep-ph].

[255] T. G. Rizzo, "Z' phenomenology and the LHC," arXiv:hep-ph/0610104 [hep-ph].

[256] **Particle Data Group** Collaboration, J. Beringer et al., "Review of Particle Physics (RPP)," Phys.Rev. **D86** (2012) 010001.

[257] F. Staub, T. Ohl, W. Porod, and C. Speckner, "A Tool Box for Implementing Supersymmetric Models," Comput.Phys.Commun. **183** (2012) 2165–2206, arXiv:1109.5147 [hep-ph].

[258] P. Bechtle, O. Brein, S. Heinemeyer, G. Weiglein, and K. E. Williams, "HiggsBounds: Confronting Arbitrary Higgs Sectors with Exclusion Bounds from LEP and the Tevatron," Comput.Phys.Commun. **181** (2010) 138–167, arXiv:0811.4169 [hep-ph].

[259] P. Bechtle, O. Brein, S. Heinemeyer, G. Weiglein, and K. E. Williams, "HiggsBounds 2.0.0: Confronting Neutral and Charged Higgs Sector Predictions with Exclusion Bounds from LEP and the Tevatron," Comput.Phys.Commun. **182** (2011) 2605–2631, arXiv:1102.1898 [hep-ph].

[260] A. Elsayed, S. Khalil, and S. Moretti, "Higgs Mass Corrections in the SUSY B-L Model with Inverse Seesaw," Phys.Lett. **B715** (2012) 208–213, arXiv:1106.2130 [hep-ph].

[261] **MEG Collaboration** Collaboration, J. Adam et al., "New constraint on the existence of the $\mu^+ \to e^+\gamma$ decay," Phys.Rev.Lett. **110** no. 20, (2013) 201801, arXiv:1303.0754 [hep-ex].

[262] A. Bartl, W. Majerotto, W. Porod, and D. Wyler, "Effect of supersymmetric phases on lepton dipole moments and rare lepton decays," Phys.Rev. **D68** (2003) 053005, arXiv:hep-ph/0306050 [hep-ph].

[263] M. Hirsch, H. Klapdor-Kleingrothaus, and S. Kovalenko, "B-L violating masses in softly broken supersymmetry," Phys.Lett. **B398** (1997) 311–314, arXiv:hep-ph/9701253 [hep-ph].

[264] G. Degrassi, P. Slavich, and F. Zwirner, "On the neutral Higgs boson masses in the MSSM for arbitrary stop mixing," Nucl.Phys. **B611** (2001) 403–422, arXiv:hep-ph/0105096 [hep-ph].

[265] A. Brignole, G. Degrassi, P. Slavich, and F. Zwirner, "On the O(alpha(t)**2) two loop corrections to the neutral Higgs boson masses in the MSSM," Nucl.Phys. **B631** (2002) 195–218, arXiv:hep-ph/0112177 [hep-ph].

[266] A. Brignole, G. Degrassi, P. Slavich, and F. Zwirner, "On the two loop sbottom corrections to the neutral Higgs boson masses in the MSSM," Nucl.Phys. **B643** (2002) 79–92, arXiv:hep-ph/0206101 [hep-ph].

[267] A. Dedes and P. Slavich, "Two loop corrections to radiative electroweak symmetry breaking in the MSSM," Nucl.Phys. **B657** (2003) 333–354, arXiv:hep-ph/0212132 [hep-ph].

[268] A. Dedes, G. Degrassi, and P. Slavich, "On the two loop Yukawa corrections to the MSSM Higgs boson masses at large tan beta," Nucl.Phys. **B672** (2003) 144–162, arXiv:hep-ph/0305127 [hep-ph].

[269] ATLAS working group, "ATLAS experiment - Public Results," 2014. https://twiki.cern.ch/twiki/bin/view/AtlasPublic.

[270] A. Nisati, "ATLAS.". Talk presented at Lepton-Photon Conference 2011, Mumbai, India.

[271] V. Sharma, "CMS.". Talk presented at Lepton-Photon Conference 2011, Mumbai, India.

[272] E. Etzion. private communication.

[273] C.-F. Chang, K. Cheung, and T.-C. Yuan, "Supersymmetric Decays of the Z' Boson," JHEP **1109** (2011) 058, arXiv:1107.1133 [hep-ph].

[274] **ATLAS Collaboration** Collaboration, G. Aad et al., "Search for dilepton resonances in pp collisions at $\sqrt{s} = 7$ TeV with the ATLAS detector," Phys.Rev.Lett. **107** (2011) 272002, arXiv:1108.1582 [hep-ex].

[275] **CMS Collaboration** Collaboration, S. Chatrchyan et al., "Search for Resonances in the Dilepton Mass Distribution in pp Collisions at $\sqrt{(}s) = 7$ TeV," JHEP **1105** (2011) 093, arXiv:1103.0981 [hep-ex].

[276] W. Kilian, T. Ohl, and J. Reuter, "WHIZARD: Simulating Multi-Particle Processes at LHC and ILC," Eur.Phys.J. **C71** (2011) 1742, arXiv:0708.4233 [hep-ph].

[277] M. Moretti, T. Ohl, and J. Reuter, "O'Mega: An Optimizing matrix element generator," arXiv:hep-ph/0102195 [hep-ph].

[278] B. Fuks, M. Klasen, F. Ledroit, Q. Li, and J. Morel, "Precision predictions for Z' - production at the CERN LHC: QCD matrix elements, parton showers, and joint resummation," Nucl.Phys. **B797** (2008) 322–339, arXiv:0711.0749 [hep-ph].

[279] F. del Aguila, J. Aguilar-Saavedra, and R. Pittau, "Heavy neutrino signals at large hadron colliders," JHEP **0710** (2007) 047, arXiv:hep-ph/0703261 [hep-ph].

[280] J. Aguilar-Saavedra, "Heavy lepton pair production at LHC: Model discrimination with multi-lepton signals," Nucl.Phys. **B828** (2010) 289–316, arXiv:0905.2221 [hep-ph].

[281] S. Das, F. Deppisch, O. Kittel, and J. Valle, "Heavy Neutrinos and Lepton Flavour Violation in Left-Right Symmetric Models at the LHC," Phys.Rev. **D86** (2012) 055006, arXiv:1206.0256 [hep-ph].

[282] S. Gopalakrishna, A. de Gouvea, and W. Porod, "Right-handed sneutrinos as nonthermal dark matter," JCAP **0605** (2006) 005, arXiv:hep-ph/0602027 [hep-ph].

[283] C. Arina and N. Fornengo, "Sneutrino cold dark matter, a new analysis: Relic abundance and detection rates," JHEP **0711** (2007) 029, arXiv:0709.4477 [hep-ph].

[284] Z. Thomas, D. Tucker-Smith, and N. Weiner, "Mixed Sneutrinos, Dark Matter and the CERN LHC," Phys.Rev. **D77** (2008) 115015, arXiv:0712.4146 [hep-ph].

[285] D. G. Cerdeno, C. Munoz, and O. Seto, "Right-handed sneutrino as thermal dark matter," Phys.Rev. **D79** (2009) 023510, arXiv:0807.3029 [hep-ph].

[286] P. Bandyopadhyay, E. J. Chun, and J.-C. Park, "Right-handed sneutrino dark matter in $\mathbf{U}(\mathbf{1})'$ seesaw models and its signatures at the LHC," JHEP **1106** (2011) 129, arXiv:1105.1652 [hep-ph].

[287] G. Belanger, J. Da Silva, and A. Pukhov, "The Right-handed sneutrino as thermal dark matter in U(1) extensions of the MSSM," JCAP **1112** (2011) 014, arXiv:1110.2414 [hep-ph].

[288] B. Dumont, G. Belanger, S. Fichet, S. Kraml, and T. Schwetz, "Mixed sneutrino dark matter in light of the 2011 XENON and LHC results," JCAP **1209** (2012) 013, arXiv:1206.1521 [hep-ph].

[289] P. C. West, "The Yukawa beta Function in N=1 Rigid Supersymmetric Theories," Phys.Lett. **B137** (1984) 371.

[290] D. Jones and L. Mezincescu, "The Chiral Anomaly and a Class of Two Loop Finite Supersymmetric Gauge Theories," Phys.Lett. **B138** (1984) 293.